

Maheswar Panda

---

# Percolation, Scaling, and Relaxation in Polymer Dielectrics

# Percolation, Scaling, and Relaxation in Polymer Dielectrics

Maheswar Panda

# Percolation, Scaling, and Relaxation in Polymer Dielectrics

 Springer

Maheswar Panda   
Multifunctional Polymer Nanocomposites  
Laboratory, Department of Physics  
Dr. Harisingh Gour Vishwavidyalaya  
(A Central University)  
Sagar, Madhya Pradesh, India

ISBN 978-3-031-27940-9      ISBN 978-3-031-27941-6 (eBook)  
<https://doi.org/10.1007/978-3-031-27941-6>

© The Editor(s) (if applicable) and The Author(s), under exclusive license to Springer Nature Switzerland AG 2023

This work is subject to copyright. All rights are solely and exclusively licensed by the Publisher, whether the whole or part of the material is concerned, specifically the rights of translation, reprinting, reuse of illustrations, recitation, broadcasting, reproduction on microfilms or in any other physical way, and transmission or information storage and retrieval, electronic adaptation, computer software, or by similar or dissimilar methodology now known or hereafter developed.

The use of general descriptive names, registered names, trademarks, service marks, etc. in this publication does not imply, even in the absence of a specific statement, that such names are exempt from the relevant protective laws and regulations and therefore free for general use.

The publisher, the authors, and the editors are safe to assume that the advice and information in this book are believed to be true and accurate at the date of publication. Neither the publisher nor the authors or the editors give a warranty, expressed or implied, with respect to the material contained herein or for any errors or omissions that may have been made. The publisher remains neutral with regard to jurisdictional claims in published maps and institutional affiliations.

This Springer imprint is published by the registered company Springer Nature Switzerland AG  
The registered company address is: Gewerbestrasse 11, 6330 Cham, Switzerland

*The whole of science is nothing more than a  
refinement of everyday thinking*

—*Albert Einstein*

*Dedicated to my father: Mr. Umakanta Panda  
for teaching me the value of being honest and  
self-disciplined*

# Preface

There is availability of a large number of books under two classes, such as: the books dealing with either the phenomena of percolation/applications of percolation phenomena or on the development of polymer composites/nanocomposites for their electrostatic energy storage applications. The books on percolation theory deal mostly with the theoretical and/or computational aspect of the systems and target very broad/large audiences comprising of statistical physicists, solid-state physicists, theoretical physicists, mathematicians, social scientists, etc., while the books on polymer nanocomposites deal with the synthesis and characterization of materials for electrostatic energy storage applications and targets the audiences comprising of experimental condensed matter physicists, materials scientists, polymer scientists, chemists, mechanical, civil, electrical, chemical and electronics engineers, etc.

Hence, a book of unique kind of this type containing both of the above contents is demanded and should be available in the market, which will target the audiences comprising from the above two different classes; i.e., it should contain both physics and applications of the polymer composites. This book contains the synthesis, structure, microstructure, phase transition, percolation, scaling, relaxation, magnetic, multiferroic, rheological behaviors, and the electrostatic energy storage applications of the polymer composites. An additional chapter is also included to have an understanding of the non-percolative polymer composites.

This book will be a concise report and will try to inculcate mostly the percolative phase transitions and the relaxation behavior of insulating polymers/conductor composites across the percolation threshold and their applications. The explanation of the critical and relaxation exponents across the phase transition point will be mostly the key features of this book. The detailed explanation of the relaxation behavior by applying dielectric spectroscopy and impedance spectroscopy in such systems will be very innovative, novel, and interesting features of this book. In addition, the multifunctional properties, such as the multiferroic, viscoelastic properties, and the physical properties of non-percolative polymer composites will also make the additional interesting parts of this book. The last chapter of the book also explains the importance of ferroelectric polymer dielectrics for future electrical energy storage applications.

Over the past 18 years of working in this area of research, I was highly curious to write a book in this area of research, which will contain a unique combination of both physics and materials science. This book will be largely beneficial for the beginners who are starting their carrier in this field of research, as they are confused with so many books, which are either targeting only the theoretical/computational aspect or the materials sciences aspect separately. Hence, this approach of finding both physics and materials sciences along with their applications, i.e., engineering of physics will make this book unique and interesting as compared to the books currently available in the market. In the writing of this book, I was highly inspired by my spouse and kids and the students of my class.

Sagar, Madhya Pradesh, India

Maheswar Panda, Ph.D.

# Acknowledgements

At the outset, I would like to thank the almighty, my motherland, and my parents: Mrs. Gouri Panda and Mr. Umakanta Panda, who had taken a lot of pain in making me to such a position, where I can deliver the book. I am highly thankful to my spouse Mrs. Binapani Panda, who has always been motivating and taking special care of me during the writing of this book and for being a constant source of inspiration throughout my academic journey. I am also highly thankful to my kids, Khushi and Ami, for their continuous fun with me and their disciplined behavior during the writing of the book. Thanks are also due to my brothers Pradeep, Chaga and my sister Bapu, and all other siblings for providing continuous encouragement and support to me at every stages of my life.

I would like to express my sincere gratitude to Prof. Neelima Gupta, Honorable Vice-chancellor of our university, who is a renowned and distinguished academician in the field of biological and animal sciences, for her continuous guidance and support in the academic development. I would like to thank Dr. Ranjan Kumar Pradhan, Registrar of our university, for his support and motivation. I am highly thankful to my Ph.D. supervisors Prof. V. Srinivas and Prof. A. K. Thakur, for their continuous support, guidance, and thorough training in their unique way for making me an independent researcher. I wish to express my sincere thanks to Prof. R. N. P. Choudhary for his continuous motivation and inspiring words throughout my professional carrier. I am very much grateful to Dr. B. Behera, Dr. V. Singh, Dr. S. K. Barik, Dr. A. Palai, Prof. H. Thomas, and Prof. V. Verma, for the timely academic discussions. I am very much grateful to my students, Mr. Sushil Kumar Behera, Ms. Harsha Chouhan, Mr. Avnish Mishra, Ms. Asmita Trivedi, Ms. Nadira Sultana, Mr. Subham Sharma, Ms. Shivangi Bidolia, Mr. Jitendra Kurmi, Mr. Soumitra Das, Mr. Sunil Soni, Ms. Jagitri Prajapti, Mr. Subhajeet Sen, Ms. Vidhi Singhai, Mr. Partha Sarathi Rout, Ms. Aditi Agarwal, Mr. Satyam Dubey, Ms. Yasika Soni, Mr. Amit Agarwal and others, who were the part of my research group. Special thanks to all the batches of PG and UG students during my teaching carrier from 2010 to till date, who were the part of my class and being friends, their intriguing and curious questions in the class, making strong to their teachers for communicating meaningful books.

I am very much grateful to all the faculty members and all my co-researchers of Dr. Harisingh Gour Vishwavidyalaya (A Central University), Sagar, M.P., for the stimulating academic discussions. I would like to thank all the faculty members/colleagues/research scholars of the physics department for giving an amicable environment, which has helped me a lot in writing this book. I am very much grateful to the reviewers, for their stimulating and intriguing questions during the process of reviewing. I would like to acknowledge SERB (DST), New Delhi, India, and UGC, New Delhi, India, for providing the financial support to carry out the related research works and also in developing the Multifunctional Polymer nanocomposites Laboratory.

Finally, I pay respect to all, who has been a part of the academic discussions, without their wholehearted support, the book would not have been completed.

Sagar, Madhya Pradesh, India

Maheswar Panda, Ph.D.

## About This Book

**Subject:** Physical sciences/Condensed matter physics/Statistical physics/Materials science/Polymer science and technology.

This book *Percolation, Scaling, and Relaxation in Polymer Dielectrics* will be a book of unique kind, highly useful to the graduate students of condensed matter physics, applied physics, statistical physics, materials sciences, polymer sciences and technology, chemistry, engineering, etc. This book will also contain a genuine flavor of both physics and applications of percolative composites based on polymer matrix and will be useful for a larger domain of audiences comprising of physicists, materials scientists, polymer scientists, chemists, engineers, etc. This book provides the fundamentals and basic understanding of polymer dielectrics based on percolative composites. This book also may be a reference book for the UG and PG students, going through some sections of phase transition of the course statistical mechanics/physics. The microstructure and the associated physical properties, e.g., dielectric, electrical, magnetic, and rheological properties of the polymer composites, are discussed. The properties have been explained based on various theoretical models and through the application of varieties of spectroscopies, such as dielectric spectroscopy, impedance spectroscopy, conductivity spectroscopy. It also discusses a chapter on non-percolative polymer composites. The book discusses the suitability of these polymer dielectrics for their electrical energy storage applications in various devices. The structure of the book in terms of various topics in different chapters is explained as follows. Chapter 1 provides a general introduction and the recent work done on polymer dielectrics. Chapter 2 describes the basic physical properties and the fundamental models and spectroscopic techniques to understand them. Chapter 3 deals with sample preparation and the experimental measurements on them. Chapters 4 and 5 explain the percolative and scaling behaviors respectively. Chapters 6 and 7 explain their electrical relaxation behavior in terms of dielectric and impedance spectroscopy respectively. Chapter 8 describes their magnetic, multiferroic, and rheological behavior. Chapter 9 discusses the electrical and dielectric properties of non-percolative polymer composites. Chapter 10 summarizes and concludes the importance of ferroelectric polymer dielectrics.

**Key Features:**

- Focuses on both the fundamentals and application of the percolative polymer composites as electrostatic energy storage materials.
- Deals with various physical properties along with their thorough understanding, through standard models.
- Includes the current state-of-the-art research focus in the field of polymer dielectrics.
- The unique combination of both physics (percolation, scaling, and relaxation) and applications of energy storage materials.
- Additional properties, such as the multiferroic and rheological properties, are also included.
- Electrical properties of additional and special non-percolative polymer composites are also included, in the book.

**Keywords:** Polymer matrix composites, Polymer-metal composites, Microstructure, Phase transition, Polymer dielectrics, Percolation, Boundary layer capacitor effect, Percolation theory, Effective medium theory, Scaling exponents, Critical exponents, Relaxation exponents, Impedance spectroscopy, Dielectric spectroscopy, Electrical conductivity, Dielectric ceramics

# Contents

<b>1</b>	<b>Introduction</b>	1
1.1	Review of Scientific Literature	4
1.2	Scope of the Book	6
1.3	Organization of the Book	7
	References	7
<b>2</b>	<b>Fundamentals of the Models and Spectroscopic Techniques</b>	11
2.1	Introduction	11
2.2	Fundamental Concepts	12
	2.2.1 Concept of Connectivity	12
	2.2.2 How Composites Work?	12
2.3	Theoretical Models	13
	2.3.1 Effective Medium Approximations	13
	2.3.2 Percolation Theory	15
2.4	Spectroscopic Techniques	18
	2.4.1 Dielectric Spectroscopy	18
	2.4.2 Impedance Spectroscopy	21
	2.4.3 Conductivity Spectroscopy	24
2.5	Magnetic Percolation Threshold	25
2.6	Summary	26
	References	26
<b>3</b>	<b>Synthesis and Characterization of Polymer Composites</b>	29
3.1	Sample Preparation	29
	3.1.1 Synthesis of Nanocrystalline Powders	31
	3.1.2 Formation of Polymer Composites	32
3.2	Physical Characterization Techniques	33
	3.2.1 Structure	33
	3.2.2 Microstructure	35
	3.2.3 Thermal Characterizations	39
	3.2.4 Electrical Characterizations	39
	3.2.5 Magnetic Characterizations	44

3.2.6	Rheological Characterizations .....	46
3.3	Summary .....	47
	References .....	47
<b>4</b>	<b>Percolation Behavior of Polymer Composites</b> .....	<b>49</b>
4.1	Introduction .....	49
4.2	Samples Reported .....	50
4.3	Results and Discussion .....	51
4.3.1	Filler Size Dependence .....	51
4.3.2	Effect of Process Conditions and Particle Size .....	60
4.3.3	Effect of Temperature and Time .....	65
4.3.4	Effect of Matrices .....	68
4.3.5	Effect of Fillers .....	73
4.3.6	Effect of Cold Pressing .....	76
4.4	Summary .....	83
	References .....	84
<b>5</b>	<b>Scaling Behavior of Percolative Polymer Composites</b> .....	<b>87</b>
5.1	Introduction .....	87
5.2	Samples Reported .....	89
5.3	Results and Discussion .....	90
5.3.1	Microstructure .....	90
5.3.2	Stability of Composites .....	90
5.3.3	Dielectric Behavior .....	93
5.3.4	Frequency-Dependent Scaling Behavior .....	100
5.4	Summary .....	102
	References .....	108
<b>6</b>	<b>Relaxation Behavior of Percolative Polymer Composites</b> .....	<b>111</b>
6.1	Introduction .....	111
6.2	Samples Reported .....	114
6.3	Results .....	115
6.3.1	Experimental Dielectric Response .....	115
6.3.2	Frequency Dependent Dielectric Response Below $f_c$ ....	117
6.3.3	Normalization of Dipolar Relaxation .....	124
6.3.4	Frequency Dependent Dielectric Response Above $f_c$ ....	126
6.4	Discussion .....	129
6.4.1	Below $f_c$ .....	131
6.4.2	Above $f_c$ .....	133
6.5	Third Kind of Universal Dielectric Response .....	136
6.5.1	Microstructure .....	136
6.5.2	Dielectric Spectroscopy .....	137
6.5.3	Impedance and Conductivity Spectroscopy .....	142
6.6	Summary .....	144
	References .....	145

<b>7</b>	<b>Impedance Spectroscopy of Percolative Polymer Composites</b> .....	147
7.1	Introduction .....	147
7.2	Samples Reported .....	149
7.3	Results and Discussion .....	149
7.3.1	Microstructure .....	149
7.3.2	Impedance Spectroscopy .....	151
7.3.3	Modulus Spectroscopy .....	159
7.3.4	Conductivity Spectroscopy .....	162
7.4	Summary .....	164
	References .....	166
<b>8</b>	<b>Magnetic and Rheological Behavior of Polymer Composites</b> .....	169
8.1	Introduction .....	169
8.2	Samples Reported .....	171
8.3	Results and Discussion .....	172
8.3.1	Magnetic Properties .....	172
8.3.2	Rheological Properties .....	177
8.4	Summary .....	180
	References .....	183
<b>9</b>	<b>Non-percolative Polymer Composites</b> .....	185
9.1	Introduction .....	185
9.2	Samples Reported .....	187
9.3	Results and Discussion .....	187
9.3.1	Microstructure .....	187
9.3.2	Dielectric Properties .....	188
9.3.3	Conductivity Properties .....	191
9.4	Summary .....	193
	References .....	193
<b>10</b>	<b>Ferroelectric Polymer Dielectrics</b> .....	195
10.1	Introduction .....	195
10.2	Samples Reported .....	196
10.3	Results and Discussion .....	196
10.4	Summary .....	198
10.5	Scope for Future Possibilities .....	199
	References .....	201
	<b>Appendix: Calculation of Volume Fraction of Any Component in a Composite</b> .....	203
	<b>Bibliography</b> .....	205

## About the Author



**Maheswar Panda** holds a Ph.D. in Physics from the Indian Institute of Technology, Kharagpur, India, in the year 2011 after qualifying through CSIR UGC NET (JRF)-2005 in the subject Physical Sciences. He is having more than 12 years of teaching experience at the UG and PG levels, currently working as an assistant professor of Physics at Dr. Harisingh Gour Vishwavidyalaya (A Central University), Sagar, M.P., India, and already worked at CURAJ (Ajmer), CUJ (Ranchi), and NIT (Raipur). He is highly popular among the students for his unique and effective style of teaching. He is a life member of both Indian Physics Association (IPA) and Indian Association of Physics Teachers (IAPT). His research interests include percolative composites, energy storage materials, phase transitions, dielectrics, ferroelectrics, multiferroics, magnetoelectrics, magnetodielectrics, EMI shielding, optical and viscoelastic properties, polymer nanocomposites for multifunctional applications, etc. Dr. Panda has published more than 30 journal articles in international journals, all being first authored, including seven single-author articles with being received two patents (one in India and one in German) and one book chapter independently. He has been an invited speaker/reviewer for several international scientific societies/journals. He has been awarded the Young Achiever Award at ICC-2017, Bikaner, INSA Visiting Scientist Fellowship Award-2019 for completing the research work at IOP,

Bhubaneswar during the year 2019 and Best Technology Award-2022 from IIT Indore. He has been the principal investigator of two projects on development of polymer dielectrics, sanctioned by SERB (DST), New Delhi and UGC, New Delhi. He is currently guiding two Ph.D. students, who have won awards & fellowships to their credits and guided 25 M.Sc. dissertation students, with good quality journal articles, who are continuing their Ph.D. as Scientific officers at the premier institutes of the country.

# Chapter 1

## Introduction



Engineering materials constitute the foundation of technology, and technological development depends on advances in the field of materials. Whatever the field may be the final limitation on advancement depends on materials. In the development of these materials, the milestone research on nanoscience and nanotechnology started 60 years ago, when in 1959, Richard P. Feynman first delivered a lecture entitled, “**There’s Plenty of Room at the Bottom**” [1]. Composite materials consisting of micro-to nanofillers in this regard represent a giant step in the ever-constant endeavor of optimization in materials, whether the technology pertains to structural, electrical, dielectric, magnetic, optical, thermal, electrochemical, environmental, mechanical, rheological, biomedical, or any other multifunctional applications. The importance of these composite materials as engineering materials is reflected by the fact that out of over 1600 engineering materials available in the market today, more than 200 are composites [2].

Composites offer several advantages over traditional engineering materials. These beneficial characteristics have enabled the rapid acceptance of these composites in many products. They offer a range of properties suitable for multifunctional applications along with their tremendous durability and high specific strength, with an ability to be formed easily and accurately into any complex geometric shape, which is impossible to match with traditional engineering materials. A composite works based on the following three types of properties [2–5] (i) sum properties, (ii) product properties, and (iii) combination properties.

Among the different matrix composites, polymer matrix composites are gaining much interest because of several advantages, such as low cost of fabrication, relatively low processing temperature, lightweight, easy processing, flexibility, moldability, non-toxicity, and ability to absorb mechanical shock. Polymer matrix composites can again be classified according to whether the matrix used is a thermoset or thermoplastic. Both thermoplastics and thermosets have been used widely as matrices for composite materials showing excellent properties. However, the thermoplastic matrix composites are under rapid development, and their advantages over thermoset-matrix composites are the cost-effectiveness and their better performance. As polymers

possess the lowest average density (1.20 g/cc) compared with other host matrices, such as metals or ceramics, polymer composites show the highest specific strength (strength/density) which cannot be met by any other composites.

In the study of these polymer composites, there is an increasing interest in nanocomposites due to their use in various fields, such as electrical engineering, memory, and biomedical and optical applications [2–20]. Composites can exhibit unprecedented features in their overall response when compared with that of their components. The emergent properties can rarely be predicted by simply knowing the behavior of individual components as the interaction between them is a defining factor. In general, such composites consist of particles, fibers, or nanotubes dispersed in a polymer matrix. The physical properties of these composites change significantly, when the conducting filler particles form a percolative network in the polymer matrix, particularly when the constituent components differ largely in their electrical properties, such as conductivity [21–30]. The combined behavior of the composites also depends on their microstructure, e.g., with decreasing particle size, the properties of the interfaces become more important and finally start to influence the composite behavior affecting permittivity, conductivity, and electromechanical and optical properties. The insulating polymer–conductor composites (PCC) undergo an insulator-to-metal transition (IMT) at a critical concentration of conductor/metal in an insulating matrix, which is called a percolation threshold ( $f_c$ ). In particular, as the filler concentration approaches  $f_c$  from below, the effective AC electrical conductivity ( $\sigma_{\text{eff}}$ ) and the dielectric constant ( $\epsilon_{\text{eff}}$ ) of the composites increase significantly. It is observed that the enhancement in  $\epsilon_{\text{eff}}$  values with low dielectric loss ( $\tan \delta$ ) at  $f_c$  is attained at lower filler concentrations for PCC as compared to polymer-ceramic composites. On the other hand, polymer-metal composites (PMC) show relatively new electrical characteristics close to those of metals, whereas the mechanical properties and processing methods are typical that of plastics. The electrical properties of PMC depend on several factors, including the kind of conducting filler, their spatial distribution, the interaction between polymer and filler, and the contact interaction between the particles. The fundamental physics of these insulator–conductor composites (ICC) in the vicinity of  $f_c$  is very interesting both from the theoretical and experimental points of view. Percolation theory states that in the critical phase transition region, the  $\epsilon_{\text{eff}}$  diverges and  $\sigma_{\text{eff}}$  increases abnormally at  $f_c$ , and they scale as the following relations

$$\epsilon_{\text{eff}}(\omega, f_{\text{con}} \approx f_c) \propto \omega^{-y} \quad (1.1)$$

$$\sigma_{\text{eff}}(\omega, f_{\text{con}} \approx f_c) \propto \omega^x \quad (1.2)$$

$$\epsilon_{\text{eff}} \propto (f_c - f_{\text{con}})^{-s} \text{ for } f_{\text{con}} < f_c$$

or

$$\varepsilon_{\text{eff}} \propto \left( \frac{\sigma_{\text{con}}}{\sigma_d} \right)^{-s} \text{ for } f_{\text{con}} < f_c \quad (1.3)$$

$$\sigma_{\text{eff}} \propto (f_c - f_{\text{con}})^{-s'} \text{ for } f_{\text{con}} < f_c \quad (1.4)$$

$$\sigma_{\text{eff}} \propto (f_{\text{con}} - f_c)^t \text{ for } f_c < f_{\text{con}}, \quad (1.5)$$

where  $f_{\text{con}}$  is the volume fraction of conductor in the composite,  $\omega$  is the frequency of applied ac signal,  $x$  and  $y$  are the critical exponents, and they are expected to satisfy the relation;  $x + y = 1$ . ‘ $s$ ’ is the dielectric exponent in the insulator region, while ‘ $s$ ’ and ‘ $t$ ’ are the conductivity exponents in the insulator and conductor region, respectively.  $\sigma_{\text{con}}$  and  $\sigma_d$  are the conductivity of the conductor and insulator, respectively. According to the percolation theory, the values of the critical exponents are only sample dimension dependent and are independent of other factors. The ideal  $f_c$  value for three-dimensional (3D) ICC is  $f_{\text{con}} = 0.16$ . The 3D universal values of the various exponents are given by;  $s = 0.7-1$ ,  $s' = 0.7-1$  and  $t = 1.6-2$ . According to the intercluster polarization model and anomalous diffusion model, the 3D universal values of critical exponents are  $x = 0.72$ ,  $y = 0.28$ , and  $x = 0.58$  and  $y = 0.42$ , respectively. In general, the percolation theory is used for explaining the observed effects, though often the obtained experimental data do not always agree well with the theoretical predictions, which indicates the role of structural peculiarities, such as the microstructure and the process conditions on the percolative characteristics. In the study of this PCC, particularly, ferroelectric or electrostrictive polymers, like polyvinylidene fluoride (PVDF), poly[(vinylidene fluoride)-co-trifluoroethylene] [P(VDF-TrFE)], polytetrafluoroethylene (PTFE), etc. (because of their higher dielectric constants as compared to normal polymers), with a variety of conductive fillers are under rapid development and large changes in  $\varepsilon_{\text{eff}}$  have also been reported in the neighborhood of  $f_c$  [31–63]. In particular, the PMC is the potential candidate for testing the theories based on the percolative approach. The dielectric relaxation behavior and the electrical properties of PCC are also interesting and have been presented experimentally across  $f_c$  to find out the consistency of the relaxation phenomenon and its universalization [64–66].

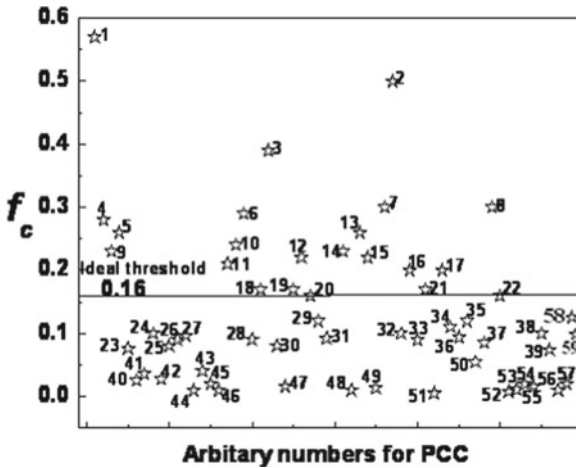
The polymer magnetic composites, in dispersing ferromagnetic and magnetostrictive materials, such as iron, nickel, and cobalt-nickel into polymer matrices, show interesting applications, such as electromagnetic interference shielding [67, 68], polymer magnetoelectrics [69–72], the magnetic percolation threshold [71–74], and other physical properties, e.g., viscoelasticity. The polymer composites showing multiferroic, viscoelastic properties, and non-presence of magnetic percolation threshold and electrical percolation threshold also have been included in this book.

## 1.1 Review of Scientific Literature

According to the percolation theory for continuum percolation systems in 3D, the ideal  $f_c$  value is  $f_{con} = 0.16$ , and the 3D ideal values of critical exponents are given by  $s = 0.7-1$ ,  $s' = 0.7-1$ , and  $t = 1.6-2$ . However, a meticulous literature survey done on ICC/PCC/PMC shows the scattered values of  $f_c$  observed experimentally in various systems as demonstrated in Fig. 1.1. Similarly, it is also observed that the values of critical exponents in the various experimental systems are largely deviating from their respective universal values. The detailed literature survey (Fig. 1.1) on PCC shows that a large number of systems comprising polymer/carbon black or carbon nanotube (multiwalled/single-walled) composites (points numbered from 40 to 57 in Fig. 1.1) give a very low value of  $f_c$ , i.e.,  $f_{con} < 0.01$ , as the conducting path in PCC is formed at very lower  $f_{con}$  due to the higher aspect ratio of the fillers. The value of scaling exponents is also found to be smaller than their respective universal values in the case of PCC having carbon nanotubes as fillers and has been attributed to the aspect ratio of the fillers. Similarly, the observation is that there are a large number of PCC systems based on carbon black and metal fillers (points numbered from 1 to 17 in Fig. 1.1), which show a higher value of  $f_c$ , and critical exponents are also found to be very high as compared to their respective universal values.

Very few reports are seen in the literature in which the experimental  $f_c$  matches with the ideal theoretical  $f_c$ . For example, although several studies show deviations from the percolation theories, interestingly the systems numbered (Fig. 1.1) as 18. PVDF/LNO, 19. PVDF/Ni, 20. Butadiene rubber/CB, 21. Butadiene rubber/CB, 22. PVDF/Ni show ideal percolative behavior. PVDF/Ni composites (points numbered 19 and 22 in Fig. 1.1) show ideal percolative behavior with  $f_c$  of 0.16–0.17 which is in agreement with the theoretically predicted value for continuum percolation systems. From Fig. 1.1, it is amply clear the scatter is quite significant though the origin for this discrepancy is still debated in PCC. The literature survey also indicates that the extent of enhancement of  $\epsilon_{eff}$  and  $\tan \delta$  at  $f_c$  in the case of this different PCC is different. The observation of an extraordinary increase of  $\epsilon_{eff} \sim 400$  with low  $\tan \delta < 0.1$  at 100 Hz and true percolative nature in PVDF/Ni composites is interesting to be investigated.

Experimental work reported in the literature also shows that as the filler concentration approaches the  $f_c$  from below, a dramatic change in  $\sigma_{eff}$  and  $\epsilon_{eff}$  occurs. In addition, above  $f_c$ , the  $\sigma_{eff}$  continues to increase before saturating, while the  $\epsilon_{eff}$  is theoretically predicted to decrease just as dramatically as it is increased. However, experimentally the  $\epsilon_{eff}$  sometimes continues to increase above  $f_c$ , although less dramatically than below it. These observations point toward the question, whether there is a problem with the sample preparation or with the theory itself (Is percolation theory correct or something is lacking in the model?). The literature also indicates that higher values of critical exponents have been observed for continuum percolation systems. These investigations suggest that the dielectric behavior of the composites depends on the physical properties of the constituents, preparation method, adhesiveness, interactions between fillers and polymer, as well as the size and shape of



1. PVDF/Ni 2. PTFE/LSCO 3. Polymer/CB 4. PVDF/Ni 5. (PVDF TrFE-CTFE)/PANI 6. PA/Fe 7. PTFE/LSCO 8. LDPE/CF 9. PVDF/n-QC 10. POM/Fe 11. PE/Fe 12. Butadiene rubber/CB 13. PVDF/Ni 14. PVDF/BaTiO<sub>3</sub>-Ni 15. Epoxy/Ag 16. PVDF/LNO 17. LDPE/CF, LDPE/Cu, LDPE/Ni 18. PVDF/LNO 19. PVDF/Ni 20. Butadiene rubber/CB 21. Butadiene rubber/CB 22. PVDF/Ni 23. Cellulose acetate/Magnetite 24. Epoxy/CB 25. Epoxy/CB 26. LDPE/Al 27. LLDPE/Al 28. PE/POM-Fe 29. Butadiene rubber/CB 30. PVDF/MWNT 31. PVC/Cabon 32. PVDF/LNO 33. PVDF/LNO 34. Epoxy/Ag 35. Polystyrene/polypyrrole 36. PVDF/SSF 37. PMMA/BaTiO<sub>3</sub>-Ni 38. PMMA/Ag 39. PVDF/CF 40. Cellulose acetate/Magnetite 41. Epoxy/CB 42. Epoxy/CB 43. LDPE/MWNT 44. Epoxy/Ag 45. LDPE/MWNT 46. PVDF/Exfoliated graphite 47. PVDF/MWNT 48. LDPE/MWNT 49. PVDF/CB 50. PMMA/BaTiO<sub>3</sub>-Ni 51. PVDF/Bi<sub>2</sub>S<sub>3</sub> 52. PVDF/MWNT 53. PVDF/MWNT 54. PVDF/MWNT 55. PVDF/MWNT 56. PVDF/BaTiO<sub>3</sub>-MWNT 57. PVDF/MWNT 58. Polyimide/Ag 59. PVDF/PCMO.

**Fig. 1.1** Experimental values of  $f_c$  for various PCC systems corresponding to the labeled numbers and the labeled numbers are given with the systems/samples studied [1–74]

the fillers. Therefore, the compositions near  $f_c$  are of fundamental interest, as they become a testing bed for various percolation mechanisms formulated from theoretical investigations. Hence, the origin of enhancement of  $\epsilon_{\text{eff}}$  and the origin of deviation of  $f_c$  value from its ideal value are some of the issues that need to be investigated. The observed critical exponents which are higher than that of the universal values have been tentatively explained based on various models, such as the random void model/the Swiss cheese model and the inverted Swiss cheese model, the position space renormalization group approximation model, and the transfer matrix method. No clear understanding of the origin of higher values observed and the extent of deviation of the critical exponents ( $s, s', t$ ) from their respective universal values (i.e., the quantification of the increment in terms of any experimentally measurable physical parameter) is found in literature till date. Hence, the quantification of the deviation of scaling exponents from their respective universal values in terms of an experimentally measurable physical parameter can provide a very clear understanding of this controversial and presently well-debated problem.

The above discussion is mainly focused on filler concentration dependencies. However, for practical reasons, it would be appropriate to be able to extract information on the homogeneity of a composite from a single measurement on a sample. In principle, such a procedure may be possible using frequency analysis. Therefore, investigation of dielectric relaxation behavior and the electrical properties of this PCC across  $f_c$  is of significant importance. Although the percolation behavior and studies on critical phase transition have been explored in the varieties of ICC and PCC described in Fig. 1.1, no systematic study on dielectric relaxation behavior and the electrical properties of this PCC across  $f_c$  is reported experimentally in a coherent way to date in this PCC. Although significant theoretical research work has been carried out on dielectric relaxation behavior, very few experimental investigations are reported. Almond et al. [65] and Calame et al. [66] have proposed a phenomenological model based on a random resistor (R)-capacitor (C) network and explained theoretically the power-law dispersions in permittivity and dielectric loss for ICC. This response was portrayed universally by the Cole–Davidson response function [64] for the composites with  $f_{\text{con}} \geq f_c$ , but very few experimental reports deal with these issues.

In addition to these, various composites are based on electrostrictive and magnetostrictive components, such as Ni/PZT/Ni, Fe/PZT/Fe, PVDF/Terfenol-D/PZT, BaTiO<sub>3</sub>/Ni, and BaTiO<sub>3</sub>/Co show magnetoelectric effects. PVDF is a semicrystalline thermoplastic having a remarkable high piezoelectric coefficient, excellent thermal stability, and chemical resistance compared with other polymers. Consequently, PVDF and its copolymers find widespread industrial applications in transducers, transistors, and capacitors. Moreover, PVDF is an attractive polymer matrix for micro and nanocomposites with superior mechanical and electrical properties. Since PVDF is a piezoelectric material, the magnetoelectric effect in PMC based on it is reported. The concept of magnetic percolation and the magnetic anomaly behavior is also reported for magnetic metal-insulator (polymer) composites at  $f_c$ . The viscoelastic properties of this PMC are also interesting and are placed in this book. A typical case of non-percolative composites is also interesting to be placed in this book.

## 1.2 Scope of the Book

The salient features of the book are

1. The microstructure of the polymer composites and the effect of various factors on their microstructure.
2. The scaling behavior, the origin of non-universality of scaling exponents, and the extent of enhancement of the electrical properties of the polymer composites.
3. The universal dielectric relaxation behavior across  $f_c$  in PCC and the evidence of the interesting third kind of Jonscher's like universal dielectric response.

4. The relationship between the microstructure and electrical properties through the various complex impedance spectroscopic techniques.
5. The magnetic, multiferroic, and rheological properties of the polymer composites.
6. Understanding the microstructure and electrical properties of the non-percolative polymer composites also.
7. Importance of ferroelectric polymer dielectrics as emerging materials of future for energy storage applications.

### 1.3 Organization of the Book

The book has been divided into ten chapters in the following way. In this chapter provides a general introduction, the work done in this area of research of percolative polymer composites as polymer dielectrics. Chapter 2 describes the basic physical properties of these composite dielectrics along with their fundamental concepts and the different models along with the spectroscopic techniques to understand the behavior of these dielectrics. The detailed theoretical background of complex spectroscopic techniques, such as; impedance spectroscopy, dielectric spectroscopy, and conductivity spectroscopy, is also included in this chapter. Chapter 3 deals with the details of the sample preparation along with their characterization by various commercial instruments and their utility also. Chapter 4 emphasizes the percolative behavior of polymer composites, prepared under various processing conditions with different fillers, as well as with varying particle sizes and shapes. Chapter 5 focuses on rigorous analysis of frequency dependence of electrical properties to unravel their origin of the extent of enhancement at their respective  $f_c$  and their non-universal scaling behavior. The interesting frequency-dependent scaling behavior of them is also included in Chap. 5. Chapter 6 deals with the study of the dielectric relaxation behavior of PCC and its quantification in terms of the dielectric relaxation exponents across  $f_c$  as a function of  $f_{con}$  and the existence of the third kind of universal dielectric relaxation phenomena. Chapter 7 deals with the correlation between microstructure and electrical properties of the PCC. Chapter 8 describes the study of the magnetic, multiferroic, and rheological behavior of the polymer composites. Chapter 9 introduces the flavor of electrical and dielectric properties of non-percolative polymer-ceramic composites. Chapter 10 gives the overall importance of ferroelectric polymer dielectrics and their emergence as future electrostatic energy storage materials.

### References

1. Feynman RP (1960) There's plenty of room at the bottom. Eng Sci 23:22–36
2. Detz AGH (1969) Composite engineering laminate. MIT Press, Cambridge
3. Chung DDL (2006) Composite materials: Science and applications. Springer, London

4. Chawla KK (2006) *Composite materials: Science and engineering*. Springer, London
5. Suchetelene JV (1972) Product properties: a new application of composite materials. *Philips Res Rep* 27:28–37
6. Zhang QM, Li H, Poh M, Xia F, Cheng ZY, Xu H, Huang C (2002) An all-organic composite actuator material with a high dielectric constant. *Nature* 419:284–287
7. Facchetti A, Yoon MH, Marks TJ (2005) Gate dielectrics for organic field-effect transistors: new opportunities for organic electronics. *Adv Mater* 17:1705–1725
8. Chu B, Zhou X, Ren K, Neese B, Lin M, Wang Q, Bauer F, Zhang QM (2006) A dielectric polymer with high electric energy density and fast discharge speed. *Science* 313:334–336
9. Rao Y, Ogitani S, Kohl P, Wong CP (2002) Novel ultra-high dielectric constant polymer based composite for embedded capacitor application. *J Appl Polym Sci* 83:1084–1090
10. Dang ZM (2018) *Dielectric polymer materials for high-density energy storage*. William Andrew, Elsevier, Amsterdam
11. Jawaid M, Khan MM (2018) *Polymer-based nanocomposites for energy and environmental applications*. Wood Head Publishing, Elsevier, Amsterdam
12. Tiwari A, Valyukh S (2014) *Advanced energy materials*. Wiley, Hoboken, New Jersey
13. Panda M (2010) *Scaling and relaxation behavior of polymer-metal composites across the percolation threshold*. Ph.D. thesis., Indian Institute of Technology Kharagpur.
14. Ray SS, Bousmina M (2006) *Polymer nanocomposites, and their applications*. American Scientific Publishers, Valencia, California
15. Mai YW, Tjong SC (2010) *Physical properties and applications of polymer nanocomposites*. Wood Head Publishing, Elsevier, Amsterdam
16. Panda M, Trivedi A (2020) Ferroelectric and piezoelectric properties of cold pressed Polyvinylidene fluoride/barium titanate Nano-composites. *Ferroelectrics* 572(1):236
17. Panda M (2022) Filler dependent microstructural and optical properties of PVDF/PEG blends versus PVDF/GO nanocomposites. *Opt Quant Electron* 54:765
18. Panda M, Sultana N, Singh AK (2022) Structural and optical properties of PVDF/GO nanocomposites. *Fuller Nano Tube Carbon Nanostruct* 30:559–570
19. Shivangi B, Panda M (2021) A spectroscopic ellipsometric study of PVDF/PEG polymer blends. *DAE SSPS-2021* 55:103–104
20. Panda M (2021) Ferroelectric, piezoelectric and dielectric properties of novel polymer nanocomposites. In: *Multifunctional ferroelectric materials*. Intech Open Publishing, Intechopen, London. <https://doi.org/10.5772/intechopen.96593>. ISBN: 978-1-83968-992-5
21. Stauffer D, Aharony A (1992) *Introduction to percolation theory*. Taylor, and Francis, London
22. Sahimi M (1994) *Applications of percolation theory*. Taylor and Francis, London
23. Nan CW (1993) *Physics of inhomogeneous inorganic materials*. *Prog Mater Sci* 37:1–12
24. Zallen R (1983) *The physics of amorphous solids*. Wiley, New York
25. Nan CW, Shen Y, Ma J (2010) Physical properties of composites near percolation. *Annu Rev Mater Res* 40:131–151
26. Shante VKS, Kirkpatrick S (1971) An introduction to percolation theory. *Adv Phys* 20:325–357
27. Sahimi M (1993) Flow phenomena in rocks: from continuum models to fractals, percolation, cellular automata, and simulated annealing. *Rev Mod Phys* 65:1393–1534
28. Kirkpatrick S (1974) Percolation and conduction. *Rev Mod Phys* 45:574–588
29. Essam JW (1980) Percolation theory. *Rep Prog Phys* 43:833–911
30. Nalwa HS (1995) *Ferroelectric polymers*. Marcel Dekkar, New York
31. Zhang QM, Bharti V, Zhao X (1998) Giant electrostriction and relaxor ferroelectric behavior in electron irradiated poly(vinylidene fluoride-trifluoro ethylene) copolymer. *Science* 280:2101–2104
32. Panda M, Srinivas V, Thakur AK (2015) Non-universal scaling behavior of polymer-metal composites across the percolation threshold. *Results in Physics* 5:136–141
33. Panda M (2019) Frequency-dependent scaling behavior of polyvinylidene fluoride/metal composites. *J. of Adv Dielect* 09:19500101–19500106
34. Yan W, Minggang Y, Rong M, Yuan Q, Yang D, Cui B, Chunrui M, Ming L, Dengwei H (2020) Design strategy of barium titanate/polyvinylidene fluoride-based nanocomposite films for high energy storage. *J Mater Chem A* 8:884–917

35. Panda M, Srinivas V, Thakur AK (2008) On the question of percolation threshold in polyvinylidene fluoride/nanocrystalline nickel composites. *Appl Phys Lett* 92:132905–132907
36. Panda M, Srinivas V, Thakur AK (2008) Surface and interfacial effect of filler particle on electrical properties of polyvinylidene fluoride/nickel composites. *Appl Phys Lett* 93:242908–242910
37. Panda M (2022) Tuned dielectric and percolation behavior of cold pressed polyvinylidene fluoride nanocomposites caused by Ni and BaTiO<sub>3</sub> filler. *Indian J Phys* 96:1699–1703
38. Panda M, Srinivas V, Thakur AK (2014) Percolation behaviour of polymer-metal composites on modification of filler. *Modern Phys Lett B* 28:1450055
39. Panda M (2018) Evidence of a third kind of Jonscher's like universal dielectric response. *J Adv Dielectr* 08:1850028
40. Huang C, Zhang Q (2004) Enhanced dielectric and electromechanical responses in high dielectric constant all-polymer percolative composites. *Adv Func Mater* 14:501–506
41. He F, Lau S, Chan HL, Fan J (2009) High dielectric permittivity and low percolation threshold in nanocomposites based on poly(vinylidene fluoride) and exfoliated graphite nanoplates. *Adv Mater* 21:710–715
42. Huang XY, Jiang PK, Kim CU (2007) Electrical properties of polyethylene/aluminum nanocomposites. *J Appl Phys* 102:1241031–1241038
43. Gonon P, Boudefel A (2006) Electrical properties of epoxy/silver nanocomposites. *J Appl Phys* 99:0243081–0243088
44. Huang C, Zhang QM, Su J (2003) High-dielectric-constant all-polymer percolative composites. *Appl Phys Lett* 82:35021–35023
45. Bauer F, Fousson E, Zhang QM (2006) Recent advances in highly electrostrictive P(VDF-TrFE-CFE) terpolymers. *IEEE Trans Dielectr Electr Insul* 13:1149–1154
46. Panda M, Mishra A, Shukla P (2019) Effective enhancement of dielectric properties in cold pressed polyvinylidene fluoride/barium titanate nanocomposites. *SN Appl Sci* 01:230–236
47. Panda M (2017) Major role of process conditions in tuning the percolation behavior of polyvinylidene fluoride-based polymer/metal composites. *Appl Phys Lett* 111:0829011–0829015
48. Panda M, Srinivas V, Thakur AK (2014) Universal microstructure and conductivity relaxation of polymer-conductor composites across the percolation threshold. *Curr Appl Phys* 14:1596–1601
49. Panda M, Srinivas V, Thakur AK (2014) Dielectric spectroscopy of polymer-metal composites across the percolation threshold. *J Adv Dielectr* 04:14500271–14500276
50. Panda M, Srinivas V, Thakur AK (2011) Role of polymer matrix in large enhancement of dielectric constant in polymer-metal composites. *Appl Phys Lett* 99:0429051–0429053
51. Prateek, Thakur VK, Gupta RK (2016) Recent progress on ferroelectric polymer-based nanocomposites for high energy density capacitors: synthesis, dielectric properties, and future aspects. *Chem Rev* 116(7):4260–4317
52. Chen Q, Shen Y, Zhang S, Zhang QM (2015) Polymer-based dielectrics with high energy storage density. *Annu Rev Mater Res* 45:433–458
53. Li Q, Chen L, Gadinski MR, Zhang S, Zhang G, Li HU, Iagodkine E, Haque A, Chen LQ, Jackson TN, Wang Q (2015) Flexible high-temperature dielectric materials from polymer nanocomposites. *Nature* 523:576–579
54. Li Q, Yao FZ, Liu Y, Zhang G, Wang H, Wang Q (2018) High-temperature dielectric materials for electrical energy storage. *Annu Rev Mater Res* 48:219–243
55. Panda M, Thakur AK, Srinivas V (2010) Thermal effects on the percolation behavior of polyvinylidene fluoride/nickel composites. *J Appl Polym Sci* 117:3023–3029
56. Dang ZM, Lin YH, Nan CW (2003) Novel ferroelectric polymer composites with high dielectric constants. *Adv Mater* 15:1625–1629
57. Zhang X, Jhiang J, Shen Z, Dan Z, Li M, Lin Y, Nan CW, Chen L, Shen Y (2018) Polymer nanocomposites with ultrahigh energy density and high discharge efficiency by modulating their nanostructures in three dimensions. *Adv Mater* 30:1707269
58. Bouharras FE, Raihane M, Ameduri B (2020) Recent progress on core-shell structured BaTiO<sub>3</sub>@polymer/fluorinated polymers nanocomposites for high energy storage: synthesis, dielectric properties and applications. *Prog Mat Sci* 113:100670

59. Xu JJ, Fu C, Chu H, Wu X, Tan Z, Qian J, Li W, Song Z, Ran X, Nie W (2020) Enhanced energy density of PVDF-based nanocomposites via a core-shell strategy. *Sci Rep* 10:17084
60. Yuan C, Zhou Y, Zhu Y, Liang J, Wang S, Peng S, Li Y, Cheng S, Yang M, Jun H, Zhang B, Zeng R, He J (2020) Polymer/molecular semiconductor all-organic composites for high-temperature dielectric energy storage. *Nat Commun* 11:3919
61. Yao Z, Song ZH, Hua Y, Zhiyong C, Minghe Z, Shujun L, Michael T, Liu H (2017) Homogeneous/inhomogeneous-structured dielectrics and their energy-storage performances. *Adv Mater* 29:1601727
62. Huang X, Jhiang P (2014) Core-Shell structured high k polymer nanocomposites for energy storage and dielectric applications. *Adv Mater* 27:546–554
63. Venketesh C, Srinivas V, Panda M, Rao VV (2010) Dielectric response in novel polyvinylidene fluoride/nanoquasicrystalline composites. *Sol Stat Comm* 150:893–896
64. Davidson DW, Cole RH (1951) Dielectric relaxation in glycerol, propylene glycol, and n propanol. *J Chem Phys* 19:1484–1490
65. Almond DP, Bowen CR (2004) Anomalous power law dispersions in ac conductivity and permittivity shown to be characteristics of micro-structural electrical networks. *Phys Rev Lett* 92:1576011–1576014
66. Calame JP (2003) Evolution of Davidson-Cole relaxation behavior in random conductor-insulator composites. *J Appl Phys* 94:5945–5957
67. Maxwell JC (1892) *A treatise on electricity and magnetism*. Dover, New York
68. Sihvola AHH (1999) *Electromagnetic mixing formulas and applications*. IEEE, London
69. Nan CW, Bichurin MI, Dong S, Viehland D, Srinivasan G (2008) Multiferroic magnetoelectric composites: historical perspective, status, and future directions. *J Appl Phys* 103:031101–031135
70. Fiebig M (2005) Revival of the magneto-electric effect. *J Phys D: Appl Phys* 38:R123
71. Stephen MJ (1981) Magnetic susceptibility of percolating clusters. *Phys Lett A* 87:67–68
72. Kalinin YE, Sitnikov AV, Skryabina NE, Spivak LV, Artem AA, Shadrin A (2004) Barkhausen effect and percolation threshold in metal-dielectric nanocomposites. *J Mag Magn Mat* E893:272–276
73. Guo Z, Park S, Hahn HT, Wei S, Moldovan M, Karki AB, Young DP (2007) Magnetic and electromagnetic evaluation of the magnetic nanoparticle filled polyurethane nanocomposites. *J Appl Phys* 101(09M):511
74. Shekhar S, Sajitha EP, Prasad V, Subramanyam SV (2008) High coercivity below percolation threshold in polymer nanocomposite. *J Appl Phys* 104:0839101–0839104

# Chapter 2

## Fundamentals of the Models and Spectroscopic Techniques



This chapter deals with the fundamental concepts of connectivity and the working of polymer composites along with the important theoretical models, which are used to describe the percolation and scaling behavior of PCC and also the non-percolative systems. The complex spectroscopies, such as dielectric spectroscopy, impedance spectroscopy, and conductivity spectroscopy, are also explained in detail to provide an understanding of the electrical parameters of these inhomogeneous and disordered materials.

### 2.1 Introduction

The word composite has come from the Latin word “compositus: com-component, ponere-to place” which means made up of distinct parts or elements. Composite materials are obtained by the artificial combination of two or more different materials to get innovative and effective properties as output, which is absent in the individual components. These multiphase materials are not formed through naturally/any reactions/phase transformations/other phenomenon, etc. In other words, a composite material, although, appears as a single structure but has identifiable interfaces among the two or more components, which are present in them. The properties of the composites are strongly influenced by the properties of their constituent materials, their distribution, and the interaction among them. The composite properties may be due to the amount of the components, due to the sum effect, or may be due to the specific combination among the components due to the combination properties. Also some times in a composite, the output is an interesting property due to the transfer of properties among the components, i.e., the product properties. The geometry (shape, size, and size distribution), orientation, and concentration of the reinforcing agent also affect the properties of these composites to a great extent as the interfacial area determines the extent of the interaction between the components.

Although the research on composites dates back 60–70 years and many theoretical approximation models for different situations have been developed to understand the experimental results, the models are undergoing modification even now. Among these models, the most important are effective medium theory (EMT) or effective medium approximation (EMA) [1–10] and the percolation theory [11–13]. Although EMT has attracted the most attention, due to certain limitations of it in the case of 3D samples, percolation theory has been developed. Before going to the detailed descriptions of the models, it would be useful to discuss some of the fundamental concepts in the case of composites.

## 2.2 Fundamental Concepts

### 2.2.1 Concept of Connectivity

On the basis of the concept of connectivity introduced by Newnham et al. [14], in the 3D space there are ten possible connectivities for a diphasic composite such as (a) 0–0, (b) 1–0, (c) 2–0, (d) 3–0, (e) 1–1, (f) 2–1, (g) 3–1, (h) 2–2, (i) 3–2, and (j) 3–3. Imagine an epoxy matrix in which small particles of other materials are dispersed so that they don't touch each other. This is an example of 3–0 connectivity, because one of the phases, namely epoxy, is self-connected in all three dimensions, whereas the other phase (comprising of the dispersed particles) is not self-connected in any dimension or direction. Similarly, for a 2–1 connectivity pattern, one phase is self-connected in two-dimensional layers; the other is self-connected in one-dimensional chains or fibers. In this way, the other connectivities can be understood [14].

### 2.2.2 How Composites Work?

A composite works based on the following three types of properties: (1) sum properties, (2) product properties [15], and (3) combination properties. A “sum property” of a composite is a weighted sum of the contributions from the individual component phases, and it is proportional to the volume or weight fractions of these phases in the composite. Physical quantities like density and resistivity are sum properties. A more interesting result of a composite structure is the product property, which is reflected in the composite structure but is absent in the individual phases. In a biphasic composite material, if one phase exhibits a property  $A \rightarrow B$  (application of an independent variable  $A$  resulting in an effect  $B$ ) with a proportionality tensor  $dB/dA = X$  (may be a constant or dependent on  $A$  or  $B$ ) and the second phase exhibits a property  $B \rightarrow C$  with a proportionality tensor  $dC/dB = Y$ , then the composite will exhibit a property  $A \rightarrow C$  which is absent in either of the initial phases. The property  $A \rightarrow C$  is called a “product property” of the composite. The proportionality tensor

$dC/dA$  is the product of the proportionality tensor of the two individual phases, i.e.,  $dC/dA = (dC/dB)(dB/dA) = Y * X$ .

In certain cases, the averaged value of the output shows the optimized result for a particular combination between the two components and will exhibit a maximum at an intermediate ratio of the phases. This is called a “combination property”. Depending on the application, the appropriate properties of the individual phases can be invoked to design a composite to yield the requisite effect for the desired application.

## 2.3 Theoretical Models

To understand the physical properties of the composites [the properties of the composites which are usually considered are effective conductivity ( $\sigma_{\text{eff}}$ ) or effective dielectric constant ( $\epsilon_{\text{eff}}$ )] made up of various components of different dielectric constants and conductivities, there are various models which are used to understand the physics and in the evaluation of their physical parameters. These parameters are interchangeable in the formulas in a whole range of models due to the wide applicability of Laplace’s equation. The problems that fall outside of this class are mainly in the field of elasticity and hydrodynamics, due to the higher-order tensorial character of the effective medium constants. A discussion about the  $\sigma_{\text{eff}}$  and  $\epsilon_{\text{eff}}$  of the composites is required.

Various models used to describe the  $\epsilon_{\text{eff}}$  and  $\sigma_{\text{eff}}$  of a composite are (i) EMA or EMT and (ii) scaling/percolation theory.

### 2.3.1 *Effective Medium Approximations*

Effective medium approximations (EMA) are physical models that describe the macroscopic properties of a medium ( $\epsilon_{\text{eff}}$  and  $\sigma_{\text{eff}}$ ) based on the properties and the relative fractions of its components. They can be discrete models such as applied to resistor networks or continuum theories as applied to elasticity or viscosity but most of the current theories have difficulty in describing percolating systems. There are many different effective medium approximations, each of them being more or less accurate in distinct and separate situations. Nevertheless, they all assume that the macroscopic system is homogeneous and typical of all mean-field theories, and they fail to predict the properties of a multiphase medium close to the  $f_c$  due to the absence of long-range correlations or critical fluctuations in the theory. Some of the important EMA for linear composites (i.e., linear relationship between fields and current densities exist) are Maxwell–Garnett approximations or mixture rule [16], Yamada [7], Landauer [17] and Bruggeman’s approximations [2], etc., which have been the basis for a vast number of studies of macroscopically inhomogeneous media

to deal, and they have been generalized by numerous authors to treat in a wide variety of problems.

In general, in the case of Maxwell-Garnett EMA, the conditions under which this approximation is expected to be valid are (a) volume fraction of the embedded material is very low as compared to the matrix (may be an insulating ceramic or polymer matrix) and (b) the domains of the embedded materials are spatially separated. Under this approximation, the  $\epsilon_{\text{eff}}$  of the composite made up of more than two components consisting of matrix and inclusions has been dealt, and it was found that this explains very few systems to match with the experimental results.

Under the earlier simplified assumptions, the experimental values of physical parameters did not match with the theoretical values, and it was found that the assumptions in obtaining the effective response from a medium in the previous cases needed to be taken care of. Hence, Bruggeman considered the shape of the filler particles to be elliptical or ellipsoidal and increased the predictive capability of EMA. Although Bruggeman EMA dates back to 1935, still the prediction of  $f_c$  for 2D samples in the case of percolation systems matches well with the experimental results.

In Landauer's assumptions, a theory for a random mixture is given based on the assumption that each crystal acts as if surrounded by a homogeneous medium whose properties are those of the mixture, and under these assumptions, some experimental results match with the theoretically predicted values.

In the case of Bruggeman's approximations for 3D Percolating systems, the EMA is of particular interest in two special cases. One is the limit for one component is of zero conductivity and the other is of finite conductivity. This corresponds to a metal-insulator composite. The other limit is one component is of finite conductivity and another one is of infinite conductivity corresponding to a composite of normal metal and perfect conductor. (not to say "superconductor" because the magnetic properties of component 1 are unspecified). In these cases,  $\sigma_{\text{eff}}$  is predicted by the EMA to have singular properties near a percolation threshold ( $f_c$ ) at  $f_c \sim 1/3$  [1]. The special concentration  $f_c = 1/3$  has a natural physical interpretation: It is the "connectivity threshold", above which there is a connected path of material 1 extending throughout the sample. The EMA predicts  $f_c$  to be  $1/3$  for a 3D sample with approximately spherical grains. In general, in D dimensions and compact grains, it is found that the Bruggeman's EMA predicts  $f_c = 1/D$ .

It is often difficult to make a direct comparison between these predictions and experiments since real materials hardly ever perfectly satisfy the geometrical expectations of the EMA in its simplest form (symmetric arrangement of the two components in the form of compact, nearly spherical grains, with no short-range order). The results show that the EMA is in excellent agreement with the computer "experiment". In particular, the broad surface plasmon band predicted by the EMA is very similar to that found in the computer results, as a function of concentration. The main discrepancies arise near  $f_c$ . These are not surprising, since it is known that the EMA, being a mean-field approximation, must give incorrect power-law relations between  $\sigma_{\text{eff}}$  and  $f_c$ .

In the above discussions in the case of systems undergoing a drastic change in their physical properties, they cannot be described by the EMA. The main approximation in EMA is that all the domains are located in an equivalent mean field. Unfortunately, it is not the case close to the  $f_c$  in a composite where the system is governed by the largest cluster of conductors, which is a fractal, and long-range correlations are absent from Bruggeman's simple formula. The  $f_c$  values are in general not correctly predicted. It is 0.33 in the EMA, in 3D, far from the 0.16 expected from percolation theory [11–13] and observed in experiments. However, in two dimensions, the EMA gives a  $f_c$  of 0.50 and has been proven to model percolation relatively well. Hence to understand further the percolation, the percolation/scaling theory has been developed.

### 2.3.2 Percolation Theory

From the above discussion of EMA, it is found that the predicted  $f_c$  for metal-dielectric composites matches with the experimental value of  $f_c$  only in 2D. However, the predicted value of  $f_c$  by EMA fails to coincide with the experimental value of  $f_c$  in 3D. That is why the percolation theory for two-component composites is developed. According to percolation theory depending upon the critical occupation probability ( $p_c$ ) of one component in the matrix of another or depending upon the fraction of one component in the component of other matrices, the physical properties, such as conductivity and dielectric constant, undergo a drastic change in their values which is known as a percolative phase transition. According to the theory at the phase transition, there will be a divergence in the real part of  $\epsilon_{\text{eff}}$  (i.e., a singularity is observed) and the  $\sigma_{\text{eff}}$  undergoes a drastic change in their values. The  $f_c$  is a mathematical term related to the percolation theory, which is the formation of long-range connectivity in random systems. The  $f_c$  is the critical value of the occupation probability or fraction of conducting component, such that infinite connectivity (percolation) first occurs. In general, there exist different types of percolation, and it can be broadly divided into two types such as (i) lattice percolation and (ii) continuum percolation which is observed depending upon the  $p_c$  or  $f_c$  in the matrix of another, respectively.

- (i) **Lattice percolation:** The most common percolation model is to take a regular lattice, like a square lattice, and make it into a random network by randomly “occupying” sites (vertices) or bonds (edges) with a statistically independent probability  $p$ . At a critical threshold, i.e., at  $p_c$ , the long-range connectivity first appears, and this is called the percolation threshold. More general systems have several probabilities  $p_1, p_2$ , etc., and the transition is characterized by a critical surface or manifold. Again depending upon the occupancy either at the sites (vertices) or bonds (edges), the lattice percolation is of two types, such as (a) site percolation and (b) bond percolation.
- (a) **Site percolation:** If the percolation of infinite connectivity occurs at critical occupation probability and the occupancy is along with the sites or vertices of the crystal structure, then the percolation is called site percolation. The

site percolation threshold value varies largely from 0.80 to 0.4 depending upon the crystal lattice structure and on the dimensionality of the samples.

- (b) **Bond percolation:** Similarly if the percolation of infinite connectivity occurs at a critical occupation probability and the occupancy is only at the edges or bonds of the crystal structure, then the percolation is called bond percolation. One of the subclasses of bond percolation is the directed percolation where connectivity along a bond depends upon the direction of the flow. The value of the percolation threshold varies largely also from 0.74 to 0.39 depending upon the crystal lattice structure and on the dimensionality of the samples. The value also varies depending upon the random or quasilattices, such as 0.66 to 0.33.

Now depending upon the percolation probability, the scaling laws have been found in the critical region of the phase transition. The different scaling laws are given by  $\epsilon_{\text{eff}}$  and  $\sigma_{\text{eff}}$  that follow universal fractional power laws as a function of frequency in the vicinity of  $p_c$ , for both site percolation and bond percolated systems as given by

$$\epsilon_{\text{eff}}(\omega, p \approx p_c) \propto \omega^{-y} \quad (2.1)$$

And

$$\sigma_{\text{eff}}(\omega, p \approx p_c) \propto \omega^x, \quad (2.2)$$

where  $p$  is the probability of occupation,  $\omega$  is the frequency of applied AC signal,  $x$  and  $y$  are the critical exponents, and they are expected to satisfy the relations  $x + y = 1$  [18–34]. According to percolation theory, the power-law behavior of  $\epsilon_{\text{eff}}$  and  $\sigma_{\text{eff}}$  in the vicinity of  $p_c$  is given by

$$\epsilon_{\text{eff}} \propto (p_c - p)^{-s} \text{ for } p < p_c \quad (2.3)$$

and

$$\sigma_{\text{eff}} \propto (p_c - p)^{-s'} \text{ for } p < p_c \quad (2.4)$$

$$\sigma_{\text{eff}} \propto (p - p_c)^t \text{ for } p > p_c, \quad (2.5)$$

where ‘ $s$ ’ is the dielectric exponent in the insulator region and ‘ $s'$ ’ & ‘ $t$ ’ are the conductivity exponents in the insulator and conductor region, respectively. The value of critical  $p_c$  is very different for different kinds of systems depending on the type of lattices.

### (ii) Continuum percolation

One can also consider continuum systems, such as overlapping disks and spheres placed randomly, or the negative space (Swiss cheese models) where the percolation

is achieved due to relative change in the fraction of one component in the matrix of another. The fraction of the component at which the percolation transition occurs is called the critical percolation threshold ( $f_c$ ). Similarly, the value of  $f_c$  also varies largely in this case depending upon the shape, size of the fillers, and dimensionality of the samples. The value varies from 0.66 to 0.004 (Fig. 1.1). However, the predicted ideal  $f_c$  for 3D continuum systems in which all the ideal approximations are there is found to be 0.16. This ideal  $f_c$  value of 0.16 is rather a very special case as long as the conducting fillers used are with micron-scale and spherical shape. The different power laws which are governed by  $\varepsilon_{\text{eff}}$  and  $\sigma_{\text{eff}}$  to follow universal fractional power laws as a function of frequency in the vicinity of  $f_c$  are given by Eqs. (1.1)–(1.2) as

$$\varepsilon_{\text{eff}}(\omega, f_{\text{con}} \approx f_c) \propto \omega^{-y}; \quad \sigma_{\text{eff}}(\omega, f_{\text{con}} \approx f_c) \propto \omega^x,$$

where  $f_{\text{con}}$  is the volume fraction of conductor in the composite,  $\omega$  is the frequency of applied AC signal,  $x$  and  $y$  are the critical exponents, and they are expected to satisfy the relations  $x + y = 1$  [18–34]. According to percolation theory, the power-law behavior of  $\varepsilon_{\text{eff}}$  and  $\sigma_{\text{eff}}$  in the vicinity of  $f_c$  is given by Eqs. (1.3)–(1.5) as

$$\varepsilon_{\text{eff}} \propto (f_c - f_{\text{con}})^{-s} \text{ for } f_{\text{con}} < f_c; \quad \sigma_{\text{eff}} \propto (f_c - f_{\text{con}})^{-s'} \text{ for } f_{\text{con}} < f_c;$$

and

$$\sigma_{\text{eff}} \propto (f_{\text{con}} - f_c)^t \text{ for } f_c < f_{\text{con}},$$

where ‘ $s$ ’ is the dielectric exponent in the insulator region and ‘ $s'$ ’, ‘ $t$ ’ are the conductivity exponents in the insulator and conductor region, respectively.

According to the two different physical models, such as the intercluster polarization/resistor-capacitor (RC) model and the anomalous diffusion model, the 3D universal values of critical exponents are  $x = 0.72$ ,  $y = 0.28$ , and  $x = 0.58$ ,  $y = 0.42$ , respectively. According to the percolation theory in 3D, under the consideration of intercluster polarization model, the relations  $x = t/(s + t)$  and  $y = s/(s + t)$  are valid and the universal values of  $s$ ,  $s'$ , and  $t$  are given by  $s_{\text{un}} = s'_{\text{un}} = 0.7-1$  and  $t = 1.6-2.0$  [18–34]. Similarly under the anomalous diffusion model, as suggested by Gefen et al. [23, 24] that polarization effects occur only within finite clusters, and the values of exponents ‘ $x$ ’ and ‘ $y$ ’ are purely independent of the transport exponents ‘ $s$ ’ and ‘ $t$ ’. In this approximation, the values of ‘ $x$ ’ and ‘ $y$ ’ are purely a combination of the geometrical exponents ‘ $\nu$ ’ and ‘ $\eta$ ’. Under this approximation, the value of ‘ $s$ ’ in the usual scaling laws is replaced by  $s' = 2\nu - \eta$ . Under this approach, the exponent values of  $x$  and  $y$  are given by  $x = t/\nu(2 + \theta)$  and  $y = 2\nu - \eta/\nu(2 + \theta)$  where the exponent  $\theta$  is related to the electrical percolation in terms of diffusion and ‘ $s$ ’, ‘ $t$ ’ characterize the divergence of  $\varepsilon_{\text{eff}}$  and  $\sigma_{\text{eff}}$  in the vicinity of  $f_c$ . According to percolation theory, the values of the critical exponents are only dimensional dependent of the samples, i.e., whether the samples studied are of 2D, 3D, or others and are

independent of other factors. The 3D universal values of  $s$ ,  $s'$ , and  $t$  are given by  $s_{\text{un}} = s'_{\text{un}} = 0.7-1$  and  $t = 1.6-2.0$ . Similarly, the 2D universal values of the exponents are given by  $s_{\text{un}} = s'_{\text{un}} = t_{\text{un}} = 1.1-1.3$ , and the universal value of critical exponents for other dimensional samples also can be referred [11, 12]. This book has discussed the experimental results of only continuum percolative systems.

## 2.4 Spectroscopic Techniques

### 2.4.1 Dielectric Spectroscopy

To understand the dielectric behavior and other related phenomena (relaxation, dispersion, saturation, etc.) in a system, several formalisms have been developed. All these formalisms describe frequency response characteristics of dielectric properties of a system and provide valuable insight into the prevailing relaxation mechanism and the distribution of relaxation times due to dipolar interaction. The observed complex relative permittivity of a system is expressed as  $\varepsilon(\omega) = \varepsilon' - i\varepsilon''$ . Debye [35] was the first to propose a law for an ideal non-interacting dipolar system, e.g., a non-viscous fluid. He gave the simplest and most ubiquitous model for the dielectric response of a monodisperse system and established that the complex permittivity  $\varepsilon(\omega) = \varepsilon' - i\varepsilon''$  varies as

$$\varepsilon(\omega) = \varepsilon'_{\infty} + (\varepsilon_s - \varepsilon'_{\infty}) \frac{1}{1 + i\omega\tau}, \quad (2.6)$$

where  $\omega$  is the angular frequency and  $\varepsilon_s$  and  $\varepsilon'_{\infty}$  denote the static ( $\omega = 0$ ) permittivity and the limiting permittivity at high frequencies ( $\omega\tau \rightarrow \infty$ ) that depend on atomic and electronic polarizabilities, respectively. It is now well established that for monodisperse ideal systems having a single characteristic relaxation time ( $\tau$ ), the complex permittivity spectrum ( $\varepsilon'$  vs.  $\varepsilon''$  plot) exhibits a semicircle with the center on the  $\varepsilon'$  axis such that it intersects this axis at  $\varepsilon' = \varepsilon_s$  and  $\varepsilon' = \varepsilon'_{\infty}$ . This approach is intuitively attractive since Eq. (2.6) in the frequency domain gives an adequate description of the behavior of the orientational polarization for many dipolar systems. However, there are practical problems in implementing Eq. (2.6) due to inherent dipolar interactions and related complexity of the material due to the distribution of relaxation times. For a continuous distribution of relaxation times, there is a need to replace the factor  $1/1 + i\omega\tau \int_0^{\infty} \left[ \frac{g(\tau)}{1+i\omega\tau} \right] d\tau$  of Eq. (2.6), to ensure normalization  $\int_0^{\infty} g(\tau) d\tau = 1$ . However, the difficulty with this interpretation is that there is no independent way of confirming the form  $g(\tau)$  required for giving the desired fit to the experimental data. In addition, frequency-domain spectroscopy indicates that pure Debye response is virtually nonexistent in solids and is hardly ever seen in condensed matter. Debye dielectric spectra are the most elementary form of dielectric response for an independent non-interacting polarizing entity. They have

the identical time-independent probability of relaxation from the stressed condition, and hence for such systems, the ratio of imaginary to real part of permittivity is given by

$$\frac{\varepsilon''(\omega)}{\varepsilon'(\omega)} = \omega\tau \text{ for } \omega \gg \omega_p, \quad (2.7)$$

where  $\omega_p$  is the frequency corresponding to the loss peak position. It indicates that the loss would increase monotonously with frequency for frequencies greater than  $\omega_p$ , which is the characteristic of non-viscous liquids. In reality, the existence of non-viscous liquid type dielectric response is hardly ever seen in solids.

Subsequently, an alternative approach for dielectric relaxation (dipolar relaxation) was developed by Cole–Cole [36], Cole–Davidson [37], and Havriliak–Negami (H-N) [38] based on experimental observations on dispersion and absorption of a considerable number of liquids and solid dielectrics. To generalize the dipolar relaxation phenomena and the practical dielectric response of materials having a distribution of relaxation times, H-N gave a purely empirical expression as

$$\varepsilon(\omega) = \varepsilon'_\infty + (\varepsilon_s - \varepsilon'_\infty) \frac{1}{[1 + (i\omega\tau)^{1-\alpha}]^{1-\beta}}, \quad (2.8)$$

where it is assumed that the non-negative quantities  $\alpha$  and  $\beta$  gauge the symmetric and asymmetric broadenings of the dielectric loss spectrum, respectively. The empirical Cole–Cole and Davidson–Cole relations are seen to be the special case of Eq. (2.8) for  $0 \leq \alpha \leq 1$  with  $\beta = 0$ , and  $0 \leq \beta \leq 1$  with  $\alpha = 0$ , respectively. Although H-N Eq. (2.8) takes care of all types of heterogeneity present in a dipolar system, it was Jonscher [39], who proposed a new insight into the understanding of universal dielectric response (JUDR) in materials based on a systematic analysis of experimental results available in the literature. According to Jonscher, there are two fundamentally different types of polarization response under a steady electric field (in frequency as well as in time domain) depending on the nature of the polarizing species. They are

- (i) a strongly correlated dipolar system with dipolar species having a finite amount of charge displacement such that the dielectric response has a loss peak in the frequency spectrum due to the delayed response of the dipolar flipping with respect to the frequency of applied electric field and
- (ii) a strongly correlated charge carrier (ionic, electronic, or a semiconductor) system with hopping electrons or ionic charges such that an indefinite amount of charge carriers may be displaced leading to the steep dispersion at low frequencies referred to as “anomalous low-frequency dispersion (ALFD)”.

JUDR laws for both the dipolar and charge carrier-dominated solid systems provide rich physics associated with relaxation and charge transport phenomena. In the case of a broader dipolar response than the Debye-type feature, polydispersive response in the frequency domain is given by Jonscher’s two fractional power laws in

two distinct regions flanking the loss peak. They occur at a unique frequency called peak frequency ( $\omega_p$ ) expressed in different frequency ranges as

at low frequencies

$$\varepsilon_s - \varepsilon'(\omega) \propto \varepsilon(\omega) \propto \omega^m \text{ for } \omega \ll \omega_p \text{ with } 0 < m < 1 \quad (2.9a)$$

and at high frequencies

$$\varepsilon'(\omega) \propto \varepsilon(\omega) \propto \omega^{n-1} \text{ for } \omega \gg \omega_p \text{ with } 0 < n < 1 \quad (2.9b)$$

The combined form of the above two power laws can be represented as

$$\varepsilon''(\omega) = \frac{1}{(\omega/\omega_p)^{-m} + (\omega/\omega_p)^{1-n}} \quad (2.10)$$

in which the exponent's  $m$  and  $1 - n$  fall in the range  $[0, 1]$  and  $\omega_p$  is temperature dependent. The universal law for the dipolar systems showing a loss peak in their frequency spectrum may therefore be represented as

$$\frac{\varepsilon''(\omega)}{\varepsilon'(\omega)} = \cot(n\pi/2) = \text{const for } \omega \gg \omega_p \text{ with } 0 < n < 1. \quad (2.11)$$

The physics associated with this Eq. (2.11) is that the ratio of energy lost per reversal of macroscopic polarization to energy stored in every macroscopic polarization for  $\omega \gg \omega_p$  is constant and independent of frequency unlike that of the Debye behavior. If the value of 'n' lies between  $1/2 < n < 1$ , then the real part  $\varepsilon'(\omega)$  of the dielectric constant is higher than the imaginary part  $\varepsilon''(\omega)$  while if 'n' is in between  $0 < n < 1/2$ , the converse is true. In the special case of  $n = 1/2$ , the two components are equal. Because of this approach due to Jonscher, H-N Eq. (2.10) can be redefined as

$$\varepsilon = \varepsilon'_\infty + (\varepsilon_s - \varepsilon'_\infty) \frac{1}{[1 + (i\omega\tau)^m]^{(1-n)/m}}. \quad (2.12)$$

It provides useful physics from the approximation of the experimental data in terms of the correct asymptotic behavior in accordance with the Eqs. (2.11) and (2.12).

On the other hand, in the case of dielectric response for a charge carrier-dominated system, there is no dielectric loss peak. Instead, two clear regions with dielectric dispersion are the typical feature of the dielectric spectrum. A region with continuously rising loss toward low frequencies arising due to the long-range DC conductivity is the most striking feature. It is referred to as the anomalous low frequency dispersion (ALFD). Another is the high-frequency dispersive region above its critical frequency ( $\omega_c$ ), which  $\omega_c$  separates the DC and AC conductivity region in the material systems and the JUDR type response may again be expected to be valid as

in the case of dipolar systems thereby giving the same physical significance. In this case,  $\omega_c$  plays the same role as that of  $\omega_p$  in dipolar systems. Hence, JUDR for a charge carrier-dominated system may be expressed in different frequency regime as at low frequencies

$$\varepsilon'(\omega) \propto \varepsilon(\omega) \propto \omega^{-p} \text{ for } \omega \ll \omega_c \text{ with } 0 < p < 1 \quad (2.13a)$$

and at high frequencies

$$\varepsilon'(\omega) - \varepsilon'_\infty \propto \varepsilon(\omega) \propto \omega^{n-1} \text{ for } \omega \gg \omega_c \text{ with } 0 < n < 1 \quad (2.13b)$$

Now combining Eqs. (2.13a) and (2.13b), we get

$$\varepsilon''(\omega) = \frac{1}{(\omega/\omega_c)^p + (\omega/\omega_c)^{1-n}}. \quad (2.14)$$

The typical frequency dependence is now characterized by the two fractional exponents 'n' and 'p'. This is the dielectric response associated with a system dominating mobile charge carriers as the polarizing species. At low frequency, for ideal charge carrier systems, the exponent  $p$  is generally close to 1. A consequence of the high-frequency behavior of Eq. (2.13b) for the ALFD is that the ratio  $\frac{\varepsilon''(\omega)}{\varepsilon'(\omega)}$  is independent of frequency and is given by

$$\frac{\varepsilon''(\omega)}{\varepsilon'(\omega)} = \cot(n\pi/2) = \text{const for } \omega \gg \omega_c \text{ with } 0 < n < 1. \quad (2.15)$$

In this book, the validity and consequences of Eq. (2.11) and (2.15) in a wide variety of polymer–conductor composites (PCC) exhibiting insulator-to-metal transition (IMT) across  $f_c$  are discussed.

### 2.4.2 Impedance Spectroscopy

Complex impedance spectroscopy (CIS) is a very convenient and non-destructive powerful experimental technique which is used to investigate the microstructural and electrical properties of the ceramics/composites. This technique enables us to separate the real and imaginary components of the electrical parameters and hence provides a true picture of the material properties. Each representation can be used to highlight a particular aspect of the response of a sample. Impedance is a complex quantity that consists of a real part and an imaginary part, which are both a function of frequency. The main advantage of using impedance spectroscopy is that it can detect the rapidly changing electrical response in the samples. Impedance data of materials that have capacitive and resistive components, when represented in the Nyquist plot, lead to a succession of semicircles arising from the contribution of bulk,

grain boundary/interface between the components, and electrode-material interface, respectively. Generally, the semicircle corresponding to the electrode-material interface comes at low frequency for ionic conductors only. But in the case of dielectric ceramics and composites, the semicircles arise from the contribution of bulk, grain boundary/interface between composite components, respectively, at different frequency ranges. CIS enables the evaluation of the relaxation frequency of the material which is only an intrinsic property of the material independent of the geometrical factors of the samples. CIS can also be used to detect the percolation in PCC. To have a complete and clear understanding regarding the electrical behavior of any material, the simultaneous analysis of the frequency-dependent electrical properties of a material, such as the impedance ( $Z$ ), dielectric constant or relative permittivity ( $\epsilon$ ), electric modulus ( $M$ ), and admittance ( $Y$ )/AC conductivity ( $\sigma_{ac}$ ), is required which is possible through CIS. These electrical parameters can be related to one another as per the equivalent circuit model. The static dielectric constant is given by  $\epsilon = Cd/\epsilon_0 A$  where  $C$  is the capacitance of the pellet,  $d$  is the pellet thickness,  $A$  is the cross-sectional area of the pellet, and  $\epsilon_0$  is the permittivity of free space ( $8.854 \times 10^{-12}$  F/m), and the loss tangent is given by  $\tan \delta = \epsilon''/\epsilon' = M''/M' = Z'/Z'' = Y'/Y''$ , where (') and (") represent the real and imaginary parts of the corresponding physical quantities. For the case of an ideal R-C combination of the electrical network (Debye-type relaxation), the impedance is given by

$$Z(\omega) = Z' - jZ'' = R_\infty + \frac{R}{1 + j\omega RC}, \quad (2.16)$$

where  $R_\infty$  is the resistance at infinite frequency and  $\omega$  is the angular frequency. For non-Debye-type relaxation, the impedance should satisfy the Cole-Cole formalism which is given by

$$Z(\omega) = R_\infty + \frac{R}{1 + j(\omega RC)^{1-\alpha}}$$

or

$$Z(\omega) = R_\infty + \frac{R}{1 + j(\omega/\omega_0)^{1-\alpha}}, \quad (2.17)$$

where  $\omega_0 = 1/RC$  is the peak relaxation frequency. The impedance corresponding to the constant phase element (CPE) which is a non-Debye circuit element is given by

$$Z_{CPE} = \frac{1}{Q(i\omega)^u}, \quad (2.18)$$

where  $i = \sqrt{-1}$ ,  $Q$ , and  $u$  are the fitting parameters and  $Q$  is called CPE such that it may behave as an electrical analog of resistance, Warburg impedance, capacitance, and inductance for different values of  $u = 0, 0.5, 1$ , and  $-1$  respectively.

The dimension of CPE is  $\Omega^{-1}s^u$ , whereas that of capacitance is  $\Omega^{-1}s$  so that CPE and capacitance may be treated as proportional to each other and they are related as  $C = Q(\omega_{\max})^{u-1}$  [40, 41]. The value of  $Q_0$  is frequency independent, while it is temperature and material dependent. The parameter  $Q_0$  describes the magnitude of dispersion. The exponents of Eqs. (2.17) and (2.18) are related to each other by  $u = 1 - \alpha$  and  $\alpha$  determines the extent of depression of the semicircle below the real axis [40]. The exponent  $\alpha$  represents the magnitude of the departure of the electrical response from an ideal condition that has a single relaxation time. In other words,  $\alpha$  gives a further representation of the distribution of the relaxation times and can be determined from the location of the centers of the semicircle. When  $\alpha$  goes to zero, ( $1 - \alpha \rightarrow 1$ ), Eq. (2.17) reduces to the classical Debye formalism. The admittance corresponding to Eq. (2.18) can be written as

$$Y(\omega) = Qj\omega^u = B_0\omega^u[\cos(u\pi/2) + j\sin(u\pi/2)] = A\omega^u + B\omega^u \quad (2.19)$$

With  $A = B_0 \cos(u\pi/2)$  and  $B = B_0 \sin(u\pi/2)$ .

The impedance analysis involves the display of the impedance data in different formalisms and provides us the maximum possible information. The display of impedance data in the complex plane plot appears in the form of a succession of semicircles attributed to relaxation phenomena with different time constants due to the contribution of grain bulk, grain boundary/interfacial polarization, and electrode polarization in a polycrystalline material or a composite. Hence, the contribution to the overall electrical property from various components in the material is separated easily. The peak of the semicircle in the complex plane plot enables us to evaluate the relaxation frequency ( $f_{\max}$ ) of the material corresponding to the origin of different type of polarization in accordance with the relation:

$$\omega_{\max} \tau_0 = \omega_{\max} RC = 2\pi f_{\max} RC = 1$$

Or

$$f_{\max} = \frac{1}{2\pi RC} \text{ and } \tau_0 = \frac{1}{2\pi f_{\max}}, \quad (2.20)$$

where  $\tau_0$  is the peak relaxation time. The impedance data also enable us to investigate the information on relaxing dipoles in the material in terms of the real and imaginary parts of the complex dielectric constant  $\varepsilon = \varepsilon' - j\varepsilon''$  through the relations:

$$\varepsilon(\omega) = \varepsilon' - j\varepsilon'' = \frac{1}{j\omega C_0 Z(\omega)} \text{ with} \quad (2.21)$$

$$\varepsilon' = \frac{-Z''}{\omega C_0 (Z'^2 + Z''^2)} \text{ and } \varepsilon'' = \frac{Z'}{\omega C_0 (Z'^2 + Z''^2)}$$

where  $C_0$  is the vacuum capacitance.

The complex modulus of the material is given by

$$M(\omega) = \frac{1}{\varepsilon(\omega)} = M' + jM'' = j\omega C_0 Z(\omega)$$

with

$$M' = -\omega C_0 Z'' = \frac{\varepsilon'}{\varepsilon'^2 + \varepsilon''^2} \text{ and } M'' = \omega C_0 Z' = \frac{\varepsilon''}{\varepsilon'^2 + \varepsilon''^2}. \quad (2.22)$$

Complex modulus formalism is an important and convenient tool to determine, analyze, and interpret the dynamical process of electrical transport phenomena. Moynihan et al. [42] gave a detailed analysis of the complex electric modulus formalism as

$$M(\omega) = \frac{1}{\varepsilon(\omega)} = M'(\omega) + jM''(\omega)$$

Or

$$M(\omega) = M_\infty \left[ 1 - \int_0^\infty \exp(j\omega t) \frac{d\varphi(t)}{dt} dt \right], \quad (2.23)$$

where  $M_\infty = 1/\varepsilon_\infty$ ,  $\varepsilon_\infty$  is the limiting high-frequency real part of permittivity and the function  $\varphi(t)$  is a relaxation function or Kohlrausch-Williams-Watts (KWW) [43] function, given as

$$\phi(t) = \exp\left(-\left(\frac{t}{\tau}\right)^\beta\right) \text{ with } 0 \leq \beta \leq 1. \quad (2.24)$$

For a realistic assessment of the modulus formalism, it is important to realize that it is based on a description of the electric response of the sample in terms of the macroscopic field decay function  $\varphi(t)$ . Empirically, the KWW function is a convenient choice for  $\varphi(t)$ , and the non-exponential parameter  $\beta$  is called the stretching exponent which is suitably varied for fitting the data. The smaller the value of  $\beta$ , the larger is the deviation of relaxation with respect to Debye-type relaxation ( $\beta = 1$ ). In other words, it can be said that for Debye-type relaxation ( $\beta = 1$ ), the full width at half maximum (FWHM) is observed to be 1.14 decades. For non-Debye-type relaxation ( $\beta < 1$ ), the observed FWHM must be greater than 1.14 decades.

### 2.4.3 Conductivity Spectroscopy

The origin of frequency dependence of conductivity in the relaxation phenomena arises due to mobile charge carriers. Jonscher attempted to explain the behavior of the real part of AC conductivity (which is calculated as  $\sigma_{ac} = \omega \varepsilon_0 \varepsilon' T \text{and}$ ) using the following universal power-law equation as

$$\sigma_{ac}(\omega) = \sigma_{dc} + \sigma_1(\omega)$$

where  $\sigma_{dc}$  is the dc conductivity

$$\sigma_{ac}(\omega) = \sigma_{dc} + A\omega^k \text{ where } \sigma_1(\omega) = A\omega^k$$

Or

$$\sigma_{ac}(\omega) = A\omega^k \text{ for } \sigma_{dc} = 0, \quad (2.25)$$

where  $k = 0$  is the frequency-independent term which is related to DC conductivity and the value of ' $k$ ' lies in between  $0 \leq k \leq 1$  is related to the pure dispersive component of AC conductivity having characteristics of power-law behavior of Eq. (2.25). The parameter ' $A$ ' is frequency independent, but may be temperature and material dependent. It is observed from above Eq. (2.25) that the AC conductivity is of the mixed type comprising  $\sigma_{dc}$  and  $\sigma_{ac}$ . There exists a frequency called hopping frequency ( $\omega_H$ ) [44–46] at which the conductivity changes from DC to AC, and the relation (2.25) can be written in the Almond-West [47] formalism as

$$\sigma_{ac} = \sigma_{dc} \left[ 1 + \left( \frac{\omega}{\omega_H} \right)^k \right] \text{ with the value of } \omega_H = \left( \frac{\sigma_{dc}}{A} \right)^{\frac{1}{k}}. \quad (2.26)$$

## 2.5 Magnetic Percolation Threshold

With decreasing particle size, a ferromagnetic material undergoes a transition from a polydomain to a single-domain state. This single-domain state is the most important cause for the intriguing physical properties displayed by nanosized magnetic materials. A single-domain particle is always in a state of uniform magnetization. This means that the constituent spins at temperatures well below the Curie temperature rotate in unison. The exchange energy is strong enough to hold all spins parallel to each other and determines the value of the particle magnetic moment, while its direction is determined by the total anisotropy energy. Superparamagnetism refers to this thermally activated switching of the magnetization over rotational energy barriers provided by magnetic anisotropy. When single-domain particles are reduced in size with their spontaneous magnetizations preserved, there begin high thermal fluctuations in the magnetization directions of the particles. Below a certain size, ambient thermal energy may be large enough to cause the moment to jump between two different stable orientations of magnetization even in the absence of an applied field. The behavior is exactly analogous to the Langevin treatment of paramagnetism with

the vital difference that the moment is not that of a single atom but rather of a single-domain particle and has a value of the order of  $10^2$ – $10^5$  Bohr magnetons (“super-spins”). Since extremely large moments and hence susceptibilities are involved, the treatment is known as superparamagnetism. Superparamagnetism is a magnetic analog of Brownian motion. In discussion with a ferromagnetic metal nanoparticle, the nanodimensional metal granule is considered as a ferromagnetic particle possessing an intrinsic magnetic moment equal to the sum of magnetic moments of the atoms contained in this granule. If the energy of the magnetostatic interaction between granules is below  $kT$  ( $k$  being Boltzmann constant and  $T$  is absolute temperature), no correlation between the magnetization vectors of such particles takes place, and the composite is expected to show its paramagnetic/superparamagnetic properties. When an infinite network of contacting granules is formed, at a critical concentration of the magnetic filler particle called magnetic percolation threshold ( $m_c$ ), conditions favoring exchange interaction between the atoms of the neighboring granules in the matrix are expected and the material should acquire a drastic change in its magnetic properties, such as DC magnetic susceptibility, coercivity, and DC magnetization [48–51].

## 2.6 Summary

Basic concepts associated with the composites have been explained. The working mechanisms of different composites that generate the net properties from the individual constituents have been discussed. The model of explaining the physical properties of composites is given in terms of the effective medium theories, such as Maxwell-Garnett, Yamada, Bruggeman, and Landauer’s approximations. Due to the limitations of these approximation models in explaining certain physical properties in some definite situations, the percolation theory has been added to account for the variation of physical properties of polymer composites. The explanation of ferromagnetism, magnetic dipolar interaction, superparamagnetism, and magnetic percolation threshold also has been added. The dielectric and impedance spectroscopies have been added to account for the microstructure, relaxation behavior, and the other electrical properties.

## References

1. Stroud D (1998) The effective medium approximations: some recent developments. *Superlattices Microstruct* 23:567–573
2. Bruggeman DAG (1935) Berechnung verschiedener physikalischer Konstanten von heterogenen Substanzen. I. Dielektrizitätskonstanten und Leitfähigkeiten der Mischkörper aus isotropen Substanzen. *Ann Phys* 416:636–664
3. Sahimi M (2003) *Heterogeneous materials I: linear transport and optical properties*. Springer, New York

4. Torquato S (2002) Random heterogeneous materials: microstructure and macroscopic properties. Springer, New York
5. Priou A (1992) Dielectric properties of heterogeneous materials. In: Progress in electromagnetics research. Elsevier, New York
6. Oppert M, Saad D (2001) Advanced mean field methods: theory and practice. MIT Press, Massachusetts
7. Yamada T, Ueda T, Kitayama T (1982) Piezoelectricity of a high content lead zirconate titanate/polymer composite. *J Appl Phys* 53:4328–4332
8. Tinga WR, Voss WAG, Blossy DF (1973) Generalized approach to multiphase dielectric mixture theory. *J Appl Phys* 44:3897–3902
9. Brosseau C (2002) Generalized effective medium theory and dielectric relaxation in particle-filled polymeric resins. *J Appl Phys* 91:3197–3204
10. Calame JP (2008) Dielectric permittivity simulation of random irregularly shaped particle composites and approximation using modified dielectric mixing laws. *J Appl Phys* 104:114108–114111
11. Stauffer D, Aharony A (1992) Introduction to percolation theory. Taylor and Francis, London
12. Sahimi M (1994) Applications of percolation theory. Taylor and Francis, London
13. Panda M, Srinivas V, Thakur AK (2015) Non-universal scaling behavior of polymer-metal composites across the percolation threshold. *Res Phys* 5:136–141
14. Newnham RE, Skinner DP, Cross LE (1978) Connectivity and piezoelectric-pyroelectric composites. *Mater Res Bull* 13:525–536
15. Ryu J, Priya S, Uchino K, Kim HE (2002) Magnetolectric effect in composites of magnetostrictive and piezoelectric materials. *J Electroceramics* 8:107–119
16. Maxwell JCG (1904) Colours in metal glasses and metal films. *Philos Trans R Soc London Sect A* 3:385–420
17. Landauer R (1952) The electrical resistance of binary metallic mixtures. *J Appl Phys* 23:779–784
18. Bergman DJ, Imry Y (1977) Critical behavior of the complex dielectric constant near the percolation threshold of a heterogeneous material. *Phys Rev Lett* 39:1222–1225
19. Grannan DM, Garland JC, Tanner DB (1981) Critical behavior of the dielectric constant of a random composite near the percolation threshold. *Phys Rev Lett* 46:375–378
20. Wilkinson D, Langer JS, Sen PN (1983) Enhancement of the dielectric constant near a percolation threshold. *Phys Rev B* 28:1081–1087
21. Song Y, Noh TW, Lee SI, Gaines JR (1986) Experimental study of the three-dimensional ac conductivity and dielectric constant of conductor-insulator composite near the percolation threshold. *Phys Rev B* 33:904–908
22. Lee SI, Song Y, Noh TW, Chen XD, Gaines JR (1986) Experimental observation of non-universal behavior of the conductivity exponent for three-dimensional continuum percolation systems. *Phys Rev B* 34:6719–6724
23. Gefen Y, Aharony A, Alexander S (1983) Anomalous diffusion on percolating clusters. *Phys Rev Lett* 50:77–80
24. Gefen Y, Aharony A, Mandelbrot BB, Kirkpatrick S (1981) Solvable fractal family, and its possible relation to the backbone at percolation. *Phys Rev Lett* 47:1771–1774
25. Knite M, Teteris V, Aulika I, Kabelka H, Fuith A (2004) Alternating-current properties of elastomer-carbon nanocomposites. *Adv Eng Mater* 6:746–749
26. Laibowitz RB, Gefen Y (1984) Dynamic scaling near the percolation threshold in thin Au films. *Phys Rev Lett* 53:380–383
27. Efros AL, Shklovskii BI (1976) Critical behaviour of conductivity and dielectric constant near the metal-non-metal transition threshold. *Phys Status Solidi (b)* 76:475–485
28. Balberg I (2002) A comprehensive picture of the electrical phenomena in carbon black-polymer composites. *Carbon* 40:139–143
29. Balberg I, Bozowski S (1982) Percolation in a composite of random stick-like conducting particles. *Solid State Commun* 44:551–554

30. Halperin BI, Feng S, Sen PN (1985) Difference between lattice and continuum percolation transport exponents. *Phys Rev Lett* 54:2391–2394
31. Feng S, Halperin BI, Sen PN (1987) Transport properties of continuum systems near the percolation threshold. *Phys Rev B* 35:197–214
32. Rubin Z, Sunshine SA, Heaney MB, Bloom I, Balberg I (1999) Critical behavior of the electrical transport properties in a tunneling-percolation system. *Phys Rev B* 59:12196–12199
33. Bug ALR, Grest GS, Cohen MH, Webman I (1987) Ac response near the percolation threshold: transfer-matrix results in two and three dimensions. *Phys Rev B* 36:3675–3682
34. Balberg I (1987) Tunnelling and non-universal conductivity in composite materials. *Phys Rev Lett* 59:1305–1308
35. Debye P (1945) *Polar molecules*. Dover, New York
36. Cole KS, Cole RH (1941) Dispersion and absorption in dielectrics I. Alternating current characteristics. *J Chem Phys* 9:341–351
37. Davidson DW, Cole RH (1951) Dielectric relaxation in glycerol, propylene glycol, and *n* propanol. *J Chem Phys* 19:1484–1490
38. Havriliak S, Havriliak SJ (1997) *Dielectric and mechanical relaxation in materials: analysis, interpretation, and application to polymers*. Hanser Publishers, Munich
39. Jonscher AK (1983) *Dielectric relaxation in solids*. Chelsea Dielectrics press, London
40. Macdonald JR (1987) *Impedance spectroscopy: emphasizing solid materials and systems*. Wiley, New York
41. Hsu CS, Mansfeld F (2001) Concerning the conversion of the constant phase element parameter  $Y_0$  into a capacitance. *Corrosion* 57:747–748
42. Moynihan CT, Boesch LP, Loberge NL (1973) Decay function for the electric field relaxation in vitreous ionic conductors. *Phys Chem Glasses* 14:122–125
43. Williams G, Watts DC (1970) Non-symmetrical dielectric relaxation behavior arising from a simple empirical decay function. *Trans Faraday Soc* 66:80–85
44. Dyre JC, Schroder TB (2000) Universality of ac conduction in disordered solids. *Rev Mod Phys* 72:873–892
45. Gerhardt R (1994) Impedance and dielectric spectroscopy revisited: distinguishing localized relaxation from long-range conductivity. *J Phys Chem Solids* 55:1491–1506
46. Sinclair DC, West AR (1989) Impedance and modulus spectroscopy of semiconducting  $\text{BaTiO}_3$  showing positive temperature coefficient of resistance. *J Appl Phys* 66:3850–3856
47. Almond DP, Duncan GK, West AR (1983) The determination of hopping rates and carrier concentrations in ionic conductors by a new analysis of ac conductivity. *Solid State Ionics* 8:159–164
48. Stephen MJ (1981) Magnetic susceptibility of percolating clusters. *Phys Lett A* 87:67–68
49. Kalinin YE, Sitnikov AV, Skryabina NE, Spivak LV, Artem AA, Shadrin A (2004) Barkhausen effect and percolation threshold in metal-dielectric nanocomposites. *J Mag Magn Mater* 272–276:E893
50. Guo Z, Park S, Hahn HT, Wei S, Moldovan M, Karki AB, Young DP (2007) Magnetic and electromagnetic evaluation of the magnetic nanoparticle filled polyurethane nanocomposites. *J Appl Phys* 101(09M):511
51. Shekhar S, Sajitha EP, Prasad V, Subramanyam SV (2008) High coercivity below percolation threshold in polymer nanocomposite. *J Appl Phys* 104:0839101–0839104

# Chapter 3

## Synthesis and Characterization of Polymer Composites



This chapter deals with the description of the procedures of preparing the polymer composites and their physical characterizations. Further, brief descriptions of the analytical instruments used for the physical characterization of the samples and some of the typical results from the respective instruments are also included for their inherent standardizations.

### 3.1 Sample Preparation

Samples in suitable shapes have been synthesized [1–4] to perform the electromagnetic experiments to minimize the geometry errors and errors from other sources. A thickness monitor glass tape caster is used for preparing the polymer composite films. The other experimental techniques used for sample preparation are (a) high-energy ball milling, (b) ultrasonic sonicator, (c) compression hot molding, and (d) hydraulic press.

/Polymer/metal composites (PMC) have been prepared with the purchased chemicals as per the following specifications. The high purity (99.9%) polymers, both a polar/weakly ferroelectric polymer of polyvinylidene fluoride (PVDF) and a non-polar polymer of low-density polyethylene (LDPE) were purchased from Alfa Aesar. The high purity (99.99%) metal powders, such as nickel ( $\mu$ -Ni), aluminum (Al), copper (Cu), iron (Fe), having an initial particle size of  $\sim(10\text{--}20)$   $\mu\text{m}$ , were purchased from Alfa Aesar. The particle size of  $\mu$ -Ni has been reduced to form nanocrystalline Ni (n-Ni), and the quasicrystal of Al, Cu, and Fe corresponding to the nominal composition of  $\text{Al}_{65}\text{Cu}_{23}\text{Fe}_{12}$  (n-QC) has been formed through ball milling, described below. The n-Ni has been annealed to form a core-shell structure of n-Ni and NiO composites, respectively, and their formation is described below.

Various specifications regarding density, percentage of crystallinity, melting temperature, presence of different phases, average particle size, surface area, and the DC conductivity of the polymer and conductor components either as purchased

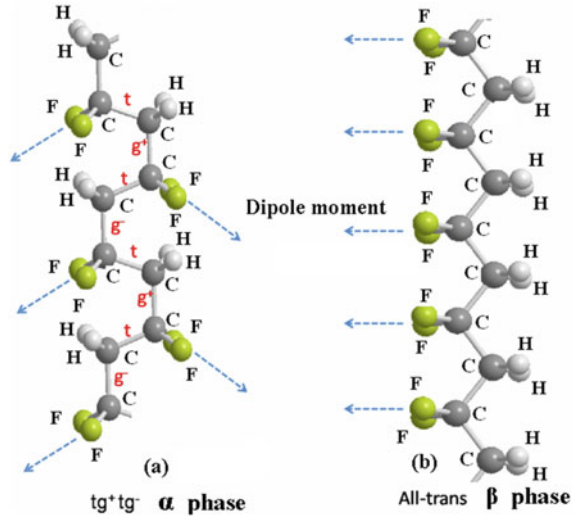
**Table 3.1** Specification of the various components

Components	Density (g/cc)	Average particle size ( $\mu\text{m}$ )	DC conductivity ( $\Omega^{-1} \text{cm}^{-1}$ )	BET surface area ( $\text{m}^2/\text{g}$ )	Series of composites	$f_c$
PVDF	1.74	0.4–0.6	$10^{-14}$	–	A	0.57
LDPE	0.92	400	$10^{-15}$	–	B	0.27
$\mu$ -Ni	8.91	8–12	$\sim 10^9$	0.03	C	0.23
$n$ -Ni	8.91	0.02–0.04	$\sim 10^6$ – $10^8$	1.30	D	$0.25 < f_c < 0.26$
$n$ -QC	4.7	0.2–0.3	$\sim 10^3$ – $10^4$	–	E	0.07
$n$ -Ni@ NiO	8.91	0.02–0.04	$\sim 10^{-5}$	–	F	0.30
					G	0.06

or synthesized are listed below in Table 3.1. The two types of polymer used in the present investigation are a polar (PVDF) and a non-polar (LDPE) polymer. The polymer PVDF is a semicrystalline polymer (50–60% crystalline), while the polymer LDPE is an amorphous polymer (30% crystalline) [5, 6]. The monomer units present in PVDF and LDPE are  $\text{CH}_2=\text{CF}_2$  and  $\text{CH}_2=\text{CH}_2$ , respectively, and in the polymeric form they are written as  $-\text{[CH}_2=\text{CF}_2\text{]}_n-$  and  $-\text{[CH}_2=\text{CH}_2\text{]}_n-$ , respectively. PVDF exists in five different structural forms, such as  $\alpha$  (TGTG'),  $\beta$  (TTTT),  $\gamma$  (TTTGT'TTG'),  $\delta$ , and  $\epsilon$  depending on the chain conformations as trans (T) or gauche (G) linkages.

Among these polymorphic forms of PVDF, three important crystalline forms of PVDF are  $\alpha$  (pseudo-orthorhombic),  $\beta$  (orthorhombic), and  $\gamma$  (monoclinic), having chain confirmations as TGTG' or  $(\text{tg}^+\text{tg}^-)$ , TTTT, TTTGT'TTG', respectively. Due to the presence of chain conformation, PVDF exists either in a non-polar ( $\alpha$ ) or in a polar (e.g.,  $\beta$ ,  $\gamma$ ) phase. The schematic diagram of the two most common conformations of PVDF, such as  $\alpha$  and  $\beta$ , is given in Fig. 3.1. We observe that there is a net permanent dipole moment exists in the  $\beta$  phase of the polymer. Each crystal phase having different molecular confirmations affects its dipolar characteristics due to the preferential orientation of the atomic groups around the carbon atom. When poled, PVDF is a ferroelectric polymer, exhibiting efficient piezoelectric and pyroelectric properties. PVDF has a glass transition temperature ( $T_g$ ) of about  $-35^\circ\text{C}$  and a melting temperature of  $170^\circ\text{C}$ . Similarly, LDPE is one of the polymeric forms of polyethylene (PE). Polyethylene is a thermoplastic polymer consisting of long chains of monomer ethylene. Polyethylene is classified into several different categories based mostly on its density and branching. With regard to sold volumes, the most important polyethylene grades are high-density polyethylene (HDPE), linear low-density polyethylene (LLDPE), and low-density polyethylene (LDPE). LDPE is defined by a density range of  $0.91$ – $0.94 \text{ g/cm}^3$ . It can withstand a temperature of  $80^\circ\text{C}$  continuously and  $95^\circ\text{C}$  for a short time. In terms of its crystal structure, it exists only in one phase as it is only 30% crystalline and it is also non-polar. The  $T_g$  and M.T. values for LDPE are  $-125^\circ\text{C}$  and  $130^\circ\text{C}$ , respectively.

**Fig. 3.1** Schematic arrangements of the H, F, and C atoms in the polymer chain of PVDF, **a** non-polar ( $\alpha$ ) phase and **b** polar ( $\beta$ ) phase



### 3.1.1 Synthesis of Nanocrystalline Powders

The synthesis of nanocrystalline elemental and alloy powders has been carried out with the help of a high-energy ball milling technique.

#### (a) Mechanical Milling

In this technique, a planetary ball mill (RETSCH PM-200 model) is used to synthesize nickel fine particles with tungsten carbide balls and vials. Toluene milling medium is chemically inert and used as a coolant to diffuse the heat generated during milling. Toluene also acts as a lubricant to prevent any damage to balls during the collision. The ball to powder weight ratio (BPR) is taken as 10:1, and the milling time is up to 60 h. After 60 h of milling, Ni nanoparticles of size 20–30 nm were obtained which was confirmed from HRTEM.

Oxide-coated Ni particles have also been prepared with NiO over the Ni metal in its nanocrystalline state. n-Ni ball-milled metal particles have been annealed at 500 °C for 5 h, and n-Ni/NiO core-shell particles have been prepared for further study.

#### (b) Mechanical Alloying

Elemental blends of Al, Cu, and Fe corresponding to the nominal composition of  $Al_{65}Cu_{23}Fe_{12}$  have been mechanically alloyed for 10 h in a high-energy planetary ball mill (RETSCH PM-200 model). The milling has been carried out in toluene and tungsten carbide milling media by maintaining BPR at 10:1. Well-ordered quasicrystalline (QC)  $Al_{65}Cu_{23}Fe_{12}$  powders (~300 nm) confirmed through HRTEM were obtained on annealing (800 °C) the as milled powder under inert gas atmosphere for 1 h. The QC structure has been confirmed through XRD patterns.

### 3.1.2 Formation of Polymer Composites

The synthesis of PMC samples in the form of pellets and thick films have been done by following a two-step process. (a) For pellets, mechanical blending is followed by hydraulic press/hot compression molding. (b) For thick films, ultrasonic sonication is followed by tape casting [1–6].

#### (I) Bulk composites

The PMC composites were prepared by mechanical blending of the two components (polymer and metal) with the help of agate mortar and pestle. The homogeneity was achieved after grinding the composites for more than 2 h. The various series of composite samples were prepared by taking different volume fractions of the conductor and mixing with a definite amount of polymer in such a way that the volume fraction of the conductor is gradually increased. Initially, a few composite pellets were made, and on subsequent measurements of properties, the number of compositions was increased as being approached the  $f_c$  to obtain the value of  $f_c$  (i.e., critical region) very accurately.

These powders were pressed with the help of a hydraulic press to get the samples in their desired cylindrical pellet form. The final samples made were of 13 mm diameter and 1.5–2 mm thickness. In this book, the experimental investigation of PMC is reported (prepared with the hydraulic press at room temperature and referred them as cold-pressed samples or room temperature consolidated samples) and the hot-molded composites.

#### Hot-molded composites

The four major steps involved in compression hot molding (Fig. 3.2) are

1. Preformed blanks, powders, or pellets are placed in the bottom section of a heated mold or die.
2. The other half of the mold is lowered and is pressure applied.
3. The material softens under heat and pressure, flowing to fill the mold. Excess material is squeezed from the mold. If the polymer used is a thermoset, then cross-linking occurs in the mold.
4. The mold is opened and the part is removed.

For thermoplastics, the mold is cooled before removal, so the part will not lose its shape. Thermosets may be ejected while they are hot and after curing is complete. This process is slow, but the material moves only a short distance to the mold and does not flow through gates or runners. Only one part is made from each mold.

#### (II) Thick Films

Thick films of the PMC were prepared with the help of a homemade thickness monitor glass tape caster after preparing the slurry of the PMC passing through ultrasonic probe sonication.



Fig. 3.2 Compression hot molding with temperature digital panel meter and pressure indicator

### 3.2 Physical Characterization Techniques

The samples have undergone various types of characterizations and have been analyzed for finding their suitability for the relevant applications [7–16].

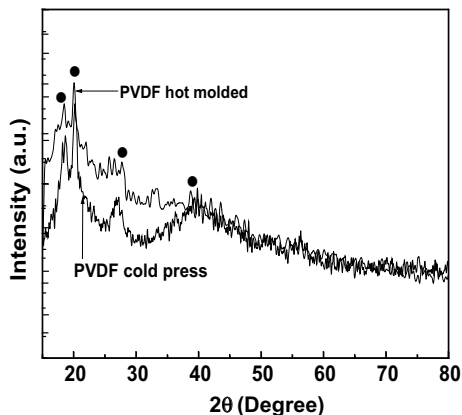
#### 3.2.1 Structure

##### (i) X-Ray Diffraction

X-ray diffraction (XRD) is a powerful tool for materials characterization as well as for the investigation of the fine structure of the materials. As the physical properties of a composite (e.g., electrical, dielectric, optical, magnetic, etc.) depend on the arrangements of the different components in the composite, the determination of the homogeneity of the samples becomes an indispensable part.

The diffraction pattern of a substance comprises both the angular positions and intensities of the diffracted beams and forms a sort of fingerprint by which the substance may be identified. Analysis of the angular positions of the diffraction lines leads immediately to a knowledge of the size, shape, and orientation of the unit cell, while the relative intensities of the lines reflect the relative quantity of the different components present in the composite. A given substance always produces a characteristic diffraction pattern, whether that substance is present in the pure state or as one constituent of a mixture of substances. Quantitative analysis of the various components is also possible because the intensities of the diffraction lines due to a

**Fig. 3.3** Typical XRD pattern of the polymer samples, such as cold-pressed and hot-molded pure PVDF



particular phase depend on the proportion of that phase in the specimen. In the case of polymeric materials, the XRD technique is used to determine the proportion of crystalline and amorphous phases in terms of the degree of crystallinity.

In this book, the X-ray diffractograms were recorded over a wide range of diffraction angles  $2\theta$  varying from  $15^\circ$  to  $80^\circ$  using  $\text{Cu K}\alpha$  radiation of wavelength  $\lambda = 1.5418 \text{ \AA}$  at a scanning rate of  $3^\circ/\text{min}$  with the help of Rigaku (model: Miniflex) and Pan-analytical X'pert PRO-PW 3040 X-ray diffractometers. The X-ray generator was operated at 40 kV, at an anode current of 20 mA from stabilized power supplies. The qualitative phase analysis was performed by the usual Hanawalt's method of comparative peak matching with standard JCPDS (Joint Committee of Powder Diffraction Standards) files. All the observed peaks/reflections were indexed based on the best agreement between the observed and the JCPDS data. The typical XRD pattern of the polymer PVDF showing both the crystalline and amorphous content is given in Fig. 3.3.

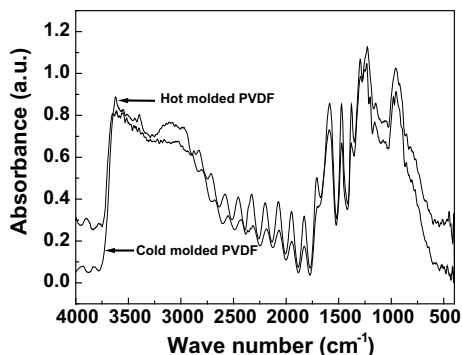
### (ii) Fourier Transform Infrared Spectroscopy (FTIR)

Fourier transform infrared spectroscopy (FTIR) studies, in general, are used to identify;

- The unknown materials and chemical groups present in the polymers or in PMC.
- To determine the quality or consistency of a sample and is also used to determine the amount of components present in a mixture.
- To determine the phase of the polymer in which it exists.
- In addition, it also gives a lot of relevant information for a polymer or PMC, such as crystallinity of the material, bond length, bond strength, and ionic motions.

In infrared spectroscopy, IR radiation is passed through a sample. Some of the infrared radiation is absorbed by the sample and some of it is transmitted through the sample. The resulting spectrum represents the molecular absorption and transmission, creating a molecular fingerprint of the sample. Like a fingerprint, no two unique molecular structures produce the same infrared spectrum and hence making

**Fig. 3.4** Typical FTIR spectrum in the specular reflection mode of the cold molded and hot-molded pure PVDF



the infrared spectroscopy a useful tool for the above several types of analysis. FTIR is advantageous over the conventional IR technique because the sample is exposed to IR radiation for a small time interval in the former case, thereby minimizing the possibility of sample damage while a spectrum is recorded. Secondly, the FTIR technique has the added advantage of recording the details of even overlapped spectral features.

In this book, the FTIR spectra of the polymer and PMC to observe the different phases present in the polymer, the phase change of the polymer due to dispersion of metal particles in the polymer matrix was taken. It is also interesting to know whether the dispersed metal particles and the polymer chain have any molecular level interactions, which may reflect in absorption or transmission spectra. The samples were in the form of thick films  $\sim 50 \mu\text{m}$  and as powders of PMC. The FTIR spectrum of the samples (in KBr) was recorded at room temperature in the mid IR range ( $400\text{--}4000 \text{ cm}^{-1}$ ) at an average scan rate of 32 with a wave number resolution of  $4 \text{ cm}^{-1}$  using Thermo Nicolet Spectrophotometer (model: NEXUS-870). Before recording the spectrum of the samples, a spectrum without sample was recorded, which was subtracted each time from the spectrum of the sample material to remove the effect of atmospheric moisture and  $\text{CO}_2$ . The typical FTIR spectrum of some of the PMC is shown in Fig. 3.4.

### 3.2.2 Microstructure

#### (i) Optical Microscopy

The technique of optical microscopy is widely used to obtain the following information: (i) It helps in phase identification and to distinguish between amorphous and crystalline materials, (ii) for observing structural transformations in crystallization as well as under the action of various effects, such as thermal cycling and deformations, (iii) for observing macroscopic morphology and crystal system information as well as in comparing the structure of a material obtained under different technical

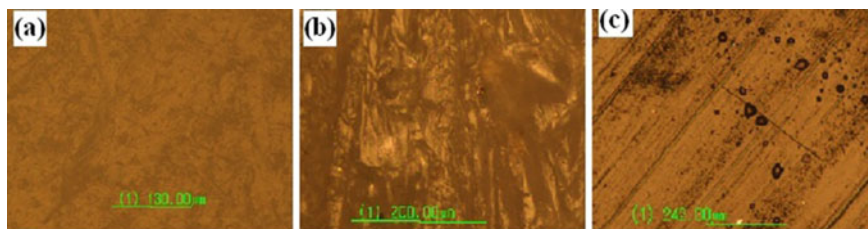


**Fig. 3.5** Typical optical micrographs of the polymer matrix, **a** cold-pressed pure PVDF, **b** hot-molded pure PVDF, and **c** hot-molded pure LDPE

conditions, (iv) for studying imperfections/defects in a material, (iv) to study the kinetics of the process of transformations, and (v) optical microscopy of polymeric electrolytes (materials) prepared in thin-film form reveals a characteristic lamellar structure when viewed in cross-polarized light.

The morphology of the polished surface of the samples has been collected with the help of a polarized optical microscope (model: Nikon ECLIPSE E400 POL). Typical optical micrographs of some of the polymer matrices after undergoing thorough treatment are shown in Fig. 3.5.

## (ii) Electron Microscopy

### (a) Scanning Electron Microscope (SEM)

The SEM is a versatile instrument for examining the microstructure of solid surfaces because it combines high spatial resolution with a depth of field in the same image. SEM produces micrographs by scanning the surface of the specimen with a small electron probe, synchronous with an electron beam from a source. The contrast in the micrograph is due to topographical variations and atomic number differences in the specimen. Two important types of analyses performed by an SEM are (i) high-resolution secondary electron imaging for knowing the specimen topography and (ii) backscattered electron imaging for knowing compositional variations on the sample surface. In addition, both qualitative and quantitative energy dispersive analysis of X-rays (EDAX) analysis of most elements can also be performed, relating elemental composition to morphological and textural features in a sample.

The principle of analysis of the characteristic X-rays emitted from samples can be used to determine both the qualitative and quantitative composition of samples constituted of different elements. The energy dispersive X-ray spectrometer discriminates between the energies of these characteristic X-rays falling on it and hence detects them. The concentration of the elements can easily be calculated from the peak heights. An important point to be noted in the case of EDAX analysis is that it can be performed either in “point analysis” mode or “area scan” mode, which is not possible by conventional X-ray analysis methods.

The instrument used in the present study is Oxford-Link ISIS 300 energy dispersive X-ray (EDX) micro-analyzer with an ECON IV detector attached to JEOL JSM

5800 scanning electron microscope. Sample composition and homogeneity were checked by employing the EDAX microprobe.

### (b) Field Emission Scanning Electron Microscope (FESEM)

The advantage of FESEM over SEM is that of its high resolving power. Although the basic principle of operation remains the same, there are some differences from that of conventional SEM. The most important difference between the two is the emitter type, i.e., the electron gun. The function of the electron gun is to provide a large and stable current in a small beam. Thermionic emitters are used in conventional SEM, while field emitters are used in FESEM. The accelerating voltage of routine FESEM instruments is  $\sim 120$ – $200$  kV.

In the present investigation, the morphology of the polished surface of the samples has been taken with the help of a FESEM (Model: Carl Zeiss, Supra 40). Experiments were performed on gold-coated samples, and FESEM micrographs were recorded through large/small area scans. The typical FESEM pattern of the polymer matrices used in the present investigation is shown in Fig. 3.6. The presence of spherulites is the clear signature of the crystalline polymer in cold-pressed PVDF (Fig. 3.6a), while they are not present for the hot-molded PVDF (Fig. 3.6b) because of the melting of the polymer at  $200$  °C. In the case of LDPE due to its non-crystalline nature in both cold-pressed and in hot-molded form, no spherulites are found (Fig. 3.6c, d).

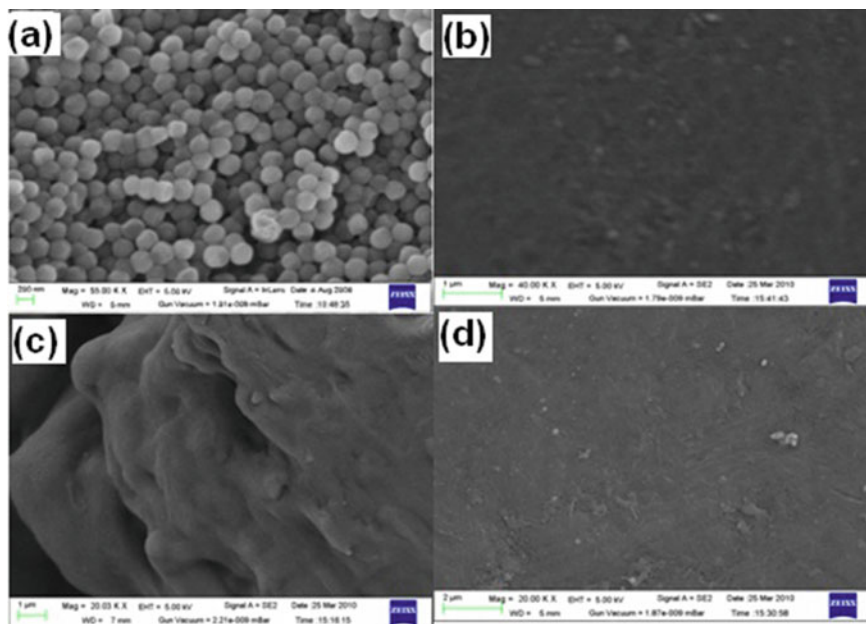


**Fig. 3.6** Typical FESEM of the polymers, **a** crystalline PVDF, **b** hot-molded PVDF, **c** non-crystalline polymer LDPE, and **d** hot-molded LDPE

### (c) **Transmission Electron Microscope (TEM)**

The TEM is a very powerful and versatile instrument that is capable of characterizing materials' crystal structure and microstructure, simultaneously by diffraction and imaging techniques. In a conventional TEM, a thin specimen is irradiated with an electron beam of uniform current density. Whatever part is transmitted is magnified by a three or four stages lens system and projected onto a fluorescent screen. When the transmitted electrons strike the fluorescent screen, light is generated allowing the user to see the image. The accelerating voltage of routine instruments is ~120–200 kV and determines the velocity and wavelength of the electrons and hence the resolution of the instrument.

In the present investigation, fine freestanding metal particles were obtained by high-power ultrasonication. A drop of this colloidal solution was taken and placed on the carbon grid for the measurements. The measurements were carried out with the help of TEM (Model: JEOL-JEM-2100) at an acceleration voltage of 200 kV.

### (iii) **Surface Area Measurement**

The instrument works based on the theory first proposed by Stephen Brunauer, Paul Hugh Emmett, and Edward Teller known as BET theory. According to this theory, at known partial pressure, the amount of N<sub>2</sub> (or any other inert gas) adsorbed by the regenerated sample at liquid N<sub>2</sub> temperature forms a single molecular layer over the surface of the sample. This adsorbed N<sub>2</sub> is then measured to calculate the surface area of the sample. In this method, gas mixture (approximately 30% N<sub>2</sub> and 70% He) continuously flows over the sample. The sample is dipped in liquid N<sub>2</sub>. At liquid N<sub>2</sub> temperature (−198 °C), N<sub>2</sub> gets adsorbed in this flow and forms a monolayer on the surface. This adsorbed N<sub>2</sub> is allowed to desorb by bringing the sample to room temperature. This desorbed N<sub>2</sub> is proportional to the surface area of the sample and so measured to calculate the surface area by using a mathematical equation. The BET theory can be expressed in the form of a mathematical equation involving physical terms, such as room temperature, partial pressure of the gas mixtures, volume for monolayer adsorption, and volume adsorbed at equilibrium pressure, and is given by

$$(P/P_0)/V_s(1 - P/P_0) = 1/V_m C + (C - 1)(P/P_0)/V_m C, \quad (3.1)$$

where  $V_m$  = monolayer volume,  $V_s$  = volume adsorbed at  $P/P_0$  at 0 °C,  $C$  = a constant, and  $P/P_0$  = partial pressure of the gas. There are two methods of dynamic measurement: the three-point and single-point method. In the present investigation, the surface area was measured with the help of the BET surface area analyzer (model: Smart Sorb 92/93) which uses the single-point dynamic method.

### 3.2.3 Thermal Characterizations

#### (i) Differential Scanning Calorimetry (DSC)

In this technique, the differential energy (enthalpy) changes of a sample required to maintain both the sample and the reference material (usually alumina, an inert material) are measured at the same temperature during a phase transformation on thermal treatment. A few milligrams of the sample and inert reference material are separately heated in a hermetically sealed container in such a way that a temperature difference between them is zero. To meet this requirement, an energy flow in terms of either absorption or evolution of heat takes place. The difference in the heat input when plotted as a function of time or temperature results in a definite pattern known as the DSC curve. The physical/chemical changes (e.g., melting, etc.) of a part or entire sample on heating, accompanied by absorption of energy to maintain zero temperature difference, appear as an “endothermic peak”. On the other hand, the changes in the materials (e.g., crystallization on cooling, etc.) involve the evolution of energy, and it appears as an “exothermic peak” in DSC curves. Particularly, in the case of polymeric materials which are mostly semicrystalline (partly crystalline and partly amorphous) in nature, it provides a range of useful information, such as glass transition temperature  $T_g$ , melting temperature  $T_m$ , decomposition temperature  $T_d$ , heat capacity, melting enthalpy  $\Delta H_m$ , and degree of crystallinity. The “degree of crystallinity” can be evaluated by determining the change in enthalpy ( $\Delta H_m$ ) from DSC during the melting of the crystalline part of the polymeric materials according to the formula  $\%X_c = \left( \Delta H_m / \Delta H_{100\%, \text{crystalline}} \right) \times 100\%$ , where  $(\Delta H_m)_{\text{DSC}}$  is the enthalpy change of the polymer corresponding to  $T_m$ . The experimental results are reported from DSC, Perkin Elmer (model: Sapphire DSC) to find out the melting temperature and phase transition of the polymer.

### 3.2.4 Electrical Characterizations

#### (a) Dielectric measurement

In the case of a dielectric material/PMC, there are several types of polarization, each of which can be explained by its intrinsic physical mechanism. The different basic types of polarizations are electronic, ionic, orientational/dipolar, interfacial/grain boundary/Maxwells Wagner Sillars (MWS), and electrode polarization. When an insulator is placed in an external electric field, electrons of the atoms are displaced slightly with respect to the nuclei, which induce dipole moments causing the electronic polarization. When the atoms of the molecule do not share their electrons symmetrically, the electron clouds are displaced eccentrically toward the stronger binding one. Thus, the ions acquire charges of opposite polarity. These net charges tend to change the equilibrium positions of the ions themselves under the action of an electric field. This displacement of charged ions or a group of ions with respect to

each other creates a second type of induced dipole moment called ionic polarization. In addition, the permanent dipole moments may exist in a material in the absence of an external electric field due to its very structure and difference of electro-negativity in a molecule. Such dipoles experience a torque due to an electric field that tends to orient them in the direction of the electric field. Consequently, an orientation polarization exists. Similarly in the case of composites (e.g., PMC) or dielectric ceramics, at the interface between two components or at the grain boundary, the charge accumulation occurs and forms an artificial dipole giving rise to interfacial polarization. Another type of artificial polarization occurs for ionic conductors at the interfacial area between the sample and electrodes giving rise to electrode polarization. These first three mechanisms of polarizations are arising due to charges locally bound in the atoms or molecules or inside the structure of solids. In addition to all these, there usually exist charge carriers that can migrate for some distance through dielectrics and those are called the later types of polarization. Generally, carriers are impeded in motion because of being trapped in the materials' interfaces. Hence, they cannot freely discharge at the electrodes and space charge results. Such distortion appears as an increase in the capacitance of the sample and may be distinguishable from a rise of the dielectric constant. Thus, the next polarization called interfacial and space charge polarization comes into play. But generally, the space charge or electrode polarization is observed for ionic conductors and hence only to consider the four types of polarization. The total polarization is the sum of the above four types of polarization. For electronic and ionic polarization, the frequency effect is negligible up to  $10^{10}$  Hz. As the optical range of frequency is reached, electronic contribution becomes the sole contributor.

When a dielectric is placed in an alternating electric field, a temporary phase shift is found to occur between the driving fields and resulting polarization; consequently, a loss current component appears giving rise to the dielectric loss of the sample. Due to the phase lag of the polarization (which gives rise to dielectric constant) with respect to the driving electric field, there will be two components of the complex dielectric constant, in which one component will try to restore the polarization while other components will contribute to the loss. The complex dielectric constant is given by  $\varepsilon = \varepsilon' - j \varepsilon''$ , where  $\varepsilon'(\omega)$  and  $\varepsilon''(\omega)$  are real and imaginary component (loss) of the complex dielectric constant, respectively. The loss factor is the primary criterion for the usefulness of a dielectric as an insulator material. So for some applications where high capacitance in the smallest physical space is required, materials with high dielectric constant and low dissipation factor must be used.

In this book, the dielectric measurements as a function of frequency have been carried out on the PMC samples in the form of thick films as well as on pellets using a high precision impedance analyzer (Agilent 4294A) in the frequency range of 40 Hz–10 MHz, with an applied voltage of 400 mV, using Agilent 16451B Dielectric Test Fixture (Inset, Fig. 3.7) is reported. The applied voltage of 400 mV has been optimized by applying different voltages of the applied electrical signal varying from 5 mV to 1 V for various PMC, taking both the percolating and non-percolating samples. We observe from the variation of capacitance and loss tangent shown in Fig. 3.8a, b, d, e for the two insulating polymers, such as polar PVDF and non-polar LDPE. The

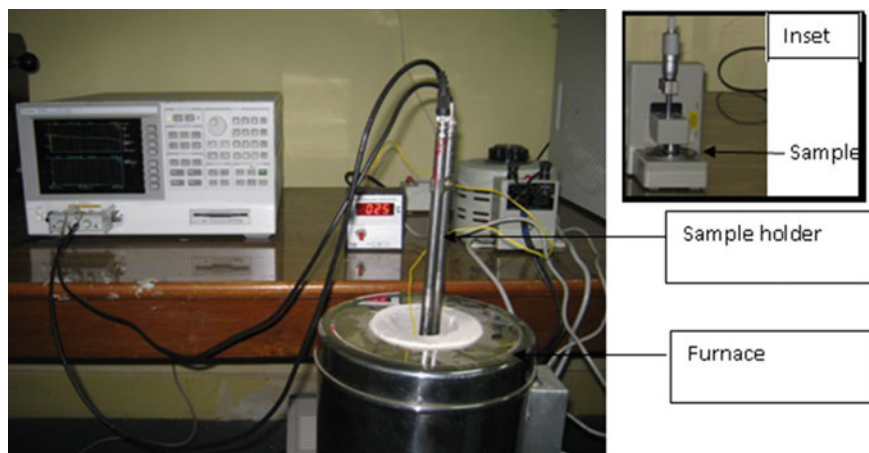


**Fig. 3.7** Agilent impedance analyzer along with the connected sample holder containing sample is placed inside the furnace for temperature variation of electrical measurement, Inset: Agilent 16451B Dielectric test fixture in which sample is placed for the room temperature measurement

scattering of data points gradually decreases with the increase of voltages from 5 mV and becomes stable for the applied voltages in the range of 100–400 mV or more than it. For the percolating PMC (Fig. 3.8c, f), even 5 mV gives stable data for all the electrical parameters. So what is concluded that for a more insulating sample, there is a requirement for higher AC voltage, and with the increase of conductivity, a less perturbing voltage is needed for getting stable data. As in the present book, to report PMC series, hence for each sample the voltage of 400 mV has been optimized. The temperature variation of the dielectric data on the prepared samples has been taken with the help of a homemade sample holder and Agilent 42941A impedance probe as shown in Fig. 3.7.

### (b) Impedance measurement

Complex impedance spectroscopy (CIS) is an experimental tool for the characterization of the electrical properties of materials. The technique is based on analyzing the AC response of a system to a sinusoidal perturbation and subsequent calculation of the impedance as a function of the frequency of the perturbation. The technique enables us to evaluate and separate the contribution to the overall electrical properties in the frequency domain due to electrode reactions at the electrode/material interface and the migration of charge carriers (ions/electrons) through the grains and across the grain boundaries within the specimen sample. In the impedance spectroscopy technique, a sinusoidal signal of low amplitude is applied across a sample and the response at the output is compared with the input signal to determine the impedance ( $Z$ ) and phase shift ( $\theta$ ). Due to this directional characteristic, the impedance data can be represented in the form of real and imaginary components making the impedance a complex quantity. So, the impedance of a sample is

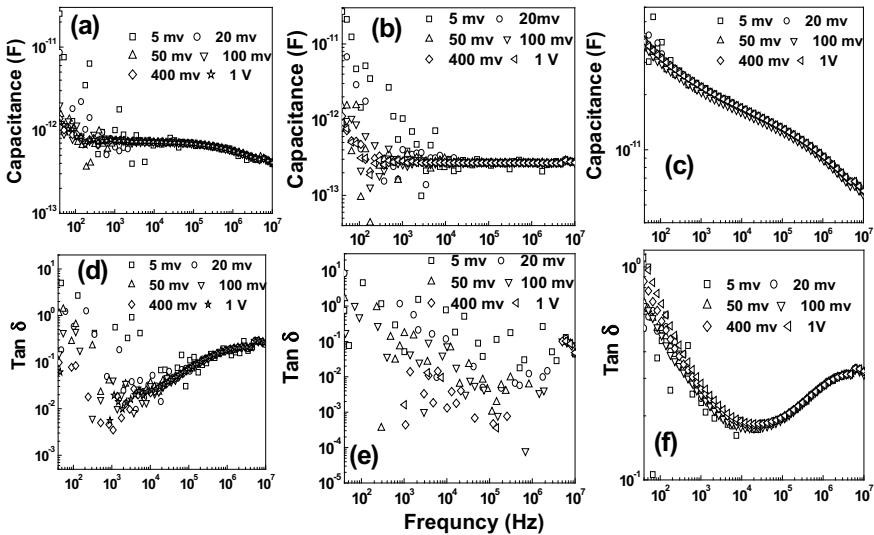


**Fig. 3.8** Variation of capacitance. **a** PVDF, **b** LDPE, **c** composite above  $f_c$  and  $\text{Tan } \delta$ , **d** PVDF, **e** LDPE, and **f** composite above  $f_c$ , at varying applied input voltages

known as the “complex impedance” consisting of both resistive (real part) and reactive (imaginary part) components. Impedance analysis involves the display of the impedance data in different formalisms and provides us the maximum possible information about the materials. The display of impedance data in the complex plane plot appears in the form of a succession of semicircles attributed to relaxation phenomena with different time constants due to the contribution of grain (bulk), grain boundary, and interface/polarization in a polycrystalline material. Hence, the contributions to the overall electrical property by various components in the material are separated easily. One of the main advantages of frequency-dependent measurements is that the contributions of the bulk material, the grain boundaries, and electrode effects can easily be separated if the time constant is different enough to allow separation. The complex plane plots result in different semicircles, intercepting along the x-axis ( $Z'$ -axis) at different regions. The intercept of the first semicircle in the high-frequency region is due to grains; the second one at intermediate frequency is due to grain boundaries/interfacial polarization, and the third one in the low-frequency region is due to electrode effect.

The impedance measurements in the present study have been carried out in the same manner as the electrical properties measurements were performed. The applied voltage of 400 mV has been optimized by applying different voltages of the applied electrical signal for two insulating polymers, PVDF (Fig. 3.9a, d) and LDPE (Fig. 3.9b, e) and for one percolating sample (Fig. 3.9c, f). The main purpose is to study (1) the electrical properties of the proposed materials using variable frequency measurements and to assign the different electrical impedance to appropriate regions of the samples (i.e., for bulk, grain boundaries/interfacial polarization,

electrode-material interface, etc.) and (2) to extract the maximum amount of useful information regarding the relaxation behavior across percolation threshold from the acquired data, namely relaxation frequency, AC and DC conductivity values, etc.

The various combinations of the samples reported in this book have been prepared through different process conditions which are given in the form of Table 3.2, with the sample name along with their method of preparation.

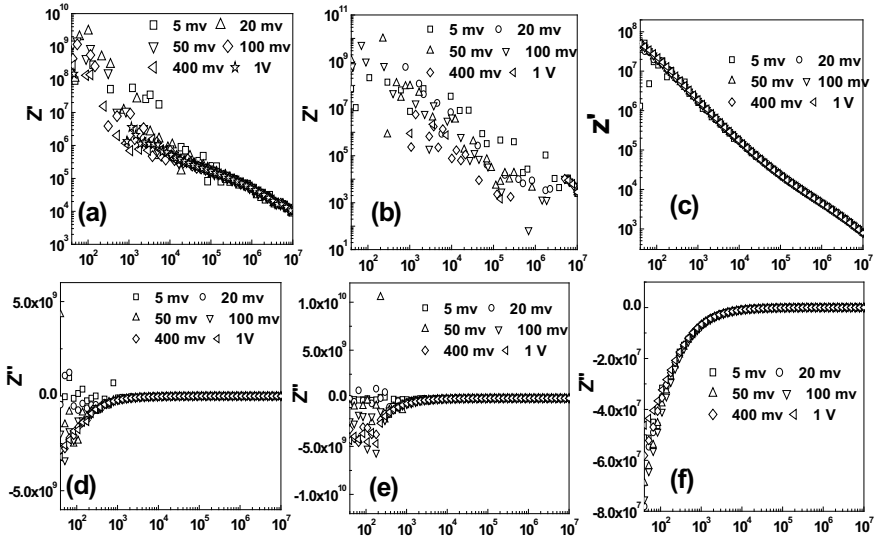


**Fig. 3.9** Variation of the real part of impedance ( $Z'$ ) given by **a** PVDF, **b** LDPE, **c** composite above  $f_c$  and imaginary part of impedance ( $Z''$ ) given by **d** PVDF, **e** LDPE, and **f** composite above  $f_c$ , at varying applied input voltages

**Table 3.2** Various composites reported along with their method of preparation

Name of the series of composites	Preparation method
PVDF/ $\mu$ -Ni	Room temperature consolidation (Cold pressed)
PVDF/ $n$ -Ni	Room temperature consolidation (Cold pressed)
PVDF/ $n$ -QC	Room temperature consolidation (Cold pressed)
PVDF/ $\mu$ -Ni	Compression hot molding with time variation
PVDF/ $\mu$ -Ni	Compression hot molding
PVDF/ $n$ -Ni	Compression hot molding
PVDF/ $n$ -Ni@NiO	Compression hot molding
LDPE/ $n$ -Ni	Compression hot molding

### (c) Spontaneous Polarization measurement

The distinguishing features of ferroelectrics in comparison to normal dielectric materials are the existence of spontaneous polarization and the presence of electric hysteresis, when polarization is plotted as a function of the applied electric field. This nonlinear nature is due to the combined effect of the following components, such as (i) dielectric polarization, (ii) remnant polarization, (iii) dielectric loss (leakage), and (iv) non-remnant polarization. The area within the hysteresis loop is a measure of the energy required to twice reverse the polarization. At zero fields, the electric displacement within a single domain (saturated value of the displacement) has two values corresponding to the opposite orientations of the spontaneous polarization. In a multidomain crystal, the average zero-field displacement can have any value between these two extremes. In principle, the spontaneous polarization is equal to the saturation value of the electric displacement extrapolated to zero fields. The remanent polarization  $P_r$  (the displacement at zero fields) may be different from the spontaneous polarization  $P_s$  if reverse nucleation occurs before the applied field reversal. The area within the loop is the measure of the energy loss per cycle. As in the present investigation, a ferroelectric polymer PVDF was chosen as the matrix; hence, the ferroelectric hysteresis loop on the unpoled samples was obtained using a precision workstation (M/S. Radiant Technologies Inc., USA) as PVDF exists in its mixed phase [ $\alpha$ ,  $\beta$ ]. The ferroelectric hysteresis test setup from M/S. Radiant Technologies Inc., USA, is capable of measuring very weak polarization. Generally, the hysteresis loop in ferroelectric thin films, ferroelectric capacitors, and ferroelectric read-only memory (FEROM) is obtained with the help of this setup. The whole setup is shown in Fig. 3.10.

## 3.2.5 Magnetic Characterizations

### (i) Permeability from Impedance Measurement

The frequency dependence of initial permeability of the composite sample was measured with the help of the turn coil method by passing 20 mA AC current through a pickup coil and the measurements were performed using an Agilent impedance analyzer (4294A) with the help of 42941A probe at room temperature in the frequency range of 10 kHz–10 MHz. A pickup coil of 40 turns was used for generating the exciting magnetic field by sending an oscillating current of 20 mA where the sample was used as the core of the pickup coil. The exciting field generated by the pickup coil is estimated to be  $\sim 1$  Oe. The length of the sample used was larger than the length of the pickup coil, and the effective area of the sample was found to be very less as compared to the pickup coil area. In this method, the measure of permeability, i.e., the relative permeability of a material with respect to vacuum or air was measured. The self-inductances were measured for all the composites with and without the samples, respectively. The complex permeability of the material can be written as  $\mu(\omega) = \mu'(\omega) - j\mu''(\omega)$ . The amplitude of ac current was kept at a constant

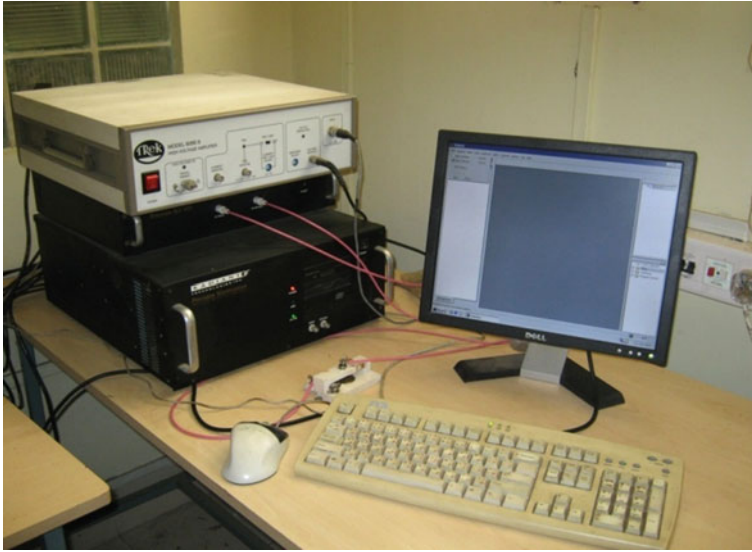


**Fig. 3.10** Ferroelectric hysteresis loop tracer from M/S. Radiant technologies

value during the frequency sweep to produce the constant amplitude of the AC field  $h(t) = h_0 e^{j\omega t}$  on the sample. The real and imaginary parts of permeability ( $\mu$ ) were determined as per the following relations

$$\mu'(\omega) = \frac{L(\omega)}{L_0(\omega)} \quad (3.2)$$

$$\mu''(\omega) = \frac{\{R(\omega) - R_0(\omega)\}}{L_0(\omega)}, \quad (3.3)$$

where  $L$  and  $R$  are the equivalent inductance and resistance with the sample and  $L_0$  and  $R_0$  are those of empty solenoid, respectively.

#### (ii) **Vibrating Sample Magnetometer (VSM)**

The operation of the VSM is based on the principle of flux change and, hence, inductions of emf in a coil when the sample is vibrated near it. When a sample is placed in a uniform magnetic field, a magnetic moment proportional to the product of the sample susceptibility and the applied field develops in it. If the sample is made to undergo sinusoidal motion in a direction at right angles to the magnetic field with the help of a mechanical vibrator, an alternating emf can be induced in suitably located stationary pickup coils. This emf has an amplitude proportional to the magnetic moment of the sample, the vibration amplitude, and the vibration frequency. Through the use of lock-in-amplifier and feedback techniques, only that portion of the signal arising from the magnetic moment is picked up and is converted

into direct readout in emu on a digital panel meter. The room temperature (300 K) M–H curves of the samples studied for this thesis work were measured with a homemade vibrating sample magnetometer with a sensitivity of  $10^{-6}$  emu in applied magnetic fields between  $\pm 7$  kOe.

### 3.2.6 Rheological Characterizations

#### (i) Rotational Rheometer

Rotational rheometry (Fig. 3.11) is a powerful technique for the measurement of properties associated with complex shear rheology across all types of material, sensitive enough to measure the viscosity of dilute polymer solutions. Rotational rheometry is ideal for discerning structural and compositional changes of materials, which are the critical controlling factors for inflow and deformation properties, and ultimately associated with product stability and performance.

The basics of the rotational rheometry technique are as follows. The sample is loaded into the gap of a measuring system, such as a concentric cylinder system, specifically designed to impose simple shear flow when rotated. The measuring system is supported by a virtually frictionless air bearing and driven by an ultra-low inertia motor, coupled to an ultra-high precision position encoder. The sample and measuring system are also temperature controlled. Various rheological characteristics of the sample can be determined by rotating, oscillating, or applying a step function to the measuring system, either by controlling motor torque (stress-controlled rheometry) or position change (strain-controlled rheometry).

**Fig. 3.11** Rotational rheometer from M/S. Anton Parr technologies



### 3.3 Summary

The various ways of preparing the polymer nanocomposites are described in detail. Special care is to be taken to prepare the samples to approach  $f_c$  as closely as possible during the observation of insulator-to-metal (IMT) transition at  $f_c$ . The experimental setups used for sample preparation, such as hydraulic press and compression hot molding, are included in detail. The working principle of various experimental setups such as XRD, FTIR, optical microscope, SEM, FESEM, TEM, BET surface area analyzer, DSC, impedance analyzer, FE hysteresis, VSM, and rheometer are included.

### References

1. Nicolais L, Carotenuto G (2004) Metal-polymer nanocomposites. Wiley-Interscience, Hoboken, New Jersey
2. Mittal V (2015) Synthesis techniques for polymer nanocomposites. Wiley-VCH Verlag GmbH, Weinheim
3. Huang X, Zhi C (2016) Polymer nanocomposites electrical and thermal properties. Springer, Switzerland
4. Hussain CM, Mishra AK (2018) New polymer nanocomposites for environmental remediation. Elsevier, Netherlands
5. Lovinger AJ (1983) Ferroelectric polymers. *Science* 220:1115–1121
6. Lovinger AJ (1981) Unit cell of the  $\gamma$  phase of poly(vinylidene fluoride). *Macromolecules* 14:322–325
7. Kaufmann EN (2012) Characterization of materials, vol 3. Wiley-Interscience, Hoboken, New Jersey
8. Flewitt PEJ, Wild RK (2017) Physical methods for materials characterization. CRC Press, Boca Raton
9. Merritt WHH, Dean LLJ, Settle JA, FA, Jr (1974) Instrumental methods of analysis, New York-Wokingham, Van Nostrand
10. Cullity BD (1978) Elements of x-ray diffraction. Addison-Wesley, USA
11. Yemu B (1999) Z Simpwin version 2, Electrochemical impedance spectroscopy (EIS) data analysis software, Princeton applied research
12. Maxwell JC (1892) A treatise on electricity and magnetism. Dover, New York
13. Wagner KW (1914) Erklärung der dielektrischen nachwirkungsvorgänge auf grund maxwellscher vorstellungen. *Arch Elektrotech* 2:371–387
14. Sillars RW (1937) The properties of a dielectric containing semiconducting particles of various shapes. *J Inst Electr Eng* 80:378–394
15. Jonscher AK (1983) Dielectric relaxation in solids. Chelsea Dielectrics Press, London
16. Macdonald JR (1987) Impedance spectroscopy: emphasizing solid materials and systems. Wiley, New York

# Chapter 4

## Percolation Behavior of Polymer Composites



In this chapter, a detailed investigation of structural, microstructural, dielectric, and percolation behavior of a variety of polymer-metal composites (PMC) comprising polar and non-polar polymers have been discussed. The effect of filler particle size, process conditions, mixing and firing time, temperature, different polymer matrices, the conductivity of filler particles, and spherulites of polymer on the percolation threshold ( $f_c$ ) and other percolation parameters have been included. All the PMC undergo an insulator-to-metal transition (IMT) at  $f_c$ , and the experimental results have been explained with the help of percolation theory, boundary layer capacitor effect, and the concept of connectivity.

### 4.1 Introduction

Recently, there have been several studies on polymer-based composites which exhibit excellent physical properties coupled with mechanical flexibility. In particular, ferroelectric polymers, like polyvinylidene fluoride (PVDF), poly[(vinylidene fluoride)-co-trifluoroethylene][P(VDF-TrFE)], and polyvinylidene fluoride-trifluoro ethylene-chlorofluoroethylene [PVDF-TrFE-CFE], etc., and composites with a variety of fillers, such as ceramics, metals, or metal-ceramic components have been investigated, and large changes in the value of effective dielectric constant ( $\epsilon_{\text{eff}}$ ) have been reported in the neighborhood of  $f_c$  [1–22]. Although the percolation theories for random continuum percolation systems predict the ideal value of  $f_c$ , i.e., the critical volume fraction for any three-dimensional (3D) random percolative insulator–conductor composites (ICC) to be at 0.16 (where the fillers are assumed to be of hard spheres and in micron size), always the experimentally observed  $f_c$  value is found to be at variance (refer Fig. 1.1 of Chap. 1). The focus of research in polymer/conductor composites (PCC) is on  $f_c$  and the critical behavior in the vicinity of IMT [23, 24]. Although half a century has passed since the initial development of the standard percolation theory, yet a consensus hasn't been reached so far as the calculation of  $f_c$

for a given material that exhibits an IMT is concerned. Many controversies exist in this area of research which requires serious attention, although several studies show deviations from the percolation theories (refer Fig. 1.1 of Chap. 1). Interestingly, Dang et al. [2] demonstrated ideal percolative behavior in hot-molded PVDF/Ni composites with a  $f_c$  value of 0.16 which is in agreement with the theoretically predicted value. Also, the value of static dielectric constant ( $\epsilon_{\text{eff}}$ ) in PVDF/Ni composites is around 400 which is comparable to the reported  $\epsilon_{\text{eff}}$  of  $\sim 450$  in case of other PMC (References in Fig. 1.1). Very few PMC show  $\epsilon_{\text{eff}} > 450$ , and it has been observed in some of the PMC the value is around 2000. As discussed in Chap. 1, the scattered values of  $f_c$  and the extent of enhancement of  $\epsilon_{\text{eff}}$  in the vicinity of  $f_c$  are the two major features exhibited in PMC which are the subject of recent debate, so these surprising results question the validity of percolation theory in PMC. On the other hand, PMC materials are tipped to be ideal for the verification of the proposed theories. Therefore, pertinent questions in the present discussion are

- (i) On what parameters the value of  $f_c$  depends on?
- (ii) What is the effect of filler particle size and shape?
- (iii) How does the process condition affect the  $f_c$  of a particular PMC?
- (iv) Does the polymer matrix play a role in the extent of enhancement of  $\epsilon_{\text{eff}}$  and in changing the value of  $f_c$ ?
- (v) Does the nature of filler affect the  $f_c$  and electrical properties of a PCC?
- (vi) Whether the critical exponents remain the same for all PMC, i.e., they only depend on the dimensionality of the samples?
- (vii) What is the role of Spherulites?

## 4.2 Samples Reported

A variety of polymers, such as a polar/weakly ferroelectric polymer (PVDF) and a non-polar polymer (LDPE), were chosen to investigate the percolation behavior in PMC/PCC. The different fillers chosen are  $\mu$ -Ni,  $n$ -Ni, composite/core-shell structure of  $n$ -Ni and  $n$ -NiO. The varieties of PMC were prepared under different process conditions. Two series of composites, such as PVDF/ $\mu$ -Ni and PVDF/ $n$ -Ni composites, were formed by mixing the powders of the two components for more than 2 h and then the blended samples were prepared in the form of pellets (diameter-13 mm and thickness  $\sim 1.5$ –2 mm) through hydraulic pressing referred to as the cold press samples (consolidation at room temperature for 5 min).

To investigate thermal effects, two series of the same PVDF/ $\mu$ -Ni composites were reported with varying temperature and time to optimize the hot molding time duration. In this process, first, a series of blended powders of PVDF/ $\mu$ -Ni composites were hot molded at a temperature of 200 °C (above the melting temperature of PVDF) for 12 min and the  $f_c$  value was found to be at  $>0.32$ . Further, one of the sample [volume fractions of the conductor ( $f_{\text{con}} = 0.22$  (above ideal  $f_c$ ))] of above series PVDF/ $\mu$ -Ni composites was hold molded at a temperature of 200 °C with varying times from 12 to 90 min to find the optimized molding time of 45 min.

After optimization of the molding time (45 min), the above two series of samples (cold-pressed samples), PVDF/ $\mu$ -Ni and PVDF/ $n$ -Ni composites, were again prepared with the hot molding procedure at the optimized time of 45 min and a temperature of 200 °C.

In addition to these, non-polar polymer (LDPE)/ $n$ -Ni composites were prepared under the optimized hot molding condition at a temperature of 130 °C for 45 min.

Air annealed  $n$ -Ni (gets converted to the core-shell structure of  $n$ -Ni and NiO) was also used as fillers to study the dielectric behavior. The composites of PVDF/core-shell structure ( $n$ -Ni and NiO) were prepared under the optimized time of 45 min at 200 °C.

Another series of PVDF/ $n$ -QC (alloy) were also prepared in the form of pellets (diameter-13 mm and thickness  $\sim$ 1.5–2 mm) through hydraulic pressing referred to as the cold press samples (consolidation at room temperature and for 5 min).

In all the series, the samples have been prepared with different  $f_{\text{con}}$  in the composites to approach the  $f_c$  as closely as possible.

## 4.3 Results and Discussion

### 4.3.1 Filler Size Dependence

The observation of high value of  $\epsilon_{\text{eff}}$  and true percolative nature in hot-molded PVDF/ $\mu$ -Ni composites prompted to investigate again the effect of  $\mu$ -Ni filler in PVDF matrix composite under different process conditions. It is also known that the size of filler particles plays a major role in the determination of  $f_c$  and the magnitude of  $\epsilon_{\text{eff}}$  for a PMC. Therefore, a comparative study of filler particle size dependence is necessary. The effect of Ni filler particle size in PVDF matrix and its relation to the magnitude of  $\epsilon_{\text{eff}}$ , loss tangent (Tan  $\delta$ ), and  $f_c$  is discussed.

Reports have been investigated on the consolidated pellets of PVDF/ $\mu$ -Ni and PVDF/ $n$ -Ni composites prepared by applying 10 MPa pressure on the composite powder mixtures at room temperature. Before the electrical characterizations, we have studied the structure and morphology of the composites to ensure constituent phases and homogenous distribution of the fillers in the polymer matrix.

With the increase of  $f_{\text{con}}$  in the composites, the intensity of XRD peaks corresponding to  $f_{\text{cc}}$ -Ni phase increases with a corresponding decrement in the intensity of peaks for PVDF (Fig. 4.1). These changes confirm the formation of a two-phase composite. However, the observed broadening of Ni peaks in the case of PVDF/ $n$ -Ni (Fig. 4.1b) in the composites as compared to the PVDF/ $\mu$ -Ni (Fig. 4.1a) is attributed to the nanocrystallinity of Ni due to the reduction of its particle size. At higher  $f_{\text{con}}$ , the signature of the peaks corresponding to the polymer PVDF is not observed due to their decreased amount of PVDF in the samples. The peak positions corresponding to Ni and PVDF have indicated with their respective Miller indices of phases observed.

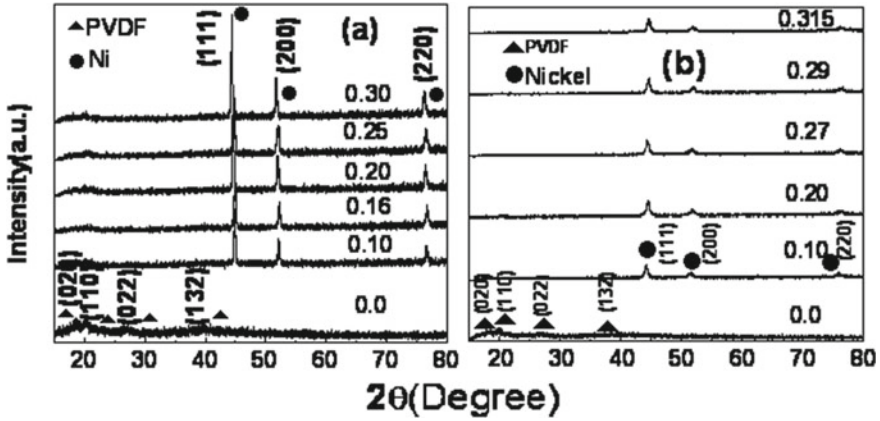


**Fig. 4.1** X-ray diffraction pattern of the PMC. **a** PVDF/ $\mu$ -Ni composites samples for  $f_{\text{con}} = 0.0$ – $0.30$  and **b** PVDF/n-Ni composites samples for  $f_{\text{con}} = 0.0$  to  $0.315$ , from bottom to top, respectively

The FTIR spectra of the PMC samples for both micron and nanocomposites in the wavenumber region of interest (i.e., fingerprint region  $\sim \nu = 1600$ – $400 \text{ cm}^{-1}$ ) are shown in Fig. 4.2. The characteristic absorption peaks due to different vibrational modes of the base polymer matrix, i.e., PVDF, are observed at  $490 \text{ cm}^{-1}$  ( $\text{CF}_2$  Bending and wagging),  $528, 615 \text{ cm}^{-1}$  ( $\text{CF}_2, \text{CCC}$ ),  $763, \text{ and } 795 \text{ cm}^{-1}$ . It has been found that most of the absorption peaks correspond to the  $\alpha$  phase of the polymer with some of the peaks remaining unidentified indicating the presence of mixed phase in the polymer PVDF matrix. With the increase of  $f_{\text{con}}$  in the composite, we do not observe any shift and broadening in absorption peak positions. We only observe the intensity of peaks gradually decreases which is due to the decrease of volume fraction of polymer in the composites with the increase of  $f_{\text{con}}$ . Hence, we confirm that there is no molecular-level interaction between the Ni clusters and the polymer matrix. This also indicates that Ni metal atoms/particles do not enter into the polymer chain of the matrix.

The typical optical micrographs of the composites in the case of PVDF/ $\mu$ -Ni composites are shown in Fig. 4.3, while the inset of Fig. 4.3a shows the surface topography of pure PVDF. The metal clusters appear as the brighter region in the matrix, while the background is the polymer matrix. It can be observed that at lower  $f_{\text{con}}$ , the metal clusters are well isolated from each other and they have been well masked by the insulating polymer matrix. With the increase of  $f_{\text{con}}$ , the micrographs indicate the random distribution of Ni clusters up to the  $f_c$  and the density of distribution of nickel clusters becomes prominent. The observation is that the density of distribution of the Ni clusters increases systematically with the increase of  $f_{\text{con}}$ . From these micrographs, it is seen that when Ni concentration is low and the particles are distributed randomly in the polymer matrix and are very isolated from each other. However, with the increase of volume fraction of Ni, the particles aggregate to

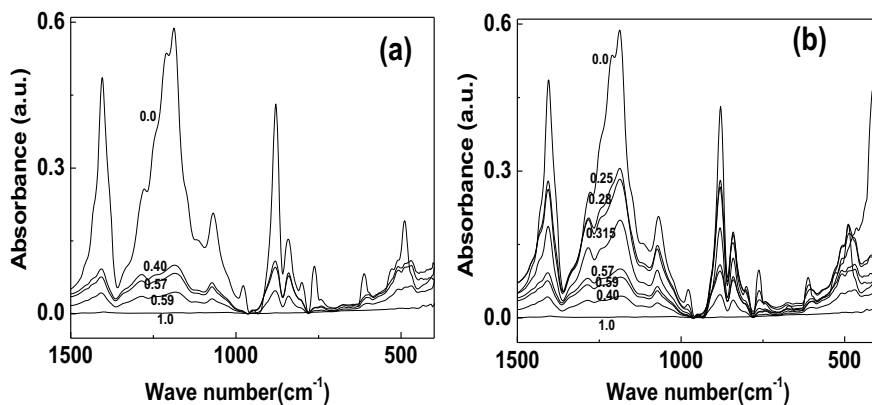


**Fig. 4.2** FTIR spectrum corresponding to some of the composites of the cold-pressed. **a** PVDF/ $\mu$ -Ni and **b** PVDF/ $n$ -Ni, composites in the wavenumber region of 1600–400  $\text{cm}^{-1}$

form large clusters and most become self-connected to form a continuous network of clusters, i.e., forming a percolation cluster. The size of the metal clusters is  $\sim 60 \mu\text{m}$ .

Similarly, the typical optical micrographs of the PVDF/ $n$ -Ni composites are shown in Fig. 4.4. Here we observe better homogeneity of the samples as compared to the

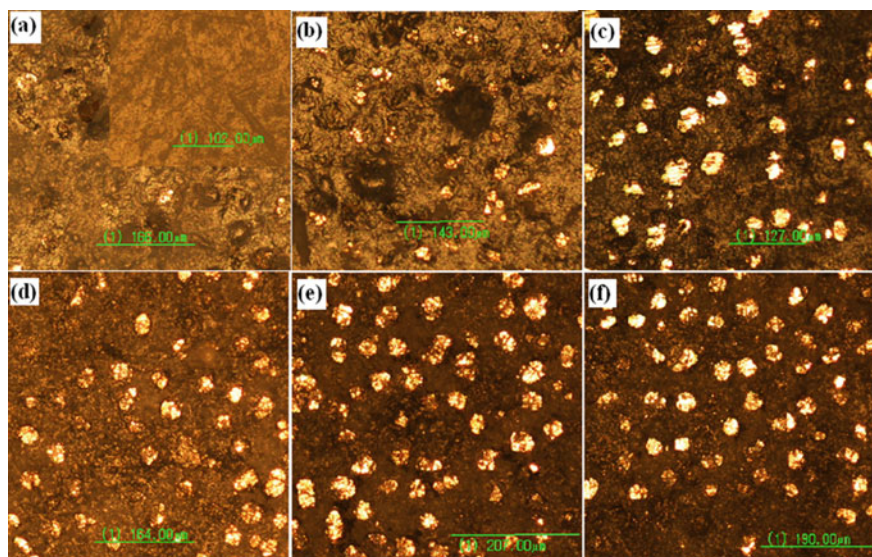


**Fig. 4.3** Optical micrographs of the polished surface of the pure PVDF and PVDF/ $\mu$ -Ni composites with different  $f_{\text{con}}$ , **a** 0.10 (inset: 0.0), **b** 0.20, **c** 0.30, **d** 0.50, **e** 0.56, and **f** 0.57, respectively, at the magnification of 50X

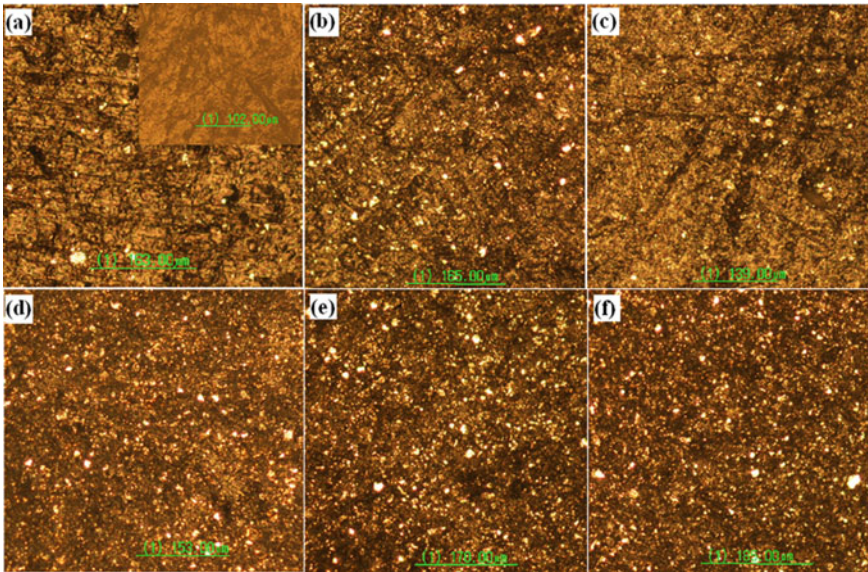


**Fig. 4.4** Optical micrographs of the polished surface of the pure PVDF and PVDF/*n*-Ni composites with different  $f_{\text{con}}$ , **a** 0.10 (inset: 0.0), **b** 0.16, **c** 0.20, **d** 0.25, **e** 0.28, and **f** 0.315, respectively, at the magnification of 50X

PVDF/ $\mu$ -Ni composites. Hence, we observe with the decrease of particle size of the metal particles that the homogeneity of the PMC can be increased.

The high-resolution FESEM surface micrographs of PMC under study are shown in Fig. 4.5a–c. From the high-resolution FESEM micrographs of the pure PVDF and PVDF/*n*-Ni composites, the Ni clusters/particles distributed randomly in the polymer matrix can be observed with particle dimensions in the range of 20–30 nm and can be estimated from high-resolution transmission electron microscope image (Fig. 4.5d).

The frequency response characteristics of  $\epsilon_{\text{eff}}$ , effective AC conductivity ( $\sigma_{\text{eff}}$ ), and  $\tan \delta$  for both  $\mu$ -Ni and *n*-Ni composites are shown in Fig. 4.6. The evolution of all the electrical parameters in both the composites appears to be the same only with the difference in their magnitudes. In the case of PVDF/ $\mu$ -Ni composites [13], the static  $\epsilon_{\text{eff}}$  of the composites increases slowly from 15 for  $f_{\text{con}} = 0.0$ –100 for  $f_{\text{con}} = 0.5$  in the lower  $f_{\text{con}}$  region. Again with the increase of  $f_{\text{con}} > 0.5$ , the static  $\epsilon_{\text{eff}}$  increases at a higher rate and its value undergoes a sharp rise to reach the value of 1300 at  $f_{\text{con}} = 0.57$  and then the decrement in static  $\epsilon_{\text{eff}}$  is observed to be 650 for  $f_{\text{con}} = 0.58$  showing a singular point in the evolution of dielectric constant as a function of  $f_{\text{con}}$ . Hence, the singular point observed in the case of PVDF/ $\mu$ -Ni composites is observed to be 0.57 which is the  $f_c$  for this series of samples. In the case of PVDF/ $\mu$ -Ni composites, the  $\epsilon_{\text{eff}}$  shows a very weak dependence of frequency over the measured frequency region, even up to a metal loading of  $f_{\text{con}} = 0.56$  at which the observed static dielectric constant was found to be 300.

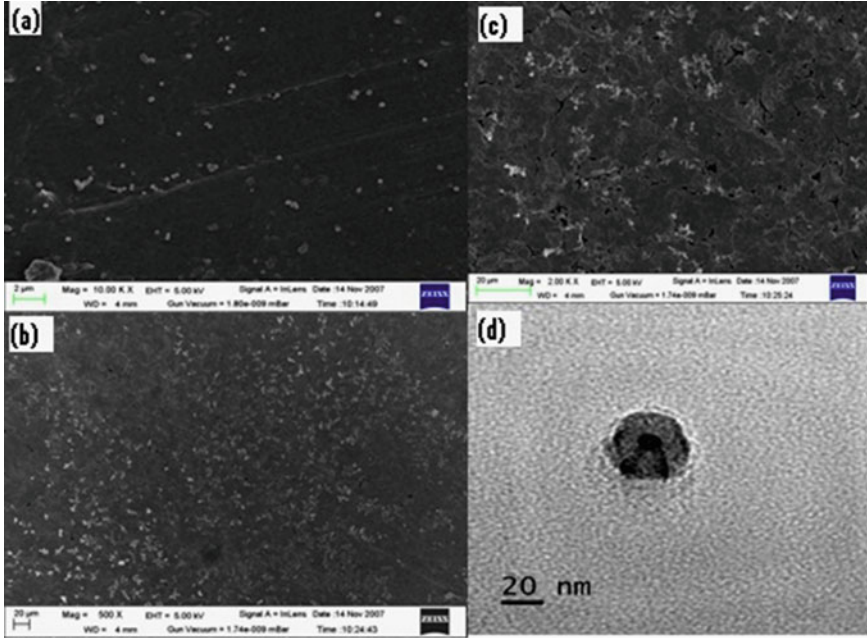


**Fig. 4.5** FESEM micrographs of the PVDF/ $n$ -Ni composites, **a**  $f_{con} = 0.0$ , **b**  $f_{con} = 0.28$  at 500X, **c**  $f_{con} = 0.28$  at 2 KX, and **d** HRTEM image of the  $n$ -Ni

Even above the  $f_c$ , ( $f_{con} = 0.57$ ) the  $\epsilon_{eff}$  in the vicinity of  $f_c$  and even after the  $f_c$  shows also a weak dependence of frequency over the whole frequency range (Fig. 4.5a). For example, in the case of  $f_{con} = 0.57$ , the  $\epsilon_{eff}$  values at 40 Hz and 10 MHz are given by 1300 and 300, maintaining a value of more than 300 at 10 MHz. Similarly for  $f_{con} = 0.58$ , the  $\epsilon_{eff}$  values at 40 Hz and 10 MHz are given by 650 and 120, respectively. Here it is interesting to mention that the observed static  $\epsilon_{eff}$  of 1300 is the highest dielectric constant among the PVDF-based PMC [12, 13]. In case of PVDF/ $n$ -Ni composites, the static  $\epsilon_{eff}$  increases from 15 for  $f_{con} = 0.0$ –2500 for  $f_{con} = 0.28$ . This value is also comparable to the magnitude of enhancement of  $\epsilon_{eff}$  in any of the PMC. The  $\epsilon_{eff}$  of the composites up to  $f_{con} = 0.25$  shows a weak dependence of frequency over the whole frequency range, but as it approaches the percolation threshold ( $f_{con} = 0.28$ ) the variation is more pronounced, i.e.,  $\epsilon_{eff}$  becomes more dispersive as compared to the PVDF/ $\mu$ -Ni composites. This may be attributed to the larger leakage currents resulting from the higher conductivity of the composites due to an increase in surface area of the particles and a decrease in the interparticle distance with reduction of metal particle size in the case of PVDF/ $n$ -Ni composites. As the measured BET surface areas of the  $\mu$ -Ni and  $n$ -Ni used are 0.03 and 1.30 m<sup>2</sup>/g, respectively, the changes in  $\epsilon_{eff}$  may be attributed to the larger leakage currents resulting from the higher conductivity of the composites as  $f_{con} \rightarrow f_c$ .

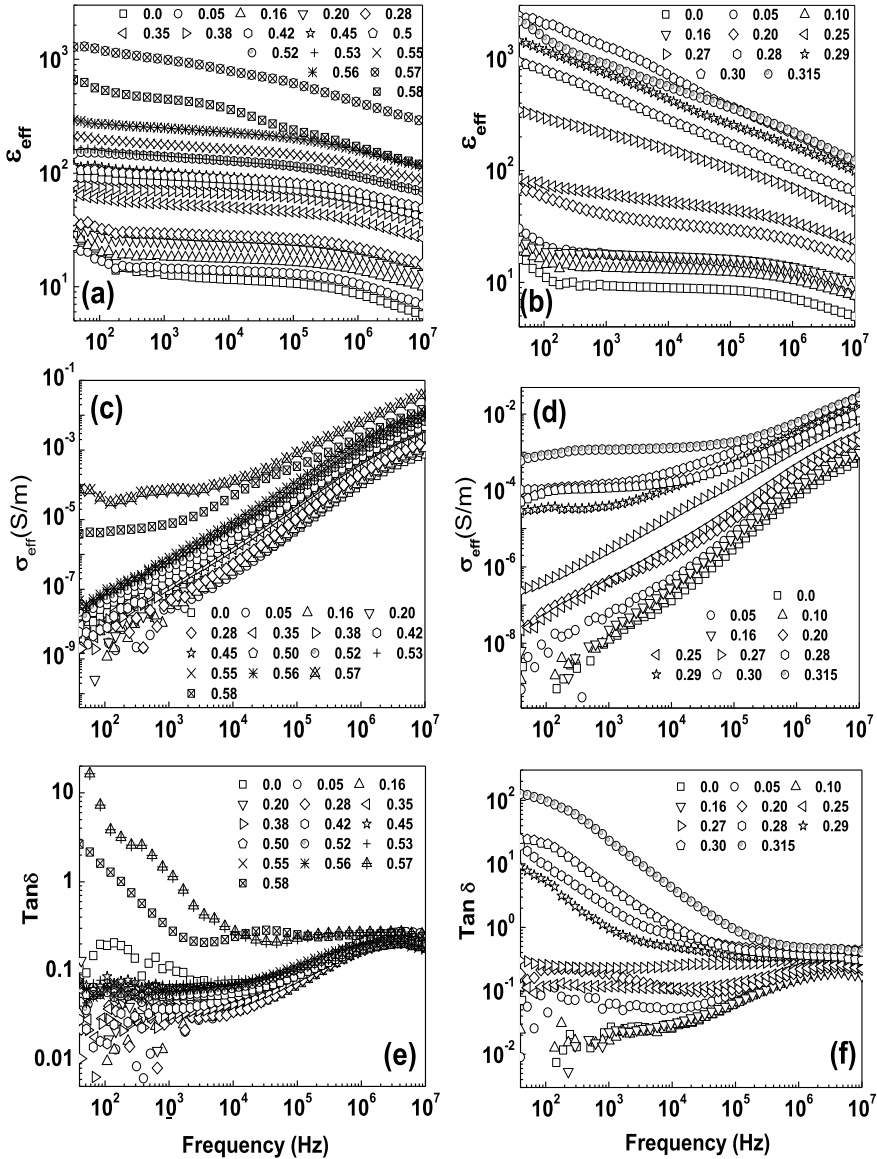


**Fig. 4.6** Dependence of the effective dielectric constant (a, b), effective conductivity (c, d), and dielectric loss tangent (e, f) on frequency for the cold-pressed PVDF/ $\mu$ -Ni and PVDF/ $n$ -Ni composites, respectively, at room temperature

The variation of  $\sigma_{\text{eff}}$  for the two series of composites is also investigated. We observe that in both cases a long-range DC conductivity plateau is observed over a certain frequency region at their respective  $f_c$ . So at  $f_c$ , a mixed conductivity of AC and DC conductivity is observed over different frequency regions, while for the samples with  $f_{\text{con}} < f_c$  only the AC conductivity is observed. Although the  $f_c$  for PVDF/ $\mu$ -Ni composites is observed at  $f_{\text{con}} = 0.57$  for  $\mu$ -Ni composites, i.e., at almost double of the concentration for PVDF/ $n$ -Ni composites ( $f_c = 0.28$ ), the conductivity values for both the percolative composites are almost of the same order over the whole frequency range (Fig. 4.6). The higher conductivity in the case of  $n$ -Ni composites is due to the enhanced extent of tunneling due to an increase in interparticle contacts and a decrease in the interparticle distance [25, 26]. It is because of the increased surface area of metal particles due to a reduction in their size. The magnitude of interparticle distance and interfacial area depends on the size and shape of the Ni particles and their volume fraction in the composite. As the particle size reduces, the number density of the particles will increase leading to a corresponding decrease in interparticle distance. This in turn increases the number of nearest neighbors for a particle due to an increase in its surface area. Further with the reduction of metal particle size, the number of clusters as well as the number of particles in a cluster increases in the matrix. As a consequence, electrons find it easier to tunnel between two and more particles/clusters due to intra (tunneling between two or more particles in the same cluster) and inter (tunneling between two or more clusters in the matrix) tunneling in the case of  $n$ -Ni composites as compared to  $\mu$ -Ni composites. So the overlapping of effective tunneling range [25, 26] of two or more particles/clusters can be obtained for  $n$ -Ni at a lower concentration than  $\mu$ -Ni in the composites. The  $\sigma_{\text{eff}}$  of the composites (Fig. 4.6) in the regime of  $f_{\text{con}} < f_c$  exhibits strong frequency dependence, while its frequency dependence becomes weaker in the regime of  $f_{\text{con}} > f_c$ .

The Tan  $\delta$  behavior for both  $\mu$ -Ni and  $n$ -Ni composites across the  $f_c$  shows identical behavior. The loss value for both the percolative composites is also of the same order over the whole frequency range (Fig. 4.6). Figure 4.6 shows the loss tangent of the composite at low frequency undergoes a sharp increase for  $f_{\text{con}} > f_c$  while maintains a value below 1 at high frequencies ( $>100$  kHz). Such a sharp rise in loss could be considered as one important feature of the percolative composite and evidence of the large leakage current in the composite. For the composite  $f_{\text{con}} < f_c$ , the loss tangent is less than 0.3 irrespective of frequency. We also observe that in both the series of composites, the Tan  $\delta$  shows a peak in its frequency evolution spectrum for  $f_{\text{con}} < f_c$  at around 2 MHz which comes due to the dipolar relaxation frequency of the polymer PVDF as there is the presence of permanent dipoles in the system. However, for  $f_{\text{con}} > f_c$ , the characteristic dipolar relaxation (DR) vanishes and a sharp rise of low-frequency dispersion of the Tan  $\delta$  is observed which is called anomalous low-frequency dispersion (ALFD). The detailed DR and ALFD have been explained in Chap. 6. The  $\sigma_{\text{eff}}$ ,  $\varepsilon_{\text{eff}}$  of the two series of cold-pressed PVDF/ $\mu$ -Ni and PVDF/ $n$ -Ni composites have been studied as a function of  $f_{\text{con}}$  and frequency. As shown in Fig. 4.7 in the case of PVDF/ $\mu$ -Ni composites, the  $\varepsilon_{\text{eff}}$  rises from 250 to 995 at 1 kHz and while  $\varepsilon_{\text{eff}}$  rises from 268 to 1218 at 100 Hz when  $f_{\text{con}}$  increases from  $f_{\text{con}} = 0.56$

to  $f_{con} = 0.57$ . Similarly, in case of PVDF/*n*-Ni composites, as shown in Fig. 4.7 the  $\epsilon_{eff}$  rises from 215 to 1273 when  $f_{con}$  increases from  $f_{con} = 0.27$  to  $f_{con} = 0.28$  at 1 kHz while it rises steeply from 255 ( $f_{con} = 0.27$ ) to 2050 ( $f_{con} = 0.28$ ) at 100 Hz (Fig. 4.7). This value of  $\epsilon_{eff}$  is comparable to the highest dielectric constant in any of the PMC reported till date.

Similarly as shown in Fig. 4.7, the value of  $\sigma_{eff}$  in case of PVDF/ $\mu$ -Ni and PVDF/*n*-Ni composites demonstrates an IMT in the vicinity of  $f_{con} = 0.57$  and  $f_{con} = 0.28$ , respectively. These experimental results have well been explained with the help of percolation theory. According to percolation theory, the power-law dependence of dielectric constant near the percolation threshold is given by Eq. (1.3).

$$\epsilon_{eff} \propto (f_c - f_{con})^{-s} \text{ for } f_{con} < f_c,$$

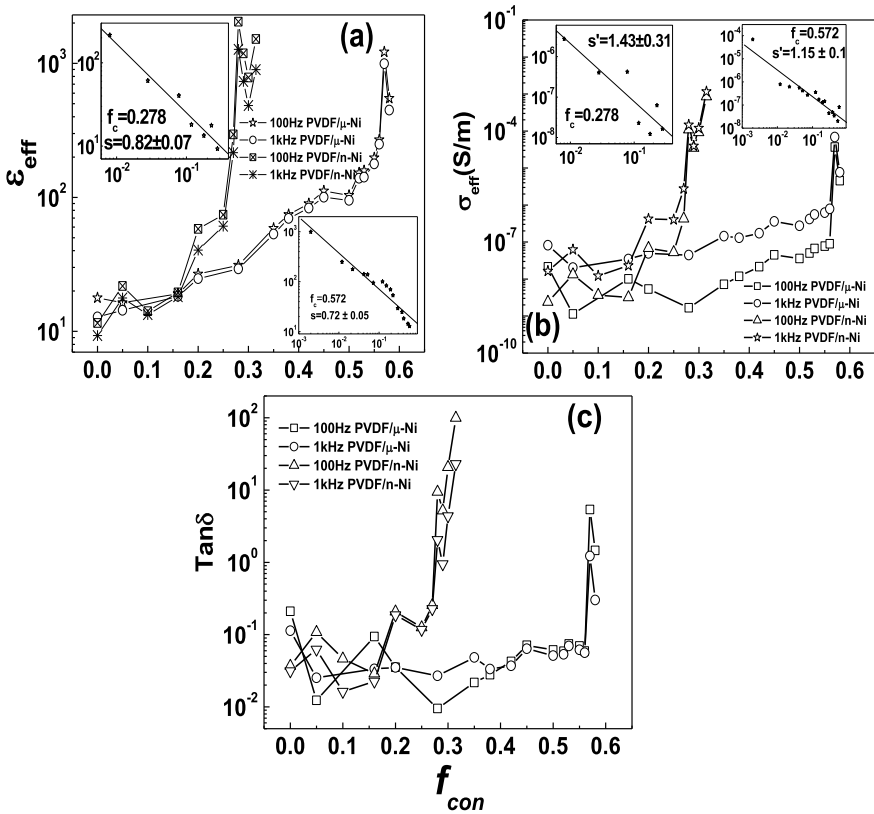


**Fig. 4.7** a Effective dielectric constant, b effective conductivity, and c effective loss tangent as a function of  $f_{con}$ , measured at 100 Hz and 1 kHz at room temperature for cold-pressed PVDF/ $\mu$ -Ni and PVDF/*n*-Ni composites, respectively. Inset a The least-square fit of  $\epsilon_{eff}$  at 1 kHz to Eq. (1.3) for cold-pressed PVDF/*n*-Ni and PVDF/ $\mu$ -Ni composites, respectively. Inset b The least-square fit of  $\sigma_{eff}$  at 1 kHz to Eq. (1.4) for cold-pressed PVDF/*n*-Ni and PVDF/ $\mu$ -Ni composites, respectively

where  $\varepsilon_{\text{eff}}$  is the effective dielectric constant,  $f_c$  is the percolation threshold, and 's' is the corresponding critical exponent in the dielectric region. In the case of PVDF/ $\mu$ -Ni composites, the measured  $\varepsilon_{\text{eff}}$  as a function of  $f_{\text{con}}$  shows divergence and follows the power-law Eq. (1.3), with  $f_c = 0.572$  and  $s = 0.72 \pm 0.05$  (Inset, Fig. 4.7a). The critical exponent  $s = 0.72$  obtained from the fit is in agreement with the universal value of  $s$  predicted for a 0–3 composite, i.e., ( $s_{\text{un}} = 0.8-1$ ). Similarly, in the case of PVDF/ $n$ -Ni composites, the measured  $\varepsilon_{\text{eff}}$  as a function of  $f_{\text{con}}$  shows divergence and follows the power-law Eq. (1.3), with  $f_c = 0.278$ ,  $s = 0.82 \pm 0.07$  (Inset, Fig. 4.7a). The critical exponent 's' is in agreement with the earlier reported value of  $s = 0.89$  [2, 12, 13] and universal value of 's' for a 0–3 composite ( $s_{\text{un}} = 0.8-1$ ).

As shown in Fig. 4.7, the  $\sigma_{\text{eff}}$  as a function of  $f_{\text{con}}$  at 1 kHz for both the series of samples increases abruptly near the critical concentration  $f_c \sim 0.57$  and 0.28 indicating the formation of the continuous conductive network in the composite. According to percolation theory, the power-law dependence of conductivity is given by Eq. (1.4)

$$\sigma_{\text{eff}} \propto (f_c - f_{\text{con}})^{-s'} \text{ for } f_{\text{con}} < f_c,$$

where  $f_{\text{con}}$  is the volume fraction of the conductor,  $f_c$  is the percolation threshold, and 's'' is the conductivity critical exponent in the insulating region. The best fit of the conductivity data of PVDF/ $\mu$ -Ni composites to Eq. (1.4) yields  $f_c = 0.572$ ,  $s' = 1.15 \pm 0.1$  (Inset, Fig. 4.7b). The exponent value  $s'$  is higher than the universal value ( $s' = 0.8-1$ ), and the higher critical exponents also have been observed in several works. The best fit of the conductivity data of PVDF/ $n$ -Ni composites to Eq. (1.4) yields  $f_c = 0.278$ ,  $s' = 1.4 \pm 0.3$  (Inset, Fig. 4.7b). The exponent value  $s'$  is higher than the universal value ( $s'_{\text{un}} = 0.8-1$ ). It is interesting to point out here that the value of  $f_c$  is consistent with the values obtained from dielectric and conductivity data, but significantly higher than that of universal values (0.16). This could be attributed to the process conditions through which the samples are prepared. This suggests that the process conditions affect only the  $f_c$  with no significant change in critical exponents. The dielectric exponent 's' found for both the composites matches well with the universal value, while the conductivity exponent in the insulating region 's'' maintains always a higher value than the universal values which is also observed from earlier pieces of literature of close to the two phases PVDF/Ni composites, i.e.,  $s' = 1.40$  [2, 12, 13]. It also observed that for both the series of samples, the dielectric loss factor (Tan  $\delta$ ) also undergoes a large change near the  $f_c$ . For PVDF/ $\mu$ -Ni composites, Tan  $\delta$  changes from 0.06 to 1.02 when  $f_{\text{con}}$  increases from 0.56 to 0.57 at 1 kHz (Fig. 4.7c) while for PVDF/ $n$ -Ni composites, Tan  $\delta$  changes from 0.25 to 2.04 when  $f_{\text{con}}$  increases from 0.27 to 0.28 at 1 kHz (Fig. 4.7c), respectively.

A significant change in  $f_c$  of 0.57 in the case of PVDF/ $\mu$ -Ni composites from the reported  $f_c$  ( $f_c = 0.16$ ) could be attributed to the sample processing conditions which give rise to an increase of adhesiveness between the filler and polymer leading to more homogeneity of the samples. But under the same processing conditions, the  $f_c$  value for PVDF/ $n$ -Ni composites was found to be at 0.28. Hence with the reduction of metal particle size, the appearance of such a change in  $f_c$  (0.28) from the respective

universal value (0.16) of  $f_c$  observed for the same system of PVDF/ $\mu$ -Ni composites could be attributed to sampling processing conditions and particle size. This may be also attributed to because the onset of percolation will occur at the same range of interparticle distance whether it may be a coarse or a fine particle. The other possibility could be because the PVDF tends to surround the nickel clusters leading to an increase of adhesiveness, such that the nickel clusters are separated by thick insulating layers (for  $f_{\text{con}} < 0.28$ ) forming a gap in the effective tunneling range of two filler clusters which probably inhibit the higher-order tunneling, similar to that has been observed in many granular composites which always show a higher value of  $f_c$  than the predicted value.

### 4.3.2 Effect of Process Conditions and Particle Size

The above analysis shows the non-ideal value of  $f_c$  in the case of PVDF/ $\mu$ -Ni and PVDF/ $n$ -Ni composites by varying the filler particle size. These composites, namely PVDF/ $\mu$ -Ni and PVDF/ $n$ -Ni, were hot molded with an idea that the  $f_c$  can be lowered by subjecting to thermal parameters (temperature and time). Due to the decrease of  $f_c$  in PMC, the flexibility of the polymer can be retained. Hence, the above two series of same composites were prepared under hot molding procedure by subjecting a difference in the process conditions to investigate the percolation behavior of these composites.

The typical optical micrographs of the composites in the case of the above two series of composites are shown in Fig. 4.8, while the inset of Fig. 4.8a shows the surface topography of pure PVDF. These micrographs indicate the random distribution of Ni clusters up to the  $f_c$  and the density of distribution of nickel clusters in the case of  $n$ -Ni composites are prominent. From these micrographs, it is seen that when Ni concentration is low, the particles are distributed randomly in the polymer matrix and are very isolated from each other. However, with the increase of  $f_{\text{con}}$ , the particles aggregate to form large clusters and most become self-connected to form a continuous network of clusters, i.e., forming a percolation cluster.

The frequency response characteristics of  $\varepsilon_{\text{eff}}$ ,  $\sigma_{\text{eff}}$ , and  $\tan \delta$  for both  $\mu$ -Ni and  $n$ -Ni composites prepared under the hot molding processing are shown in Fig. 4.9, and the evolution of all the electrical parameters appears to be identical with the previous two series of cold-pressed  $\mu$ -Ni and  $n$ -Ni composites with only the difference of  $f_c$ . In the case of PVDF/ $\mu$ -Ni composites, in the region of  $f_{\text{con}} < f_c$  ( $f_c = 0.26$ ) the  $\varepsilon_{\text{eff}}$  of the composites shows a weak dependence of frequency over the whole frequency range (Fig. 4.9) and also the static  $\varepsilon_{\text{eff}}$  increases from 10 for  $f_{\text{con}} = 0.0$  to 310 for  $f_{\text{con}} = 0.25$ . For  $f_{\text{con}} = 0.26$ , the sample becomes completely conducting, and a negative value of static  $\varepsilon_{\text{eff}}$  is observed. Hence, the value of  $f_c$ , in this case, exists definitely between 0.25 and 0.26. In the case of PVDF/ $n$ -Ni composites, the  $\varepsilon_{\text{eff}}$  of the composites up to  $f_{\text{con}} = 0.065$  shows a weak dependence of frequency over the whole frequency range, and the value of static  $\varepsilon_{\text{eff}}$  increases from 10 for  $f_{\text{con}} = 0.0$  to 300 for  $f_{\text{con}} = 0.65$ . The  $f_c$  observed for the PVDF/ $n$ -Ni composites is at  $f_{\text{con}} = 0.07$

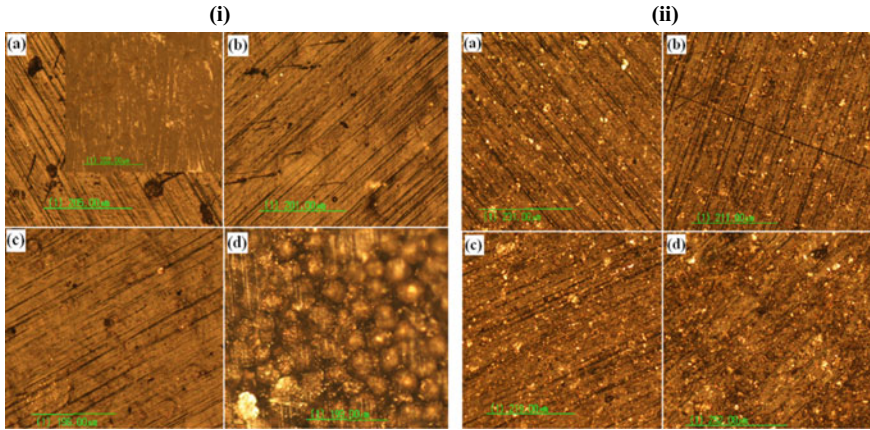


**Fig. 4.8** Optical micrographs of the polished surface of the hot molded (i) PVDF/ $\mu$ -Ni composites with different  $f_{\text{con}}$ , **a** 0.10, inset: Pure PVDF, **b** 0.16, **c** 0.20, **d** 0.26, and (ii) PVDF/ $n$ -Ni composite samples with different  $f_{\text{con}}$ , **a** 0.03, **b** 0.05, **c** 0.06, and **d** 0.07, respectively

at which the observed static  $\epsilon_{\text{eff}}$  is found to be 3000. We observe for both the series of composites as  $f_{\text{con}} \rightarrow f_c$  the variation of  $\epsilon_{\text{eff}}$  over the measured frequency region is more pronounced, i.e., dielectric constant becomes more dispersive. This may be attributed to the larger leakage currents resulting from the higher conductivity of the composites due to the increase in connectivity of the metal filler particles due to the difference in process conditions.

It can be observed from Fig. 4.9 that in the case of  $f_{\text{con}} = 0.26$  in case of PVDF/ $\mu$ -Ni composites, only pure DC conduction is observed which is due to the complete connectivity among the metallic clusters giving rise to a metallic behavior while for  $f_{\text{con}} = 0.07$  in case of PVDF/ $n$ -Ni composites a mixed conductivity comprising DC and AC conduction is observed. Although the  $f_c$  value is achieved at  $f_{\text{con}} = 0.26$  for  $\mu$ -Ni composites and  $f_{\text{con}} = 0.25$  remains as an insulator (Fig. 4.9), i.e., at almost containing four times of the  $f_c$  for  $n$ -Ni composites (i.e.,  $f_c = 0.07$ ), the conductivity value for  $f_c = 0.07$  in case of PVDF/ $n$ -Ni composites is higher than the  $f_{\text{con}} = 0.25$  in case of PVDF/ $\mu$ -Ni composites even if it contains a higher metallic fraction. The higher conductivity in the case of  $n$ -Ni composites is due to the enhanced extent of overlapping of the tunneling range of the filler particles which is feasible due to the development of connectivity among the metallic clusters due to different processing conditions, and as a consequence, electrons find it easier to tunnel between two or more particles/clusters. The  $\text{Tan } \delta$  pattern with frequency shows identical evolution for both the series of composites. The  $\text{Tan } \delta$  shows a dipolar relaxation for all the samples corresponding to  $f_{\text{con}} < f_c$ , while it shows an anomalous low-frequency dispersion for  $f_{\text{con}} > f_c$ . The value of low-frequency  $\text{Tan } \delta$  undergoes a sharp change in its value across the  $f_c$ .

The  $\sigma_{\text{eff}}$  and  $\epsilon_{\text{eff}}$  of the two series of hot-molded PVDF/ $\mu$ -Ni and PVDF/ $n$ -Ni composites have been studied as a function of  $f_{\text{con}}$  and frequency. As shown in

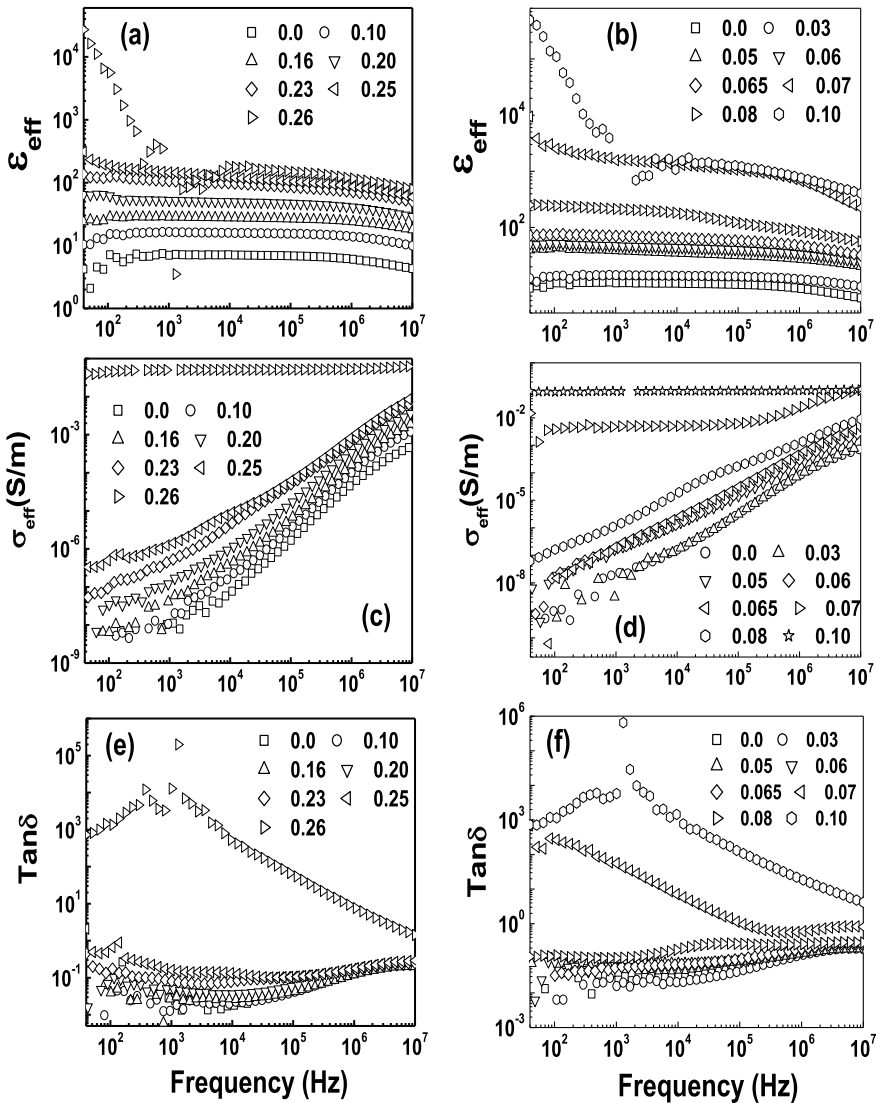


**Fig. 4.9** Dependence of the effective dielectric constant (a, b), effective conductivity (c, d), and dielectric loss tangent (e, f) on frequency for the hot-molded PVDF/ $\mu$ -Ni and PVDF/ $n$ -Ni composites, respectively, at room temperature

Fig. 4.10a in the case of PVDF/ $\mu$ -Ni composites, the  $\epsilon_{\text{eff}}$  rises from 145 to a negative value  $-69$  (metallic) at 1 kHz and while  $\epsilon_{\text{eff}}$  rises from 186 to 5500 (metallic) at 100 Hz when  $f_{\text{con}}$  increases from  $f_{\text{con}} = 0.25$  to  $f_{\text{con}} = 0.26$ . Similarly, in case of PVDF/ $n$ -Ni composites, the  $\epsilon_{\text{eff}}$  rises from 70 to 1560 when  $f_{\text{con}}$  increases from  $f_{\text{con}} = 0.065$  to  $f_{\text{con}} = 0.07$  at 1 kHz, while it rises steeply from 74 ( $f_{\text{con}} = 0.065$ ) to

2762 ( $f_{con} = 0.07$ ) at 100 Hz (Fig. 4.10a). This value of  $\epsilon_{eff}$  is also comparable to the highest  $\epsilon_{eff}$  in any of the PMC reported till date. Similarly as shown in Fig. 4.10b, the value of  $\sigma_{eff}$  in case of PVDF/ $\mu$ -Ni and PVDF/ $n$ -Ni composites demonstrates an IMT in the vicinity of  $f_{con} = 0.26$  and  $f_{con} = 0.07$ , respectively.

These experimental results have well been explained with the help of percolation theory. In the case of hot-molded PVDF/ $\mu$ -Ni composites, the measured  $\epsilon_{eff}$  as a function of  $f_{con}$  shows divergence and follows the power-law Eq. (1.3), with  $f_c = 0.259$  and  $s = 0.90 \pm 0.10$  (Inset, Fig. 4.10a). The critical exponent  $s = 0.75$  obtained from the fit is in agreement with the universal value of ‘ $s$ ’ predicted for a 0–3 composite, i.e., ( $s_{un} = 0.8–1$ ). Similarly, in the case of hot-molded PVDF/ $n$ -Ni composites, the measured  $\epsilon_{eff}$  as a function of  $f_{con}$  shows divergence and follows the power-law Eq. (1.3), with  $f_c = 0.07$ ,  $s = 0.75 \pm 0.10$  (Inset, Fig. 4.10a). The critical exponent ‘ $s$ ’ is in agreement with the earlier reported value of  $s = 0.89$  and universal value of ‘ $s$ ’ for a 0–3 composite ( $s_{un} = 0.8–1$ ) [23, 24].

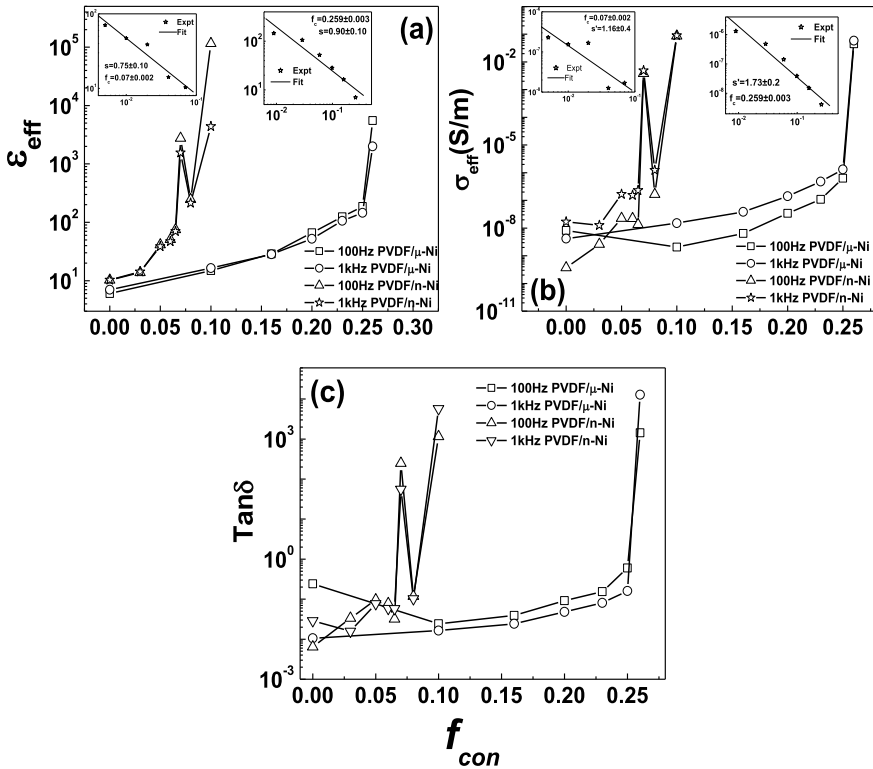


**Fig. 4.10** **a** Effective dielectric constant, **b** effective conductivity, **c** effective loss tangent as a function of  $f_{con}$ , measured at 100 Hz and 1 kHz at room temperature for hot-molded PVDF/ $\mu$ -Ni and PVDF/ $n$ -Ni composites, respectively. Inset **a** The least-square fit of  $\epsilon_{eff}$  at 1 kHz to Eq. (1.3) for hot-molded PVDF/ $n$ -Ni and PVDF/ $\mu$ -Ni composites, respectively. Inset **b** The least-square fit of  $\sigma_{eff}$  at 1 kHz to Eq. (1.4) for hot-molded PVDF/ $n$ -Ni and PVDF/ $\mu$ -Ni composites, respectively

As shown in Fig. 4.10b, the  $\sigma_{\text{eff}}$  as a function of  $f_{\text{con}}$  at 1 kHz for both the series of samples increases abruptly near the critical concentration  $f_c \sim 0.259$  and 0.07 indicating the formation of the continuous conductive network in the composite. The best fit of the conductivity data of PVDF/ $\mu$ -Ni composites to Eq. (1.4) yields  $f_c = 0.259$ ,  $s' = 1.73 \pm 0.20$  (Inset, Fig. 4.10b). The best fit of the conductivity data of PVDF/ $n$ -Ni composites to Eq. (1.4) yields  $f_c = 0.07$ ,  $s' = 1.16 \pm 0.4$  (Inset, Fig. 4.10b). The exponent value  $s'$  is higher than the universal value ( $s'_{\text{un}} = 0.8-1$ ). It is interesting to point out here that the value of  $f_c$  is consistent with the values obtained from dielectric and conductivity data, but significantly different from that of cold-pressed composites as well as also from that of universal value (0.16). This could be attributed to the process conditions through which the samples are prepared. The dielectric exponent ' $s$ ' found for both the composites matches well with the universal value, while the conductivity exponent in the insulating region ' $s'$ ' maintains always a higher value than the universal values. We also observe that the process conditions affect the value of  $f_c$ , the magnitude of critical exponents, and also the electrical parameters are found to be different from that of the cold press composites. A detailed description regarding these features has been discussed in Chap. 5.

We also observe that for both the series of samples, the  $\text{Tan } \delta$  also undergoes a large change near the  $f_c$ . For PVDF/ $\mu$ -Ni composites,  $\text{Tan } \delta$  changes from 0.16 to 12,828 at 1 kHz, while it changes from 0.59 to 1434 at 100 Hz (Fig. 4.10c), respectively, when  $f_{\text{con}}$  increases from 0.25 to 0.26. For PVDF/ $n$ -Ni composites,  $\text{Tan } \delta$  changes from 0.05 to 55 when  $f_{\text{con}}$  increases from 0.065 to 0.07 at 1 kHz, while it changes from 0.03 to 247 at 100 Hz (Fig. 4.10c), respectively.

A significant change in  $f_c$  of 0.259 and 0.07 in the case of PVDF/ $\mu$ -Ni and PVDF/ $n$ -Ni composites, respectively, from the same cold-pressed composites as 0.57 and 0.28, respectively, could be attributed to the sample processing conditions which give rise to an increase of extent of connectivity and decrease of adhesiveness between the filler and polymer leading to more heterogeneity of the samples. Hence in the case of hot-molded samples also, with reduction of metal particle size, a huge change in  $f_c$  (0.07) of PVDF/ $n$ -Ni from the  $f_c = 0.259$  of PVDF/ $\mu$ -Ni composites occurred and none of the values of  $f_c$  for four series of composites does coincide with the universal value of  $f_c$  (i.e., 0.16).

Hence what we observed from the hot-molded and cold-pressed samples is that the value of  $f_c$  has sharply changed with respect to the cold press samples. The magnitude of  $\varepsilon_{\text{eff}}$  observed is greater than the cold press composites, with a lower amount of metallic content but of course with a higher value of  $\text{Tan } \delta$ . The magnitude of critical exponents is found to be different for different series of PMC. With the reduction of metal particle size, the  $f_c$  has been greatly changed. Now in the following discussion how the external parameters, like temperature and time, process conditions, nature of filler, and polymer matrices, affect the percolation behavior in PMC is discussed.

### 4.3.3 Effect of Temperature and Time

In this section, a systematic study is taken up to optimize  $f_c$  as a function of various parameters including materials processing conditions, shape, and size of the fillings, time of mixing, temperature and time of compression hot molding, etc., for PVDF/ $\mu$ -Ni composites. The aim is to investigate the effect of heat treatment and its duration on tailoring the value of  $f_c$  in a PMC. It is seen that the thermal effects do play an important role in lowering the value of  $f_c$  [16].

Figure 4.11 shows the variation of  $\epsilon_{\text{eff}}$ ,  $\sigma_{\text{eff}}$ , and  $\text{Tan } \delta$  of all the composite samples of  $f_{\text{con}} = 0.0, 0.05, 0.10, 0.16, 0.18, 0.22, 0.27, 0.32, 0.40,$  and  $0.403$  molded under  $200^\circ\text{C}$  and for 12 min. We can observe from Fig. 4.11a that there is a sudden increment in  $\epsilon_{\text{eff}}$  for the sample 0.40 as compared to the sample 0.32. The static  $\epsilon_{\text{eff}}$  increases from 50 for  $f_{\text{con}} = 0.32$  to 133 for  $f_{\text{con}} = 0.40$  (Fig. 4.11a). The  $\epsilon_{\text{eff}}$  at 0.40 is 13 times the dielectric constant of the pure polymer matrix. As this is a macroscopically heterogeneous system consisting of two components of significantly different permittivity and conductivity, because of Maxwell [27], Wagner [28], Sillars [29] (MWS) interfacial polarization due to the accumulation of charges at the interface of a metal and insulating polymer, the charge is blocked. That is the charge suffers resistance to flow and indirectly leads to the storage of charge and thereby increases the capacitance and hence the  $\epsilon_{\text{eff}}$ . This increase continues with an increase in more interfaces with the increase in metal content in the composite. Below the critical concentration of the filler loading, the interparticle distance is large enough, so that neighboring local fields do not interact. Thus, dielectric factor in this region increases slowly. But as the filler loading increases, the MWS effect increases due to a reduction in the interaggregate/cluster/particle distance giving rise to higher dielectric properties. The contribution to  $\epsilon_{\text{eff}}$  for the pure PVDF and as well as for all other samples below  $f_c$  from dipolar polarization becomes negligible at high frequencies, i.e., above  $10^5$  Hz (Fig. 4.11a) which is attributed to the dipolar relaxation within that frequency range and can be observed from Fig. 4.11c that there is also a relaxation peak in  $\text{Tan } \delta$  versus frequency over that frequency range for all the samples below 0.32, i.e., in the insulating side. The 0.40 sample doesn't show any dipolar relaxation peak because it is in the deep metallic region and it becomes a charge carrier-dominated system. When it becomes a charge carrier-dominated system, the response from the permanent dipoles of PVDF in the composites becomes dominated. As it is a charge carrier-dominated system, 0.40 shows anomalous low-frequency dispersion (ALFD) [94] in its  $\epsilon_{\text{eff}}$  and  $\text{Tan } \delta$  as a function of frequency (See for 0.40 sample in Fig. 4.11a, c) discussed in Chap. 6. The dipolar relaxation occurring for all the samples below 0.32, i.e., below  $f_c$  is attributed to the presence of polar groups ( $-\text{F}$ ) in PVDF in all the composites. We can observe from the dielectric data for 0.403 samples (Fig. 4.11a) for which there is a very fluctuation in  $\epsilon_{\text{eff}}$  and also shows the negative value of  $\epsilon_{\text{eff}}$  over certain frequencies is observed which is because the 0.403 sample becomes completely metallic. The static  $\epsilon_{\text{eff}}$  for this sample is also very high, i.e.,  $>50,000$ , and this infinite value of  $\epsilon_{\text{eff}}$  occurs for conductors only.

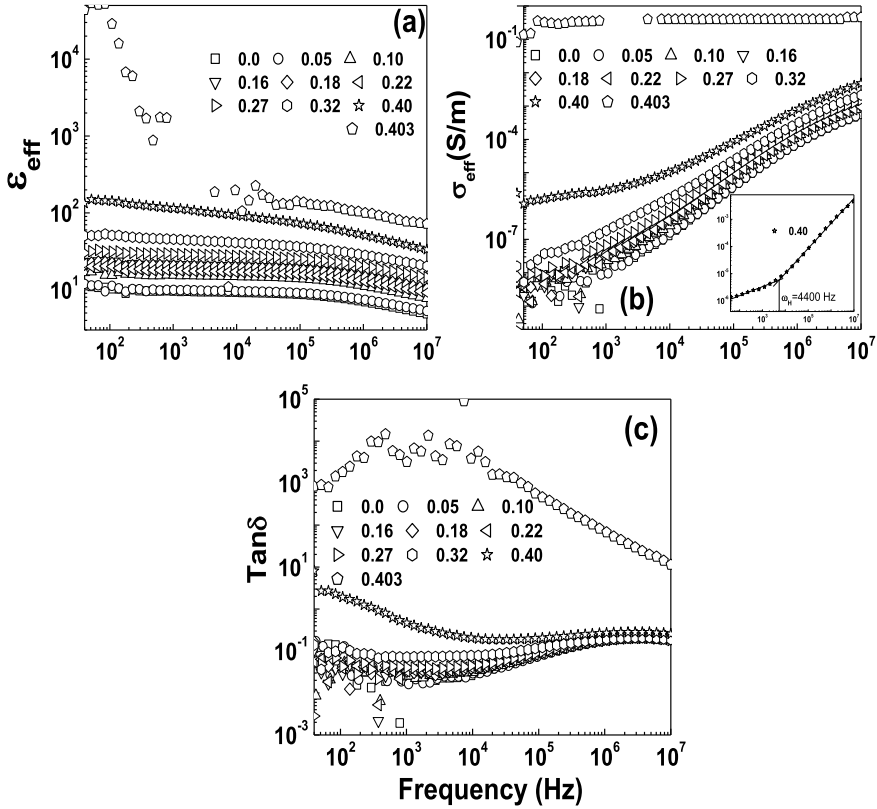


**Fig. 4.11** Variation of **a** effective dielectric constant, **b** effective conductivity, and **c** loss tangent as a function of frequency for all the composites molded under 200 °C for 12 min with different  $f_{con}$ . The solid line for the sample  $f_{con} = 0.40$  in the inset of Fig. 4.11b shows the fits in evaluating  $\omega_c$  value, which is found to be 4400 Hz

From the AC conductivity graph (Fig. 4.11b), it can be noticed that there is an abrupt increase in DC conductivity at low frequencies for  $f_{con} = 0.40$  as compared to  $f_{con} = 0.32$  which is also expected from the percolation theory. Thus from this data, it is obvious that  $f_c$  lies between 0.32 and 0.40. One can observe for the sample 0.40 that AC conductivity is independent of frequency up to a limiting frequency beyond which the AC conductivity increases with frequency obeying Jonscher's universal power-law [30]. The DC conductivity independent of frequency is coming due to long-range connectivity across the bulk resistance of the composite due to the occurrence of physical contacts among the filler clusters, while the increase in AC conductivity after a certain frequency is explained due to the hopping of localized charge carriers within the localized sites. Jonscher's universal dielectric response law is given by Eq. (2.25)

$$\sigma_{ac} = \sigma_{dc} + A\omega^k,$$

where  $\sigma_{dc}$  is the DC conductivity and  $\omega$  is the angular frequency. The fitting of the above equation to the conductivity data for 0.40 sample shows that the value of ‘ $k$ ’ was found to be 0.78 which is well within Jonscher’s universal value of between 0 and 1. The frequency which separates the region of AC and DC conductivity region is called critical frequency or hopping frequency ( $\omega_H$ ). The  $\omega_H$  is normally determined by locating the intersection of the lines that are tangent to the frequency-dependent and frequency-independent regions. Above  $\omega_H$ , the conductivity increases according to Jonscher’s power-law behavior  $\sigma(\omega) \propto \omega^k$ , where  $\omega$  is the frequency of the applied electric signal. The  $\omega_H$  value is found from the fits which is 4400 Hz (Inset, Fig. 4.11b) and separates the region of AC and DC conductivity. For other samples, i.e., from 0.0 to 0.32, the DC conductivity value is very less as there is no physical contact between the filler clusters. For the sample 0.403, the conductivity is complete of DC conduction and there is no effect of frequency on the conductivity which is because of the development of complete physical connectivity among the filler clusters giving rise to a completely metallic nature.

The sudden increment in  $\tan \delta$  which is also a feature of percolation can be observed for the sample 0.40 as compared to the 0.32 sample (Fig. 4.11c). For the sample 0.403, very high loss of  $>1000$  is observed as it becomes metallic. The difference in microstructure and how the filler clusters approach each other with the increase of concentration of the metallic filler can be observed from the optical micrographs shown in Fig. 4.12.

Thus, it can be concluded from the above discussion that the value of  $f_c$  found under this condition of sample preparation is between 0.32 and 0.40. But under the same processing conditions, the  $f_c$  was found at 0.16 for the same composites of PVDF/ $\mu$ -Ni. These differences could be attributed to the processing time. Therefore, by varying the duration of hold time it may be possible to further lower the value of  $f_c$ . With this idea, one of the samples, i.e., 0.22 just above 0.16, i.e., the ideal  $f_c$  was hot molded for different hold times by keeping temperature fixed at 200 °C.

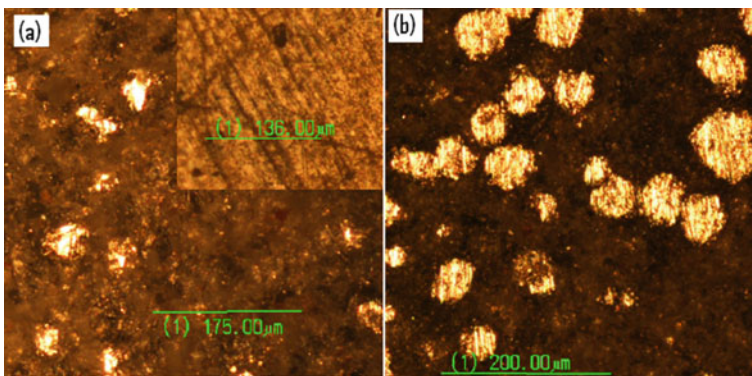


**Fig. 4.12** Optical micrographs of the composites with different  $f_{con}$  molded at 200 °C for 12 min, **a**  $f_{con} = 0.22$  and **b**  $f_{con} = 0.32$ . Inset:  $f_{con} = 0.0$ , i.e., pure polymer PVDF

The composite 0.22 shows a value of static  $\epsilon_{\text{eff}}$  of 15 for the room temperature compacted sample. With the increase of heat treatment for different timings, the value of static  $\epsilon_{\text{eff}}$  increases slowly to 18 for the sample with a cure time of 12 min, 43 for 30 min, 50 for 45 min, and 50 for 90 min (Inset, Fig. 4.13a). We observe that the thermal effects do play a role up to a certain limiting time (for a particular concentration of the conductor) and after that, there is no impact of time on percolation and interparticle distance. We can observe also from Fig. 4.13b, c that the value of  $\sigma_{\text{eff}}$  and  $\text{Tan } \delta$  also increases with the increase of hold time for the composite sample 0.22. The  $\sigma_{\text{eff}}$  is found to increase from  $10^{-8}$  to  $10^{-7} \Omega^{-1} \text{ m}^{-1}$  at 1 kHz for  $f_{\text{con}} = 0.22$  (Inset, Fig. 4.13b). The value of  $\text{Tan } \delta$  also increases from 0.02 to 0.04 at 1 kHz for  $f_{\text{con}} = 0.22$  for different hot molding timings (Inset, Fig. 4.13c). The overall mechanism is that the interfacial area and interparticle distance are likely the key parameters in controlling the properties of the composites. The increase in dielectric constant is due to the decrease in intercluster/particle distance and decrease in viscosity of the polymer leading to less adhesiveness of the polymer with metal such that it helps in increase of accumulation of charges at the metal/polymer interface. The increase in AC conductivity and loss tangent is due to more probability of tunneling with a decrease in interfiller cluster distance and increase in the overlapping of the effective tunneling range of the two filler clusters and decrease in viscosity of the polymer with an increase of heat content leading to less adhesiveness of the polymer with metal which can be observed from the optical micrographs (Fig. 4.14). But the effect of increment occurs up to a certain extent and after that heat treatment cannot lower down the percolation if the concentration of filler and spatial distribution connectivity is not there. This is evidenced by invariant values of  $\epsilon_{\text{eff}}$ ,  $\sigma_{\text{eff}}$ , and  $\text{Tan } \delta$  for the sample molded for 45 and 90 min (Fig. 4.13). In fact, these values tend to saturate instead of undergoing IMT as a function of molding time. Thus what we conclude that the effective range of metal concentration for percolation lies above 0.22 and below 0.40, i.e.,  $(0.22 < f_c \leq 0.40)$ . Previous reports on identical systems give  $f_c = 0.16$  and  $f_c = 0.57$  observed by us [12, 13]. The large change in  $f_c$  from 0.57 to less than 0.40, i.e.,  $(0.22 < f_c \leq 0.40)$  is explained as due to the heat energy which helps in the diffusion of the metal particles into the polymer matrix; as a consequence, the cluster size of the metal particles increases. Due to an increase in cluster size, more physical contacts are developed giving rise to long-range DC conductivity which is a typical feature of percolation. Due to the increase in heat treatment, viscosity of the polymer decreases leading to a decrease in intercluster distance and wetting of the polymer to metal also. Thus, we observed the value of  $f_c$  in PMC/PCC is predominantly controlled by the processing conditions.

#### 4.3.4 Effect of Matrices

In the earlier sections, it has been discussed the effect of filler particle size and process conditions on the value of  $f_c$  and the different electrical parameters. Now the role of the matrix to answer the questions like whether the polymer matrix plays any

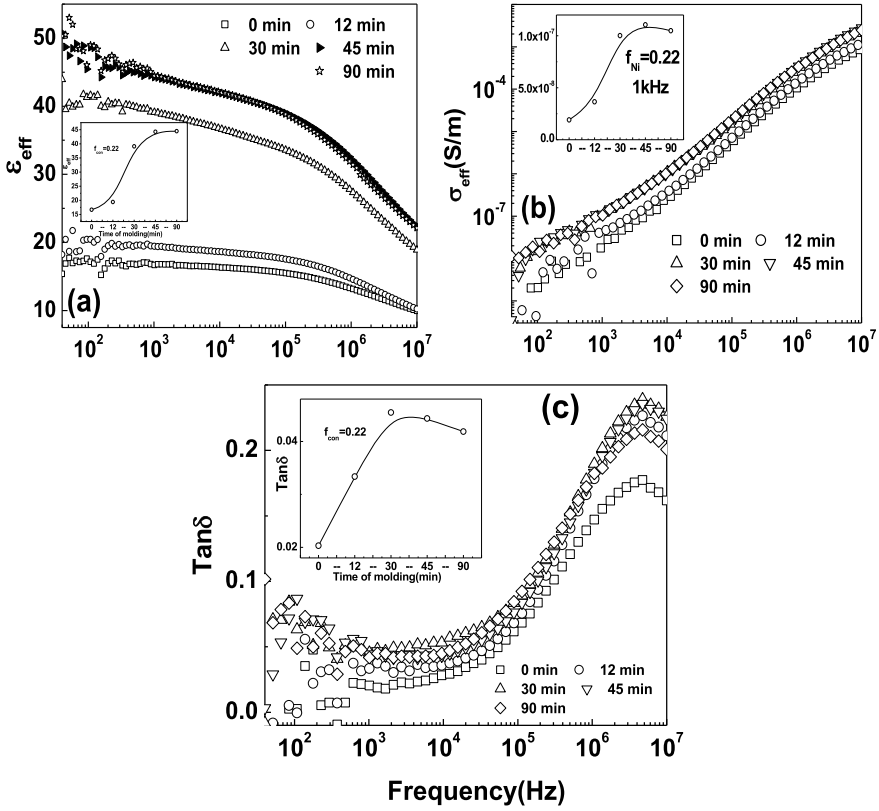


**Fig. 4.13** Variation of **a** effective dielectric constant, **b** effective AC conductivity, and **c** loss tangent for the sample with  $f_{con} = 0.22$  molded for different timings as a function of frequency; Inset: **a** effective dielectric constant, **b** effective AC conductivity, and **c** loss tangent versus molding time at 1 kHz for  $f_{con} = 0.22$  sample

role in enhancing  $\epsilon_{eff}$  or in the extent of enhancement of  $\epsilon_{eff}$  will be discussed. The composites have been prepared with a non-polar polymer matrix, and the percolation behavior in the case of PMC has been compared with that of the previously discussed PMC based on polar/ferroelectric polymer matrix, i.e., PVDF. The non-polar polymer matrix (LDPE) is a very good insulator whose dielectric constant is very low  $\sim 2$  due to the non-contribution of dipolar polarization. It is shown that with the increase of  $f_{con}$ , the  $\epsilon_{eff}$  of a PMC is increased and the magnitude of the extent of enhancement of  $\epsilon_{eff}$  becomes very low as compared to the polar PMC at  $f_c$ .

Before discussing the electrical properties, the structural and morphological properties of these non-polar PMC have been studied. With the increase of  $f_{con}$  in the composites, the intensity of XRD peaks corresponding to  $fcc$ -Ni phase increases with a corresponding decrement in the intensity of peaks for LDPE (Fig. 4.15a). These changes confirm the formation of a two-phase composite. However, the observed broadening of Ni peaks in the composites is attributed to the nanocrystallinity of

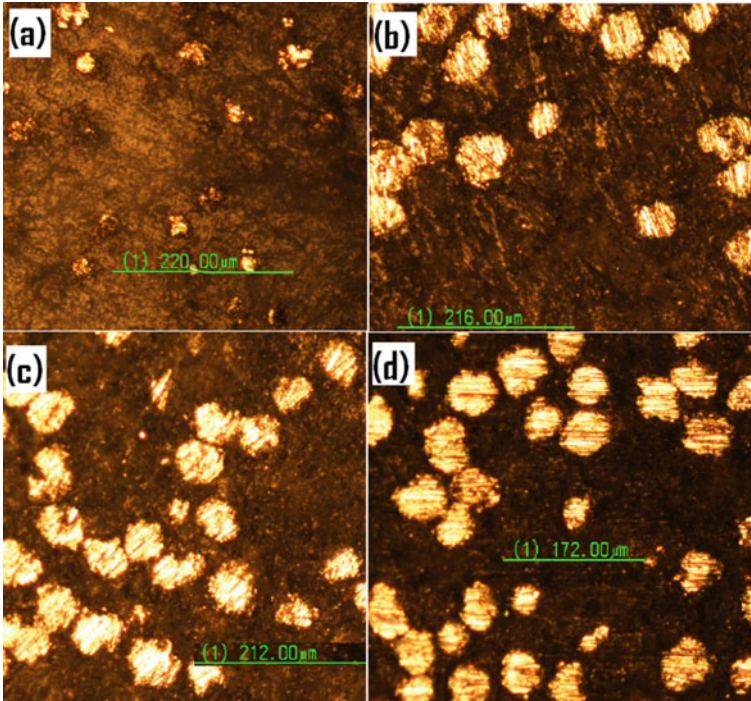


**Fig. 4.14** Optical micrographs of the composite sample with  $f_{\text{con}} = 0.22$  molded at 200 °C for different timings, **a** 0 min, **b** 30 min, **c** 45 min, and **d** 90 min

Ni due to the reduction of its particle size. The optical micrographs of four typical composites with  $f_{\text{con}} = 0.03$ – $0.07$  in the LDPE matrix are shown in Fig. 4.15b–e. From these micrographs, it is seen that when  $n$ -Ni concentration is low the particles are distributed randomly in the polymer matrix. However with the increase of the particles, they become aggregated to form large clusters and most become self-connected to form a continuous network of clusters.

The  $\sigma_{\text{eff}}$ ,  $\varepsilon_{\text{eff}}$ , and  $\tan \delta$  of the composites based on the LDPE matrix have been studied as a function of frequency and  $f_{\text{con}}$  at 300 K. As shown in Fig. 4.16a, the static  $\varepsilon_{\text{eff}}$  value rises from 2 to 25 when  $f_{\text{con}}$  varies from 0.0 to 0.05. However, even at  $f_{\text{con}} = 0.06$ , which is observed to be the  $f_c$  for these composites, the static  $\varepsilon_{\text{eff}}$  value is only 74, while the value of static  $\varepsilon_{\text{eff}}$  in the case of PVDF matrix composites maintains at a level of  $>2000$  (Refer Fig. 4.9b). Hence, we observe that polymer matrix plays a major role in the enhancement of  $\varepsilon_{\text{eff}}$  at  $f_c$ . Due to the high dielectric constant of PVDF having permanent dipolar polarization, the extent of enhancement in  $\varepsilon_{\text{eff}}$  is tuned while it does not happen in the case of non-polar LDPE composites. The  $\varepsilon_{\text{eff}}$  of the composites up to  $f_{\text{con}} = 0.05$  shows a weak dependence of frequency over the whole frequency range, but as it approaches  $f_c = 0.06$ , the variation is more

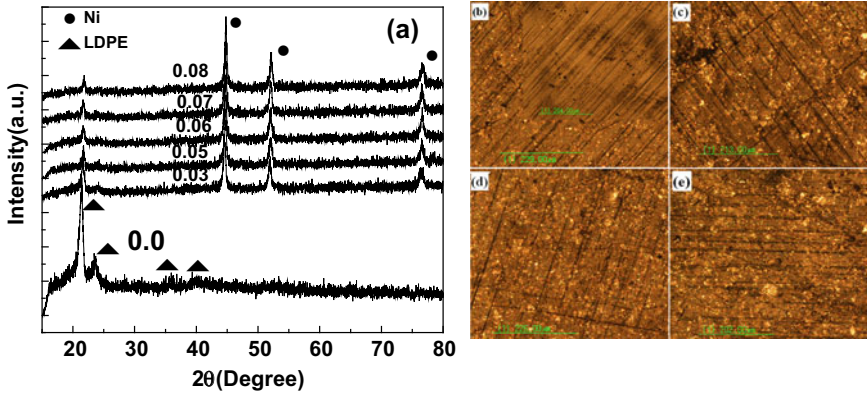


**Fig. 4.15** **a** X-ray diffraction pattern of LDPE/*n*-Ni composite samples for  $f_{\text{con}} = 0.0$ – $0.08$  from bottom to top, respectively; Optical micrographs of the polished surface of the pure LDPE and LDPE/*n*-Ni composite with different  $f_{\text{con}}$ , **b**  $f_{\text{con}} = 0.03$ , Inset: pure LDPE, **c**  $f_{\text{con}} = 0.05$  and **d**  $f_{\text{con}} = 0.06$ , **e**  $f_{\text{con}} = 0.07$

pronounced (Fig. 4.16a). The changes in  $\varepsilon_{\text{eff}}$  may be attributed to the larger leakage currents resulting from the higher conductivity of the composites as  $f_{\text{con}} \rightarrow f_c$ .

The  $\sigma_{\text{eff}}$  of the composites (Fig. 4.16b) in the regime of  $f_{\text{con}} < f_c$  exhibits a strong frequency dependence, while its frequency dependence becomes gradually weaker in the regime of  $f_{\text{con}} > f_c$ . In this PMC, at  $f_c$  a mixed conductivity comprising AC and DC conductivity is also obtained, but the region of DC plateau remains over a very narrow range of frequencies, while a broader region of DC conductivity was found for hot-molded PVDF/*n*-Ni composites (Fig. 4.9d), which is entirely due to the properties of the matrix and the process conditions. The obtained  $f_c$  in the case of LDPE composites of 0.06 matches with the  $f_c$  of 0.07 in the case of PVDF/*n*-Ni hot-molded composites. Figure 4.16c shows the value of  $\tan \delta$  of the composites at low frequency undergoes a sharp increase for  $f_{\text{con}} > f_c$  while maintains a value below 1 at high frequencies ( $>100$  kHz). For the composites with  $f_{\text{con}} < f_c$ ,  $\tan \delta$  is less than 0.1 irrespective of frequency. Here also the DR for these composites was not observed [unlike that of PVDF composites] below  $f_c$  which is due to the non-presence of dipoles in the LDPE polymer matrix. It is attributed to the higher extent of increment of  $\varepsilon_{\text{eff}}$  in hot-molded PVDF/*n*-Ni composites at  $f_c$  as compared to the  $\varepsilon_{\text{eff}}$  value in LDPE/*n*-Ni composites at  $f_c$  which is due to the broader region of DC conductivity. But this is not the case as even for one of highly conducting sample ( $>f_c$ ) in the case of LDPE/*n*-Ni (e.g.,  $f_{\text{con}} = 0.10$ ), the static  $\varepsilon_{\text{eff}}$  is 1200 (Fig. 4.16a) as compared to the static  $\varepsilon_{\text{eff}}$  of 3000 at  $f_c$  for PVDF/*n*-Ni composites (Fig. 4.9b) although the DC conductivity region in the previous case is larger than the latter (Figs. 4.9d and 4.16b).

As shown in Fig. 4.16d in the case of LDPE/*n*-Ni composites, the  $\varepsilon_{\text{eff}}$  rises from 19 to 36 at 1 kHz and while  $\varepsilon_{\text{eff}}$  rises from 24 to 60 at 100 Hz when  $f_{\text{con}}$  increases from  $f_{\text{con}} = 0.05$  to  $f_{\text{con}} = 0.06$ . Thus with the non-polar polymer matrix, a very

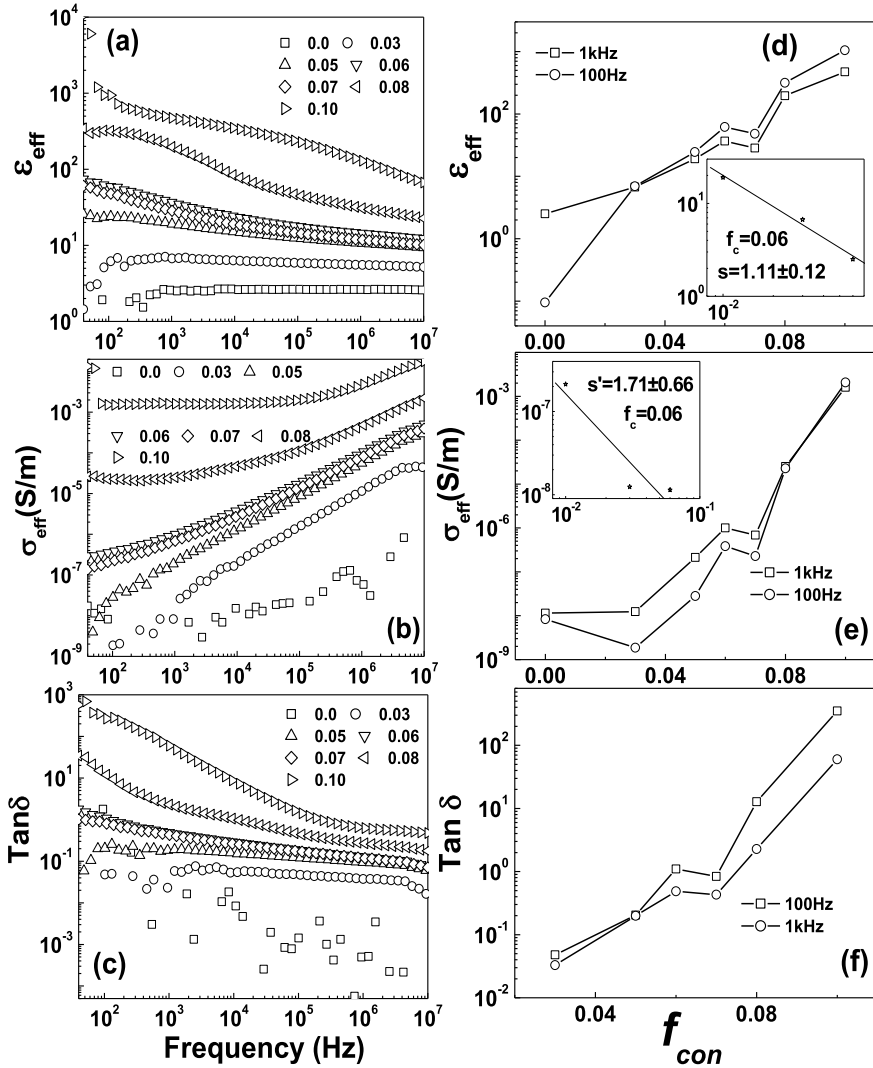


**Fig. 4.16** **a** Effective dielectric constant, **b** effective AC conductivity, and **c** loss tangent as a function of the frequency at 300 K; **d** effective dielectric constant, **e** effective AC conductivity, and **f** loss tangent as a function of  $f_{con}$ , Inset **d** The least-square fit of  $\epsilon_{eff}$  at 1 kHz to Eq. (1.3). Inset **d** least-square fit of  $\sigma_{eff}$  at 1 kHz to Eq. (1.4)

low value of  $\epsilon_{eff}$  is achieved. The measured  $\epsilon_{eff}$  as a function of  $f_{con}$  shows a sharp rise in its value and follows the power-law Eq. (1.3), with  $f_c = 0.06$  and  $s = 1.11 \pm 0.12$  (Inset, Fig. 4.16d). The critical exponent  $s = 1.11$  obtained from the fit isn't in agreement with the universal value of  $s$  predicted for a 0–3 composite, i.e.,  $s_{un} = 0.8-1$ . Similarly as shown in Fig. 4.16e, the value of  $\sigma_{eff}$  in the case of LDPE/n-Ni

composites demonstrates an IMT in the vicinity of  $f_{\text{con}} = 0.06$ . The  $\sigma_{\text{eff}}$  as a function of  $f_{\text{con}}$  increases abruptly near the critical concentration  $f_c \sim 0.06$  indicating the formation of the continuous conductive network in the composite. The best fit of the conductivity data of LDPE/*n*-Ni composites to Eq. (1.4) yields  $f_c = 0.06$ ,  $s' = 1.71 \pm 0.66$  (Inset, Fig. 4.16e). The exponent value  $s'$  is very higher than the universal value ( $s'_{\text{un}} = 0.8-1$ ). It is interesting to point out that the value of  $f_c$  is consistent with the values obtained from dielectric and conductivity data. In this case, both the dielectric exponent ' $s$ ' and conductivity exponent  $s'$  are found to be largely different from their respective universal values. We also observe that for LDPE/*n*-Ni composites,  $\text{Tan } \delta$  undergoes large change near the  $f_c$  which varies from 0.19 to 0.5 at 1 kHz, while it changes from 0.2 to 1.09 at 100 Hz, respectively, when  $f_{\text{con}}$  increases from 0.05 to 0.06 (Fig. 4.16f). A significant coincidence in the value of  $f_c$  of 0.06 in case of LDPE/*n*-Ni composites matches well with the earlier results of hot-molded PVDF/*n*-Ni composites whose  $f_c$  was found to be 0.07. However, the  $f_c$  value does not coincide with the universal ideal value of 0.16. Hence, we observe that as long as different matrices used are of the same order of conductivity, the value of  $f_c$  will not change much for particular processing conditions; however, the magnitude of critical exponents may be affected by the process conditions.

### 4.3.5 Effect of Fillers

In the foregoing sections, we have observed different values of  $f_c$  for different series of samples. However, at  $f_c$  we always observed a higher value of  $\text{Tan } \delta$  which is not required as far as the PMC materials will find application as high  $\epsilon_{\text{eff}}$  materials. Hence as always, the materials are searched with high  $\epsilon_{\text{eff}}$  and low  $\text{Tan } \delta$ , we aim to have high  $\epsilon_{\text{eff}}$  with low  $\text{Tan } \delta$  in a PMC. The idea was that by coating an oxide layer over the *n*-Ni filler particles,  $\text{Tan } \delta$  can be decreased with the tuned value of  $\epsilon_{\text{eff}}$ . To do that the *n*-Ni particles are air annealed at 500 °C for 5 h. At last, what we found a composite of core-shell structure of *n*-Ni and NiO. The XRD results corresponding to composites of PVDF/*n*-Ni and NiO are shown in Fig. 4.17a. With the increase of volume fraction of (*n*-Ni and NiO) in the composite, the intensity corresponding to *n*-Ni and NiO peaks goes on increasing while the intensity of peaks corresponding to pure PVDF decreases. The optical micrographs of some of the typical composites with  $f_{\text{con}} = 0.10$  to  $f_{\text{con}} = 1.0$  are shown in Fig. 4.17b–e. From these micrographs, it is seen that when filler concentration is low, the particles are distributed randomly in the polymer matrix. However, with the increase of  $f_{\text{con}}$ , the particles aggregate to form large clusters and most become self-connected to form a continuous network of clusters.

The  $\epsilon_{\text{eff}}$ ,  $\sigma_{\text{eff}}$ , and  $\text{Tan } \delta$  of the PVDF/*n*-Ni and NiO composites based on PVDF matrix have been studied as a function of frequency and  $f_{\text{con}}$  at 300 K. As shown in Fig. 4.18a, the static  $\epsilon_{\text{eff}}$  value rises from 10 to 92 when  $f_{\text{con}}$  varies from 0.0 to 0.27. However, on approaching  $f_c$  at  $f_{\text{con}} = 0.30$ , the static  $\epsilon_{\text{eff}}$  value is found to be 280. In this case also at/above  $f_c$ , a mixed conductivity comprising AC and DC conductivity

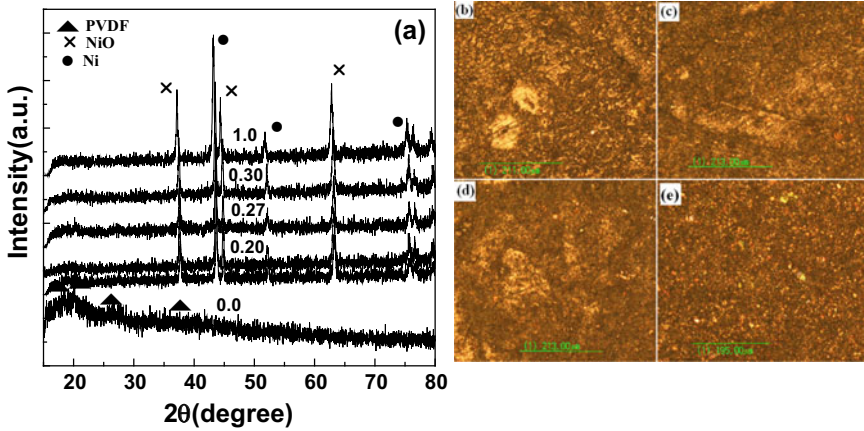


**Fig. 4.17** a X-ray diffraction pattern of PVDF/ Ni and NiO composite samples for  $f_{\text{con}} = 0.0$  to 1.0 from bottom to top, respectively; Optical micrographs of the polished surface of the pure PVDF and PVDF/ $n$ -Ni-NiO composites with different  $f_{\text{con}}$ , **b** 0.10, **c** 0.20, **d** 0.30, and **e** 1.0

is obtained (Fig. 4.18b). The obtained value of  $f_c$  in the case of PVDF/ $n$ -Ni and NiO composites is found to be at  $f_{\text{con}} = 0.30$  which is largely different from that of the  $f_c$  value of 0.07 in the case of PVDF/ $n$ -Ni hot-molded composites. Figure 4.18c shows that the value of  $\text{Tan } \delta$  of the composites at low frequency undergoes a transition for  $f_{\text{con}} > f_c$ . As shown in Fig. 4.18d in the case of PVDF/ $n$ -Ni and NiO composites, the  $\epsilon_{\text{eff}}$  rises from 73 to 120 at 1 kHz and while  $\epsilon_{\text{eff}}$  rises from 92 to 281 at 100 Hz when  $f_{\text{con}}$  increases from  $f_{\text{con}} = 0.27$  to  $f_{\text{con}} = 0.30$ . Hence even with the coating of an oxide layer over the metallic filler, the static  $\epsilon_{\text{eff}}$  value achieved is found to be 281. The power-law Eq. (1.3) was fitted to the experimental results which give the value of  $f_c = 0.30$  and  $s = 1.77 \pm 0.6$  (Inset, Fig. 4.18d). Similarly, the best fit of the conductivity data of PVDF/ $n$ -Ni and NiO composites to Eq. (1.4) yields  $f_c = 0.30$ ,  $s' = 3.14 \pm 0.2$  (Inset, Fig. 4.18e). The critical exponents obtained from the fits aren't in agreement with the universal values. The value of  $f_c$  is consistent with the values obtained from dielectric and conductivity data, but significantly different from the  $f_c$  value of 0.07 of the hot-molded PVDF/ $n$ -Ni composites with the difference from that of universal value (0.16). The very difference in  $f_c$  value is attributed to the formation of an artificial insulating layer making an obstacle for the easy tunneling of the free electrons and thereby a huge change in  $f_c$  value is observed.

It is also observed that for PVDF/ $n$ -Ni and NiO composites,  $\text{Tan } \delta$  undergoes a very small change (Fig. 4.18f) as compared to hot-molded PVDF/ $n$ -Ni composites (Fig. 4.9f), as it changes from 0.16 to 0.81 at 1 kHz and from 0.3 to 1.16 at 100 Hz, respectively, when  $f_{\text{con}}$  increases from 0.27 to 0.30.

In this case, the  $f_c$  value does not coincide with the universal ideal value ( $f_{\text{con}} = 0.16$ ) of  $f_c$  and a significant change in  $f_c$  (0.30) from the universal value (0.16) as well as from the  $f_c$  value (0.07) for hot-molded PVDF/ $n$ -Ni composites could be attributed to the nature of filler particle having one insulating oxide layer (NiO)

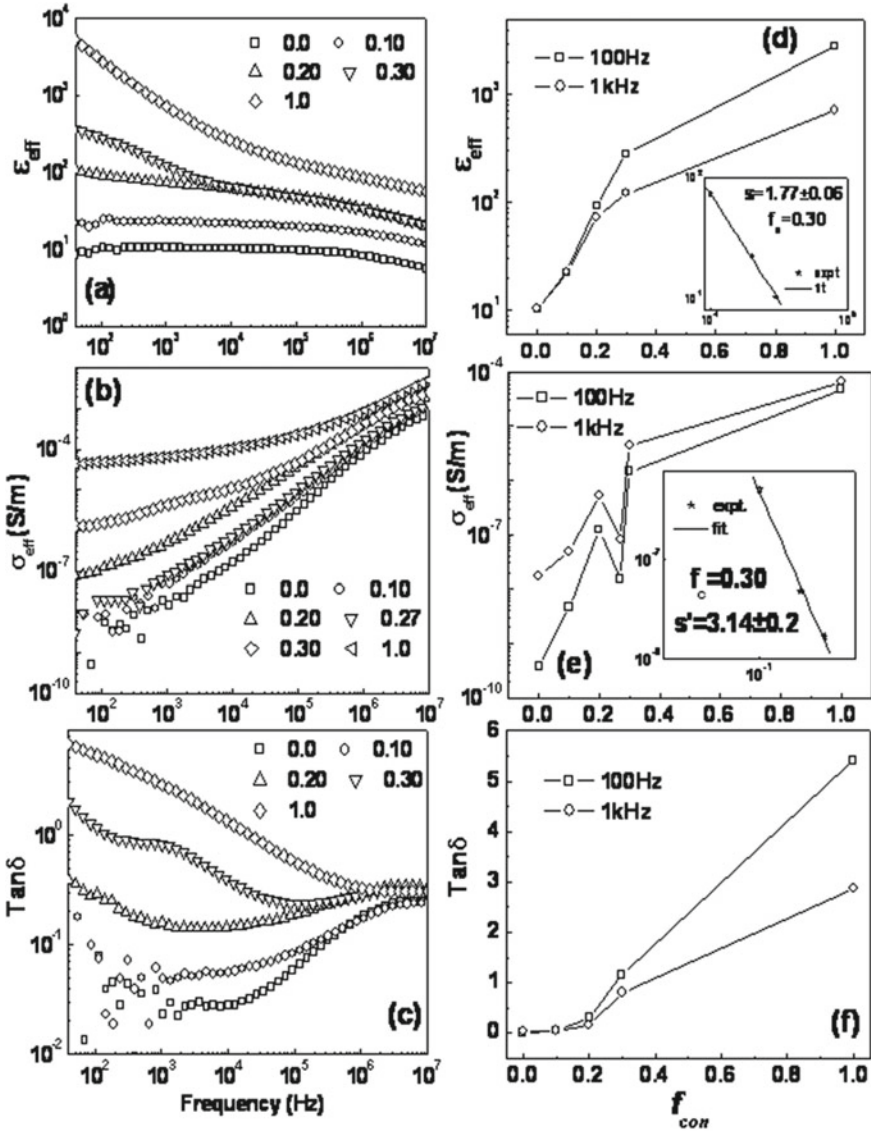


**Fig. 4.18** **a** Effective dielectric constant, **b** effective AC conductivity, and **c** loss tangent as a function of the frequency at 300 K; **d** effective dielectric constant, **e** effective AC conductivity, and **f** loss tangent as a function of  $f_{con}$ , Inset **d** The least-square fit of  $\epsilon_{eff}$  at 1 kHz to Eq. (1.3). Inset **d** Least-square fit of  $\sigma_{eff}$  at 1 kHz to Eq. (1.4)

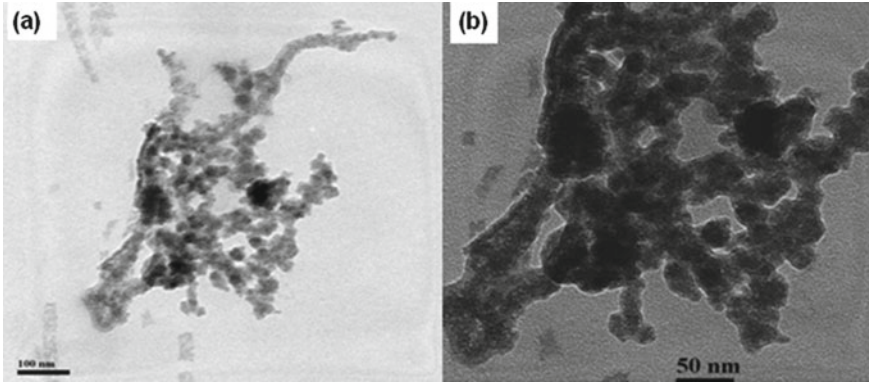


**Fig. 4.19** TEM micrographs of core-shell n-Ni and NiO filler used **a** lower and **b** higher magnification

which can be observed from the high-resolution TEM micrographs showing the inner black core as Ni and outer diffused layer with a different color as the oxide coating (Fig. 4.19).

In a description, we have also studied the effect of filler particles in their alloy form by preparing composites of PVDF/*n*-QC [11]. We observed the same typical features for all the electrical parameters across  $f_c$  for that series of PMC only with the difference of values of  $f_c$ ,  $\epsilon_{\text{eff}}$ ,  $\sigma_{\text{eff}}$ ,  $\text{Tan } \delta$ , and the critical exponents. The observed value of  $f_c$  for the cold-pressed PVDF/*n*-QC composites was observed to be 0.23 with a very high value of  $\epsilon_{\text{eff}} = 3000$  and  $\text{Tan } \delta = 100$ . We also observed the same typical features of large deviation of critical exponents of the scaling laws from their respective universal values.

### 4.3.6 Effect of Cold Pressing

Although everybody predicts the effect of process conditions plays a major role, no systematic study of experimental report is available, where the effect of process condition on the percolation behavior of PMC has undergone a systematic investigation. Hence, to investigate the role of process conditions in altering the percolation behavior, two series of PMC have been prepared through the two different methods [4]. The methods are (1) s series of PVDF/*n*-Ni was prepared as a room temperature (300 K) consolidation at 10 MPa pressure (cold press) and (2) a series of PVDF/*n*-Ni was prepared by hot molding at a temperature of 200 °C (above the melting temperature of PVDF (~135 °C)) and 10 MPa pressure (hot press).

The optical micrographs of the percolating samples of the two series of PMC with  $f_c = 0.28$  and  $f_c = 0.07$  prepared through cold press and hot press method are shown in Fig. 4.20a, b, respectively. The micrographs suggest a random distribution

of bright metal clusters ( $n$ -Ni) in the PVDF matrix with the formation of a self-connected network of  $n$ -Ni clusters. The distribution of metal clusters and the extent of connectivity of the fillers in the PVDF matrix appear to be different since their methods of preparation are different. The cold-pressed samples appear to be highly homogenous with a lower cluster size as compared to the hot-pressed samples. The cold press PVDF (inset, Fig. 4.20a) shows a smooth surface, which indicates possibly no effect has occurred on the internal molecular structure of PVDF due to cold pressing (without any heating), while the hot press PVDF (inset, Fig. 4.20b) shows a flow like behavior (due to heating up to 200 °C during hot molding), suggesting the possibility of a change in relative crystallinity of the polymer.

The FESEM micrographs of the pure PVDF, prepared through the cold press and hot press methods, are shown in Fig. 4.21a, b respectively. The presence of spherulites (the spherical semicrystalline regions of the polymer) in the cold-pressed PVDF (Fig. 4.21a) in comparison to the hot-molded PVDF, where the spherulites have been lost (Fig. 4.21b), confirms the lowering of crystallinity of the polymer due to heating up to 200 °C during hot molding. The diameter of the spherulites present in the polymer is of the order of  $\sim 0.1 \mu\text{m}$  (Fig. 4.21a), while the  $n$ -Ni taken in preparing the PMC was of particle size (20–30 nm) confirmed from the high-resolution TEM micrograph (inset, Fig. 4.21b) and possibly the  $n$ -Ni cluster size in the PVDF matrix is also of the order of the diameter of the spherulite.

**Fig. 4.20** (Color online) Optical micrographs of percolative samples corresponding to two different methods of preparation based on PVDF matrix, **a** cold press ( $f_c = 0.28$ ), inset: pure PVDF. **b** Hotpress ( $f_c = 0.07$ ), inset: pure PVDF

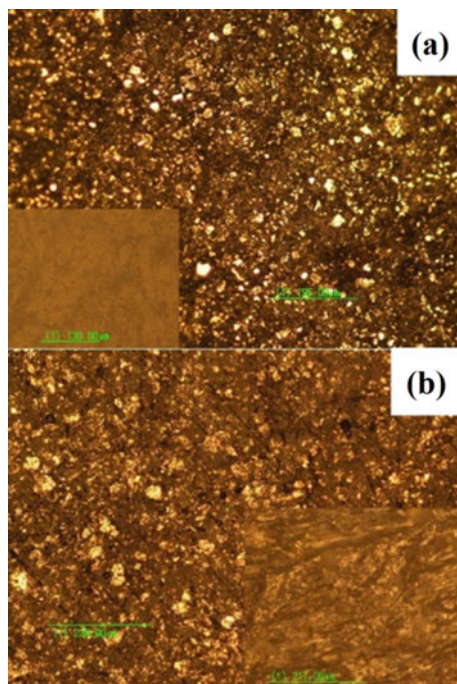
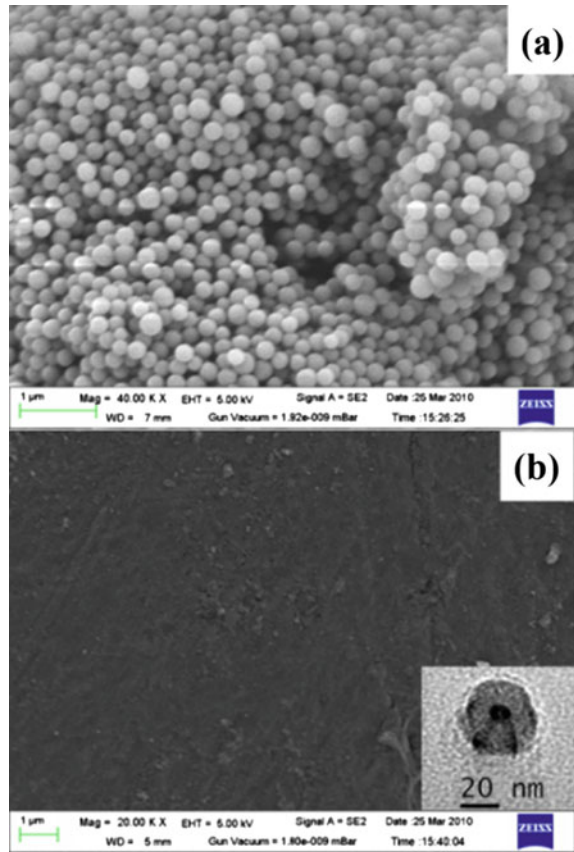


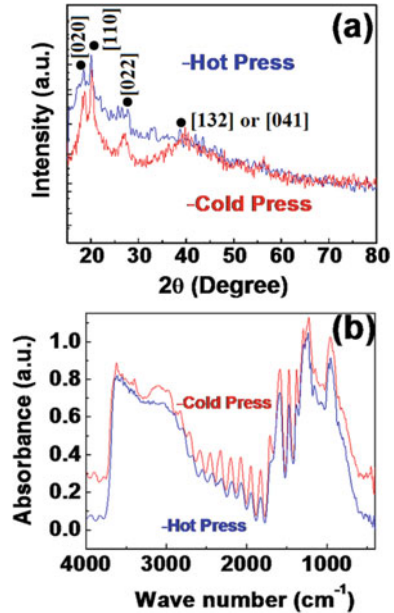
**Fig. 4.21** FESEM micrographs of the pure PVDF, **a** cold press and **b** hot press, Inset: HRTEM image of the nanocrystalline Nickel



The supporting experimental evidence of lowering of relative crystallinity of the pure PVDF during hot molding can be analyzed with the help of XRD (Fig. 4.22a) and FTIR (Fig. 4.22b) data, respectively. The typical XRD pattern of the pure PVDF of all the observed peaks/reflections was indexed based on the best agreement between observed and the JCPDS data of both the cold-pressed and hot-pressed PVDF. This shows that there is a slight relative change in both the crystalline and amorphous content of the PVDF due to hot molding since  $\% \text{ crystallinity} = (\text{total area of crystalline peaks}) / (\text{total area of all peaks})$  and the area of crystalline peaks has undergone a slight decrement (Fig. 4.22a). The FTIR data of the hot-molded sample also support the lowering of relative crystallinity (since the absorbance at different wavenumbers for the hot-molded sample is lower in comparison with cold press sample attributed to the lowering of surface area due to loss of spherulites during hot molding). Hence, the presence of spherulites in the PVDF matrix is the deciding factor in determining the properties of PMC, suitable for their dielectric applications.

The presence of spherulites of the cold-pressed sample may be supportive in providing a large surface area for the storage of electrical charge, which may lead to

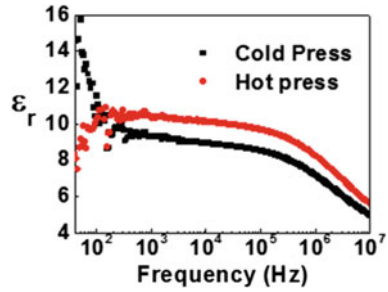
**Fig. 4.22** Change of relative crystallinity of pure PVDF. **a** X-ray diffractometry data of cold press and hot press samples and **b** FTIR data of cold press and hot press samples



improvement of  $\epsilon_{\text{eff}}$  of the PMC in comparison with the hot-molded sample. With this aim, the comparison of the dielectric behavior of the PVDF sample prepared through two different methods is shown in Fig. 4.23. This shows that the static and low frequency (less than 100 Hz) dielectric constant ( $\epsilon_r$ ) of the cold-pressed PVDF is higher ( $\sim 10$ – $16$ ) than the hot-pressed PVDF ( $\sim 10$ ), while the value of  $\epsilon_r$  for both the samples remains constant above 100 Hz. The difference of  $\epsilon_r$  between the cold press and hot press PVDF in the range of 100 Hz–10 MHz may be taken within the experimental error (Fig. 4.23). The static higher value of  $\epsilon_r$  for cold-pressed PVDF in comparison with hot-pressed PVDF is attributed to the storage of electrical charge at the surfaces of spherulites of cold-pressed PVDF. The low-frequency dispersion of  $\epsilon_r$  (from 16 at 40 to 10 at 100 Hz) of the cold-pressed PVDF is attributed to the electrical charge migration/conduction across the boundary of the surface of the spherulites with the increase of frequency.

The  $\epsilon_{\text{eff}}$  and  $\sigma_{\text{eff}}$  of both the series of PMC as a function of  $f_{\text{con}}$  at 1 kHz and 300 K are shown in Fig. 4.24a, b, respectively. In the case of cold-pressed PMC (Fig. 4.24a), the  $\epsilon_{\text{eff}}$  rises from 200 to 1300, when  $f_{\text{con}}$  increases from 0.27 to 0.28, while for the hot-pressed PMC the  $\epsilon_{\text{eff}}$  undergoes a comparatively sharp transition from 100 to 1600, when  $f_{\text{con}}$  increases from 0.065 to 0.07 due to the IMT at the critical concentration of the conductor. The critical transition region for the hot-pressed PMC is narrower in comparison with the critical transition region for the cold-pressed PMC, attributed to the different methods of preparation of the PMC leading to the formation of different extent of connectivity among the fillers, as well as the filler cluster size. The cluster size for hot-pressed PMC is higher in comparison

**Fig. 4.23** (Color online)  
Comparison of dielectric behavior of pure PVDF prepared through cold press and hot press methods

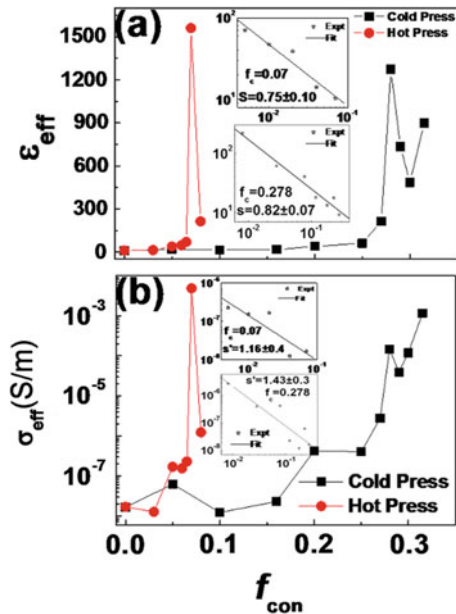


with cold-pressed PMC, leads to a lowering of homogeneity and hence the observed sharp transition. The  $\epsilon_{\text{eff}}$  as a function of  $f_{\text{con}}$  for both the PMC follows the power-law Eq. (1.3)

$$\epsilon_{\text{eff}} \propto (f_c - f_{\text{con}})^{-s} \text{ for } f_{\text{con}} < f_c.$$

For cold-pressed and hot-pressed PMC, the values found for  $f_c$  are 0.28 and 0.07, respectively, and the value of ‘s’ is found to be  $0.82 \pm 0.07$  and  $0.75 \pm 0.10$  (Insets: Fig. 4.24a), respectively. The critical exponent ‘s’ for both the PMC is almost the same (since the matrix and filler of both PMC are the same and that leads to the same interaction) and is in agreement with the universal value of  $s$  ( $s_{\text{un}}$ ) predicted for a 0–3 composite, i.e.,  $s_{\text{un}} = 0.8-1$ . Similarly,  $\sigma_{\text{eff}}$  clearly shows an IMT for both the series of PMC in the vicinity of  $f_{\text{con}} = 0.28$  and 0.07, respectively (Fig. 4.24b). As shown

**Fig. 4.24** (Color online)  
Variation of **a**  $\epsilon_{\text{eff}}$  and **b**  $\sigma_{\text{eff}}$  as a function of  $f_{\text{con}}$  at 1 kHz and 300 K for both the series of PMC prepared through cold press and hot press, respectively. Inset: **a** least-square fit to Eq. (1.3), upper: PMC through the hot press, lower: PMC through the cold press, **b** least-square fit to Eq. (1.4), upper: PMC through the hot press, lower: PMC through cold press



in Fig. 4.24a, the value of  $\sigma_{\text{eff}} \sim 10^{-2}$  S/m for the percolative ( $f_c = 0.07$ ) hot-molded sample is 100 times higher than the  $\sigma_{\text{eff}} \sim 10^{-4}$  S/m for the percolative ( $f_c = 0.28$ ) cold press sample; hence, the cold press PMC may be a suitable candidate for energy storage. The best fit of conductivity data of both the cold press and hot press PMC to Eq. (1.4) yields  $f_c = 0.28$  &  $0.07$ ,  $s' = 1.43 \pm 0.3$ , and  $1.16 \pm 0.4$ , respectively (Insets: Fig. 4.24b). The exponent value ' $s'$ ' for both the PMC is almost of the same value, but in both the cases ' $s'$ ' is greater than the universal value  $s'_{\text{un}} = 0.8-1$  and is explained based on the Swiss cheese model/inverted Swiss cheese model [23, 24]. The non-universality of ' $s'$ ' is a common problem for most PCC. The  $f_c$  value calculated for both the PMC independently from the dielectric and conductivity data largely coincides, but they largely deviate from the universal  $f_c$  value [ $f_c = 0.16$  for a three-dimensional (0–3) composite], which is attributed to the process conditions, adhesiveness of the polymer PVDF, and metal filler particle size.

$$\sigma_{\text{eff}} \propto (f_c - f_{\text{con}})^{-s'} \text{ for } f_{\text{con}} < f_c$$

The comparison of the variation of  $\epsilon_{\text{eff}}$ ,  $\sigma_{\text{eff}}$ , and  $\text{Tan}\delta$  of both the series of PMC as a function of frequency at 300 K is given in Fig. 4.25. As shown in Fig. 4.25a, b, the static value of  $\epsilon_r$  for the cold-pressed pure PVDF at 40 Hz is 16 and undergoes low-frequency dispersion to reach a value of 10 at 100 Hz, while the  $\epsilon_r$  for the hot-pressed pure PVDF at 40 Hz is 10 and maintains this value also up to 100 Hz. The higher value of  $\epsilon_r$  (Fig. 4.23) for cold-pressed pure PVDF is explained based on charge accumulation at the surface of spherulites at lower frequencies. However, above 100 Hz, the dielectric constant of both cold press and hot press PVDF remains the same. With the increase of  $f_{\text{con}}$  for both the PMC, the enhancement of  $\epsilon_{\text{eff}}$  occurs. For the cold-pressed PMC, the original low-frequency dispersion present in the pure PVDF is also maintained for all other PMC with different  $f_{\text{con}}$  (since the spherulites of PVDF are not lost with the addition of  $n$ -Ni into the polymer matrix) and a  $\epsilon_{\text{eff}}$  of 2400 at 40 Hz (for  $f_{\text{con}} = f_c = 0.28$ ) was achieved. However, for the hot-pressed PMC, no low-frequency dispersion was observed, even up to the  $f_{\text{con}} = f_c = 0.07$  and is attributed to loss of spherulites of the PVDF matrix during hot molding. The  $\sigma_{\text{eff}}$  of all the samples of both the series of PMC (Fig. 4.25c, d) shows strong variation with frequency for  $f_{\text{con}} < f_c$ . As  $f_{\text{con}} \sim f_c$ , the conductivity sharply rises to show an IMT and higher  $\sigma_{\text{eff}}$  for the hot-pressed percolative sample was observed in comparison with the cold-pressed percolative sample, which confirms the better applicability of the cold-pressed samples. For  $f_{\text{con}} \geq f_c$ , a mixed conductivity comprising AC and DC was observed, while only AC conduction was observed for  $f_{\text{con}} < f_c$ . The  $\text{Tan } \delta$  variation for both the series of PMC (Fig. 4.25e, f) shows the loss tangent undergoes a sudden increase at the  $f_c$ . The higher  $\text{Tan}\delta$  is observed for the hot-pressed PMC even if the fraction of conductor loading is only 0.07 in comparison with 0.28. This large deviation is attributed to the hot press process condition, giving rise to a lowering of homogeneity (inhomogeneous cluster size throughout the matrix) and developing a better network of connectivity for the metal filler clusters, which forms a suitable path for electrical conduction and the large loss tangent. Hence, the cold press samples having better homogeneity, low loss tangent, high dielectric constant, broader critical

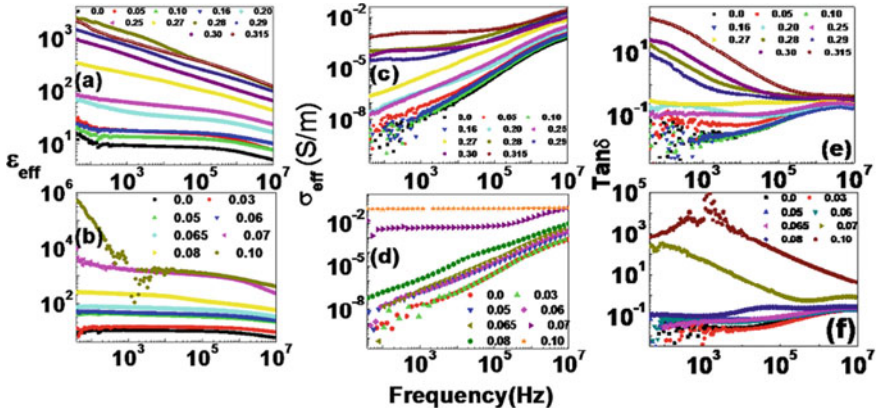


**Fig. 4.25** (Color online) Comparison of variation of  $\epsilon_{\text{eff}}$  (a, b),  $\sigma_{\text{eff}}$  (c, d), and  $\text{Tan } \delta$  (e, f) as a function of frequency at 300 K for both cold-pressed and hot-pressed PMC, respectively

region, and the high static dielectric constant would be better candidates for energy storage applications in comparison with hot press samples.

In a nutshell, the static value of  $\epsilon_{\text{eff}}$  and  $\text{Tan } \delta$  at 1 kHz for different PMC studied under present investigation at their respective  $f_c$  along with their experimental values of critical exponents and the universal values is given in Table 4.1. We observe from Table 4.1 that the magnitude of enhancement of  $\epsilon_{\text{eff}}$  and  $\text{Tan } \delta$  for the PMC/PCC having a lower  $f_c$  is higher as compared to the PMC with a higher value of  $f_c$  which questions the explanation of enhancement of  $\epsilon_{\text{eff}}$  in terms of boundary layer capacitor effect. Similarly, the magnitude of the critical exponents also becomes higher than that of their respective universal values and the interesting feature observed is that their magnitudes for various PMC/PCC become very different from each other, although the values of the critical exponents are supposed to be only dependent on dimensionality of the samples. In this case, as all the PMC samples are 3D samples; hence, the value of critical exponents for various series of PMC should not change much and that should remain within the experimental error which is not observable from the present results. Hence to find the origin of enhancement of  $\epsilon_{\text{eff}}$  for a PMC at its  $f_c$  and its non-universal scaling behavior of showing different values of critical exponents, a systematic and detailed analysis of the scaling behavior of these PMC/PCC has been carried out in Chap. 5 and the concept of boundary layer capacitor effect has been modified by the proposed concept of connectivity which appears to be more valid for PMC.

**Table 4.1** Magnitudes of  $\epsilon_{\text{eff}}$  and  $\text{Tan } \delta$  at 1 kHz for various PMC [prepared under different temperature ( $T$ ) and time ( $t$ )] under investigation at their respective  $f_c$ , along with their experimental and theoretical values of critical exponents

Series of PMC	$f_c$	Ideal $f_c$	$\epsilon_{\text{eff}}$ at 1 kHz	$\text{Tan } \delta$ at 1 kHz	$s$	$S'$	$s_{\text{un}}$	$s'_{\text{un}}$
Coldpressed PVDF/ $\mu$ -Ni	0.57	0.16	995	1.22	$0.72 \pm 0.05$	$1.15 \pm 0.1$	0.7-1	0.7-1
Cold pressed PVDF/ $n$ -Ni	0.28	0.16	1273	2.04	$0.82 \pm 0.07$	$1.43 \pm 0.31$	0.7-1	0.7-1
Hot molded PVDF/ $\mu$ -Ni <b>T = 200 °C, t = 45 min</b>	0.26	0.16	-ve	12,828	$0.90 \pm 0.1$	$1.73 \pm 0.2$	0.7-1	0.7-1
Hot molded PVDF/ $n$ -Ni <b>T = 200 °C, t = 45 min</b>	0.07	0.16	1560	55	$0.75 \pm 0.1$	$1.16 \pm 0.4$	0.7-1	0.7-1
Hot molded LDPE/ $n$ -Ni <b>T = 200 °C, t = 45 min</b>	0.06	0.16	36	048	$1.11 \pm 0.12$	$1.71 \pm 0.66$	0.7-1	0.7-1
Hot molded PVDF/ $n$ -Ni@NiO <b>T = 200 °C, t = 45 min</b>	0.30	0.16	121	0.81	$1.77 + 006$	$3.14 \pm 0.2$	0.7-1	0.7-1
Cold pressed PVDF/ $n$ -QC	0.23	0.16	544	146	$0.69 \pm 0.09$	$1.09 \pm 0.15$	0.7-1	0.7-1

## 4.4 Summary

A variety of combinations of PMC/PCC for investigating the percolation and scaling behavior of these composites are studied, and it is found that at  $f_c$  a very large enhancement in  $\epsilon_{\text{eff}}$  and  $\sigma_{\text{eff}}$  has been observed.

The large enhancement in  $\epsilon_{\text{eff}}$  in the neighborhood of percolation threshold can be understood based on the “boundary layer capacitor effect”, i.e., near the  $f_c$  there are many conducting particles isolated by very thin dielectric insulating layer forming a large number of microcapacitors which give rise to very high  $\epsilon_{\text{eff}}$  and on the basis MWS polarization effect. Similarly, the abrupt change in  $\sigma_{\text{eff}}$  in the neighborhood of  $f_c$  can be understood from percolation theory, i.e., near the  $f_c$  the effective tunneling range of two filler particles overlaps leading to a sudden increment in the probability of nearest neighbor as well as higher-order tunneling.

- (i) High value of  $\epsilon_{\text{eff}}$  with low  $\text{Tan } \delta$  at different  $f_c$  has been observed. The achieved  $\epsilon_{\text{eff}}$  is the highest value in magnitude with a comparable loss among the PMC based on the PVDF matrix. The highest value of  $\epsilon_{\text{eff}}$  achieved in the present investigation is also comparable to  $\epsilon_{\text{eff}}$  in any of the PMC reported to date.

- (ii) The difference in  $f_c$  is attributed mainly due to the filler particle size, process condition, nature of filler particles, homogeneity, temperature, mixing and firing time, etc.
- (iii) The electrical properties of the composites in the vicinity of  $f_c$  are explained based on the boundary layer capacitor effect, the concept of connectivity, and conventional percolation theory with the values of critical exponents deviating from their respective universal values.
- (iv) With the reduction of filler particle size, the low-frequency  $\epsilon_{\text{eff}}$  is increased due to an increase in surface area, but the dielectric behavior becomes more dispersive over the whole frequency range because of more leakage current resulting from the decrease in interparticle distance and more interparticle contacts due to increase in surface area.
- (v) It is concluded that the observation of an ideal  $f_c$  is a matter of coincidence as it depends on various parameters simultaneously.
- (vi) It is observed that by creating an artificial insulating layer over the metallic filler, the  $\tan \delta$  is reduced drastically with a moderate value of  $\epsilon_{\text{eff}}$  with huge change in  $f_c$ .
- (vii) It has been found that the enhancement of dielectric constant of PMC based on polyvinylidene fluoride matrix is largely tuned by the process conditions and that plays a major role in the development of polymer dielectrics for their suitability to static and low-frequency applications. The spherulites present in the PVDF matrix are always helpful in maintaining and increasing the  $\epsilon_{\text{eff}}$  of PMC. Hence, utmost care should be taken in preparing the PMC based on PVDF at room temperature or at a comparatively low temperature so that the spherulites may be retained, which are highly helpful in achieving higher  $\epsilon_{\text{eff}}$  of PMC. It is also being suggested that the cold-pressed PMC would be a better candidate over the hot molding samples for static and low-frequency dielectric applications.

## References

1. Nalwa HS (1995) Ferroelectric polymers. Marcel Dekkar, New York
2. Dang ZM, Lin YH, Nan CW (2003) Novel ferroelectric polymer composites with high dielectric constants. *Adv Mater* 15:1625–1629
3. Huang C, Zhang Q (2004) Enhanced dielectric and electromechanical responses in high dielectric constant all-polymer percolative composites. *Adv Func Mater* 14:501–506
4. Panda M (2017) Major role of process conditions in tuning the percolation behavior of polyvinylidene fluoride based polymer/metal composites. *Appl Phys Lett* 111:0829011–0829015
5. Fan J (2008) High dielectric permittivity and low percolation threshold in nanocomposites based on poly(vinylidene fluoride) and exfoliated graphite nanoplates. *Adv Mater* 21:710–715
6. Panda M (2022) Tuned dielectric and percolation behavior of cold pressed polyvinylidene fluoride nanocomposites caused by Ni and BaTiO<sub>3</sub> filler. *Indian J Phys* 96:1699–1703
7. Panda M, Soni S (2018) A comparative study of visco-elastic properties of non-polar and polar polymer dielectrics. *Mater Today: Proc* 05:2123–2131

8. Panda M, Srinivas V, Thakur AK (2014) Percolation behaviour of polymer-metal composites on modification of filler. *Mod Phys Lett B* 28:14500551–14500556
9. Panda M, Srinivas V, Thakur AK (2011) Role of polymer matrix in large enhancement of dielectric constant in polymer-metal composites. *Appl Phys Lett* 99:0429051–0429053
10. Panda M, Thakur AK, Srinivas V (2010) Thermal effects on the Percolation behavior of polyvinylidene fluoride/nickel composites. *J Appl Polym Sci* 117:3023–3028
11. Venketesh C, Srinivas V, Panda M, Rao VV (2010) Dielectric response in novel polyvinylidene fluoride/nanoquasicrystalline composites. *Solid State Commun* 150:893–896
12. Panda M, Srinivas V, Thakur AK (2008) On the question of percolation threshold in polyvinylidene fluoride/nanocrystalline nickel composites. *Appl Phys Lett* 92:132905–132907
13. Panda M, Srinivas V, Thakur AK (2008) Surface and interfacial effect of filler particle on electrical properties of polyvinylidene fluoride/nickel composites. *Appl Phys Lett* 93:242908–242910
14. Panda M, Srinivas V, Thakur AK (2008) Dielectric behavior of a metal-polymer composite with reduction of metal particle size. In: 53rd DAE solid state physics symposium, vol 53, pp 1035–1036
15. Panda M, Thakur AK, Srinivas V (2007) Enhancement of dielectric constant in PVDF/Ni composites. In: 52nd DAE solid state physics symposium, vol 52, pp 569–570
16. Dang ZM, Yuan JK, Zha JW, Zhou T, Hu GH (2012) Fundamentals, processes, and applications of high-permittivity polymer-matrix composites. *Prog Mat Sci* 57:660–723
17. Dang ZM, Wu JP, Xu HP, Yao SH, Jiang MJ, Bai J (2007) Dielectric properties of upright carbon fiber-filled poly(vinylidene fluoride) composite with low percolation threshold and weak temperature dependence. *Appl Phys Lett* 91:0729121–0729123
18. Shen Y, Nan CW, Li M (2004) Anisotropic electrical properties of semiconductive Bi<sub>2</sub>S<sub>3</sub> nanorod filled ferroelectric polyvinylidene fluoride. *Chem Phys Lett* 396:420–423
19. Yao SH, Dang ZM, Jiang MJ, Xu HP, Bai J (2007) Influence of aspect ratio of carbon nanotube on percolation threshold in ferroelectric polymer nanocomposite. *Appl Phys Lett* 91:2129011–2129013
20. Wang L, Dang ZM (2005) Carbon nanotube composites with high dielectric constant at low percolation threshold. *Appl Phys Lett* 87:0429031–0429033
21. Yao SH, Dang ZM, Jiang MJ, Bai J (2008) BaTiO<sub>3</sub>-carbon nanotube/polyvinylidene fluoride three-phase composites with high dielectric constant and low dielectric loss. *Appl Phys Lett* 93:1829051–1829053
22. Chandrasekhar KD, Venimadhav A, Das AK. High dielectric permittivity in semiconducting Pr<sub>0.6</sub>Ca<sub>0.4</sub>MnO<sub>3</sub> filled polyvinylidene fluoride nanocomposites with low percolation threshold. *Appl Phys Lett* 95:0629041–0629043
23. Stauffer D, Aharony A (1992) Introduction to percolation theory. Taylor and Francis, London
24. Sahimi M (1994) Applications of percolation theory. Taylor and Francis, London
25. Toker D, Azulay D, Shimon N, Balberg I, Millo O (2003) Tunnelling and percolation in metal-insulator composite materials. *Phys Rev B* 68:041403
26. Balberg I, Azulay D, Toker D, Millo O (2004) Percolation and tunneling in composite materials. *Int J Mod Phys B* 18:2091
27. Maxwell JC (1892) A treatise on electricity and magnetism. Dover, New York
28. Wagner KW (1914) Erklärung der dielektrischen nachwirkungsvorgänge auf grund maxwellscher vorstellungen. *Arch Elektrotech* 2:371–387
29. Sillars RW (1937) The properties of a dielectric containing semiconducting particles of various shapes. *J Inst Electr Eng* 80:378–394
30. Jonscher AK (1977) The 'universal' dielectric response. *Nature* 267:673–679

# Chapter 5

## Scaling Behavior of Percolative Polymer Composites



This chapter deals with the study of the origin of enhancement of effective dielectric constant ( $\epsilon_{\text{eff}}$ ) in the vicinity/at percolation threshold ( $f_c$ ) in a polymer/metal composite (PMC). From the analysis of data, the enhancement of  $\epsilon_{\text{eff}}$  in PMC at/in the vicinity of  $f_c$  has been explained based on the concept of connectivity and the loss tangent ( $\tan \delta$ ) over the long-established boundary layer capacitor effect. The origin of the deviation of scaling exponents from their respective universal values and also the quantification of the deviation have been explained based on the concept of connectivity of the metallic fillers in a PMC. The widely used percolative equations are well-fitted with the experimental results of all PMC at all values of the frequency. The value of  $f_c$  is found to be independent of the frequency of the applied signal, suggesting the studied PMC are real percolating systems. The critical exponents ( $s$  and  $s'$ ) which characterize the divergence of  $\epsilon_{\text{eff}}$  and  $\sigma_{\text{eff}}$  in the vicinity of  $f_c$  are found to be frequency-dependent and increase with the increase of frequency. The divergence of  $\epsilon_{\text{eff}}$  and  $\sigma_{\text{eff}}$  in the vicinity of  $f_c$  is found to decrease with the increase of frequency. The rate of decrease of  $s$  and  $s'$  with an increase of frequency is attributed to the method of preparation, size of the fillers, adhesiveness of polymer/filler, and the rate of decrease of ' $\epsilon_{\text{eff}}$ ' with frequency (due to the absence of different extents of contributions of various types of conventional polarization).

### 5.1 Introduction

Insulating polymer/conductor composites (PCC) are of recent interest due to their superior physical properties like high dielectric constant with mechanical flexibility making them suitable for several applications, such as high electric energy density materials and embedded capacitor applications. A variety of PCC is fabricated by incorporation of different types of conductor, such as metals, metallic alloys, carbon

black, carbon nanofibers and nanotubes, graphite nanoplatelets, and conducting polymers into the polymer matrix (Fig. 1.1). These composites undergo an insulator-to-metal transition (IMT) at  $f_c$  at which they show an abnormal increase in  $\varepsilon_{\text{eff}}$  and dc conductivity. Among various types of PCC, the PMC are of particular interest due to their easier processing, cost-effectiveness, high dielectric constant, and better flexibility. However, from Chap. 4 we have found that the value of  $f_c$  depends on several parameters, such as size, the shape of the filler, wetting, and adhesiveness of the polymer, interfacial interaction, and spatial distribution of both the components. In addition to these, processing parameters, such as temperature, curing time, mixing time, and thickness of the composite are also crucial in determining the  $f_c$ . Since several parameters affect the  $f_c$  value, the experimental observation of an ideal  $f_c$  is very rare, and the percolation behavior of PCC/PMC still requires a clear and better understanding. Therefore the samples must be prepared under identical conditions for the comparison of properties and to propose any possible physical reason to explain the unusual behavior exhibited in such PCC/PMC. Theoretical calculation on PCC/PMC suggested that at  $f_c$  a singularity in  $\varepsilon_{\text{eff}}$  is expected. However, experimentally the value of  $\varepsilon_{\text{eff}}$  and its extent of enhancement at  $f_c$  for different PMC are found to be different (References of Fig. 1.1). Although PMC gives higher  $\varepsilon_{\text{eff}}$  as compared to ceramic polymer composites, further enhancement of  $\varepsilon_{\text{eff}}$  is also desirable for various applications. Thus, the study on the origin of large values of  $\varepsilon_{\text{eff}}$  and its extent of enhancement at  $f_c$  for PMC is important to investigate.

On the theoretical front, it is predicted that in a random distribution of conducting particles embedded in an insulating matrix through a three-dimensional (3D) random circuit network in which the components are either pure resistances or pure capacitances, assumed that  $\varepsilon_{\text{eff}}$  and  $\sigma_{\text{eff}}$  follow universal fractional power laws of Eqs. (1.1) and (1.2) as a function of frequency in the vicinity of  $f_c$ , which are given by

$$\varepsilon_{\text{eff}}(\omega, f_{\text{con}} \approx f_c) \propto \omega^{-y} \text{ and } \sigma_{\text{eff}}(\omega, f_{\text{con}} \approx f_c) \propto \omega^x,$$

where  $f_{\text{con}}$  is the volume fraction of conductor in the composite,  $\omega$  is the frequency of applied ac signal,  $x$  and  $y$  are the critical exponents and they are expected to satisfy the relations  $x + y = 1$ , with  $x = t/(s + t)$  and  $y = s/(s + t)$  under the intercluster polarization, i.e., the RC model, where  $s$  and  $t$  characterize the divergence of  $\varepsilon_{\text{eff}}$  and  $\sigma_{\text{eff}}$  in the vicinity of  $f_c$ . According to percolation theory, the power-law behavior of  $\varepsilon_{\text{eff}}$  and  $\sigma_{\text{eff}}$  in the vicinity of  $f_c$  is given by Eqs. (1.3)–(1.5) as;

$$\varepsilon_{\text{eff}} \propto (f_c - f_{\text{con}})^{-s} \text{ for } f_{\text{con}} < f_c \quad \sigma_{\text{eff}} \propto (f_c - f_{\text{con}})^{-s'} \text{ for } f_{\text{con}} < f_c$$

$$\sigma_{\text{eff}} \propto (f_{\text{con}} - f_c)^t \text{ for } f_c < f_{\text{con}}$$

where ‘ $s$ ’ is the dielectric exponent in the insulator region and ‘ $s$ ’, ‘ $t$ ’ are the conductivity exponents in the insulator and conductor region, respectively. According to the two different physical models, such as the intercluster polarization model (RC model)

and the anomalous diffusion model, the 3D universal values of critical exponents are  $x = 0.72$ ,  $y = 0.28$ , and  $x = 0.58$ ,  $y = 0.42$ , respectively. According to the percolation theory in 3D, under the consideration of intercluster polarization model, the relations  $x = t/(s + t)$  and  $y = s/(s + t)$  are valid and the universal values of  $s$ ,  $s'$ , and  $t$  are given by  $s_{un} = s'_{un} = 0.7-1$  and  $t = 1.6-2.0$ . But in most of the practical continuum percolation systems (PCC), the critical exponents are found to be higher than the universal values which have been explained by various unusual models [1–8], such as the random void model/the swiss cheese model and the inverted swiss cheese model, the position space renormalization group approximation model, and the transfer matrix method. No clear understanding regarding the increment and the extent of increment of the critical exponents ( $s$ ,  $s'$ ,  $t$ ) from their respective universal values (i.e., the quantification of the increment in terms of any experimentally measurable physical parameter) is found in the literature to date. Hence, the quantification of the increment of scaling exponents from their respective universal values in terms of an experimentally measurable physical parameter that tailors the extent of increment of the critical exponents will give a very clear understanding in a different way over the long-standing understanding.

## 5.2 Samples Reported

The results of the following samples given in Table 5.1 are discussed below.

Among the different composites, the cold-pressed PVDF/ $\mu$ -Ni (as purchased Ni ( $\mu$ -Ni), PVDF/nanocrystalline Ni ( $n$ -Ni), PVDF/ $n$ -quasicrystal ( $n$ -QC) composites are denoted as series A, B, and E, respectively. Two series of PVDF/ $\mu$ -Ni and PVDF/ $n$ -Ni composites are denoted as series C and D, respectively, which were hot molded under a pressure of 10 MPa and a temperature of 200 °C for 45 min to get samples

**Table 5.1** Preparation method and notation for the particular series of samples

Name of the series of composites	Preparation method	Notation for the particular series
PVDF/ $\mu$ -Ni	Room temperature consolidation	A
PVDF/ $n$ -Ni	Room temperature consolidation	B
PVDF/ $\mu$ -Ni	Compression hot molding	C
PVDF/ $n$ -Ni	Compression hot molding	D
PVDF/ $n$ -QC	Room temperature consolidation	E
LDPE/ $n$ -Ni	Compression hot molding	F

with diameter 13 mm and thickness  $\sim 1.8$  mm. Low-density polyethylene (LDPE)/*n*-Ni composites denoted as series F were also hot molded under a pressure of 10 MPa and a temperature of 130 °C for 30 min. The series of samples along with their preparation method and notation used for the particular series is given in Table 5.1.

## 5.3 Results and Discussion

### 5.3.1 Microstructure

The morphological connectivity of the filler particles/clusters of the respective percolative PCC corresponding to the various series of samples can be observed from Fig. 5.1. In the optical micrographs, the brighter regions are the filler particles/clusters and the faint background is the polymer matrix. We observe in the case of the percolative cold-pressed samples for series B and E the size of nanofiller clusters are of the same order and are well-isolated from each other giving more homogeneity to the samples. In the case of series A samples due to the micron size particles, only the cluster size is higher than the series B and E samples while the homogeneity of the samples is maintained. In the case of the hot-molded samples [series C, D, and F], the cluster size of the metal filler particles increases, and the extent of homogeneity decreases. The microstructure of the percolating samples in all cases has been confirmed as the parallel combination of resistor and capacitor networks and its correlation with the various electrical parameters, and the different electrical relaxation mechanisms have been explained in Chaps. 6 and 7. Although the network of connectivity appears to be identical of consisting of a random distribution of resistors and capacitors in all cases with a difference in the size of the metal filler clusters, however, the extent of connectivity of metal fillers in all cases is observed to be different at their respective  $f_c$  as shown in Fig. 5.1.

The visual evidence of the approach of connectivity of metal filler particles/clusters in the base polymer matrix with the increase of  $f_{con}$  under a particular processing condition for a particular series can be observed from earlier chapters (Figs. 4.3 and 4.4 for series A and B, respectively). For series C, D, E, and F the visual evidence of connectivity of metal filler clusters with an increase of  $f_{con}$  can be seen from Figs. 5.2, 5.3, 5.4 to 5.5 respectively.

### 5.3.2 Stability of Composites

To probe whether the melting temperature of the composite changes with the varying fraction of the filler content we have carried out a thermal analysis study on two samples of series B, one is very near to  $f_c$  and the other is well below the  $f_c$ , such as  $f_{con} = 0.05$  and  $f_{con} = 0.25$ . As shown in the DSC curve (Fig. 5.6), we observe that

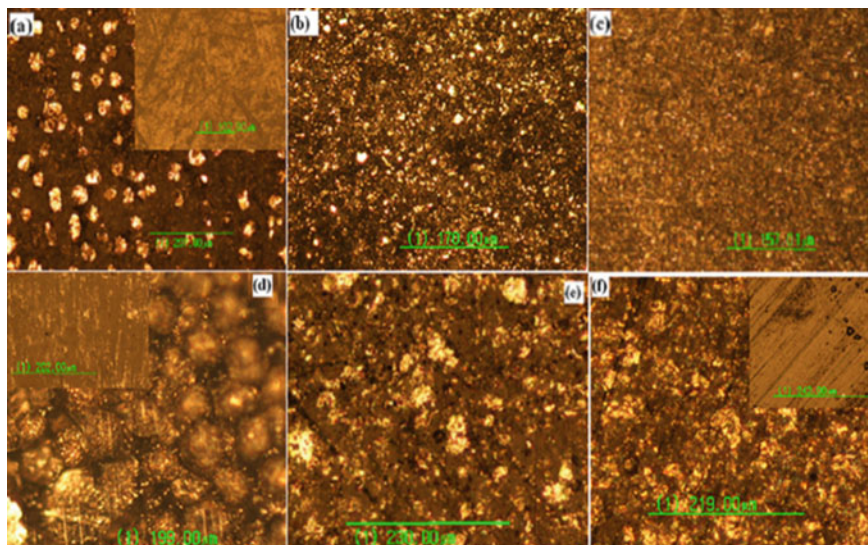


**Fig. 5.1** (Color online) Optical micrographs of the percolative composites corresponding to different series of PCC showing the morphological connectivities of filler particles/clusters respectively. **a** A, Inset: Pure PVDF. **b** B. **c** E. **d** C, Inset: Pure PVDF. **e** D. **f** F, Inset: Pure LDPE

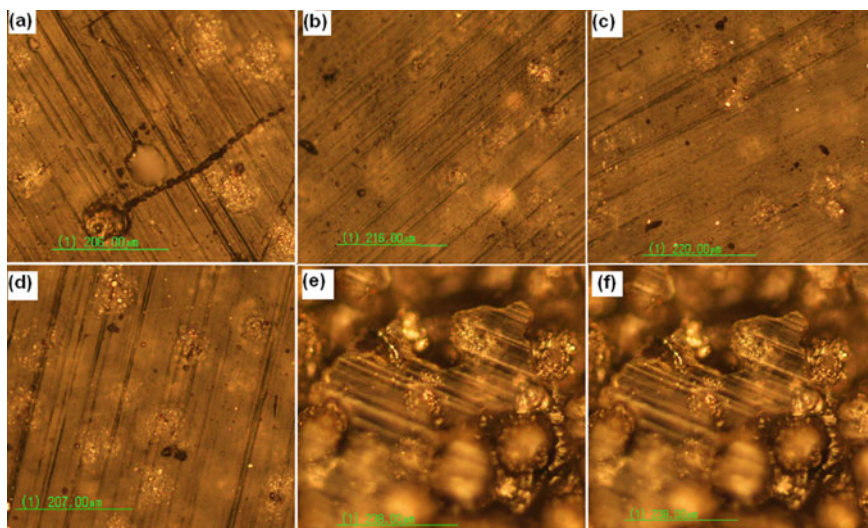


**Fig. 5.2** (Color online) Optical micrographs of the composites corresponding to different  $f_{\text{con}}$  of series C, i.e., hot-molded PVDF/ $\mu$ -Ni composites showing the morphological connectivities of filler particles/clusters, respectively, **a**  $f_{\text{con}} = 0.10$ , **b**  $f_{\text{con}} = 0.16$ , **c**  $f_{\text{con}} = 0.20$ , **d**  $f_{\text{con}} = 0.23$ , **e**  $f_{\text{con}} = 0.25$ , **f**  $f_{\text{con}} = 0.26$

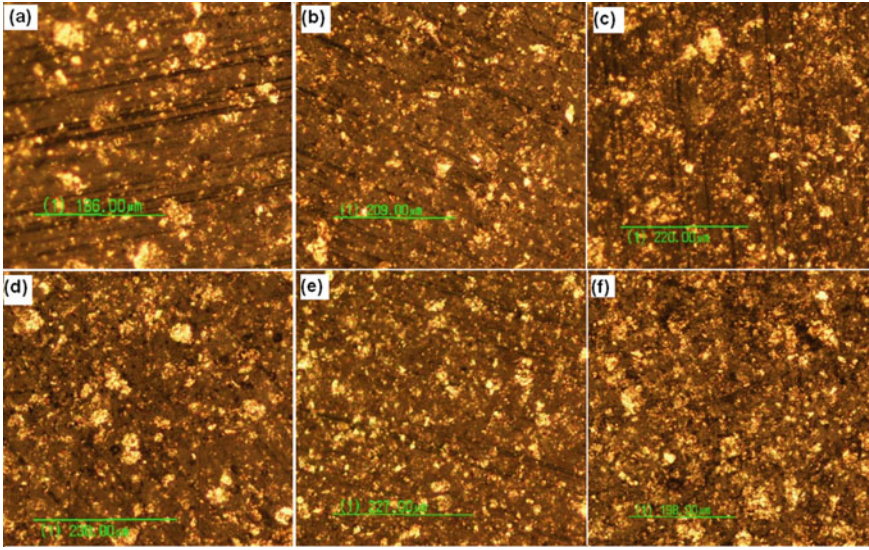


**Fig. 5.3** (Color online) Optical micrographs of the composites corresponding to different  $f_{\text{con}}$  of series D, i.e., hot-molded PVDF/n-Ni composites showing the morphological connectivities of filler particles/clusters, respectively, **a**  $f_{\text{con}} = 0.03$ , **b**  $f_{\text{con}} = 0.05$ , **c**  $f_{\text{con}} = 0.06$ , **d**  $f_{\text{con}} = 0.07$ , **e**  $f_{\text{con}} = 0.08$ , **f**  $f_{\text{con}} = 0.10$

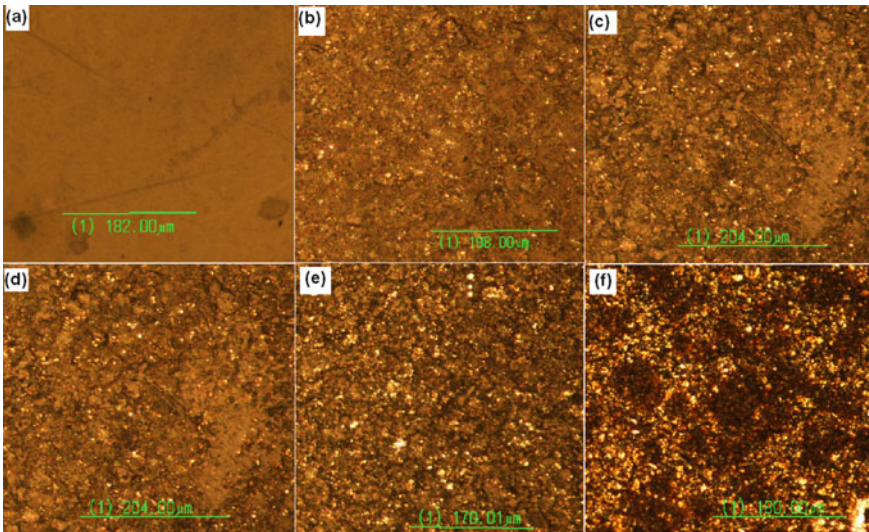


**Fig. 5.4** (Color online) Optical micrographs of the composites corresponding to different  $f_{\text{con}}$  of series E, i.e., cold-pressed PVDF/n-QC composites showing the morphological connectivities of filler particles/clusters, respectively, **a**  $f_{\text{con}} = 0.0$ , **b**  $f_{\text{con}} = 0.17$ , **c**  $f_{\text{con}} = 0.20$ , **d**  $f_{\text{con}} = 0.22$ , **e**  $f_{\text{con}} = 0.23$ , **f**  $f_{\text{con}} = 1.0$

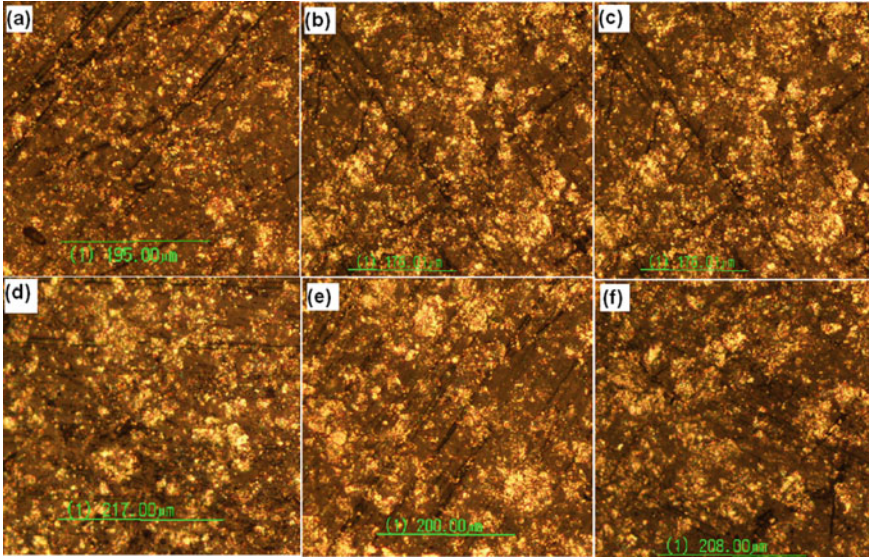


**Fig. 5.5** (Color online) Optical micrographs of the composites corresponding to different  $f_{\text{con}}$  of series F, i.e., hot-molded LDPE/n-Ni composites showing the morphological connectivities of filler particles/clusters, respectively, **a**  $f_{\text{con}} = 0.03$ , **b**  $f_{\text{con}} = 0.05$ , **c**  $f_{\text{con}} = 0.06$ , **d**  $f_{\text{con}} = 0.07$ , **e**  $f_{\text{con}} = 0.08$ , **f**  $f_{\text{con}} = 0.10$

all the samples undergo sharp transition and exhibit a peak in the endotherm at about 160 °C. This indicates that the melting in all the composites occurs at 160 °C as that is the melting temperature of pure polymer PVDF. We observe that with the increase of  $f_{\text{con}}$  only the heat of fusion decreases as the fraction of polymer in the composite decreases and less amount of heat is required at the melting temperature of the polymer for melting of the whole composite. To see whether the pattern of evolution of the heat of fusion during melting changes with different  $f_{\text{con}}$ , the normalized DSC curves are plotted in Fig. 5.6b. Hence, we find that the filler concentration does not affect the melting temperature of the polymer and also on the pattern of evolution of the phase transition of the composites. This indicates that PVDF polymer and PVDF/Ni composites respond similarly to the thermal treatment.

### 5.3.3 Dielectric Behavior

To find the relationship between the extent of enhancement of  $\epsilon_{\text{eff}}$  at  $f_c$  to the connectivity of fillers in PMC,  $\epsilon_{\text{eff}}$ , and change in loss tangent [ $\Delta \text{Tan } \delta$ ] [9, 10] (which is calculated as a measure of connectivity of the filler particles/clusters in a PMC) with respect to the pure polymer as a function of  $f_{\text{con}}$  for all series are shown in Fig. 5.7. The  $\epsilon_{\text{eff}}$  rises with an increase of  $f_{\text{con}}$  and increases abnormally at their respective

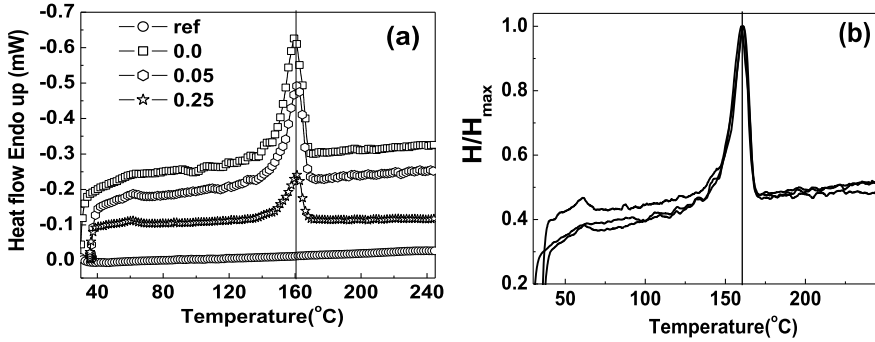


**Fig. 5.6** Typical differential scanning calorimetry (DSC) plots of the PMC corresponding to  $f_{con} = 0.05$  and  $f_{con} = 0.25$  of the series B, i.e., cold-pressed PVDF/n-Ni composites

$f_c$  for the different PMC. The  $f_c$  found for series A, B, C, D, E, and F are 0.57, 0.28,  $0.25 < f_c < 0.26$ , 0.07, 0.23, 0.06, respectively. We observe the difference in magnitude and the extent of enhancement of  $\epsilon_{eff}$  for all PMC at their respective  $f_c$ . Generally, the enhancement in  $\epsilon_{eff}$  in the neighborhood of  $f_c$  is explained based on the “boundary layer capacitor effect” [11–16]. Earlier reports (Fig. 1.1) show that a higher fraction of metal loading enhances the  $\epsilon_{eff}$  due to the formation of more interfaces in a composite and thus leading to an increase in accumulation of charges at the interfaces and enhancement in  $\epsilon_{eff}$ . It was also believed that the number of microcapacitors increases with increasing metal content in the composites which gives rise to high  $\epsilon_{eff}$ . But we observe from Fig. 5.7a that even though the  $f_c$  value is significantly different for the different series of samples under study, the magnitude of  $\epsilon_{eff}$  for all the composites at their respective  $f_c$  is comparable. It is further interesting to note that the higher  $\epsilon_{eff}$  is accompanied by a higher value of  $\Delta \tan \delta$ , which suggests that there is some correlation between the  $\epsilon_{eff}$  and  $\Delta \tan \delta$ . Although earlier assumptions seem to be logical, we confirm from our experimental results that the difference in spatial distribution and connectivity, arising due to the difference in process conditions are the most dominant factors, which play a key role in the extent of enhancement of  $\epsilon_{eff}$  at  $f_c$ . The network of microcapacitors and the distance between them (because only at a critical distance the local electric field of two clusters/particles can overlap) seem to play a major role in the enhancement of  $\epsilon_{eff}$ . From the published data in the literature and present data on various PMC composites, it is seen that the magnitude of  $\epsilon_{eff}$  is tuned by the dc conductivity (i.e., the loss tangent of the samples) as metals have very large values of static dielectric constant. To bring out these features more clearly, the  $\Delta \tan \delta$  and  $\sigma_{eff}$  for all the series of samples are plotted in Fig. 5.7b, c respectively. We observe that the pattern of evolution of all the electrical parameters, such as  $\epsilon_{eff}$ ,  $\Delta \tan \delta$ , and  $\sigma_{eff}$ , remains identical for all the series of samples as a function of  $f_{con}$ . It is observed that even though different composites exhibit different values of  $f_c$  the magnitude of  $\tan \delta$  and  $\sigma_{eff}$  for the composites containing less  $f_{con}$  is higher than the other composites of the present study, which is similar to the variation of  $\epsilon_{eff}$ . This indicates that connectivity and dc conductivity of the samples are the

important factors, which contribute to the extent of enhancement of  $\epsilon_{\text{eff}}$  as well as the loss tangent. The differences in  $f_c$  value observed for these systems from the ideal  $f_c = 0.16$  value is attributed to the difference in the size of the filler particles and process conditions which give rise to different extent of connectivity and overlapping of the effective tunneling range of the filler particles/clusters. It seems the “boundary layer capacitor effect” will work predominantly as long as the connectivity of filler particles is not developed (i.e., in the neighborhood of  $f_c$  and in the region for  $f_{\text{con}} \leq f_c$ ). We also observe that if we compare the extent of enhancement of  $\epsilon_{\text{eff}}$ ,  $\Delta \text{Tan} \delta$  and  $\sigma_{\text{eff}}$  between the PMC based on different matrices, i.e., in between series (A, B, C, D, and E) and the series F, we observe that the nature of polymer matrix also plays a significant role in the extent of enhancement of the electrical parameters for PMC at their respective  $f_c$  as have been already explained in the case of hot-molded PVDF/n-Ni and LDPE/n-Ni composites.

These qualitative arguments can be quantified by the critical exponents and their dependence on the extent of connectivity. To see the validity of  $x + y = 1$  in the vicinity of  $f_c$ , the scaling laws (1.1) and (1.2) have been fitted to the experimental results (Fig. 5.8) of all series of samples and the results are shown in Table 5.2. We

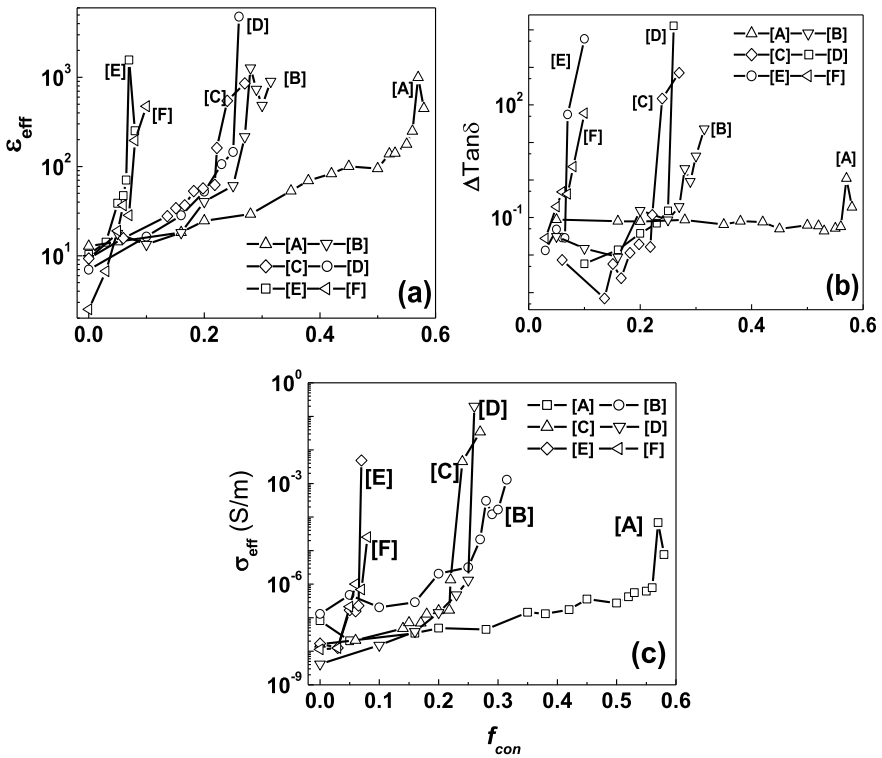


**Fig. 5.7** Dependence of the **a** Effective dielectric constant, **b** Change in Loss tangent, **c** Effective ac conductivity as a function of  $f_{\text{con}}$ , measured at 1 kHz and 300 K for all series of PMC

observe from Fig. 5.8 that the scaling laws (1.1) and (1.2) hold good for  $f_{\text{con}} \approx f_c$  as compared to  $f_{\text{con}} < f_c$ . The critical exponents  $x$  and  $y$  have been found for both the cases, and it has been found that the universal scaling behavior of  $x + y = 1$  at  $f_c$  best hold good for all the series of samples except for series D and F (Table 5.2). For series D the value of  $x + y = 1.19$ , i.e., higher than 1, is attributed to as the data for  $f_{\text{con}} = 0.065$  is taken which is below  $f_c = 0.07$  and for 0.07 also the scaling laws (1.1) and (1.2) doesn't hold good due to higher dc conductivity. We observe that due to the particular processing conditions and micron size of the filler particles for series D samples, the  $f_c$  value comes over a very narrow range of  $f_{\text{con}}$  beyond 0.065. For series F samples, we observe that  $x + y = 0.9$  for both  $f_{\text{con}} = 0.03$  and  $f_{\text{con}} = 0.05$  sample (i.e., for  $f_{\text{con}} < f_c$ ) while for  $f_{\text{con}} \approx f_c = 0.06$ , the value of  $x + y = 0.77$ . Hence, we observe the difference in the sum of the critical exponents ( $x + y$ ) for  $f_{\text{con}} < f_c$  and  $f_{\text{con}} \approx f_c$ . It can be seen from Table 5.2 that the values of  $x$  and  $y$  are different for different series of samples but interestingly the experimental values of  $x$  and  $y$  are closer to those predicted by the intercluster polarization (RC) model than those due to the effect of anomalous (fractal) diffusion [17, 18] on 3D percolating clusters. This result is also consistent with the observation of Song et al. [7] and Achour et al. [19] in CB-Teflon and CB-epoxy composites, respectively.

Since the exponents of the scaling laws (1.3)–(1.5) are related to  $x$  and  $y$  under the intercluster polarization (RC) model, the experimental results of all PMC are fitted to Eqs. (1.3) and (1.4) and the values of critical exponents  $s$  and  $s'$  are shown in Fig. 5.9 and Table 5.2. Although the critical exponent ' $s$ ' obtained from the fits is in agreement with the universal value of ' $s$ ' predicted for a 0–3 composite, i.e., ( $s_{\text{un}} = 0.7-1$ ) except for the series F sample, its value is different for different series of samples. As shown in Fig. 5.9b,  $s'$  is the conductivity critical exponent in the insulating region shows a higher value than the universal value ( $s' = 0.8-1$ ) for all series of samples, and  $s'$  is also different for different series of samples.

Further,  $s'$  also varies from one series of samples to another. The higher critical exponents also have been observed in many other continuum systems (references of Fig. 1.1), which have been explained by unusual models, such as the random void model/the swiss cheese model and the negative space/the inverted swiss cheese model, the position space renormalization group approximation model, and the transfer matrix method. Although the universality of percolation theory suggests that the dielectric constant should exhibit the same power-law dependence on  $f_{\text{con}}$  below  $f_c$ , so that  $s_{\text{un}} = s'_{\text{un}} = 0.8-1$ , this is not always observed in practical continuum systems and mostly in all practical cases  $s' \geq s$ . Since ' $t$ ' is related to the critical exponents ' $s$ ' and ' $s'$ ', and as  $s$  and  $s'$  vary for different series of samples, we expect the value of ' $t$ ' to be different for different series of samples. We observe from Fig. 5.9 that as the value of ' $s$ ' increases,  $s'$  also increase for all series of samples, and hence ' $t$ ' also should increase. There is a systematic increment of both  $s$  and  $s'$  for all the PMC in the same order.

The increase of  $s$ ,  $s'$ , and  $t$  can be correlated with the increase of  $\text{Tan } \delta$  and  $\sigma_{\text{eff}}$  (i.e., the extent of connectivity) at  $f_c$  for all the series of samples (Fig. 5.7b, c). It is observed that the higher the  $\Delta \text{Tan } \delta$  and  $\sigma_{\text{eff}}$  as a function of  $f_{\text{con}}$  for a particular PMC, the more becomes the extent of increment of the critical exponents,  $s'$  and  $t'$

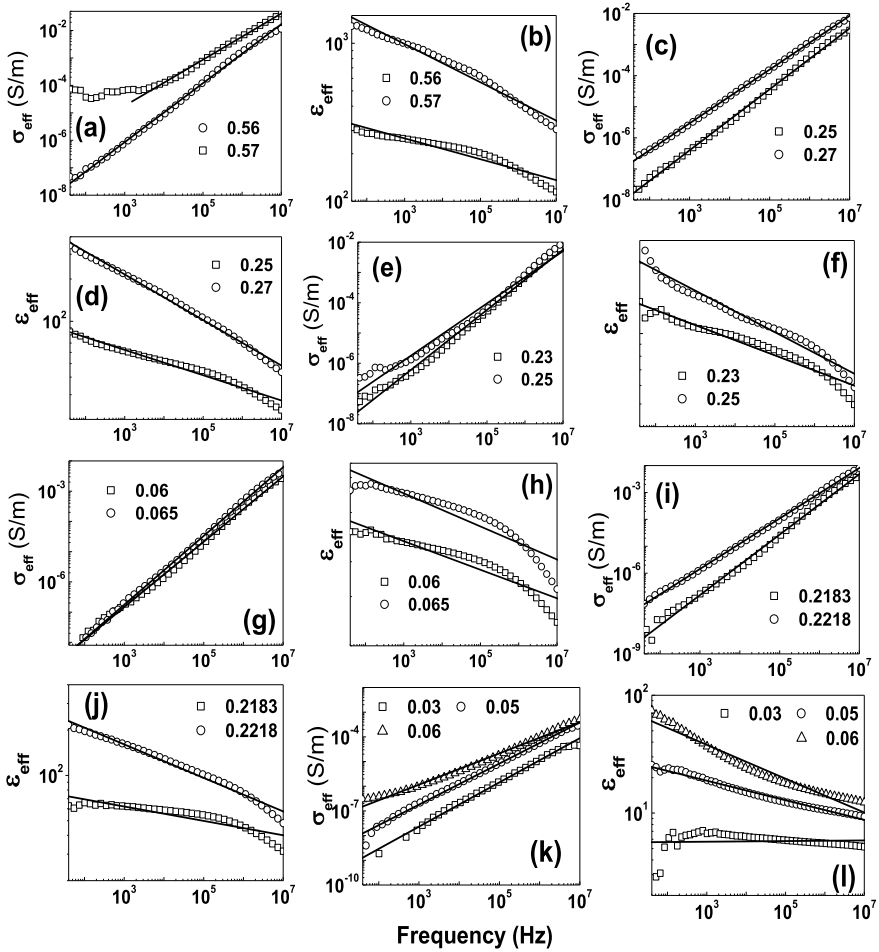


**Fig. 5.8** Fitting of Eqs. (1.1) and (1.2) to the experimental results of all the series of samples under study to obtain the critical exponents  $x$  and  $y$  in the vicinity of  $f_c$  for all the series of samples respectively at 300 K. The solid lines represent the fit to the corresponding experimental data, **a**  $x$  of series A, **b**  $y$  of series A, **c**  $x$  of series B, **d**  $y$  of series B, **e**  $x$  of series C, **f**  $y$  of series C, **g**  $x$  of series D, **h**  $y$  of series D, **i**  $x$  of series E, **j**  $y$  of series E, **k**  $x$  of series F, **l**  $y$  of series F

from their respective universal values in a PMC as can be observed from Figs. 5.7b, c and 5.9. We observe from Fig. 5.7b for series A, B, C that  $\Delta \text{Tan } \delta$  and  $\sigma_{\text{eff}}$  at  $f_c$  is in the order of  $C > B > A$ . Similarly, the value of  $s$  for series A, B, C are given by  $0.90 > 0.82 > 0.72$ , i.e., in the order of  $C > B > A$ . The value of  $s'$  for series A, B, C is also given by  $1.73 > 1.43 > 1.15$ , i.e., in the order of  $C > B > A$ . Thus, the increase of  $s, s', t, \epsilon_{\text{eff}}, \Delta \text{Tan } \delta$  and  $\sigma_{\text{eff}}$  for different PCC follows the same order. Similarly, the other group of series of samples can be compared which can suggest that there is a relationship between the critical exponents and dielectric tangent loss,

**Table 5.2** Critical exponents  $s$  and  $s'$  along with their  $f_c$  values and the values of  $x$  and  $y$  corresponding to  $f_{con} < f_c$  and  $f_{con} \approx f_c$  for all series of samples under study

Series	$f_c$	$s$	$s'$	$f_{con} < f_c$	$x = \frac{f}{(s+t)}$	$y = \frac{s}{(s+t)}$	$x + y > 1$	$f_{con} \approx f_c$	$x = \frac{f}{(s+t)}$	$y = \frac{s}{(s+t)}$	$x + y = 1$
A	0.572	$0.72 \pm 0.05$	$1.15 \pm 0.1$	0.56	1.07	0.065	1.135	0.57	0.844	0.13	0.973
B	0.278	$0.82 \pm 0.07$	$1.43 \pm 0.31$	0.25	0.98	0.09	1.07	0.27	0.863	0.16	1.023
C	0.259	$0.90 \pm 0.10$	$1.73 \pm 0.20$	0.23	0.99	0.06	1.05	0.25	0.863	0.09	0.953
D	0.07	$0.75 \pm 0.10$	$1.16 \pm 0.4$	0.06	1.08	0.05	1.13	0.065	1.13	0.06	1.19
E	0.23	$0.69 \pm 0.09$	$1.09 \pm 0.15$	0.21	1.12	0.04	1.16	0.222	0.94	0.11	1.05
				83							
F	0.06	$1.11 \pm 0.12$	$1.71 \pm 0.66$	0.05	0.83	0.08	0.92	0.06	0.63	0.14	0.77
				0.03	0.90	0.002	0.902				

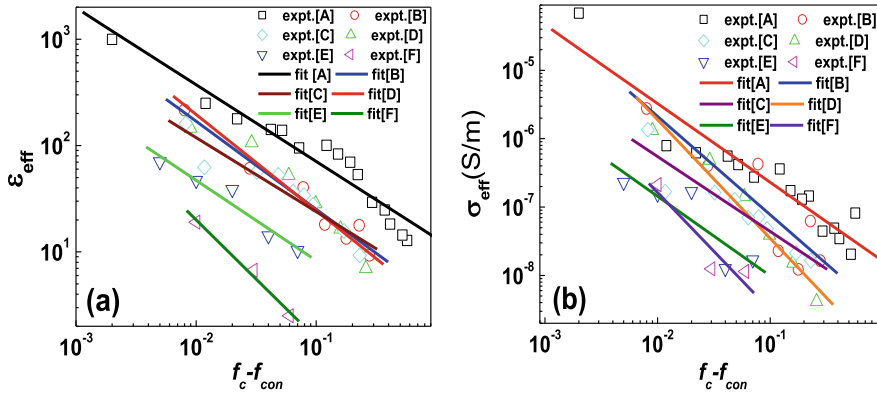


**Fig. 5.9** (Color online) Fitting of Eqs. (1.3) and (1.4) to the experimental results of all the series of PMC under study to obtain the critical exponents at 300 K, **a**  $s$  and **b**  $s'$

i.e., the extent of connectivity. However, on comparison with all the series of PMC at the same time, the clear distinction of the relationship between the increment of critical exponents and  $\Delta \text{Tan } \delta$  is not possible among the different PMC as some series of samples are having approximately the same loss tangent and that time the instruments inaccuracy of measuring the exact tangent loss also. In addition to that also the relationship is going to be masked due to the error introduced for calculation of the critical exponents for individual PMC which can be observed as the different extent of error in measurement of critical exponents is found for different series of samples.

To provide the supporting experimental evidence of connectivity of metal filler particles/clusters in the PMC is the origin which gives rise to a large enhancement of dielectric loss tangent, dielectric constant/capacitance, and large deviation of critical exponents from their respective universal values, the typical capacitance/dielectric constant as a function of temperature is performed on some of the samples of series B (Fig. 5.10). The samples chosen were  $f_{\text{con}} = 0.25$  and  $0.05$  in which one was very close to the  $f_c$ , i.e.,  $f_{\text{con}} = 0.25$  and the other one was well below  $f_c$ , i.e.,  $f_{\text{con}} = 0.05$ . We observe from Fig. 5.10 that with the increase of temperature from 25 to 110 °C for the sample  $f_{\text{con}} = 0.05$ , the value of capacitance which is of the order of Pico Farad remains almost constant over the experimentally measured whole frequency region. With further increase of temperature up to 215 °C, the magnitude of capacitance increases and undergoes the initiation of low-frequency dispersion. With further increase of temperature anomalous low-frequency dispersion of the capacitance and a sudden rise in loss tangent occurs at 250 °C and the  $\text{Tan } \delta$  value goes on increase beyond 250 °C. As a function of temperature, the sample 0.05 which was insulator at room temperature and also up to 215 °C becomes gradually a conductor at  $\geq 250$  °C. This occurs due to the melting of the polymer which occurs at 160 °C (Fig. 5.6) and the metallic filler particles approach each other, thereby making an infinite network of metal clusters forming a conductor. On the other hand,

when similar experiments were carried out in the case of sample  $f_{\text{con}} = 0.25$  the IMT occur at a lower temperature of 200 °C showing the different features (Fig. 5.11). We observe that across the IMT temperature, both the capacitance and dielectric loss tangent in the case of  $f_{\text{con}} = 0.25$  and  $f_{\text{con}} = 0.05$  undergoes a sharp rise in their value from the ordered of  $10^{-12}$  F to the ordered of  $10^{-9}$  F occurring at different temperatures (Fig. 5.11). The sharp increase of capacitance and loss tangent can be explained due to the combined effect of the increase of connectivity of the metal filler clusters in the polymer matrix and may be partly due to the change in thickness of the samples. However, we observe that up to 200 °C in both cases of  $f_{\text{con}} = 0.25$  and  $f_{\text{con}} = 0.05$  (Figs. 5.10 and 5.11) the capacitance and loss tangent does not change significantly although at that time the change of thickness of the sample has occurred. However, even after 200 °C the capacitance and loss tangent undergoes a transition at different temperatures for the two different samples. Thus, we interpret that due to the difference in  $f_{\text{con}}$  the density of distribution of metal filler particles in the polymer matrix is higher in case of  $f_{\text{con}} = 0.25$  as compared to  $f_{\text{con}} = 0.05$  and with the increase of temperature, the polymer matrix starts melting and the extent of isolation of metal filler particles/clusters decrease and in the two different cases, the appearance of a network of connectivity of filler clusters becomes different. Hence, the network of infinite connectivity of the metal filler particles occurs at percolation and occurs at two very different temperatures, i.e., at 200 °C and 250 °C, respectively, for the two typical cases of  $f_{\text{con}} = 0.25$  and  $f_{\text{con}} = 0.05$  samples. Hence, the different IMT temperature observed for two different sample with  $f_{\text{con}} = 0.05$  and  $f_{\text{con}} = 0.25$  is due to the different density of filler particles in the matrix and different extent of connectivity of the metal filler particles/clusters for the two samples with  $f_{\text{con}} = 0.05$  and  $f_{\text{con}} = 0.25$  at any constant temperature. Hence, the temperature at which the network of infinite connectivity of the conducting clusters will occur must be different for different  $f_{\text{con}}$  samples.

### 5.3.4 Frequency-Dependent Scaling Behavior

To understand the scaling behavior at exactly the percolation threshold, Eqs. (1.1) and (1.2) (given in the introduction section) of percolation theory have been used to understand the experimental results as a function of the whole range of frequencies and are given in Fig. 5.12 and Table 5.3. The critical exponents  $x$  and  $y$  have been found for both the cases, and it has been found that the universal scaling behavior of  $x + y = 1$  at  $f_c$  best holds good for all the series of samples. The exponents ( $x = 0.72$  and  $y = 0.28$ ) obtained under the intercluster polarization model for the case of 3D systems are consistent with the experimental values.

Since the exponents of the scaling laws (1.3)–(1.5) are related to  $x$  and  $y$  under the intercluster polarization (RC) model, the experimental results of the series A are fitted to Eqs. (1.3) and (1.4) and the values of critical exponents  $s$  and  $s'$  at different frequencies are shown in Fig. 5.13 and Table 5.3.

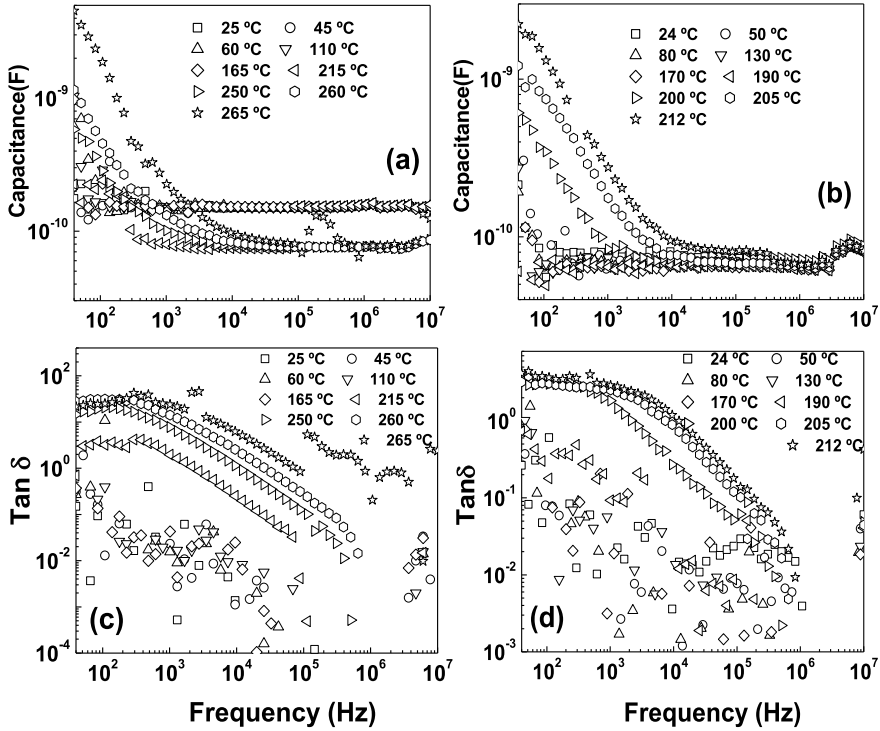


**Fig. 5.10** Variation of capacitance, **a**  $f_{con} = 0.05$ , **b**  $f_{con} = 0.25$  and  $\tan \delta$ , **c**  $f_{con} = 0.05$ , **d**  $f_{con} = 0.25$  as a function of frequency for different temperatures for two typical samples of series B

It is observed that the universal values of the critical exponent  $s$  and  $s'$  are found at certain particular frequencies, *while* with the increase of frequency, the value of exponent decreases. To see the general trend the same analysis was extended to all other series of PMC and obtained results are already given in Table 5.4 and Figs. 5.14, 5.15, 5.16 and 5.17. Already The non-universality of  $s$ ,  $s'$ ,  $t$  is correlated with the extent of spatial connectivity of filler particles, and the experimental values of  $\tan \delta$ .

To find the variation of critical exponents ( $s$  and  $s'$ ) as a function of frequency, the data of ( $s$  and  $s'$ ) obtained from the fitting of experimental data of PMC at various frequencies (Figs. 5.13, 5.14, 5.15, 5.16 and 5.17) are given in Fig. 5.18 for getting a clear picture. In all PMC, the value of critical exponents ( $s$  and  $s'$ ) is found to be universal as well as non-universal at different frequency domains. The values of ( $s$  and  $s'$ ) are found to decrease with the increase of frequency, while the observation of increase of critical exponents with the increase of frequency has been reported in some other reported dielectric conductor composites also. The decrease of ( $s$  and  $s'$ ) with the increase of frequency is attributed to the method of preparation, particle size, adhesiveness of polymer/filler, and the rate of decrease of  $\epsilon_{eff}$  with frequency (due to the absence of different extent of contribution of various types polarizations present in the PMC).

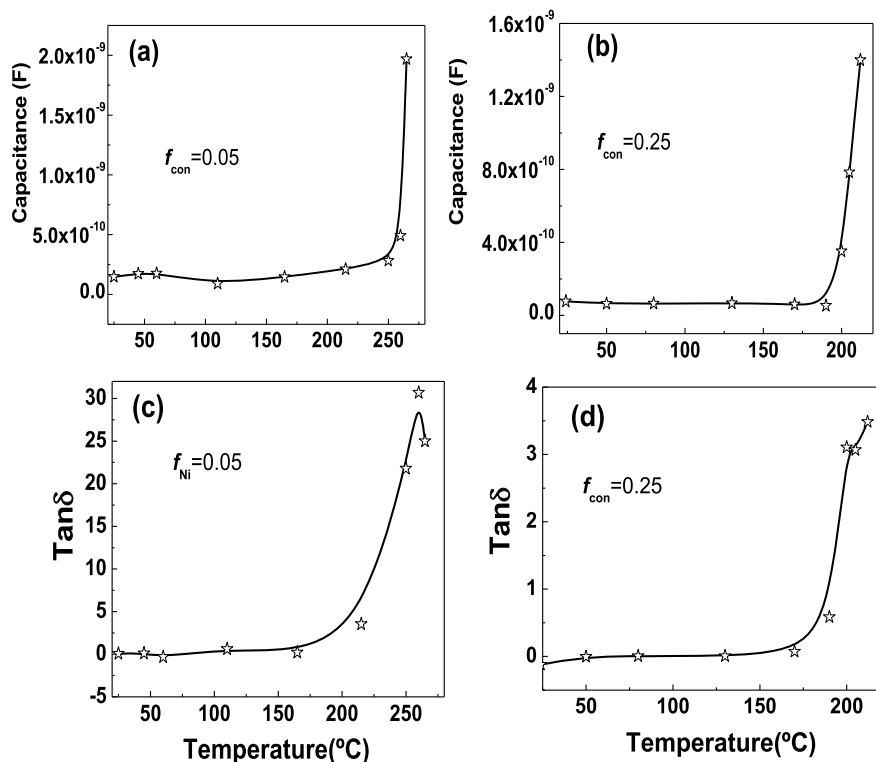


**Fig. 5.11** Variation of capacitance, **a**  $f_{\text{con}} = 0.05$ , **b**  $f_{\text{con}} = 0.25$  and  $\tan \delta$ , **c**  $f_{\text{con}} = 0.05$ , **d**  $f_{\text{con}} = 0.25$  as a function of temperature for the two typical samples of series B at 100 Hz

## 5.4 Summary

The origin of the extent of enhancement of dielectric constant ( $\epsilon_{\text{eff}}$ ) value for insulating polymer-metal composites (PMC) at their respective percolation threshold ( $f_c$ ) is attributed to spatial distribution, connectivity (coupling between the two individual phases), intercluster distance, and dc conductivity of the samples. The universal percolation behavior in the vicinity of  $f_c$ , is satisfied; with  $x + y = 1$ , with the exponents ( $x = 0.72$  and  $y = 0.28$ ) under the intercluster polarization model. The critical exponents  $s$ ,  $s'$ , and  $t$  which characterize the divergence of  $\epsilon_{\text{eff}}$  and  $\sigma_{\text{eff}}$  in the vicinity of  $f_c$  are related to  $x$  and  $y$  under the intercluster polarization model and are found to be greater than their respective universal values. These variations are correlated to the extent of connectivity of the conducting filler particles in PMC, which is reflected in the experimental values of loss tangent for these composites. The  $f_c$  value decreases with the increase of the extent of connectivity of the metal fillers in PMC due to the difference in process conditions. In the practical continuum percolation systems, the non-universality of critical exponents occurs and it is shown that the

**Fig. 5.12** (Color online) Fitting of Eqs. (1.1) and (1.2) to the experimental results of all the PMC to obtain the critical exponents  $x$  and  $y$  in the vicinity of  $f_c$  for all the series of samples, respectively, at 300 K. The solid lines represent the fit to the corresponding experimental data, **a**  $x$  of series A, **b**  $y$  of series A, **c**  $x$  of series B, **d**  $y$  of series B, **e**  $x$  of series C, **f**  $y$  of series C, **g**  $x$  of series D, **h**  $y$  of series D, **i**  $x$  of series E, **j**  $y$  of series E

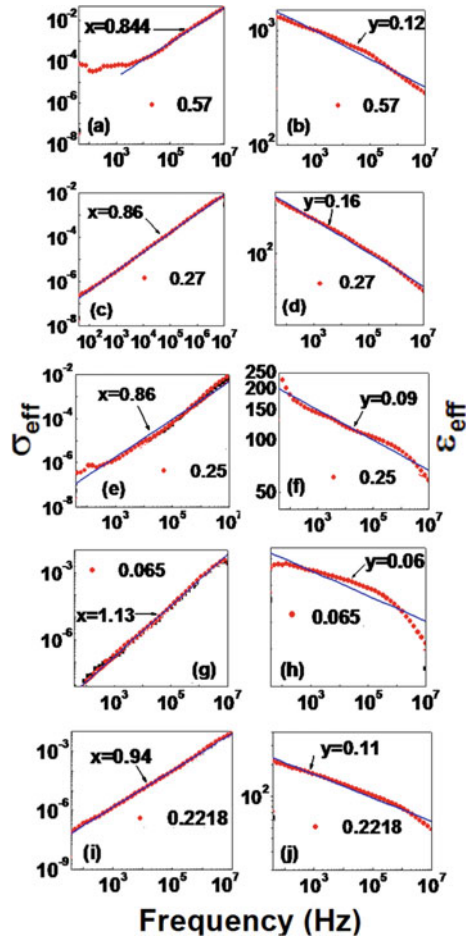


**Table 5.3** Values of exponents  $x$  and  $y$  corresponding to  $f_{con} \approx f_c$  for all series of PMC and the verification of intercluster (RC) model, i.e.,  $x + y = 1$

Series	$f_c$	$f_{con} \approx f_c$	$x$	$y$	$x + y = 1$
A	0.572	0.57	0.844	0.13	0.973
B	0.278	0.27	0.863	0.16	1.023
c	0.259	0.25	0.863	0.09	0.953
D	0.07	0.065	1.13	0.06	1.19
E	0.23	0.222	0.94	0.11	1.05

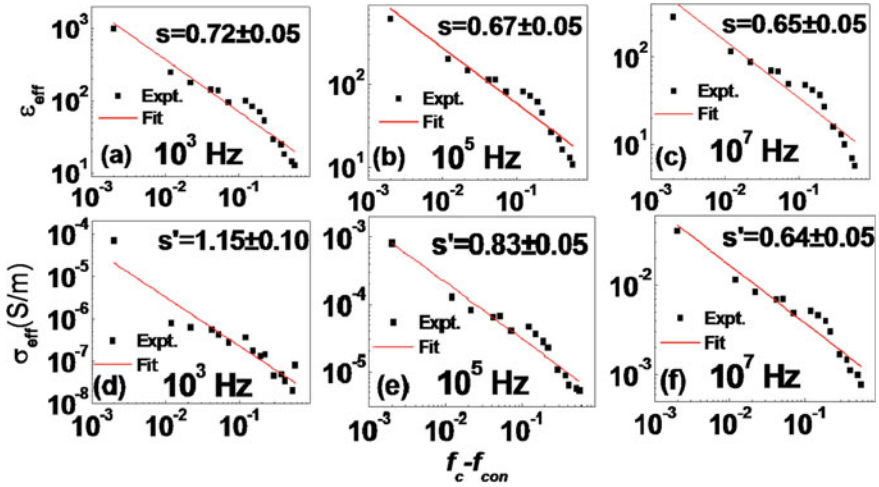


**Fig. 5.13** (Color online) Fitting of Eqs. (1.3) and (1.4) to the experimental results of the PMC of series A to obtain the critical exponents at 300 K and various frequencies,  $s$  at **a**  $10^3$  Hz, **b**  $10^5$  Hz, **c**  $10^7$  Hz and  $s'$  at **d**  $10^3$  Hz, **e**  $10^5$  Hz, **f**  $10^7$  Hz

values of critical exponents vary with the extent of connectivity of the filler particles/clusters in the composites. Hence, the origin of dielectric constant and deviation of critical exponents from the universal values in a PCC is related to the connectivity of conductive filler particles, i.e., the loss tangent. The different PMC gave different values of  $f_c$  with different extent of enhancement of  $\epsilon_{\text{eff}}$  and  $\sigma_{\text{eff}}$  at their respective  $f_c$  for different frequencies. The values of  $f_c$  are found to be non-universal as compared to the theoretically predicted ideal value. The non-universal values of  $f_c$  for different PMC have been attributed to a variety of parameters, such as size, shape, and process conditions. The value of  $f_c$  is found to be independent of the frequency of the applied ac signal since the universal percolation equations are satisfied in the vicinity of IMT, suggesting the investigated PMC systems are real percolating systems. The analysis of the experimental data of a variety of different classes of PMC confirms the obtained scaling exponents [ $s$ ,  $s'$ ] to be both universal and non-universal and is dependent on the frequency of the applied ac signal. The decrease of critical exponents with the increase of frequency is attributed to the method of preparation, size of fillers, adhesiveness of polymer/filler, and the rate of decrease of  $\epsilon_{\text{eff}}$  with frequency in case of all PMC.

**Table 5.4** Values of critical exponents  $s$  and  $s'$  across the IMT for all series of PMC at different frequencies

Series	$f_c$	$f_{con} \sim f_c$	$s$			$s'$		
			$10^3$ Hz	$10^5$ Hz	$10^7$ Hz	$10^3$ Hz	$10^5$ Hz	$10^7$ Hz
A	0.572	0.57	$0.72 \pm 0.05$	$0.67 \pm 0.05$	$0.65 \pm 0.05$	$1.15 \pm 0.10$	$0.83 \pm 0.05$	$0.64 \pm 0.05$
B	0.278	0.27	$0.82 \pm 0.07$	$0.75 \pm 0.06$	$0.57 \pm 0.05$	$1.43 \pm 0.31$	$1.04 \pm 0.12$	$0.65 \pm 0.07$
C	0.259	0.25	$0.90 \pm 0.10$	$0.80 \pm 0.13$	$0.76 \pm 0.14$	$1.73 \pm 0.20$	$1.14 \pm 0.16$	$0.86 \pm 0.13$
D	0.07	0.065	$0.75 \pm 0.10$	$0.70 \pm 0.08$	$0.67 \pm 0.10$	$1.16 \pm 0.40$	$0.95 \pm 0.17$	$0.71 \pm 0.06$
E	0.23	0.23	$0.69 \pm 0.09$	$0.61 \pm 0.08$	$0.59 \pm 0.08$	$1.09 \pm 0.15$	$0.80 \pm 0.11$	$0.65 \pm 0.09$

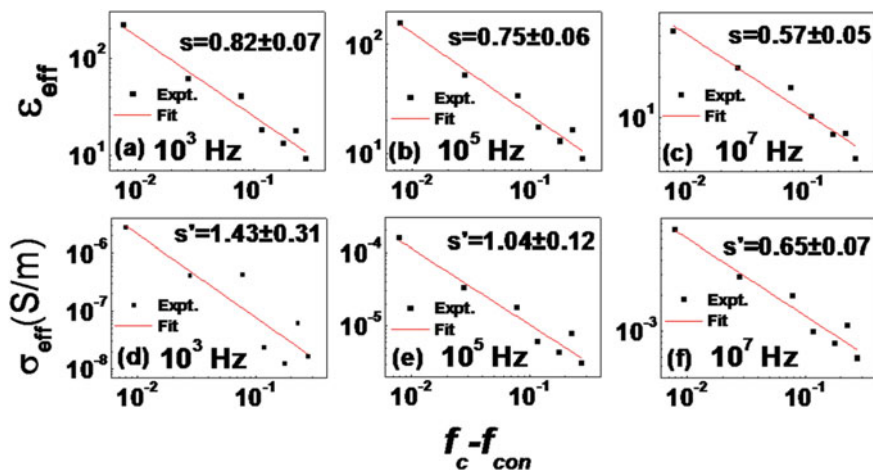


Fig. 5.14 (Color online) Fitting of Eqs. (1.3) and (1.4) to the experimental results of the PMC of series B to obtain the critical exponents at 300 K and at various frequencies,  $s$  at a  $10^3$  Hz, b  $10^5$  Hz, c  $10^7$  Hz, and  $s'$  at d  $10^3$  Hz, e  $10^5$  Hz, f  $10^7$  Hz

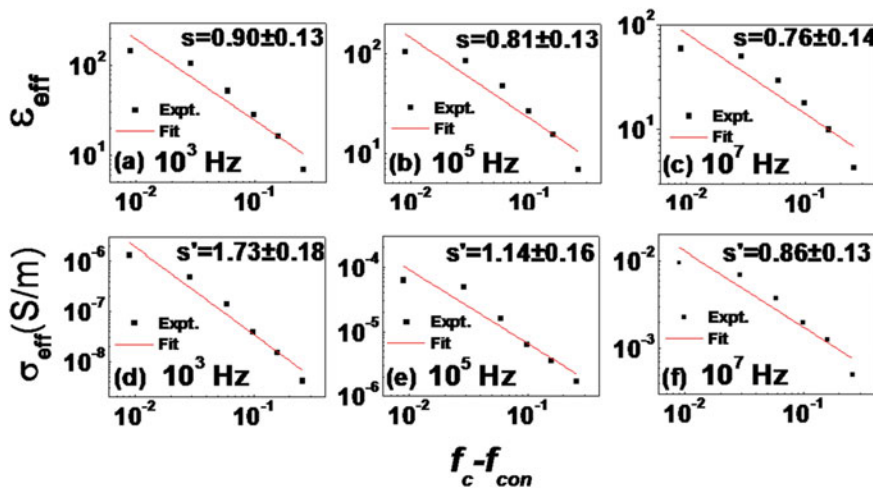


Fig. 5.15 (Color online) Fitting of Eqs. (1.3) and (1.4) to the experimental results of the PMC of series C to obtain the critical exponents at 300 K and various frequencies,  $s$  at a  $10^3$  Hz, b  $10^5$  Hz, c  $10^7$  Hz and  $s'$  at d  $10^3$  Hz, e  $10^5$  Hz, f  $10^7$  Hz

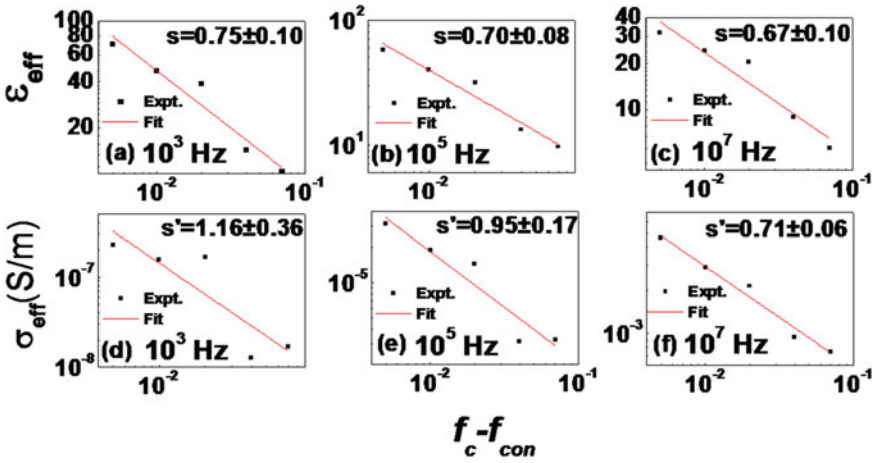


Fig. 5.16 (Color online) Fitting of Eqs. (1.3) and (1.4) to the experimental results of the PMC of series D to obtain the critical exponents at 300 K and various frequencies,  $s$  at a  $10^3$  Hz, b  $10^5$  Hz, c  $10^7$  Hz and  $s'$  at d  $10^3$  Hz, e  $10^5$  Hz, f  $10^7$  Hz

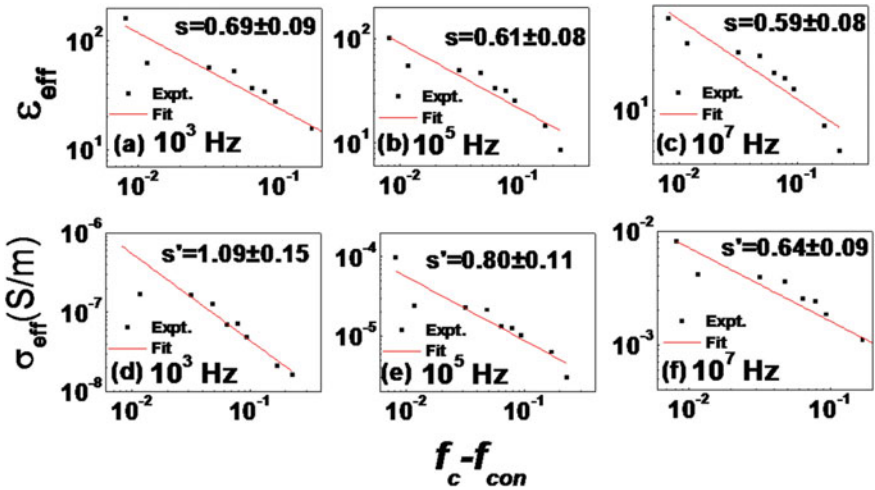
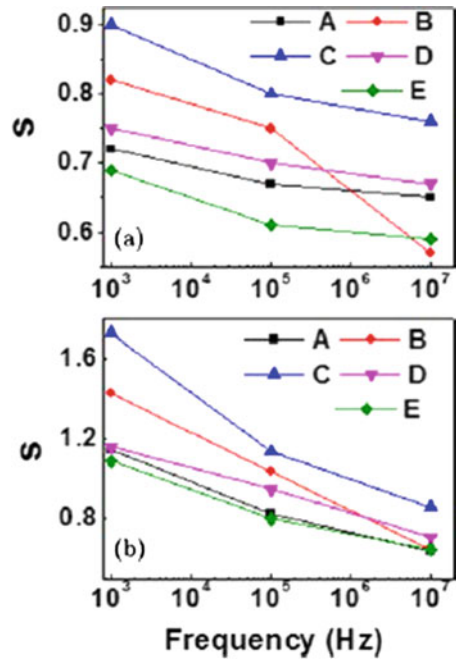


Fig. 5.17 (Color online) Fitting of Eqs. (1.3) and (1.4) to the experimental results of the PMC of series E to obtain the critical exponents at 300 K and various frequencies,  $s$  at a  $10^3$  Hz, b  $10^5$  Hz, c  $10^7$  Hz and  $s'$  at d  $10^3$  Hz, e  $10^5$  Hz, f  $10^7$  Hz

**Fig. 5.18** (Color online)  
Variation of critical exponents ( $s$  and  $s'$ ) with the increase of frequency



## References

1. Halperin BI, Feng S, Sen PN (1985) Difference between lattice and continuum percolation transport exponents. *Phys Rev Lett* 54:2391–2394
2. Feng S, Halperin BI, Sen PN (1987) Transport properties of continuum systems near the percolation threshold. *Phys Rev B* 35:197–214
3. Balberg I (1987) Tunnelling and non-universal conductivity in composite materials. *Phys Rev Lett* 59:1305–1308
4. Rubin Z, Sunshine SA, Heaney MB, Bloom I, Balberg I (1999) Critical behavior of the electrical transport properties in a tunneling-percolation system. *Phys Rev B* 59:12196–12199
5. Bug ALR, Grest GS, Cohen MH, Webman I (1987) ac response near the percolation threshold: transfer-matrix results in two and three dimensions. *Phys Rev B* 36:3675–3682
6. Wilkinson D, Langer JS, Sen PN (1983) Enhancement of the dielectric constant near a percolation threshold. *Phys Rev B* 28:1081–1087
7. Song Y, Noh TW, Lee SI, Gaines JR (1986) Experimental study of the three dimensional ac conductivity and dielectric constant of conductor-insulator composite near the percolation threshold. *Phys Rev B* 33:904–908
8. Lee SI, Song Y, Noh TW, Chen XD, Gaines JR (1986) Experimental observation of non-universal behavior of the conductivity exponent for three-dimensional continuum percolation systems. *Phys Rev B* 34:6719–6724
9. Panda M, Srinivas V, Thakur AK (2015) Non-universal scaling behavior of polymer-metal composites across the percolation threshold. *Res Phys* 5:136–141
10. Panda M (2019) Frequency-dependent scaling behavior of polyvinylidene fluoride/metal composites. *J Adv Dielect* 09:19500101–19500106
11. Panda M (2017) Major role of process conditions in tuning the percolation behavior of polyvinylidene fluoride-based polymer/metal composites. *App Phys Lett* 111:0829011–0829015

12. Panda M, Srinivas V, Thakur AK (2014) Percolation behaviour of polymer-metal composites on modification of filler. *Mod Phys Lett B* 28:14500551–14500556
13. Panda M, Srinivas V, Thakur AK (2011) Role of polymer matrix in large enhancement of dielectric constant in polymer-metal composites. *App Phys Lett* 99:0429051–0429053
14. Venketesh C, Srinivas V, Panda M, Rao VV (2010) Dielectric response in novel polyvinylidene fluoride/nanoquasicrystalline composites. *Solid State Communications* 150:893–896
15. Panda M, Srinivas V, Thakur AK (2008a) On the question of percolation threshold in polyvinylidene fluoride/nanocrystalline nickel composites. *Appl Phys Lett* 92:132905–132907
16. Panda M, Srinivas V, Thakur AK (2008b) Surface and interfacial effect of filler particle on electrical properties of polyvinylidene fluoride/nickel composites. *Appl Phys Lett* 93:242908–242910
17. Gefen Y, Aharony A, Alexander S (1983) Anomalous diffusion on percolating clusters. *Phys Rev Lett* 50:77–80
18. Laibowitz RB, Gefen Y (1984) Dynamic scaling near the percolation threshold in thin Au films. *Phys Rev Lett* 53:380–383
19. Achour ME, Brosseau C, Carmona F (2008) Dielectric relaxation in carbon black-epoxy composite materials. *J Appl Phys* 103(1–10):094103

# Chapter 6

## Relaxation Behavior of Percolative Polymer Composites



In this chapter, the universality of dielectric relaxation behavior in a wide variety of polymer–conductor composites (PCC) is discussed. The quantification of dielectric relaxation behavior in the PCC has been done in terms of the relaxation exponents of Jonscher’s universal dielectric response (JUDR) laws. The magnitude of relaxation exponents ‘ $m$ ’, ‘ $n$ ’, and ‘ $p$ ’, evaluated from the experimental results using JUDR laws, has been studied as a function of  $f_{\text{con}}$ . The physical significance of these exponents has been discussed in terms of  $f_{\text{con}}$  and the percolation mechanism. The experimental results have been rationalized by the use of Hill plots. The two kinds of generalized Jonscher’s universal dielectric response (JUDR) laws on both sides of IMT hold good, while for the percolative sample, none of the two laws hold good. Neither the concept of dipolar relaxation nor anomalous low-frequency dispersion stands valid for  $f_c = 0.27$ , while a completely different, neutral, and competing electrical behavior is observed over the entire range of frequencies. The emerged the third kind of Jonscher’s like UDR for  $f_c$  is observed, and the relaxation law has been formulated as the ratio of imaginary and real part of dielectric constant remains constant over the entire range of frequency starting from dc to any higher frequency. The value of the constant is attributed to depend on the PMC, the dielectric constant of the polymer, the differences of conductivity and fractions of the components of the PMC, and also on their connectivity arising due to the difference of their process conditions. The emerged unique dielectric relaxation consists of multiple relaxations arising due to the combination of other relaxations (arising due to the two different types of species) present in the sample,  $f_{\text{con}} = 0.27$ . This novel material may be suitable for certain specific applications in electrical and electronics engineering.

### 6.1 Introduction

The earlier Chaps. 4 And 5 have mainly dealt with the static behavior of the PCC and their dependences on  $f_{\text{con}}$  across the percolation threshold ( $f_c$ ). However, to be

able to extract information on the homogeneity of a composite sample from a single measurement, that may be possible in principle by the analysis of various electrical parameters as a function of frequency. Therefore, the detailed investigation of dielectric relaxation behavior for all PCC as a function of frequency and  $f_{\text{con}}$  is discussed in this chapter, while their electrical properties have been discussed in Chap. 7. The detailed theoretical background of understanding the dielectric relaxation phenomena in various systems has already been given in Chap. 2.

There has been a significant amount of theoretical as well as experimental work, reported on insulator–conductor composites (ICC)/PCC to unravel and understand issues related to percolation in these composites. These heterostructures provide an opportunity to analyze generic problems, such as percolation, scaling, and universality, low dimensional transport properties, appearing in many strongly correlated systems [1, 2]. The quantity that characterizes the collective response to an external ac electric field excitation in this PCC/ICC is the effective dielectric constant ( $\epsilon_{\text{eff}}$ ). While studying these composites, significant attention has been devoted to effective medium theory (EMT) [3] in terms of volume averages, thereby enabling electrical measurements to monitor these properties. The basic idea is to describe the system by a simple average permittivity measured using a self-consistent procedure, such that a grain of one of the constituents is assumed to have a well-defined shape (usually taken as spherical or ellipsoidal) and is considered to be embedded in an effective medium (homogeneous) whose properties are self-consistent. This requires the wavelength of the electromagnetic radiation probing the system has to be larger than a typical length scale that characterizes the in-homogeneities in the material medium. In this limit, we can interpret our experimental data using EMT without any loss of generality. If the above conditions are not obeyed, there would be a definite possibility that the internal structure of the medium can diffract as well as refract radiation. Further, multiple scattering losses due to random walk diffusion of the wave from one scattering center to another through the composite system determines the dielectric response of heterostructures a complicated task. From the perspective of the theory of homogenization, one can explain at least partially, many of the observed features by simply considering a quasistatic approach, thereby ignoring altogether the details of the microstructure and any other complications (e.g., aggregation and adsorption).

Liu [4] recognized that the understanding of the processes governing the electrical (charge and wave) transport under alternating fields in percolation clusters of PCC/ICC is of prime interest. Further, the dielectric relaxation behavior in particle-filled polymeric systems is complex and an understanding of polarization mechanisms in these materials over frequency remains incomplete. Dielectric relaxation in these types of in-homogenously disordered solids (PCC) continues to be of interest due to the important technological applications in the context of microwave and optical remote sensing and communication. Although dielectric relaxation behavior has been studied theoretically and experimentally in many PCC, still it requires to be investigated and verified experimentally to find out the consistency of the dielectric relaxation phenomenon and its universalization in the case of PCC [5–9]. As PCC are composites of two components, their properties may be expected to be controlled

by either of them (for any ratio of conductor to polymer in the PCC) due to the competition between the properties of two individual components as a function of their volume or weight fractions in the composite. In the case of PCC based on a polar polymer and a conductor, composites appear to be dominated by the dipolar behavior of the polymer as long as it is in the insulator side and exhibits strong charge carrier-dominated behavior beyond  $f_c$ , where the appearance of the long-range dc conductivity is the normal phenomena (References of Fig. 1.1). On the other hand, for a PCC containing a non-polar polymer, charge carrier-dominated behavior may only be expected beyond  $f_c$ . To confirm it experimentally, a wide variety of possible PCC combinations based on different polymers (polar and non-polar) with different conductors of varying particle sizes are prepared under different process conditions.

Recent researches have proved the ongoing development of high-temperature polymer dielectrics, both experimentally as well as theoretically/computationally. Out of these polymer dielectrics, ferroelectric polymer dielectrics (FPD) have proven themselves as the emerging materials of the future for electrostatic energy storage and dielectric applications, due to their higher dielectric constant, lower loss tangent and higher dielectric field strength [10]. In the development of this FPD, the hit and trial combination method comprising of varieties of ferroelectric polymers [polyvinylidene fluoride (PVDF), polyvinylidene fluoride trifluoroethylene [PVDF (TrFE)], etc., and varieties of fillers [metal, carbon nanotube, carbon black, graphene, etc.] are undergoing extensive investigations through various experimental methods. Out of these methods (hot molding, cold pressing, etc.), recent results have confirmed the importance and usefulness of the cold pressing method in the case of FPD as compared to the traditional hot molding process, since the cold pressing method develops better polymer dielectrics by retaining the spherulites as well as the flexibility of PVDF.

However, in the process of development of this FPD, a thorough understanding of dielectric relaxation behavior in this type of filler dispersed polymeric systems is required for their better design and development. The dielectric relaxation behavior has been reported theoretically and experimentally in a lot of dielectric systems, by the use of the various standard formalisms, such as Debye [11], Cole–Cole [12], Cole–Davidson [13], Havriliak–Negami [14], Hill [15], Macdonald [16], and Jonscher [17]. According to Jonscher, there are fundamentally two different types of polarization response due to the presence of two different types of polarization species in a dielectric system, under a steady electric field, such as (i) a strongly correlated dipolar system and (ii) a strongly correlated charge carrier (ionic or electronic) system.

Interestingly, it can also do believe that there must be different dielectric systems, completely different from the traditional fundamental systems as discussed above, which must be neither a dipolar nor a charge carrier-dominated system or must be an equally dipolar/charge carrier-dominated system and that must be at the exact boundary of the insulator to metal transition (IMT) of the polymer/metal composites (PMC). Since it has been found that PVDF/Ni composites have proven themselves as very good materials for energy storage, and electromagnetic interference shielding applications. Hence with the expectation of getting this unique type of dielectric relaxation behavior, a variety of series of PVDF/Ni composites with varying size &

type of filler and varying process conditions (hot molding and cold pressing) are reported. Although a variety of series of PVDF/Ni composites has been investigated, the expected dielectric relaxation behavior was observed in the cold-pressed PVDF/nanocrystalline nickel (nc-Ni) composites, which opens an interesting and novel dielectric response associated with the novel physical phenomena, which may make the material suitable for their possible electrical and electronics engineering applications.

## 6.2 Samples Reported

To prepare a variety of PCC, the different possible types of conductor chosen are (a) metal (b) alloy (quasicrystal, i.e., a semiconductor) (c) nanocrystalline metal (d) composite of a nanocrystalline metal and its oxide taking into account the effect of conductivity, density, particle size, surface area, etc., of the conducting fillers. The different possible insulating polymers are a polar polymer/weakly ferroelectric polymer and a non-polar polymer. Various series of possible combinations of PCC composites are prepared to approach  $f_c$  as closely as possible by varying  $f_{con}$  with different process conditions, such as cold-pressed (i) PVDF/ $\mu$ -Ni (ii) PVDF/ $n$ -Ni (iii) PVDF/ $n$ -QC and hot-molded (iv) PVDF/ $\mu$ -Ni (v) PVDF/ $n$ -Ni (vi) PVDF/composite of  $n$ -Ni and NiO (vii) LDPE/ $n$ -Ni denoted as series A, B, C, D, E, F, and G, respectively. For preparing the series A, B, and C samples, the components of the corresponding composites were blended with the help of agate mortar and pestle for about 1.5 h and then prepared in the form of pellets (diameter 11 mm, thickness  $\sim$  1.6 mm) under 10 MPa pressure at room temperature. For preparing Series D, E, F, and G the blended powders of the composite were hot molded under 10 MPa at a temperature of 200 °C, 200 °C, 200 °C, and 130 °C for 45 min, 45 min, 45 min, and 30 min, respectively. The final samples were prepared in the form of pellets (diameter 13 mm and thickness  $\sim$  1.8 mm). The series of samples along with their preparation method and notations used for the particular series is given in the form of Table 6.1. Subsequently, the electrical characterizations have been performed on all these samples. The detailed method of image processing of the optical micrographs of the samples with different  $f_{con}$  done through MATLAB software is described as follows. The image processing is done for seeking the percolation channels formed in the host polymer PVDF due to varying  $f_{con}$  introduced into the PMC. In the image processing, firstly the background in the image is estimated, and then it was subtracted from the original image to create a uniform background. Further, the contrast is adjusted by saturating 1% of the data at both low and high intensities. From this image, a binary image is created to see the objects in the image. The functions used in the processing of the images are as follows: (i) Imopen: morphological opening operation to estimate the background illumination, (ii) Imadjust: to adjust the contrast of the image, (iii) Im2bw: to change the grayscale image into a binary image.

**Table 6.1** Prepared samples reported for their study

Name of the series of composites	Preparation method	Notation for the particular series
PVDF/ $\mu$ -Ni	Room temperature consolidation	<b>A</b>
PVDF/ $n$ -Ni	Room temperature consolidation	<b>B</b>
PVDF/ $n$ -QC	Room temperature consolidation	<b>C</b>
PVDF/ $\mu$ -Ni	Compression hot molding	<b>D</b>
PVDF/ $n$ -Ni	Compression hot molding	<b>E</b>
PVDF/ $n$ -Ni@NiO	Compression hot molding	<b>F</b>
LDPE/ $n$ -Ni	Compression hot molding	<b>G</b>

## 6.3 Results

### 6.3.1 Experimental Dielectric Response

This section describes the experimental dielectric response of the host polymers (PVDF/LDPE) as well as the seven different varieties of PCC systems based on these two polymers as the host matrix [18–22]. The description in this section begins with the dielectric response of PVDF. Figure 6.1a shows the dielectric response of pure PVDF. This result illustrates the strong frequency dependence of  $\varepsilon'$  and  $\varepsilon''$ . The pure PVDF is an insulating polar dielectric polymer having a low static dielectric constant (15) and very low loss tangent (0.01). The origin of dielectric properties in PVDF is attributed to the presence of polar group ( $-F$ ) in its monomer ( $CH_2 = CF_2$ ) unit imparting it a weakly ferroelectric character. The magnitude of  $\varepsilon'$  at low frequency is found to be 16, and  $\varepsilon''$  shows a dipolar relaxation peak at frequency,  $\omega_p = 2.71$  MHz. Hence, it may be expected to exhibit dipolar relaxation as a function of frequency in accordance with JUDR laws expressed by Eq. 2.9. The exponents ' $m$ ' and ' $n$ ' evaluated by using Eqs. 2.9a, 2.9b, given as;

$$\varepsilon_s - \varepsilon'(\omega) \propto \varepsilon(\omega) \propto \omega^m \text{ for } \omega \ll \omega_p \text{ with } 0 < m < 1$$

$$\text{and } \varepsilon'(\omega) \propto \varepsilon(\omega) \propto \omega^{n-1} \text{ for } \omega \gg \omega_p \text{ with } 0 < n < 1$$

in the relevant range of frequencies (i.e., for  $\omega \ll \omega_p$  and  $\omega \gg \omega_p$ , respectively) gives an estimate for the exponents. The values from the fits are  $m = 0.43$  and  $n = 0.75$ , respectively, and agree well with Jonscher's universal regime of [0, 1]. We observe

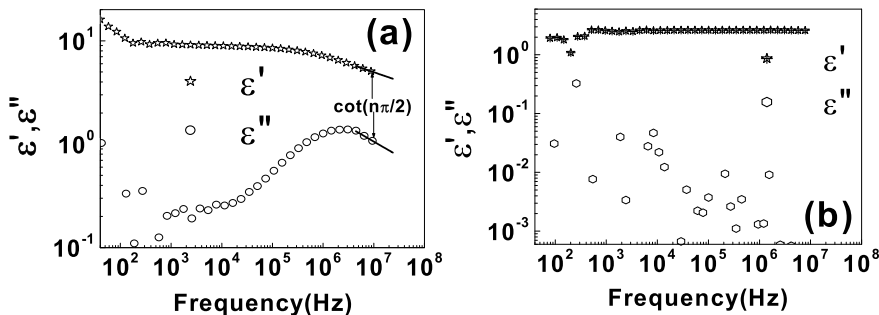


**Fig. 6.1** Log-log plot of the real ( $\epsilon'$ ) and imaginary ( $\epsilon''$ ) complex permittivity as a function of the frequency. **a** The neat PVDF matrix. The solid lines through the data show good agreement with Eqs. 2.9 & 2.11;  $\omega_p = 2.71$  MHz. **b** The pure LDPE matrix

from Fig. 6.1a that the ratio  $\epsilon''(\omega)/\epsilon'(\omega) = \cot(\pi/2) = \text{const}$  is independent of frequency for  $\omega \gg \omega_p$  is in good agreement with Eq. (2.11). Application of JUDR to the experimental results gives the value of frequency exponent as  $n = 0.75$  for pure PVDF. It is also found that the real part of dielectric constant  $\epsilon'(\omega)$  is higher than the imaginary part of dielectric constant  $\epsilon''(\omega)$  in good consistency with JUDR of a capacitor (Fig. 6.1a). Figure 6.1b shows the frequency dependence of  $\epsilon'(\omega)$  and  $\epsilon''(\omega)$  for pure LDPE which is a non-polar polymer due to the absence of net dipole moment. This seems logical because of the very structure of its monomer ( $\text{CH}_2=\text{CH}_2$ ).  $\epsilon'$  shows a flat response with a constant value of 2.5 without any fall in magnitude with frequency, whereas  $\epsilon''$  also doesn't show any relaxation behavior unlike that of pure PVDF. It is due to the absence of dipolar entities in it. The scattered data points corresponding to  $\epsilon''$  are attributed to the insulating nature of the polymer (resistivity  $\sim 10^{16} \Omega \text{ cm}$ ). Thus, JUDR of dipolar type could not be validated for a non-polar polymeric system as expected.

In the case of PCC, it is observed that all the seven series of PCC under study exhibit sharp IMT at  $f_c$ , irrespective of the type of conductor, following the percolation theory. Experimental results indicated that  $f_c$  represents a critical volume fraction of the filler loading in the PCC across which the dielectric response is governed by two different and independent mechanisms. The inherent electrical behavior of the host polymer also plays a crucial role in modulating the dielectric (permittivity/loss tangent) response. It is observed that below  $f_c$ , it is dominated by the dipolar contribution of the host polymer component which is predominantly an insulator. Above  $f_c$ , it becomes a charge carrier-dominated system. Hence, examining the validity of the JUDR for dipolar as well as charge carrier-dominated regime in the PCC in experimental results would provide significant insight into the physics associated with the IMT and dielectric relaxation process over a range of filler loading in the PCC. In addition, the role of the inherent polarity in the host polymer on dielectric relaxation in the PCC has also been examined. It is discussed below separately based on experimental evidence on all the seven series of PCC.

### 6.3.2 Frequency Dependent Dielectric Response Below $f_c$

We begin with the results of series A (PVDF/ $\mu$ -Ni) samples prepared using the cold-pressed technique. The frequency response of complex permittivity is shown in Fig. 6.2a, b. It shows a typical variation of  $\varepsilon'$  and  $\varepsilon''$  for different  $\mu$ -Ni loadings over a broad range of frequencies for the composite samples corresponding to  $f_{\text{con}} < f_c$ . It is observed from Fig. 6.2a that  $\varepsilon'$  decreases with the increase of frequency for all the composite concentrations and it becomes flat for low Ni loadings. As the  $\mu$ -Ni fraction in the composite increases and approaches  $f_c$ ,  $\varepsilon'$  increases to 200 (for  $f_{\text{con}} = 0.56$ ) from an initial value  $\sim 12$  (for  $f_{\text{con}} = 0.0$ ). This large enhancement ( $>16$  times) is attributed to the accumulation and entrapment of charges at the interface of the two components due to the boundary layer capacitor effect and MWS polarization. It seems reasonable and logical due to the blocking of charge carriers across the insulating boundaries in the PCC. As the composite concentration approaches  $f_c$  (i.e.,  $f_{\text{con}} \rightarrow f_c$  with  $f_{\text{con}} = 0.57$ ), clear frequency dispersion of  $\varepsilon'$  occurs over the whole frequency range of measurement in the present studies. It is related to leakage current resulting from higher metallic fractions. Secondly, the evolution pattern of  $\varepsilon''(\omega)$  data clearly shows a peak corresponding to  $\varepsilon'' = \varepsilon''_{\text{max}}$  at  $\omega_p = 2.71$  MHz. It is directly related to the presence of dielectric relaxation, i.e., dipolar relaxation. The origin of this relaxation lies in the presence of the polar  $[-F]$  group in the pure polymer matrix backbone of the PCC. In comparison with the relaxation peak of the pure polymer, a very small shift in loss peak position on either side of  $\omega_p = 2.71$  MHz is observed with an increase in the volume fraction of  $\mu$ -Ni in the PCC. The shift in loss peak position doesn't follow any regular order with  $\mu$ -Ni content. The minor shift in the loss peak with an increase in Ni content can be considered to be insignificant well within experimental error. It is also observed that the broadening/flattening in the loss peaks increases with a relative decrement in the dielectric relaxation strength with an increase in  $\mu$ -Ni concentration. The broadening/flattening is attributed to enhanced heterogeneity of the composites giving rise to a distribution of relaxation times caused by an additional polarization (interfacial/MWS polarization) aided by an increase in the activity of interfaces with the increase of  $\mu$ -Ni fraction in the composites. This effect is in addition to the existing dipolar polarization. The decrease in relaxation strength is attributed to a corresponding reduction in the number of dipoles of the polymer with an increase in  $f_{\text{con}}$ . With further increase of  $f_{\text{con}}$ , the magnitude of  $\varepsilon''$  increases which is attributed to the higher leakage current in the composite samples with enhanced filler loading. In general, the variation of  $\varepsilon''(\omega)$  with frequency for all the composite samples of the series A shows a dipolar relaxation peak below  $f_c$ . These results suggest that even with a higher amount of conducting components, the dielectric response of the composite is completely dominated by the insulating properties of the polymer.

Thus, all the composites below  $f_c$  (i.e., for  $f_{\text{con}} \leq 0.56$ ) show a dipole-dominated dielectric response and each of them exhibits dipolar relaxation. Typical representative pattern for  $f_{\text{con}} = 0.20$  and  $f_{\text{con}} = 0.56$  is shown in Fig. 6.2c, d, respectively, for comparison. So, JUDR should hold good for all these samples below  $f_c$ . Indeed

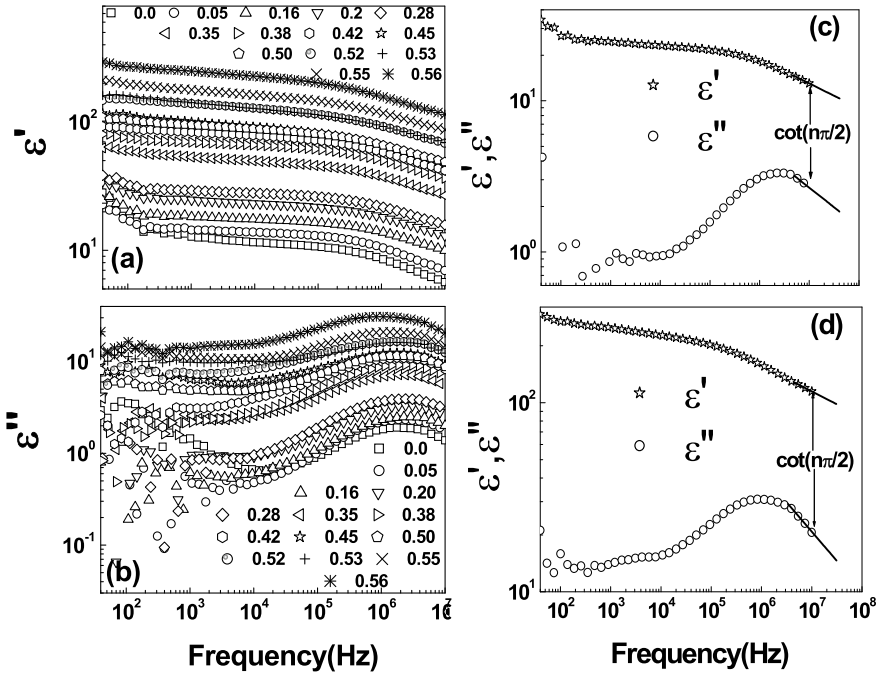


**Fig. 6.2** Comparison of the **a**  $\epsilon'$ , real part of the effective complex permittivity, **b**  $\epsilon''$ , imaginary part of the effective complex permittivity versus frequency for series A samples below  $f_c$ , i.e.,  $f_{con} < 0.57$ ; typical log–log plot of  $\epsilon'$  and  $\epsilon''$  as a function of frequency for the samples, **c**  $f_{con} = 0.20$ , **d**  $f_{con} = 0.56$  below  $f_c$ ; the solid lines through the data show good agreement with Eqs. 2.9a, 2.9b

Eq. 2.11 fit well with the experimental results of all the composites below  $f_c$ . Typical representative patterns are shown in Fig. 6.2c, d. We observe from Fig. 6.2c, d that  $\frac{\epsilon''(\omega)}{\epsilon'(\omega)}$  is independent of frequency for  $\omega \gg \omega_p$  for  $f_{con} = 0.20$  and  $f_{con} = 0.56$ , respectively, in accordance with Eq. (2.11). It is observed from the dielectric response of the above series A that the number of dipoles, as well as  $\mu$ -Ni/PVDF interfaces, play a significant role in modulating the characteristic properties of the composites.

To identify the role of the interface effect clearly, we have reduced the Ni particle size to nanoscale and prepared another series of composites (PVDF/n-Ni) intending to investigate the effect of size and surface area of the filler particles. It is observed from Fig. 6.3a that  $\epsilon'$  has a flat response with a frequency up to 100 kHz beyond which it shows a decrease for low n-Ni loadings. As the n-Ni fraction increases and approaches  $f_c$ ,  $\epsilon'$  increases possibly due to the combined effect of more charge accumulation at the n-Ni/PVDF interfaces in the composite phase as well as due to boundary layer capacitor effect. As a result,  $\epsilon'$  shows more dispersion over the whole frequency range because of more leakage current at higher metallic loading. It is very interesting to see the evolution pattern of  $\epsilon''(\omega)$  with frequency (Fig. 6.3b). It clearly shows a peak with  $\epsilon''(\omega) = \epsilon''_{max}$  at  $\omega_p = 2.71$  MHz for the pure polymer with a traceable shift in loss peak position, on either side of 2.71 MHz like that of

series A, with the increase in n-Ni content. This shift in the loss peak position with an increase in  $f_{\text{con}}$  can be considered insignificant well within experimental limits. A relatively large increase in the magnitude of dielectric constant  $\epsilon'$  is attributed to the formation of MWS dipoles at the interface of the PVDF/n-Ni phase in the composites due to charge accumulation at the interfacial boundary. The strength of MWS relaxation depends on particle size and surface area, unlike dipolar relaxation. Thus, it is observed that all the samples of series B exhibit both dipolar relaxation and MWS polarization phenomena simultaneously below  $f_c$  and show their effect independently. Therefore, it will be interesting to examine the validity of JUDR law for this series of PCC samples. The fits of Eq. 2.9 to the corresponding experimental data below  $f_c$  for the PVDF/n-Ni series confirmed an excellent agreement with JUDR law. Typical results of the fits are shown in Fig. 6.3c, d for  $f_{\text{con}} = 0.16$  and  $f_{\text{con}} = 0.25$ , respectively. Identical response and constancy of the ratio  $\epsilon''(\omega)/\epsilon'(\omega)$  agree with Eq. 2.11. A scientifically significant observation on comparing the results of the series A and B (PCC) is that with a reduction in particle size, large tailoring of  $f_c$  occurs from 0.57 (for PVDF- $\mu$ -Ni) to 0.27 (for PVDF- $n$ -Ni). This is attributed to relative enhancement in the overlapping of the effective tunneling range of the filler particles without imparting any deleterious effect on the dielectric relaxation behavior in the PCC. It is also important to mention that interfacial polarization plays a crucial role in bringing down the value of  $f_c$  without affecting the inherent phenomena of IMT across  $f_c$ .

A similarity in the dielectric response of the two series of PCC, with the essential distinction of tailored  $f_c$  prompted us to examine the pattern of this phenomena over a variety of systems to make out an evaluation for its universality [22]. In the preceding discussion, we have analyzed the validity of Jonscher's law below  $f_c$  for PCC with Ni of varying particle size. Now we attempt the same analysis on another PCC series C based on a complex alloy (a quasicrystal) in nanocrystalline form, i.e.,  $\text{Al}_{65}\text{Cu}_{23}\text{Fe}_{12}$ , denoted as n-QC. It is a PVDF/n-QC composite (series C samples). Analysis of this series would provide sufficient insight on the effect of alloy-type conductive filler on the dielectric relaxation of the PCC. We observe from Fig. 6.4a that  $\epsilon'$  decreases slowly with frequency for the composites with  $f_{\text{con}} < f_c$  for a low value of n-QC loading. As the n-QC fraction increases and approaches  $f_c$ , the  $\epsilon'$  exhibits a manifold jump. It may be related to enhanced charge accumulation at the interface of the two phases/boundary layer capacitor effect. The relaxation behavior also seems to be identical in this case exhibited by the appearance of  $\epsilon''_{\text{max}}$  peak at  $\omega_p = 2.71$  MHz. It has typical features of broadening/flattening followed by a slight shift of the loss peak position with an increase in the fraction of n-QC in the PCC (Fig. 6.4b). The basic mechanism for the changes in the dielectric response of the n-QC based PCC (i.e., dipolar contribution and MWS polarization) remains the same as before with an essential difference in the magnitude of the dielectric parameter. The experimental results of all the samples below  $f_c$  are fitted to Eq. 2.9 and typical representative fits corresponding to  $f_{\text{con}} = 0.13$  and  $f_{\text{con}} = 0.22$  are shown in Fig. 6.4c, d, respectively. A comparison from Fig. 6.4c, d suggest that the JUDR law of Eq. (2.11) is well-satisfied in the dipolar relaxation region below  $f_c$ . The dielectric response results

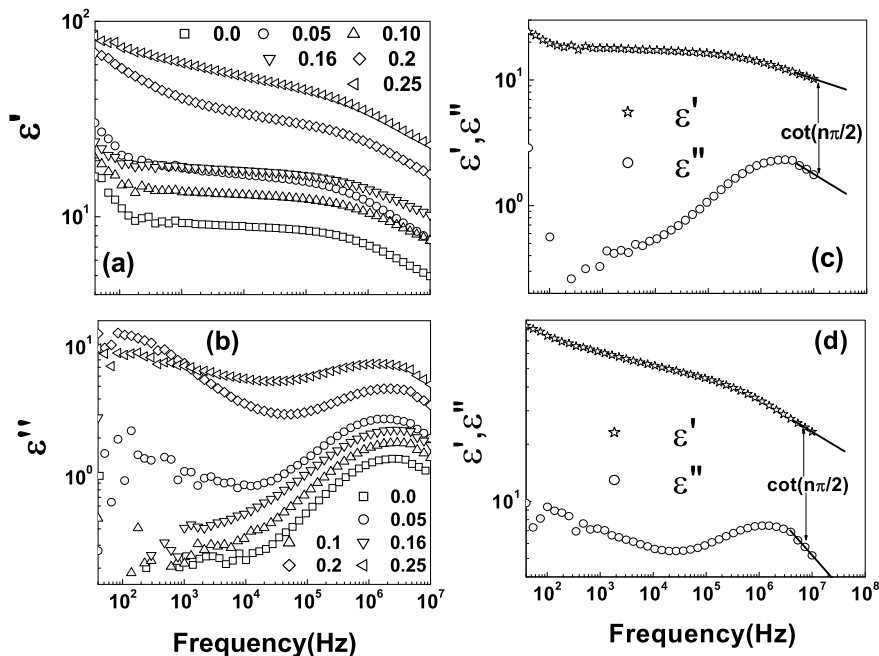


**Fig. 6.3** Comparison of the **a**  $\epsilon'$ , the real part of the effective complex permittivity, **b**  $\epsilon''$ , the imaginary part of the effective complex permittivity versus frequency for series B samples below  $f_c$ , i.e.,  $f_{\text{con}} < 0.27$ ; typical log–log plot of  $\epsilon'$  and  $\epsilon''$  as a function of frequency for the samples, **c**  $f_{\text{con}} = 0.16$ , **d**  $f_{\text{con}} = 0.25$  below  $f_c$ ; the solid lines through the data show good agreement with Eq. 2.9

discussed so far indicate that the three different series of PCC prepared via cold-pressed technique have exhibited identical behavior below  $f_c$ . The tunability of  $f_c$  depends on the particle size and conductivity of the conducting component.

To confirm the universality of JUDR on PCC, without any loss of generality, we have examined its validity on a few more PCC samples prepared under different “process conditions”. The same composite combination (series A and B) are now prepared under hot molding process conditions and are referred to as series D and E, respectively. The experimental results indicate that the value of  $f_c$  is drastically different with a change in process conditions for the D and E series of composites even if the composite components are identical to series A and B, respectively. This change is attributed to the difference in the spatial distribution of the filler particles and the extent of their connectivity in the composite phase. This, in turn, gives rise to a different extent of overlapping of the effective tunneling range of fillers arising due to differences in the process conditions. The dielectric response ( $\epsilon'$  vs. frequency) for D and E series of composites is shown in Figs. 6.5a and 6.6a. The general features of the frequency response behavior of  $\epsilon'$  for the composites below  $f_c$  remain the same as before. This can be inferred easily by comparing the results of Figs. 6.2, 6.3

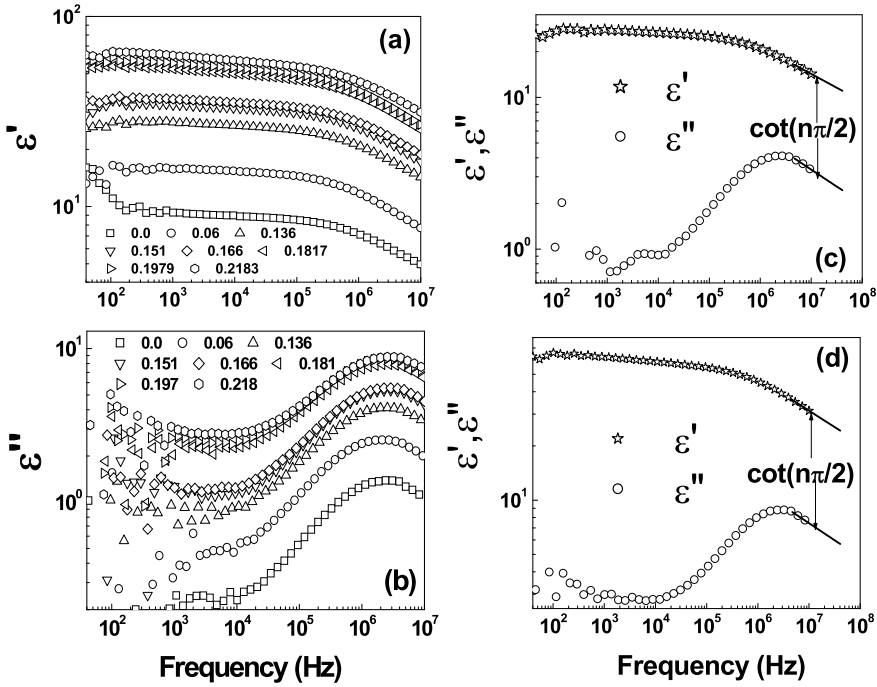


**Fig. 6.4** Comparison of the **a**  $\epsilon'$ , the real part of the effective complex permittivity, **b**  $\epsilon''$ , the imaginary part of the effective complex permittivity versus frequency for series C samples below  $f_c$ , i.e.,  $f_{con} < 0.23$ ; typical log–log plot of  $\epsilon'$  and  $\epsilon''$  as a function of frequency for the samples, **c**  $f_{con} = 0.13$ , **d**  $f_{con} = 0.218$  below  $f_c$ ; the solid lines through the data show good agreement with Eqs. 2.9a, 2.9b

and 6.4 with that of Figs. 6.5a and 6.6a. However, it is interesting to note, for the series D and E samples, that  $\epsilon''(\omega)$  variation shows a peak ( $\epsilon''_{max}$ ) at  $\omega_p = 2.48$  MHz for the pure polymer with a slight shift of the loss peak position with additional features of broadening/flattening in the peak (Fig. 6.5b and 6.6b). A comparison of the dielectric relaxation behavior of the hot molded, series D and E, PCC samples with that of the cold-pressed series A and B samples indicates an unambiguous resemblance for  $f_{con} < f_c$ . The only difference is a shift in the dielectric relaxation peak toward lower frequency (2.71 MHz for cold-pressed PCC to 2.48 MHz for the hot-molded PCC) which is insignificant well within the experimental error. The application of Jonscher’s power-law to the experimental results of series D and E samples suggests that the JUDR law expressed in Eq. (2.11) is satisfied for  $f_{con} < f_c$ . It is indicated by the fitted plots shown in Figs. 6.5c and 6.6c, d. However, the results shown in Fig. 6.5d suggest that the JUDR law breaks down because the composite has entered into the percolation region such that the dipolar contribution of polymer gets overshadowed by the dominance of the filler particles.

Before arriving at any definite conclusion on the universality of JUDR for PCC, two more distinct classes of PCC have been studied. The series F samples refer to

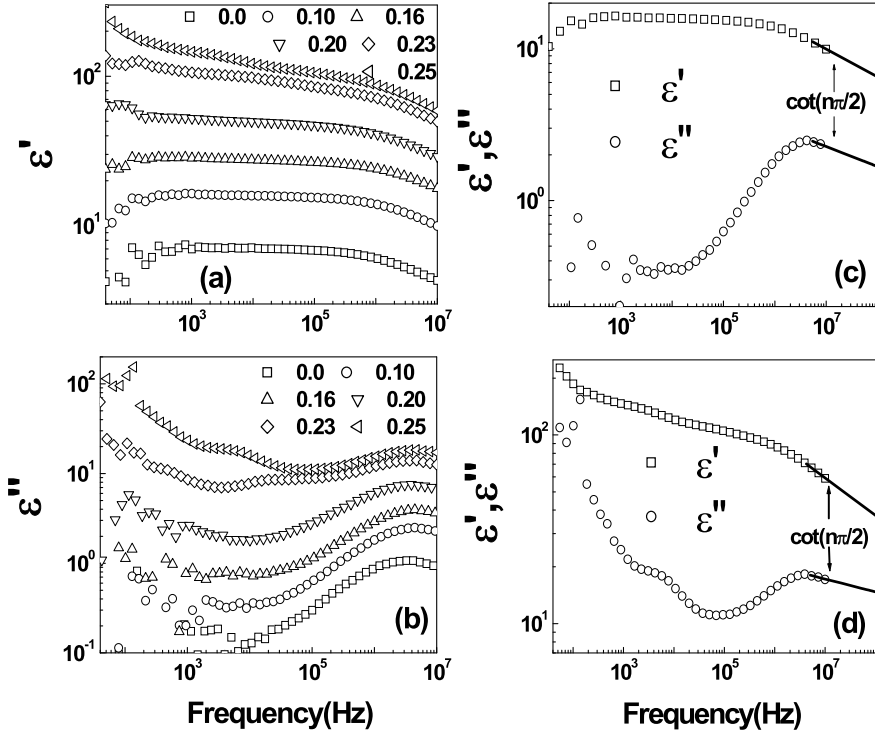


**Fig. 6.5** Comparison of the **a**  $\epsilon'$ , the real part of the effective complex permittivity, **b**  $\epsilon''$ , the imaginary part of the effective complex permittivity versus frequency for series D samples below  $f_c$ , i.e.,  $f_{con} < 0.259$ ; typical log–log plot of  $\epsilon'$  and  $\epsilon''$  as a function of frequency for the samples, **c**  $f_{con} = 0.05$ , **d**  $f_{con} = 0.25$  below  $f_c$ ; the solid lines through the data show good agreement with Eqs. 2.9a, 2.9b

a composite of PVDF/*n*-Ni-NiO where NiO is created artificially by annealing *n*-Ni for 6 h at 500 °C in air. We observe from Fig. 6.7a that the variation of  $\epsilon'$  with respect to frequency for the composites below  $f_c$  remains identical and analogous when compared with the results of other series of PCC in the present studies. The basic physics associated with the changes also remain the same. The frequency response of  $\epsilon''(\omega)$  clearly shows a peak ( $\epsilon''_{max}$ ) at  $\omega_p = 2.48$  MHz for the pure polymer like series D and E samples. In the case of F series composites, a small shift of the loss peak position has been observed with an increase in filler content as shown in Fig. 6.7b. Figure 6.7c, d confirm the validity of JUDR law in accordance with Eq. (2.11).

In this part of our experimental investigation, we move finally to a PCC based on non-polar polymers, such as LDPE/*n*-Ni composites. It is referred to as the series G samples. The experimental results have indicated that  $f_c$  for the G-series samples is drastically low than all other series under study. The static  $\epsilon'$  value found for LDPE is 2.5, and the magnitude remains the same over the whole frequency range due to the absence of dipolar (orientational) polarization in the polymer matrix (Fig. 6.1b).

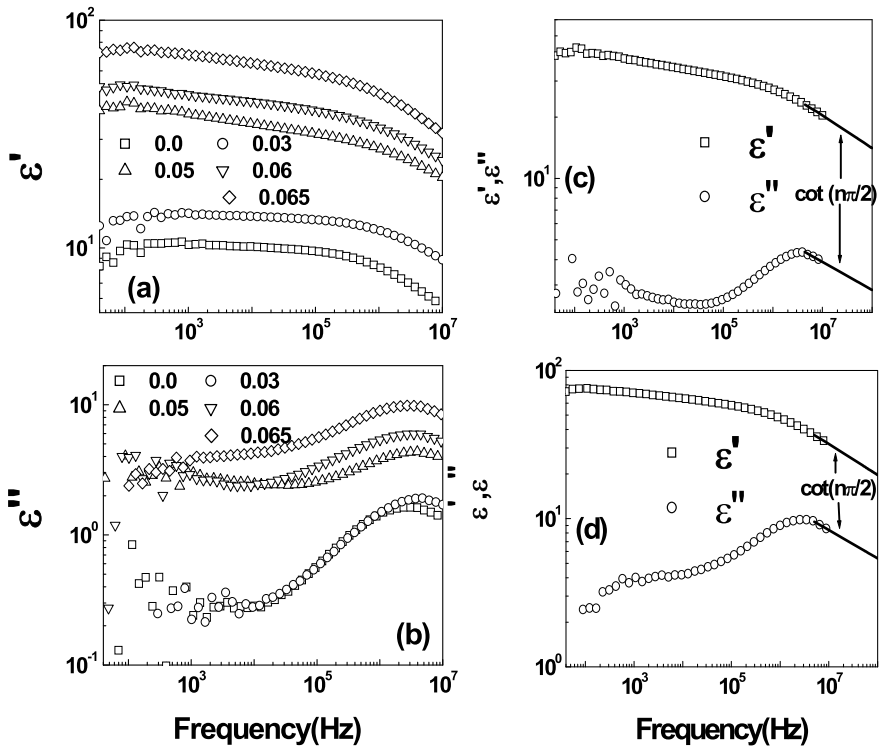


**Fig. 6.6** Comparison of the **a**  $\epsilon'$ , the real part of the effective complex permittivity, **b**  $\epsilon''$ , the imaginary part of the effective complex permittivity versus frequency for series E samples below  $f_c$ , i.e.,  $f_{con} < 0.07$ ; typical log–log plot of  $\epsilon'$  and  $\epsilon''$  as a function of frequency for the samples, **c**  $f_{con} = 0.03$ , **d**  $f_{con} = 0.065$  below  $f_c$ ; the solid lines through the data show good agreement with Eqs. 2.9a, 2.9b

With the dispersion of  $n$ -Ni in the composite, the magnitude of  $\epsilon'$  increases due to an increase in the strength of MWS interfacial polarization/boundary layer capacitor effect. An increase in the  $n$ -Ni concentration causes visible dispersion over the whole frequency range due to higher leakage current (Fig. 6.8a). However, no evidence of any dipolar relaxation could be traced for the composites below  $f_c$ . The result is understandable and logical because of the absence of dipoles in the host polymer matrix itself (Fig. 6.8b). Figure 6.8c, d shows the typical frequency response of the real and imaginary part of the effective complex permittivity for the G-series samples below  $f_c$ , where JUDR law fails to agree with the experimental results at all.

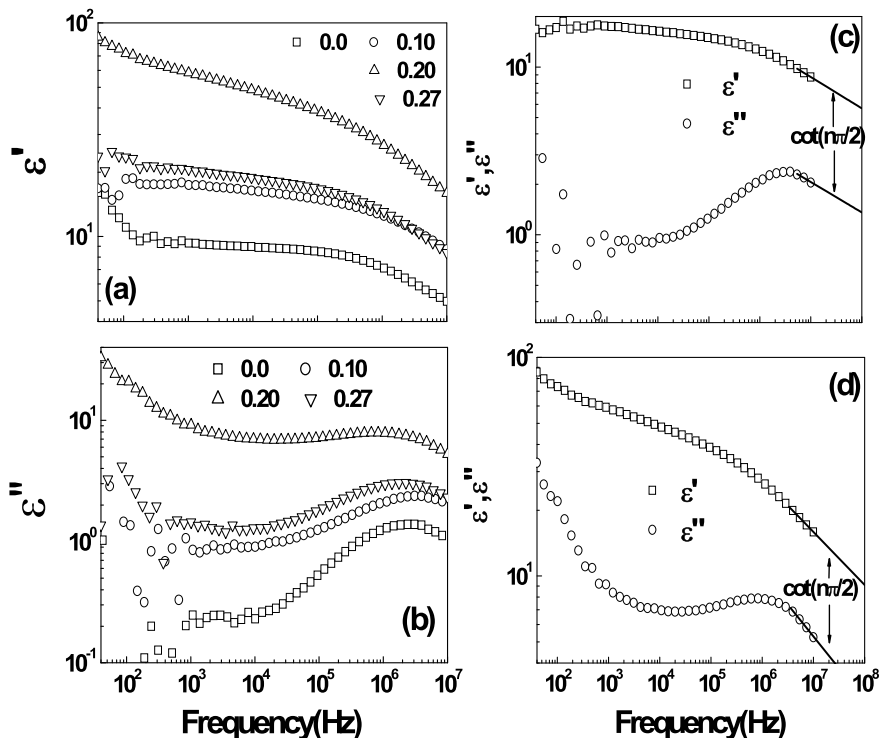


**Fig. 6.7** Comparison of the **a**  $\epsilon'$ , the real part of the effective complex permittivity, **b**  $\epsilon''$ , the imaginary part of the effective complex permittivity versus frequency for series F samples below  $f_c$ , i.e.,  $f_{con} < 0.30$ ; typical log–log plot of  $\epsilon'$  and  $\epsilon''$  as a function of frequency for the samples, **c**  $f_{con} = 0.10$ , **d**  $f_{con} = 0.20$  below  $f_c$ ; the solid lines through the data show good agreement with Eq. 2.9

### 6.3.3 Normalization of Dipolar Relaxation

To obtain clear and convincing information on the role of conductive fillers on the relaxation behavior below  $f_c$  in all the PCC, the dielectric parameters have been normalized. The normalized dielectric master curves are analyzed for all the series of PCC under study. Some representative plots are shown in Fig. 6.9a–d for series A, B, C, and F, respectively. An identical dielectric relaxation response is emerging in all the cases. It is observed that all the curves merge at a higher frequency (i.e., above  $10^5$  Hz) where the pure polymer host exhibits a dipolar relaxation peak. The relaxation peak of PCC also appears to collapse with the polymer relaxation peak. It is a clear indication that the dipolar interaction is a cooperative phenomenon for the composite samples just below  $f_c$ . In sharp contrast, the normalized curves diverge at lower frequencies (i.e., below  $10^5$  Hz) due to an effective contribution of MWS interfacial polarization arising due to the different conductivity and dielectric constant of the two components of PCC. The overall picture from the analysis indicated that for all

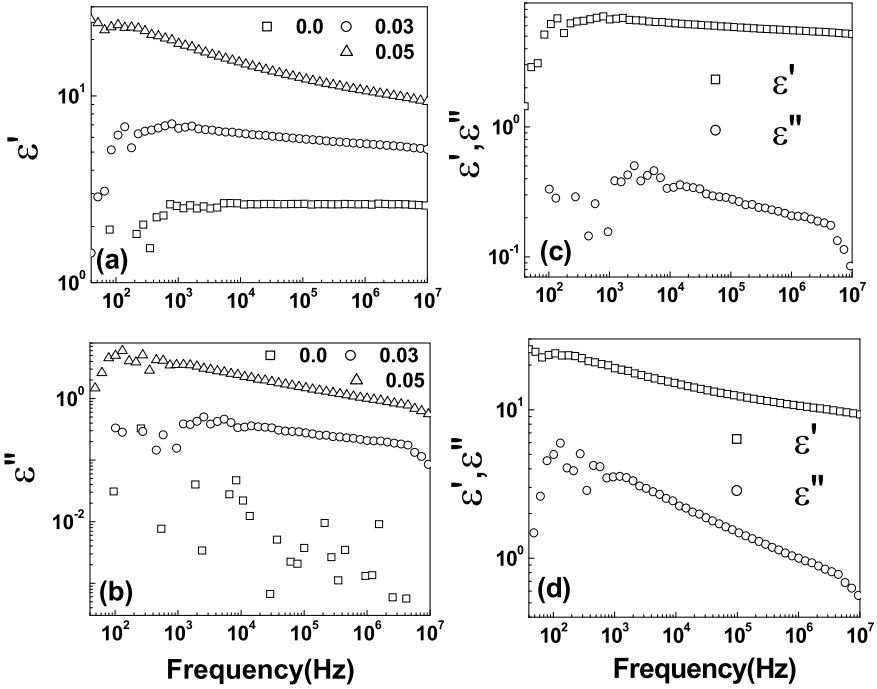


**Fig. 6.8** Comparison of the **a**  $\epsilon'$ , the real part of the effective complex permittivity, **b**  $\epsilon''$ , the imaginary part of the effective complex permittivity versus frequency for series G samples below  $f_c$ , i.e.,  $f_{con} < 0.06$ ; typical log–log plot of  $\epsilon'$  and  $\epsilon''$  as a function of frequency for the samples, **c**  $f_{con} = 0.03$ , **d**  $f_{con} = 0.05$  below  $f_c$

the series of PCC samples below  $f_c$ , the dynamics of charge transport is dependent on the filler concentration in the low-frequency region while it is independent of the filler factor in the high-frequency region. The origin of filler concentration-independent dipolar relaxation in the composites lies in the permanent dipoles of the host polymer matrix. The strength of relaxation depends on the number of dipoles. The dielectric dispersion at low frequency depends predominantly on the number of interfaces that vary from one composite concentration to another giving rise to more leakage current with increased filler loading. These features become clearer from the master curves (Fig. 6.10) plotted for all the series of samples under the normalized scale. Further, it is observed consistently from the experimental results that with the gradual increase in the conductor loading into the polymer matrix, a critical concentration ( $f_c$ ) is reached where all the seven composite series undergo a sharp transition in their electrical transport properties. As discussed previously, there is an unambiguous transition from insulating behavior below  $f_c$  to conducting one above  $f_c$ . So, it becomes a prerequisite in the present studies to examine the validity of JUDR law also above  $f_c$  for all the series of PCC. It is discussed below.

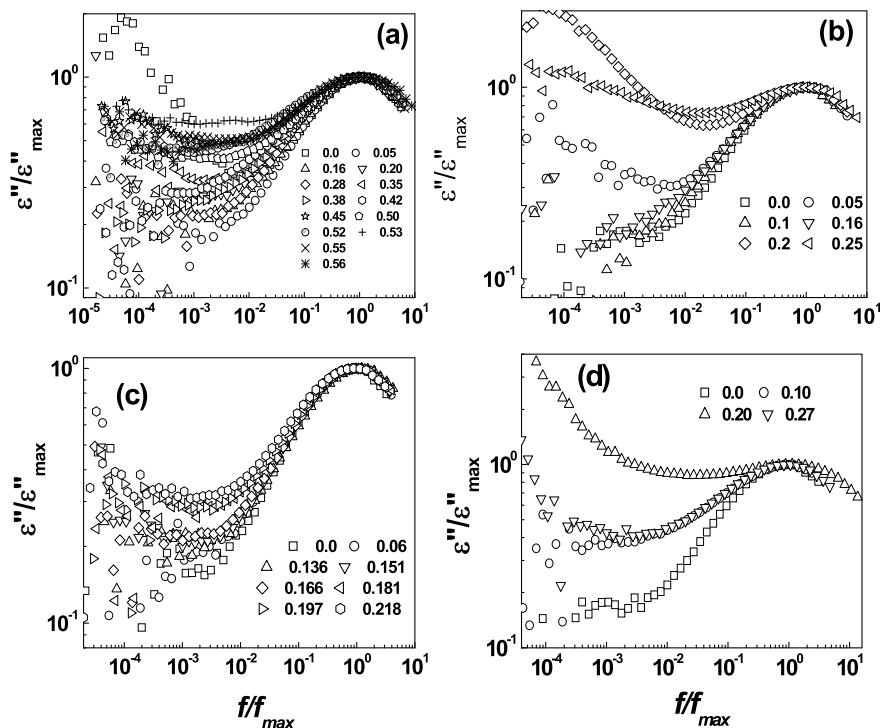


**Fig. 6.9** Typical normalized dielectric master curve of the imaginary complex permittivity for all the samples below  $f_c$  for series. **a** A, **b** B, **c** C and **d** F, respectively

### 6.3.4 Frequency Dependent Dielectric Response Above $f_c$

The typical frequency response characteristics for the real and imaginary part of complex permittivity for series A samples at/above  $f_c$  are discussed in Fig. 6.11a, b. A sudden increase in the dielectric constant occurs at  $f_c$ . It is attributed to the largest number of interfaces/interfacial areas available for charge accumulation. At the same time, more surface area is available for the charges to be blocked because of the boundary layer capacitor effect. As a result, the magnitude of dielectric constant ( $\epsilon'$ ) increases drastically to the tune of 1600 at  $f_{\text{con}} = 0.57$  and then decreases for  $f_{\text{con}} = 0.58$ , i.e., a divergence (singular point) in the real part of dielectric constant is observed. So,  $f_{\text{con}} = 0.57$  refers to the critical concentration  $f_c$ . According to percolation theory, this divergence observed at  $f_c$  is due to the IMT phenomena in the PCC system. Above  $f_c$ ,  $\epsilon'$  decreases due to the formation of a continuum of particles, and it appears to be consistent with the previous reports in literature (Fig. 1.1).  $\epsilon''$  also shows higher magnitudes with complete dispersion at low frequency due to higher leakage current assisted by filler-filler interaction at  $f_{\text{con}} > f_c$ . The interpretation seems convincing and provides a reasonable understanding in terms of scaling

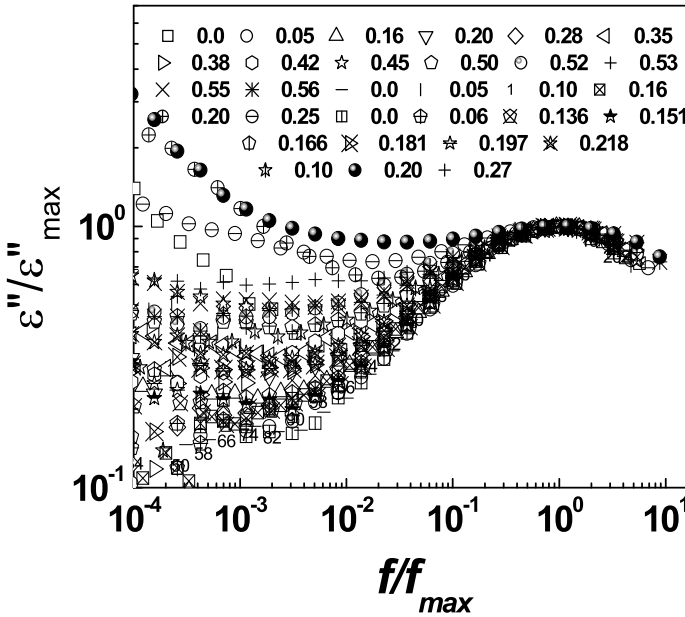


**Fig. 6.10** Typical normalized dielectric master curve of the imaginary complex permittivity for all the samples below  $f_c$  for all the PCC series of samples

laws of the percolation theory reported in the literature and earlier (Chaps. 4 and 5). There is a complete absence of loss ( $\epsilon''$ ) peak at  $f_{con} > f_c$  invariably for all the seven series of PCC in their  $\epsilon'' \sim \omega$  curve. Instead, the magnitude of  $\epsilon''$  decreases monotonically with frequency and it shows strong ALFD with two distinct regions of linear response at low and high frequencies (Fig. 6.11b). The origin of ALFD lies in the appearance of long-range dc conductivity caused by the resistive conduction through the bulk composites. Such a charge transport occurs under the partial physical contacts between the fillers which are the typical behavior of a charge carrier-dominated system. According to JUDR law of type-II, a charge carrier-dominated system showing ALFD will exhibit two regions of dispersion in the  $\epsilon'' \sim \omega$  curve obeying the power laws of Eq. 2.13a and 2.13b, respectively, which are given by.

$$\epsilon'(\omega) \propto \epsilon(\omega) \propto \omega^{-p} \text{ for } \omega \ll \omega_c \text{ with } 0 < p < 1$$

$$\text{and } \epsilon'(\omega) - \epsilon'_\infty \propto \epsilon(\omega) \propto \omega^{n-1} \text{ for } \omega \gg \omega_c \text{ with } 0 < n < 1$$

The underlying mechanism can be understood by examining the validity of Eqs. 2.13a and 2.13b for  $f_{con} \geq f_c$ , when fitted to the experimental results in the corresponding frequency regions for the PCC series samples. A comparison suggests an excellent fit of the experimental results and provides the value of critical frequency ( $\omega_c$ ) for charge carrier-dominated region (Fig. 6.11c, d).  $\omega_c$  is the frequency which

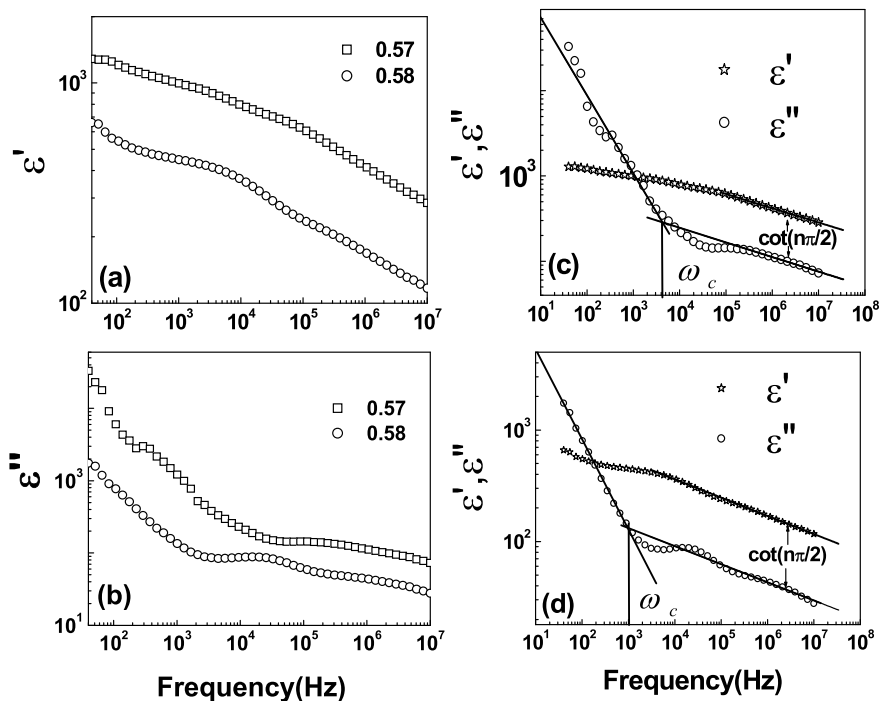


**Fig. 6.11** Comparison of the **a**  $\epsilon'$ , the real part of the effective complex permittivity, **b**  $\epsilon''$ , the imaginary part of the effective complex permittivity versus frequency for series A samples above  $f_c$ , i.e.,  $f_{con} \geq 0.57$ . Typical log–log plot of  $\epsilon'$  and  $\epsilon''$  as a function of frequency for the samples, **c**  $f_{con} = 0.57$ , **d**  $f_{con} = 0.58$  above  $f_c$ . The solid lines through the data show good agreement with Eq. 2.13.  $\omega_c$  is the frequency separating the ac and dc conductivity region

separates the ac and dc conductivity region of the composites and bears a direct analogy to the relaxation frequency ( $\omega_p$ ) in the case of the dipole-dominated region ( $f_{con} < f_c$ ). Such an analogy provides a basis to infer that frequency  $\omega_c$  refers to the frequency where the MWS interfacial polarization/conductivity relaxation occurs in the PCC series of samples. It is therefore a natural expectation that  $\omega_c$  should be dependent on  $f_{con}$  and show an increase with the increase in  $f_{con}$  due to the formation of the continuum of filler particles. However, the value  $\omega_c$  estimated from the fitted data for 0.57 and 0.58 samples of the series A PCC is 4 kHz and 3 kHz, respectively (Fig. 6.11c, d). This discrepancy may be attributed to experimental error arising due to smaller conductivity differences between the two composite samples.

In the case of series B (PVDF/n-Ni) samples at/above  $f_c$ , the real part of dielectric constant  $\epsilon'$  shows more dispersion due to higher leakage current resulting from higher probability of tunneling of charge carriers assisted by an enhanced surface area of the filler particles.  $\epsilon''$  also shows higher magnitudes at low frequency and exhibits strong dispersion due to the higher leakage current caused by well-connected conducting

network at higher filler fractions (Fig. 6.12a). The magnitude of  $\varepsilon''$  decreases monotonically with frequency at lower frequencies, and it shows an ALFD behavior exhibiting two distinct linear regions at low and high frequencies (Fig. 6.12b). The ALFD type behavior is related to the long-range dc conductivity assisted by direct physical contacts between the fillers at/above  $f_c$ . A comparison of the JUDR law of the type-II, expressed by Eq. 2.15 for charge carrier-dominated systems, with the experimental results in the corresponding frequency region for all the samples above  $f_c$  give an excellent fit (Fig. 6.12c, d). The estimated  $\omega_c$  value for the charge carrier-dominated systems is 20 kHz and 150 kHz for  $f_{\text{con}} = 0.28$  and  $f_{\text{con}} = 0.315$ , respectively, which agrees well with the conceptual expectation. Figure 6.13a, b shows the frequency dependence of complex permittivity for series C samples above  $f_c$ . To examine the validity of JUDR law, Eq. 2.15 are fitted with experimental results in the corresponding frequency region for all the samples above  $f_c$  and it also gives an excellent agreement as shown in (Fig. 6.13c, d). The estimated  $\omega_c$  value found for the cases  $f_{\text{con}} = 0.24$  and  $f_{\text{con}} = 0.27$  remains the same (4 MHz). A comparison indicates critical frequency ( $\omega_c$ ) for series C composites above  $f_c$  shows a higher value relative to series A and B composites. This is attributed to the complete physical connectivity of the filler particles in the polymer matrix giving rise to long-range dc conductivity. Visual evidence of such a possibility is noticed in the optical micrographs shown in Fig. 6.14. An identical analysis carried for all the samples of series D, E, F, and G at/above  $f_c$  suggest similar outcome and the typical results for the series F and G samples at/above  $f_c$  is shown in Figs. 6.15 and 6.16, respectively. No loss peak could be observed in their  $\varepsilon'' \sim \omega$  plot. Instead, two distinct dispersive regions have been observed as the common features of dielectric response obeying Eq. 2.15

## 6.4 Discussion

In the foregoing sections, we have examined and analyzed various aspects of the dielectric response in several PCC. This PCC have two distinct regions of dielectric behavior governed by different types of power laws across  $f_c$  [18]. The dielectric response in the region  $f_{\text{con}} < f_c$  is dominated by the dipolar contribution from the polymer host (PVDF). On the other hand, for  $f_{\text{con}} > f_c$  the dielectric properties are controlled by the uncorrelated charge carrier interaction and their response to the frequency of the applied electric field. The frequency response characteristics of the dielectric properties of the various PCC throughout the conductor composition range may therefore be expected to provide significant and rich insight into the physics associated with (i) dipolar interaction and extent of charge displacement, (ii) frequency-dependent dipolar flips with respect to an external applied electric field, (iii) dipolar relaxation, (iv) relaxation strength and its dependence on  $f_{\text{con}}$ , (v) relaxation time and its distribution, (vi) dielectric dispersion with frequency, and (vii) the dependence of dielectric response on the interaction among the charge carriers due to the difference of  $f_{\text{con}}$ .

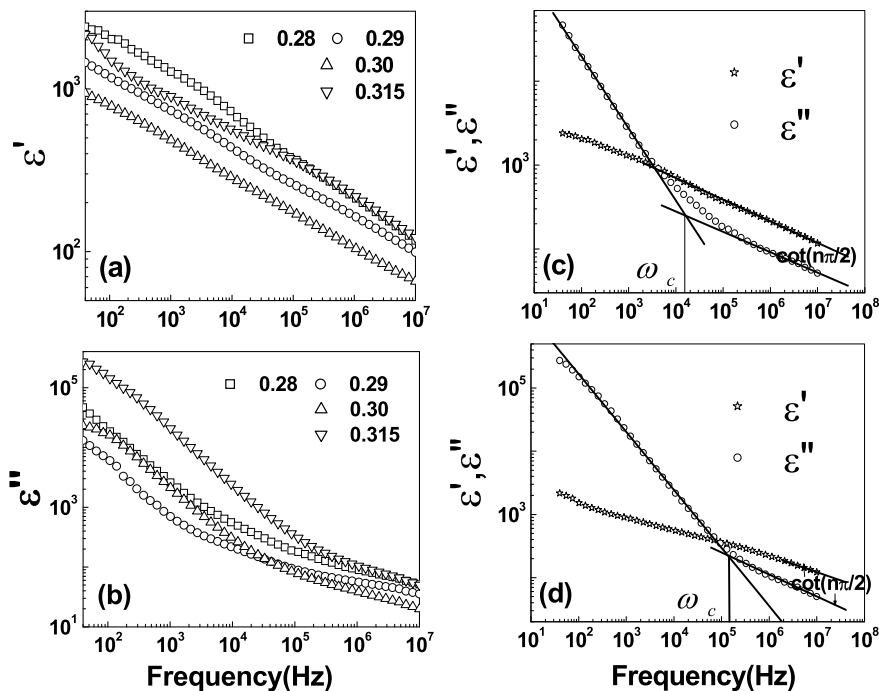


**Fig. 6.12** Comparison of the **a**  $\epsilon'$ , the real part of the effective complex permittivity, **b**  $\epsilon''$ , the imaginary part of the effective complex permittivity versus frequency for series B samples above  $f_c$ , i.e.,  $f_{con} \geq 0.28$ ; typical log–log plot of  $\epsilon'$  and  $\epsilon''$  as a function of frequency for the samples, **c**  $f_{con} = 0.28$ , **d**  $f_{con} = 0.315$ ; the solid lines through the data show good agreement with Eq. 2.13,  $\omega_c$  is the frequency separating the ac and dc conductivity region

Further, the present investigation has indicated that  $f_c$  for a specific combination of PCC is not unique. Rather, it depends on several factors including filler (conductor) particle size, their distribution, processing conditions, nature of host polymer matrix, and the external parameters (temperature, pressure, hold time, etc.) during sample processing. Therefore, to obtain a clear picture of the physics associated with the dielectric response of PCC prepared under the conditions mentioned above, the validity of JUDR laws for dipolar and charge carrier-dominated systems have been examined across  $f_c$ . Jonscher's power laws for dipolar systems have two relaxation exponents ' $m$ ' and ' $n$ ' (Eq. 2.9), whereas for charge carrier systems the two relaxation exponents are ' $p$ ' and ' $n$ ' (Eq. 2.13). Essentially, the exponents ' $m$ ' and ' $p$ ' carry different meanings with the condition that the limiting values of all the three exponents lie in between 0 and 1.

Further,  $m = 0$  in Eq. (2.9) refers to a situation in a dipolar system having completely non-interacting dipoles (uncorrelated dipoles). On the other hand,  $m = 1$  is attributed to a dipolar system having strongly interacting dipoles. In the direct analogy with the above,  $p = 1$  in Eq. (2.13) refers to an ideal charge carrier system,

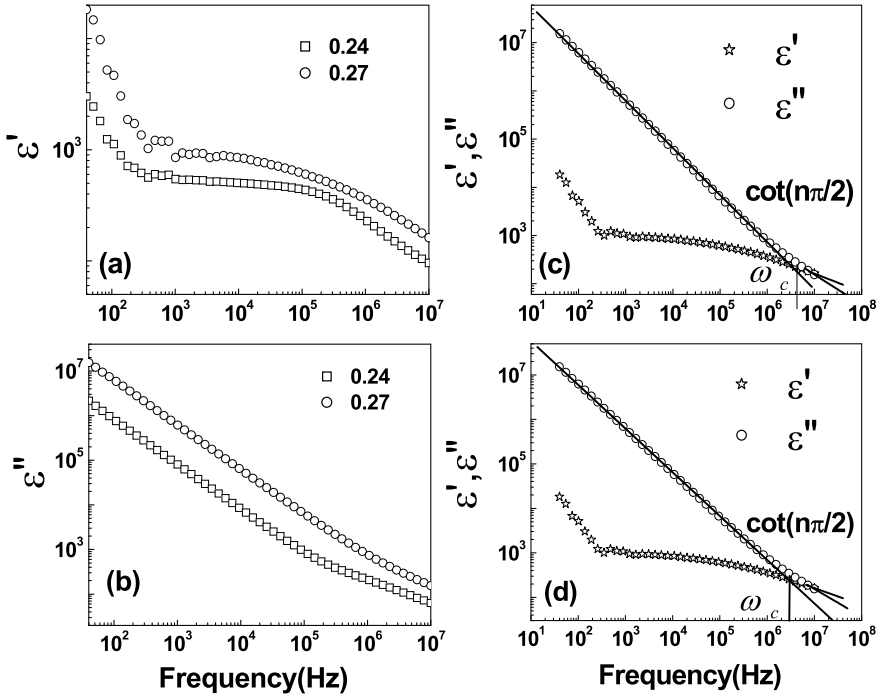


**Fig. 6.13** Comparison of the **a**  $\epsilon'$ , the real part of the effective complex permittivity, **b**  $\epsilon''$ , the imaginary part of the effective complex permittivity versus frequency for series C samples above  $f_c$ , i.e.,  $f_{con} \geq 0.22$ ; typical log–log plot of  $\epsilon'$  and  $\epsilon''$  as a function of frequency for the samples, **c**  $f_{con} = 0.24$ , **d**  $f_{con} = 0.27$  above  $f_c$ ; the solid lines through the data show good agreement with Eq. 2.13

whereas  $p = 0$  indicates that the charge carrier system would be non-responsive to the changes in frequency (i.e., non-dispersive behavior). The relaxation exponent ‘ $n$ ’ appearing in Eqs. (2.9)–(2.15) for dipolar/charge carrier systems provide information related to the dipolar dynamics for  $\omega \gg \omega_p$  and charge carriers transport for  $\omega \gg \omega_c$ . JUDR law suggests that ‘ $n$ ’ should remain constant because of the constancy of the ratio of energy stored to energy lost ( $\epsilon''(\omega) / \epsilon'(\omega)$ ) in a dipolar ( $\omega \gg \omega_p$ ) and charge carrier ( $\omega \gg \omega_c$ )-dominated system. Because of the physical phenomena described by the magnitude of the relaxation exponents,  $m$ ,  $p$ , and  $n$ , which of course depends on  $f_{con}$  in the composite, the following two cases arise.

### 6.4.1 Below $f_c$

This region refers to the dipolar region. In this case, the magnitude of the exponent ‘ $m$ ’ for all the seven series of PCC has relatively lower values lying in the range

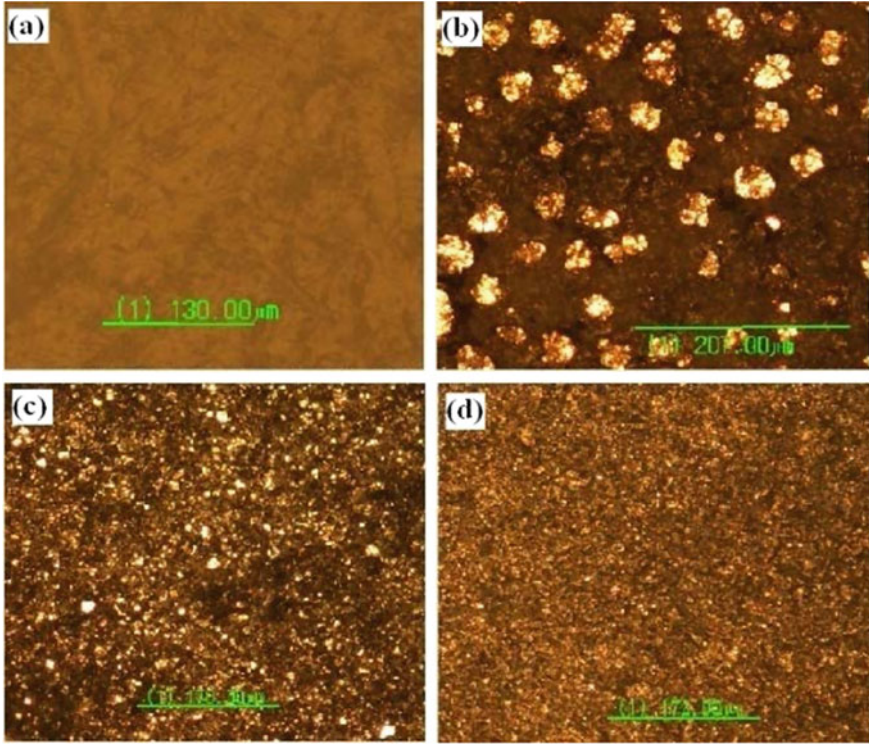


**Fig. 6.14** Typical optical micrographs of the pure PVDF and the percolative composites of the series A, B, and C, respectively. **a** PVDF, **b**  $f_{\text{con}} = 0.57$ , **c**  $f_{\text{con}} = 0.28$  and **d**  $f_{\text{con}} = 0.23$

of  $0.11 < m < 0.43$  (Fig. 6.17a). This is well within the limiting value  $[0, 1]$  as per the predictions of the JUDR law of type-I. The experimental value of ‘ $m$ ’ indicates that the increase in the  $\varepsilon_{\text{eff}}$  in the region  $f_{\text{con}} < f_c$  is due to the predominance of correlated dipolar contribution. A previous report on CB/Epoxy [23] has indicated a typical ‘ $m$ ’ value in the range of  $0.06 < m < 0.50$ . This result and the experimental investigation over a wide variety of PCC in the present studies appear to be consistent with the concept that it is impossible to have, in practice, a dipolar dielectric system that is completely interacting/perfectly non-interacting. In other words, all dipolar systems in practice have mutually interacting dipoles with a difference in their dipolar relaxation strength, relaxation time distribution, and dipolar response (flips) with the frequency of the external applied electric field. These parameters depend on  $f_{\text{con}}$  and reflect changes in their property in terms of the magnitude of the critical exponents ‘ $m$ ’ that can be observed from Fig. 6.17a. It appears that the magnitude of ‘ $m$ ’ decreases with an increase in  $f_{\text{con}}$  invariably for all the PCC under investigation. This change can be understood in terms of the relative decrease in the number of dipoles of the host polymer in the PCC with the increase in  $f_{\text{con}}$ . In addition, an increase of  $f_{\text{con}}$  enhances the heterogeneity in the PCC leading to a wide distribution of relaxation

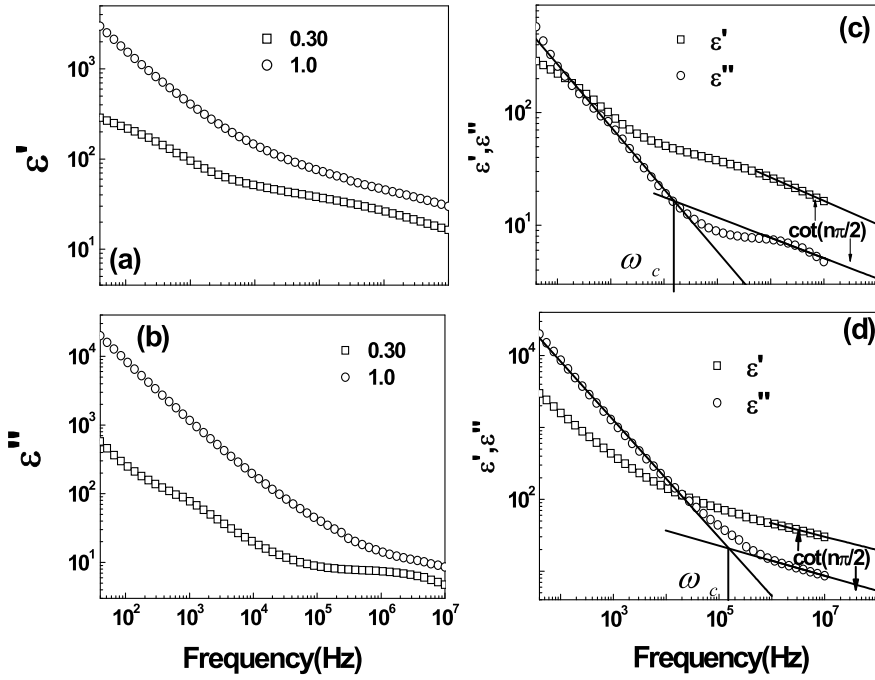


**Fig. 6.15** Comparison of the **a**  $\epsilon'$ , the real part of the effective complex permittivity, **b**  $\epsilon''$ , the imaginary part of the effective complex permittivity for series F samples versus frequency for all the samples above  $f_c$ , i.e.,  $f_{con} \geq 0.30$ ; typical log–log plot of  $\epsilon'$  and  $\epsilon''$  as a function of frequency for the samples, **c**  $f_{con} = 0.30$ , **d**  $f_{con} = 1.0$  above  $f_c$ ; the solid lines through the data show good agreement with Eq. 2.13

time and weakening of the dipolar interaction. This can be explained based on the uncorrelated behavior of the dipoles of the polymer due to the obstructions offered by the filler clusters/particles.

On the other hand, the typical values of the critical exponent ' $n$ ' for  $f_{con}/f_c < 1$  lying in the range  $0.68 < n < 0.85$  are shown in Fig. 6.18. It indicates that ' $n$ ' is nearly constant with an average value of  $\sim 0.75$  which is close to the pristine polymer phase (0.75). An analogous finding for CB/epoxy composite with  $0.95 < n < 0.98$  has also been reported. These results suggest that the dielectric behavior of the PCC below  $f_c$  depends strongly on the dynamics of the dipoles present in the polymer host.

### 6.4.2 Above $f_c$

This region refers to the charge carrier-dominated regime of the PCC. In this case, the typical values of the exponent ' $p$ ' for all the seven series of PCC lies in the range of  $0.5 < p < 1$ . The lower bound values of ' $p$ ' differ from a previous report

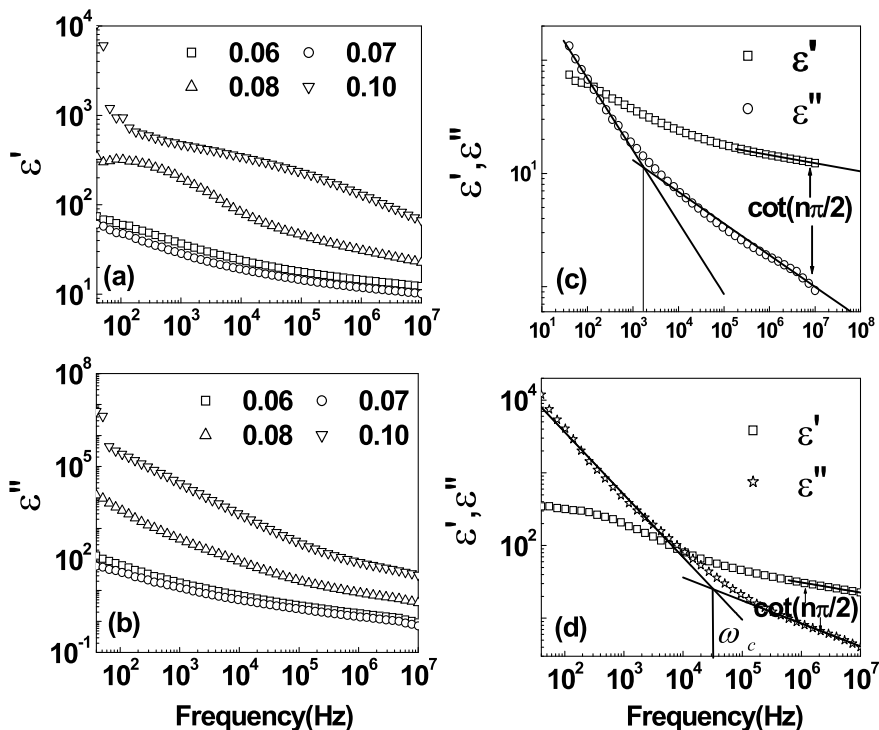


**Fig. 6.16** Comparison of the **a**  $\epsilon'$ , the real part of the effective complex permittivity, **b**  $\epsilon''$ , the imaginary part of the effective complex permittivity versus frequency for series G samples above  $f_c$ , i.e.,  $f_{con} \geq 0.06$ . Typical log–log plot of  $\epsilon'$  and  $\epsilon''$  as a function of frequency for the samples, **c**  $f_{con} = 0.06$ , **d**  $f_{con} = 0.08$  above  $f_c$ . The solid lines through the data show good agreement with Eq. 2.13

in literature for CB/epoxy composite for which  $p = [0.9, 1]$  [23]. This deviation in the magnitude of the exponent ' $p$ ' in the present report may be related to an active role of the conducting component in the composite phase above  $f_{con}$ . It has been attributed to the combined effect of two distinct processes: (a) correlated dipolar and (b) uncorrelated charge carrier contribution. The two competing phenomena exhibit sharp changes at  $f_c$  undergoing a transition from a dipole-dominated behavior to a charge carrier-dominated transport behavior for  $f_{con} > f_c$ . The more becomes the charge carrier domination, i.e., for  $f_{con} \gg f_c$ , the higher is the probability for ' $p$ ' to approach to the ideal limit of 1. The experimental results in the present studies suggest that for PCC sample with  $f_{con} \gg f_c$ ,  $p \sim 1$  (Fig. 6.17b). A relative difference in the value of  $p$  for different PCC may be related to the difference in  $f_{con}$ , the extent of connectivity, loss tangent, process conditions, and properties of the individual components of the PCC, etc.

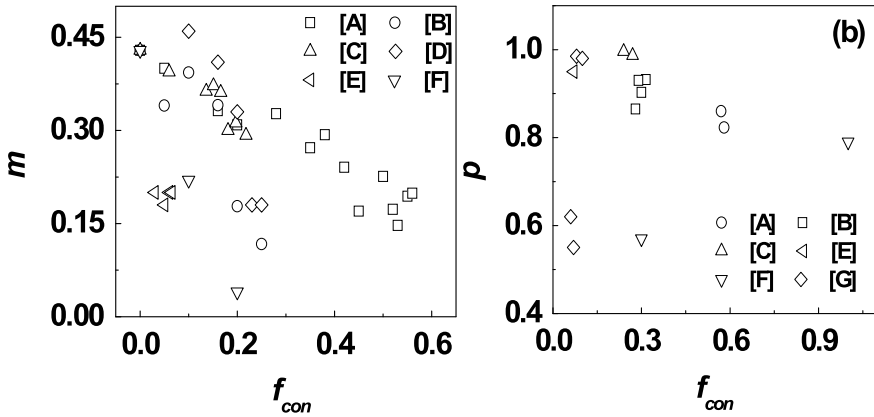
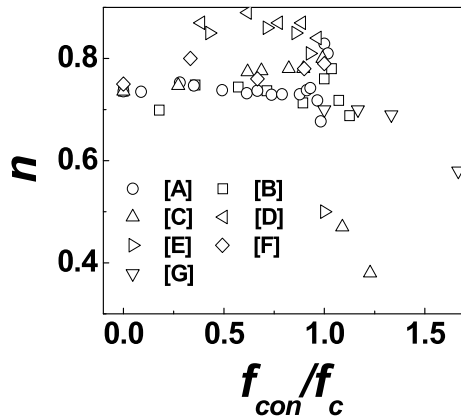


**Fig. 6.17** Variation of the exponent, **a**  $m$ , **b**  $p$  as a function of  $f_{con}$  for all the PCC series of composites under study. Each value of ‘ $m$ ’ corresponding to  $f_{con} < f_c$  is obtained from fitting of experimental data of  $\epsilon''$  to Eq. 2.9. Each value of ‘ $p$ ’ corresponding to  $f_{con} \geq f_c$  is obtained from fitting of experimental data of  $\epsilon''$  to Eq. 2.13

**Fig. 6.18** Variation in the exponent ‘ $n$ ’ as a function of  $f_{con}$  for all the series of PCC under study. Each value of ‘ $n$ ’ is obtained from fitting of experimental data of  $\epsilon''$  to Eqs. 2.9, 2.13 corresponding to all the samples of  $f_{con} < f_c$  and  $f_{con} \geq f_c$ , respectively



On the other hand, the magnitude of the critical exponent ‘ $n$ ’ has been observed to decrease linearly with  $f_{con}$  for  $f_{con}/f_c > 1$  (Fig. 6.18). This results in a direct manifestation of the dominance of uncorrelated charge carriers in the PCC. This decrease of ‘ $n$ ’ may be intuitively understood by noting that the dielectric phenomena, in this case, results from the prevalence of polarization by the deformation of the electronic cloud where the movements of the electrons are uncorrelated. The experimental value of ‘ $n$ ’ for the pristine polymer phase is 0.75, and it decreases with  $f_{con}/f_c > 1$  irrespective of the PCC. An analogous finding of a decrease in the exponent ‘ $n$ ’ for CB/epoxy composite [23] has also been reported. This dependence of ‘ $n$ ’ on  $f_{con}/f_c$  was also previously reported by Brosseau et al. [24], Mc Lachlan et al. [25], and Bardhan et al. [26]. Thus, we find that the critical exponent ‘ $n$ ’ in the PCC is

a crucial factor whose magnitude is distinctly different across  $f_c$ . So,  $f_c$  is the key parameter in tailoring the exponent 'n' which in turn governs the transport properties as well as the 3D topological arrangement of the conductor components in the PCC.

A comparison of the relaxation exponents 'n' and 'm' for  $f_{\text{con}} < f_c$  for all polar PCC is also expressed conventionally in terms of Hill plot. The typical results of the Hill plot for series A, B, C, and F are shown in Fig. 6.19. The top right-hand corner with  $m = 1$  and  $1 - n = 1$  corresponds to the ideal Debye behavior. The diagonal corresponds to symmetric peaks, i.e., the Cole–Cole equation. The top side refers to the points compatible with the empirical Cole–Davidson formula. It appears from a comparison of Fig. 6.19a–c that the experimental data points accumulate above the diagonal of the  $(m, 1 - n)$  plane and it approaches close toward the diagonal for nearly percolating networks. Another interesting feature is that polar PCC under study exhibit non-Debye-type polydispersive dipolar relaxation behavior in the regime of  $f_{\text{con}} < f_c$ . So, the correct representations require two independent parameters, such as the exponents  $\alpha$  and  $\beta$  in the H-N law and the exponents  $m$  and  $1 - n$  in the JUDR law of type-I for dipolar materials. We observe that for series A, more data points are below the diagonal of the hill plot and also are more scattered as compared to series B and C. It may be attributed to more heterogeneity in the case of series A leading to multiple scattering losses due to random walk diffusion type phenomena from scatterer to scatterer through the material. When the system is more heterogeneous, a more general form of H-N law for a dielectric response seems to provide useful information where the relaxation exponents are completely unsymmetrical.

## 6.5 Third Kind of Universal Dielectric Response

### 6.5.1 Microstructure

The optical micrographs of the pure PVDF and the composite samples such as non-percolated [ $(f_{\text{con}}) = 0.25 < \text{percolation threshold } (f_c)$ ], percolated [ $f_{\text{con}} = 0.28 > f_c$ ] and just percolated [ $f_{\text{con}} = 0.27 = f_c$ ] of PVDF/nc-Ni composites is shown in Fig. 6.20. The micrographs suggest a random distribution of bright metal clusters (nc-Ni) in the PVDF matrix with the formation of a self-connected network of nc-Ni clusters. The distribution of metal clusters and the extent of connectivity of the fillers in the PVDF matrix appear to be different with the increase of  $f_{\text{con}}$ , since the increase of  $f_{\text{con}}$  decreases the interparticle/cluster distance. The non-percolated, percolated, and just percolated phenomena can also be judged from the digital processed optical micrographs (Fig. 6.21) of corresponding samples with  $f_{\text{con}} = 0.20$  &  $0.25$ ,  $0.28$ , and  $0.27$ , respectively, since it can be seen through the processed images that formation of channels occurred as  $f_{\text{con}}$  increases in the PVDF matrix.

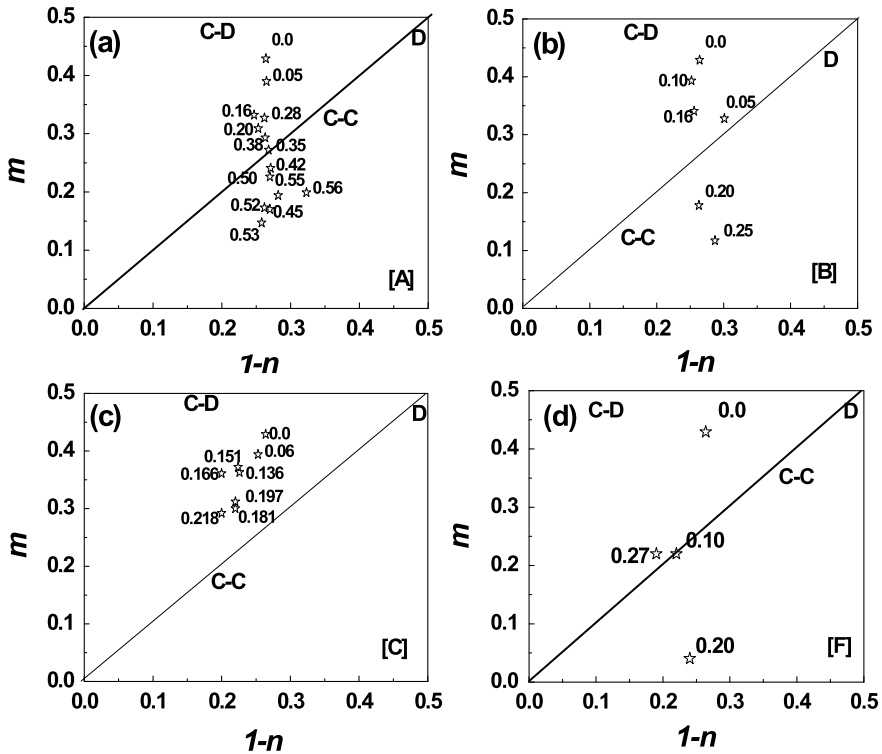


**Fig. 6.19** A compilation of the exponents ‘ $m$ ’ and ‘ $1 - n$ ’ defined by Eqs. 2.9a, 2.9b for the series of composites A, B, C, and F under study below  $f_c$ . Each sample is described by a point in the  $(m, 1 - n)$  plane. A pure Debye process corresponds to the top right-hand corner. Within this Hill plot, the Cole–Davidson model corresponds to  $m = 1$  and  $0 < 1 - n < 1$ , and the Cole–Cole model corresponds to the diagonal of the series of samples. **a** A. **b** B. **c** C. **d** F, respectively

### 6.5.2 Dielectric Spectroscopy

The dielectric and impedance data of  $f_{con} = 0.25 < f_c, f_{con} = 0.28 > f_c$  &  $f_{con} = 0.27 = f_c$  of the series of PMC across the IMT are analyzed [19]. For  $f_{con} = 0.25 < f_c$ , the expected dipolar relaxation, as a function of frequency is observed (Fig. 6.22a) and Jonscher’s two fractional power laws in two distinct regions flanking the loss peak frequency ( $\omega_p = 2.71$  MHz) obeys Eqs. (2.9a, 2.9b), given by, at low frequencies.

$$\epsilon_s - \epsilon'(\omega) \propto \epsilon''(\omega) \propto \omega^m \text{ for } \omega \ll \omega_p \text{ with } 0 < m < 1$$

and at high frequencies

$$\epsilon'(\omega) \propto \epsilon''(\omega) \propto \omega^{n-1} \text{ for } \omega \gg \omega_p \text{ with } 0 < n < 1$$

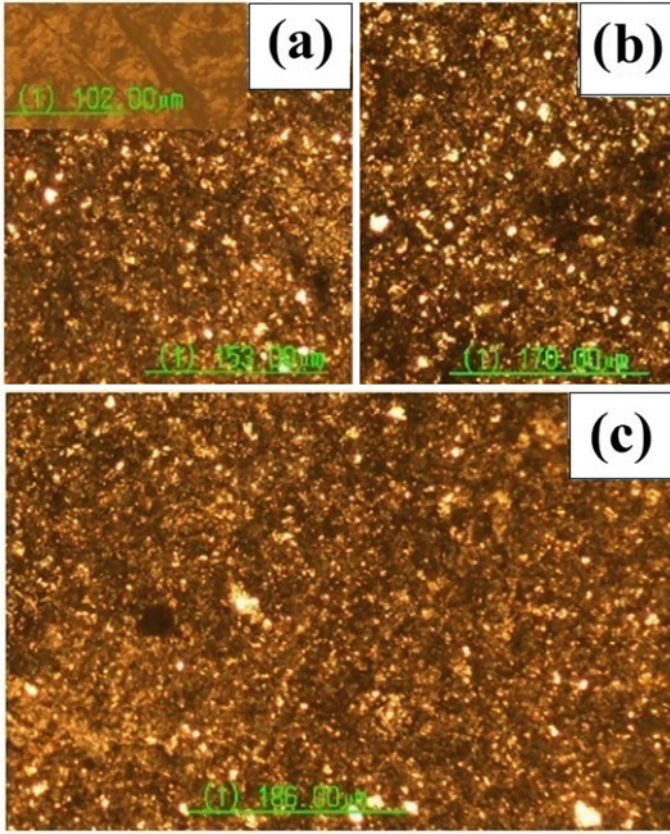


**Fig. 6.20** (Color online) Optical micrographs of the samples showing the differences of connectivity, **a** non-percolated ( $f_{\text{con}} = 0.25$ ) [inset: pure PVDF], **b** percolated ( $f_{\text{con}} = 0.28$ ). **c** Just Percolated ( $f_{\text{con}} = 0.27$ )

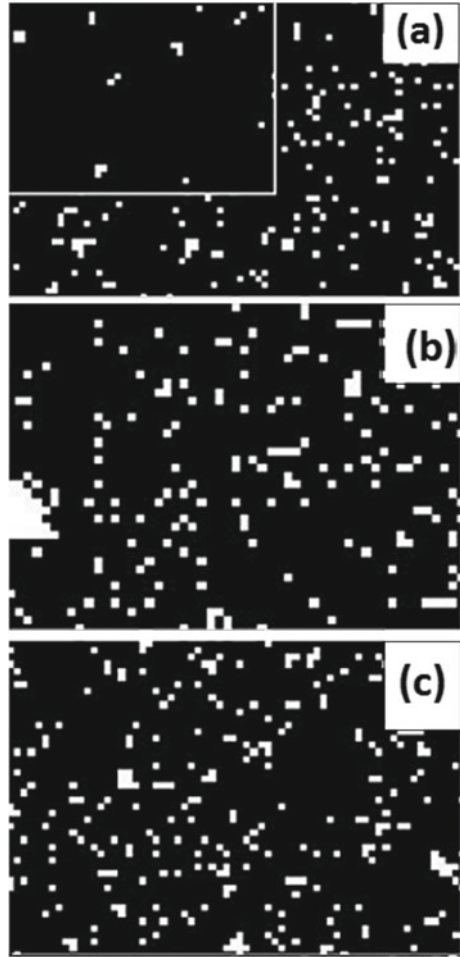
The exponent values estimated from the fits agree well with Jonscher's universal regime  $\sim [0, 1]$ . It can also be observed from Fig. 6.3a, that the ratio  $\varepsilon''(\omega)/\varepsilon'(\omega)$  is independent of frequency for  $\omega \gg \omega_p$  and is in good agreement with Eq. (2.11), given by

$$\frac{\varepsilon''(\omega)}{\varepsilon'(\omega)} = \cot(n\pi/2) = \text{const for } \omega \gg \omega_p \text{ with } 0 < n < 1$$

which says that the ratio of energy lost per reversal of macroscopic polarization to energy stored in every macroscopic polarization for  $\omega \gg \omega_p$  in the case of correlated dipolar systems is constant.

Similarly, for  $f_{\text{con}} = 0.28 > f_c$  (Fig. 6.22b), the expected correlated charge carrier relaxation as a function of frequency is observed and Jonscher's two fractional power

**Fig. 6.21** MATLAB processed optical micrographs, **a** non-percolated ( $f_{\text{con}} = 0.25$ ) [inset:  $f_{\text{con}} = 0.20$ ], **b** percolated ( $f_{\text{con}} = 0.28$ ), **c** just percolated ( $f_{\text{con}} = 0.27$ )



laws in two distinct regions flanking the critical frequency [ $\omega_c = 20$  kHz,  $\omega_c$  is the frequency that bears a direct analogy to  $\omega_p$ ] obeys Eq. (2.13a, 2.13b), given by, at low frequencies

$$\varepsilon'(\omega) \propto \varepsilon''(\omega) \propto \omega^{-p} \text{ for } \omega \ll \omega_c \text{ with } 0 < p < 1$$

and at high frequencies

$$\varepsilon'(\omega) - \varepsilon'_\infty \propto \varepsilon''(\omega) \propto \omega^{n-1} \text{ for } \omega \gg \omega_c \text{ with } 0 < n < 1$$

The obtained exponents lie well within the limiting values [0, 1] as per the predictions of Jonscher’s universal dielectric responses. From Fig. 6.22b, the ratio

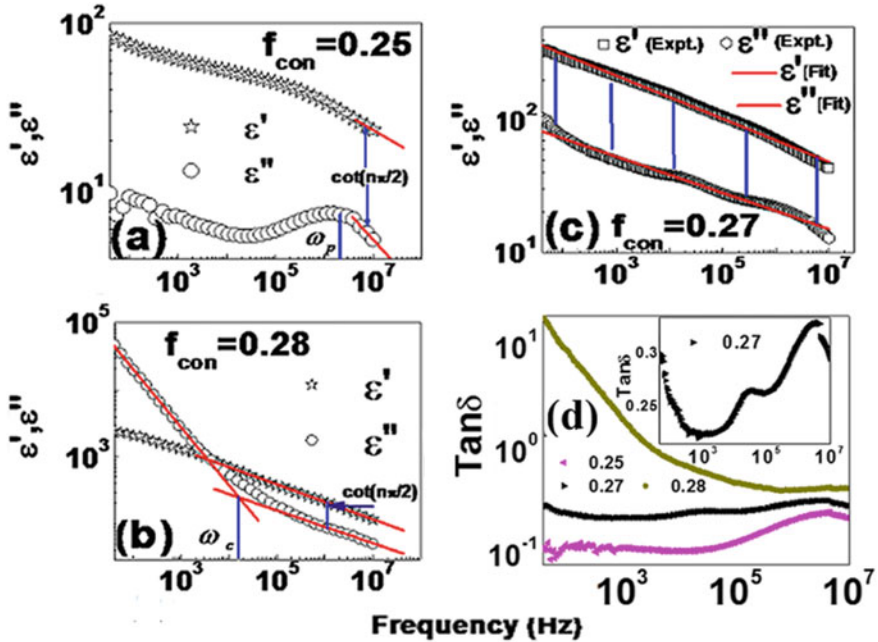


**Fig. 6.22** (Color online) Log–log plot of the real ( $\epsilon'$ ) and imaginary ( $\epsilon''$ ) complex permittivity as a function of the frequency, **a** non-percolated ( $f_{\text{con}} = 0.25$ ), the solid lines through the data show good agreement with Eqs. (2.9a, 2.9b) and (2.11), **b** Percolated ( $f_{\text{con}} = 0.28$ ), the solid lines through the data show good agreement with Eqs. (2.13a, 2.13b) and (2.15), **c** Just Percolated ( $f_{\text{con}} = 0.27$ ), the solid lines through the data show good agreement with Eqs. (2.9a, 2.9b), (2.13a, 2.13b) and (6.1). **d**  $\text{Tan } \delta \sim$  frequency for all the samples, inset:  $\text{Tan } \delta \sim$  frequency for the  $f_{\text{con}} = 0.27$  sample

$\epsilon''(\omega)/\epsilon'(\omega)$  remains constant and is independent of frequency for  $\omega \gg \omega_c$  with  $0 < n < 1$  and is in good agreement with Eq. (2.15), given by;

$$\frac{\epsilon''(\omega)}{\epsilon'(\omega)} = \cot(n\pi/2) = \text{const for } \omega \gg \omega_c \text{ with } 0 < n < 1$$

But for  $f_{\text{con}} = 0.27 = f_c$  (Fig. 6.22c), none of the relaxation phenomena, such as correlated dipolar relaxation/charge carrier relaxation were observed or an equally dipolar/charge carrier-dominated system with a completely different, neutral and competing electrical behavior is observed over the entire range of frequency. All the above equations starting from Eqs. (2.9a, 2.9b) and (2.13a, 2.13b) were found to be valid over the entire range of frequencies with values of the exponents well within Jonscher's universal regime [0, 1]. This suggests the emerged unique behavior of the sample is due to being an equally 50% dipolar and a 50% charge carrier system. Additionally, also both Eqs. (2.11) and (2.15) in a modified manner over the entire range of frequencies is demanded to be developed and is given in Eq. (6.1) as,

$$\frac{\varepsilon(\omega)}{\varepsilon'(\omega)} = \text{const} \quad (6.1)$$

which is the most awaited and modified Jonscher's like third kind of universal dielectric response behavior suitable for this type of dielectric systems. The validity of Eq. (6.1) is guaranteed as we observe from the experimental values of dielectric constants at different frequencies. At 40 Hz, the value of  $\varepsilon'(\omega)$  and  $\varepsilon''(\omega)$  are given by 400 and 100, respectively. At  $10^4$  Hz, the value of  $\varepsilon'(\omega)$  and  $\varepsilon''(\omega)$  is given by 160 and 40, respectively. At 10 MHz, the value of  $\varepsilon'(\omega)$  and  $\varepsilon''(\omega)$  is given by 50 and 13, respectively. Thus from all the above experimental results at different frequencies, it is observed for the  $f_{\text{con}} = 0.27$  sample that the value of Eq. (6.1) remains constant ( $\sim 0.25$ ) over the entire range of frequency at each value of the scanned frequency. The constant ratio for the sample can be interpreted as the rate at which the energy lost occurs per reversal of macroscopic polarization is equal to the energy stored in every macroscopic polarization at any frequency. This observation is also well-supported by analyzing the plot of loss tangent ( $\text{Tan } \delta$ ) as a function of frequency (Fig. 6.22d), which shows very drastic differences in the behavior of  $\text{Tan } \delta$  as a function of frequency for all the three samples with  $f_{\text{con}} = 0.25, 0.28,$  and  $0.27$ . The plot shows dipolar relaxation of PVDF polymer at 2.71 MHz for the sample with  $f_{\text{con}} = 0.25$ , while the low-frequency dispersion is observed for the sample with  $f_{\text{con}} = 0.28$  at less than 1 kHz. However, the value of  $\text{Tan } \delta$  is maintained at a constant value  $\sim 0.25$  (Fig. 6.22d) over the entire experimental range of the frequencies for the sample with  $f_{\text{con}} = 0.27$ , which is attributed to the rate at which the energy lost occurs per reversal of macroscopic polarization is equal to the energy stored in every macroscopic polarization at any frequency. In general, the value of this constant will be different for different PMC and is attributed to depend on the dielectric constant of the polymer, the differences of conductivity and fractions of the components of the PMC, and also on their connectivity arising due to their differences of process conditions. This equally dipolar-dominated/charge carrier-dominated behavior, i.e., the 50:50 behavior, exactly at the interface of IMT for the  $f_{\text{con}} = 0.27$  can also be observed from the initiation of percolated paths, just going to be developed in its digital image processed optical micrograph (Fig. 6.21c). The non-percolated and percolated behavior for  $f_{\text{con}} = 0.20, 0.25,$  and  $0.28$  can also be observed (Fig. 6.21) from their respective digital image processed optical micrographs. The relaxation behavior ( $\text{Tan } \delta \sim \text{frequency}$ ) of  $f_{\text{con}} = 0.27$  sample is given as an inset in Fig. 6.22d, which shows interestingly the three types of relaxations, present in the sample over the frequency ranges of 40 Hz–1 kHz, 1 kHz– $10^5$  Hz, and  $10^5$  Hz– $10^7$  Hz, respectively. The relaxation in the frequency range of 40 Hz–1 kHz is attributed to the low-frequency dispersion relaxation mechanism, while the relaxation in the frequency range  $10^5$ – $10^7$  Hz is attributed to the dipolar relaxation present in the polymer PVDF/PMC. Hence, the general trend observed is that electric conduction dominates the  $\text{Tan } \delta$  in the low-frequency region while the dielectric relaxation (dipolar relaxation) dominates in the high-frequency region. Interestingly, again the combination of the above-described relaxations emerged as a new type of relaxation in the mid-frequency region of 1 kHz  $\sim 10^5$  Hz for the  $f_{\text{con}} = 0.27$  sample due to the competing dynamics between the two

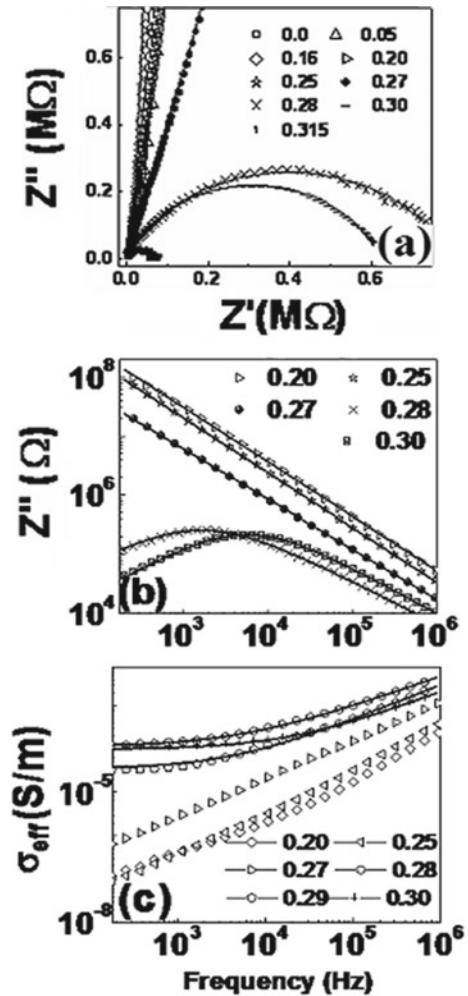
types of species present in the sample (inset, Fig. 6.22d). The presence of multiple relaxations for the  $f_{\text{con}} = 0.27$  sample may also be attributed to the competing dynamics of the two types of the carrier (dipolar as well as charge carrier) present in the sample over different frequency domains.

### 6.5.3 Impedance and Conductivity Spectroscopy

The supporting explanation of both an equally dipolar and charge carrier system for the  $f_{\text{con}} = 0.27$  sample can also be verified from the fitted experimental values of impedance and electrical conductivity with the help of a commercial software ZSIMPWIN version 2 [27], from Fig. 6.23. The observation is that for  $f_{\text{con}} < f_c$ , the Nyquist plot typically displays a straight line for all the PMC with  $f_{\text{con}} = 0.25 < f_c$  as shown in Fig. 6.23a. The straight line is attributed to the pure insulating nature of the polymer arising due to only the capacitive behavior. Further, it is observed that the profile of the Nyquist plot changes from straight-line behavior to an arc for  $f_{\text{con}} = 0.27$ , while a single depressed semicircle with the center below the real axis for  $f_{\text{con}} > f_c$ , with the frequency decreasing from left to right is observed. Thus, the behavior of  $f_{\text{con}} = 0.27$  is exactly in the middle of  $f_{\text{con}} < f_c$  &  $f_{\text{con}} > f_c$ . The appearance of a single semicircle indicates a single relaxation process originating from the Maxwell, Wagner, and Sillars (MWS) interfacial polarization at the host polymer–metal interface. Similarly, in observation with the variation of  $Z'' \sim$  frequency (Fig. 6.23b),  $Z''$  decreases linearly with frequency for  $f_{\text{con}} \leq f_c$  for all the PMC. The value of  $Z'' \sim 10^8 \Omega$  for the samples with  $f_{\text{con}} = 0.20$  and  $0.25$ , while it decreases by one order for the  $f_{\text{con}} = f_c = 0.27$  sample and it reaches  $\sim 10^7 \Omega$  and for  $f_{\text{con}} > f_c$ , it again decreases by orders reaching the value  $\sim 10^5 \Omega$ – $10^4 \Omega$  for  $f_{\text{con}} = 0.28$  &  $0.30$ . It can also be seen that  $Z'' \sim$  frequency pattern displays broad and low-intensity peaks. This behavior has been reported for several materials being evidence of actuation or a hopping type mechanism as electrons start hopping between two filler clusters due to the gradual decrease in distance between the filler clusters/particles due to the increase of  $f_{\text{con}}$ . These behaviors may be considered due to the  $f_{\text{con}}$  dependence of electrical relaxation phenomena in the materials. The relaxation peak observed for the PMC for  $f_{\text{con}} > f_c$  in the lower frequency region is due to the development of long-range dc conduction, which is attributed to the conductivity relaxation/MWS relaxation. Figure 6.23c shows the dispersion of ac conductivity ( $\sigma_{\text{ac}}$ ) with frequency for all the samples corresponding to  $f_{\text{con}} < f_c$  with the dc conductivity ( $\sigma_{\text{dc}}$ ) part becomes zero, whose detailed analysis can be found from earlier literature. The value of low-frequency  $\sigma_{\text{ac}}$  is less than  $10^{-7}$  S/m for the samples  $f_{\text{con}} = 0.20$  and  $0.25$ , while it increases by one order for the  $f_{\text{con}} = f_c = 0.27$  sample and it reaches  $\sim 10^{-6}$  S/m, and after that, it increases by orders reaching the value  $\sim 10^{-4}$ – $10^{-5}$  S/m for  $f_{\text{con}} = 0.28$  to  $0.30$ . Thus, it is found that the conductivity of  $f_{\text{con}} = f_c = 0.27$  sample lies exactly in between the  $f_{\text{con}} < f_c$  &  $f_{\text{con}} > f_c$  samples. Again for  $f_{\text{con}} = 0.28$ – $0.30$  with  $f_{\text{con}} > f_c$ , a mixed conductivity is found, i.e., a dc plateau up to a certain frequency separated by ac conductivity beyond that frequency. The dc plateau occurs due to the appearance

of long-range dc conductivity with the increase of  $f_{con}$  separated from the frequency-dependent conductivity part. The frequency at which dispersion in the ac conductivity starts shifts to the higher frequency side with a rise in  $f_{con}$  and this frequency at which the change in slope takes place is the “hopping frequency  $\omega_H$ ”. Thus from all the results of Fig. 6.23, it is confirmed that  $f_{con} = 0.27$  is tuned to the exact boundary of IMT and has opened a completely different and novel dielectric response behavior suitable for a variety of unique electrical and electronics engineering applications.

**Fig. 6.23** **a** Nyquist plots of all the samples of PMC. The solid lines are the fits to the experimental data. **b** The variation of imaginary part of impedance ( $Z''$ ) as a function of frequency for  $f_{con} = 0.20, 0.25, 0.27, 0.28,$  and  $0.30,$  respectively. **c** The variation of ac conductivity with frequency for  $f_{con} = 0.20, 0.25, 0.27, 0.28, 0.29,$  and  $0.30,$  respectively



## 6.6 Summary

The universality of dielectric relaxation in a wide variety of PCC exhibiting simultaneous dipolar and charge carrier-dominated transport over different  $f_{\text{con}}$  is discussed. The experimental results on polar and non-polar PCC provide convincing evidence for an electrical transport mechanism governed by DR and ALFD phenomena. In polar PCC, DR plays a predominant role below  $f_c$ , whereas ALFD becomes dominant above  $f_c$ . On the other hand, ALFD above  $f_c$  is the only likely possibility for non-polar PCC. The quantification of dielectric relaxation behavior in the PCC has been done in terms of the relaxation exponents of the JUDR laws and the magnitude of relaxation exponents ' $m$ ', ' $n$ ', and ' $p$ ', falls within the universal limit  $\sim [0, 1]$  with the additional feature of strong dependence on  $f_{\text{con}}$ . A decrease in the relaxation exponent ' $m$ ' with an increase of  $f_{\text{con}}$  is directly linked with a decrease in the number of dipoles of the polymer in the composite phase. This decrease is accompanied by a distribution of relaxation time due to increased heterogeneity in the system. The magnitude of ' $p$ ' increases and approaches the limiting value  $\sim 1$  with the increase of  $f_{\text{con}}$  beyond  $f_c$  due to the dominance of charge carrier transport in the system. The magnitude of the relaxation exponent ' $n$ ' decreases at  $f_c$ , due to the prevalence of MWS polarization contributed by uncorrelated electrons. Below  $f_c$ , electrical transport is controlled by strongly correlated dipoles whereas above  $f_c$  charge carrier transport becomes predominant. The two regimes across  $f_c$  on the concentration scale in the PCC indicated contrasting features in polar polymer host-based PCC. On the other hand, PCC based on the non-polar polymer could not show any significant effect below  $f_c$  while its behavior remains identical to the polar polymer-based PCC above  $f_c$ . A comparison of this feature between PCC based on different polymer host indicated a direct role of the dipoles present in the host in controlling their dielectric relaxation behavior for  $f_{\text{con}} < f_c$ . The results confirmed a general validity of the JUDR laws for a wide variety of PCC with different possible polymer/conductor combinations in the composite form prepared under different process conditions. The universality of both the JUDR laws in polar polymer-based PCC is also confirmed. Our results appear to be of universal significance for ICC. Although this chapter gives an investigation of dielectric relaxation behavior in the case of PCC, the detailed study of different other ac electrical parameters across  $f_c$  will make the study complete and will give a very clear understanding regarding the electrical relaxation behavior in this PCC, which is discussed in Chap. 7. A very different, neutral, and competing electrical relaxation phenomena for the  $f_{\text{con}} = f_c = 0.27$  sample is also observed, which suggests a novel dielectric response, as well as a very special phenomenon at the exact boundary of IMT for which both Jonscher's laws are equally validated over the entire range of frequencies and the ratio of imaginary and real part of dielectric constant, remains constant over the entire range of frequency, which makes the material as a very unique material. Also, the interesting feature is that the emerged new relaxations show the presence of multiple relaxations in addition to the conventional relaxations present in the sample due to the competing dynamics of two different

types of carriers present in the sample. These types of materials may find their unique and special applications in electrical and electronics engineering.

## References

1. Dyre JC, Schroder TB (2000) Universality of ac conduction in disordered solids. *Rev Mod Phys* 72:873–892
2. Dyre JC (1988) The random free energy barrier model for ac conduction in disordered solids. *J Appl Phys* 64:2456–2468
3. Bergman DJ, Stroud D (1992) Solid state physics, advances in research and applications. In: Ehrenreich H, Turnbull D, vol 46. Academic, New York
4. Liu SH (1986) Solid state physics, advances in research and applications. Academic, New York
5. Tuncer E, Gubanski SM, Nettelblad B (2001) Dielectric relaxation in dielectric mixtures: application of the finite element method and its comparison with dielectric mixture formulas. *J Appl Phys* 89:8092–8100
6. Adohi BJP, Brosseau C (2009) Dielectric relaxation in particle-filled polymer: influence of the filler particles and thermal treatments. *J Appl Phys* 105:054108
7. Cheng Y, Chen X, Wu K, Wu S, Chen Y, Meng Y (2008) Modeling and simulation for effective permittivity of two-phase disordered composites. *J Appl Phys* 103:034111
8. Mejdoubi A, Brosseau C (2007) Numerical calculations of the intrinsic electrostatic resonances of artificial dielectric heterostructures. *J Appl Phys* 101:084109
9. Fourn C, Lasquellec S, Brosseau C (2007) Finite-element modeling method for the study of dielectric relaxation at high frequencies of heterostructures made of multilayered particle. *J Appl Phys* 102:124107
10. Panda M (2018) Ferroelectric polymer dielectrics: emerging materials for future electrostatic energy storage applications. *AIP Conf Proc* 1953(1–4):020001
11. Debye P (1945) Polar molecules. Dover, New York
12. Cole KS, Cole RH (1941) Dispersion and absorption in dielectrics I. Alternating current characteristics. *J Chem Phys* 9:341–351
13. Davidson DW, Cole RH (1951) Dielectric relaxation in glycerol, propylene glycol, and *n* propanol. *J Chem Phys* 19:1484–1490
14. Havriliak S, Havriliak SJ (1997) Dielectric and mechanical relaxation in materials: analysis, interpretation, and application to polymers. Hanser Publishers, Munich
15. Dissado LA, Hill RM. Non-exponential decay in dielectrics and dynamics of correlated systems. *Nature* 279:685
16. Macdonald JR (1987) Impedance spectroscopy: emphasizing solid materials and systems. Wiley, New York
17. Jonscher AK (1983) Dielectric relaxation in solids. Chelsea Dielectrics press, London
18. Panda M, Srinivas V, Thakur AK (2014) Dielectric spectroscopy of polymer-metal composites across the percolation threshold. *J Adv Dielectr* 04:14500271–14500276
19. Panda M (2018) Evidence of a third kind of Jonscher's like universal dielectric response. *J Adv Dielectr* 08(1–6):1850028
20. Panda M, Srinivas V, Thakur AK (2015) Non-universal scaling behavior of polymer-metal composites across the percolation threshold. *Results Phys* 5:136–141
21. Panda M, Thakur AK, Srinivas V (2010) Thermal effects on the Percolation behavior of polyvinylidene fluoride/nickel composites. *J Appl Polym Sci* 117:3023–3028
22. Venketesh C, Srinivas V, Panda M, Rao VV (2010) Dielectric response in novel polyvinylidene fluoride/nanoquasicrystalline composites. *Solid State Communications* 150:893–896
23. Achour ME, Brosseau C, Carmona F (2008) Dielectric relaxation in carbon black-epoxy composite materials. *J Appl Phys* 103(1–10):094103

24. Brosseau C (2002) Generalized effective medium theory and dielectric relaxation in particle-filled polymeric resins. *J Appl Phys* 91:3197
25. Wu J, McLachlan DS (1998) Scaling behavior of the complex conductivity of graphite-boron nitride percolation systems. *Phys Rev B* 58:14880–14887
26. Chakrabarty RK, Bardhan KK, Basu A (1991) Nonlinear I–V characteristics near the percolation threshold. *Phys Rev B* 44:6773–6779
27. Yemu B (1999) Z Simpwin version 2, electrochemical impedance spectroscopy (EIS) Data analysis software. Princeton applied research

# Chapter 7

## Impedance Spectroscopy of Percolative Polymer Composites



In this chapter, the correlation between the microstructure of the polymer/conductor composites (PCC) series of samples with their corresponding electrical properties has been discussed. AC technique of complex impedance spectroscopy (CIS) has been used to evaluate the electrical response in terms of impedance, modulus, and ac conductivity as a function of frequency and volume fraction of conductor ( $f_{\text{con}}$ ) for the PCC across the percolation threshold ( $f_c$ ). The presence of electrical relaxation has been observed in terms of the frequency response of electrical parameters, such as impedance ( $Z$ ) and modulus ( $M$ ). An equivalent electrical circuit model has been proposed to correlate the electrical response of the various PCC series with their microstructure. The correlation between the two independent experimental results appears to be in excellent agreement with each other. The studies on these different PCC show identical microstructure agreeing well with their electrical properties and observed relaxation across  $f_c$ . The observed conductivity relaxation in all the seven series of PCC provides convincing evidence for proposing the universality of the phenomena.

### 7.1 Introduction

Generally, the polymer/conductor composites (PCC) are flexible and can be easily fabricated into various shapes as compared to polymer-ceramic composites. The interesting properties of these PCC are that they undergo an insulator-to-metal transition (IMT) at a critical volume fraction of the conductor ( $f_{\text{con}}$ ) called percolation threshold ( $f_c$ ) which is characterized by the divergence of the real part of the dielectric constant and abnormal increase of ac conductivity. To design new composite materials with desirable properties, the understanding of electrical properties of ICC/PCC is of great significance [1–5]. Despite numerous research results reported up to now,

little is known about the relationship between the microstructure and electrical properties of PCC experimentally although some scattered results are available on electrical properties for a few PCC. Almond et al. [1–4] and Calame [5] explained theoretically that for insulator–conductor composites (ICC) (i.e., for a random resistor ( $R$ )–capacitor ( $C$ ) networks) the power-law dispersions in permittivity and dielectric loss is characterized universally by the Cole–Davidson response function for the composites with  $f_{\text{con}} \geq f_c$ . The experimental verification of the power-law dispersion of permittivity is reported universally in a variety of PCC for both the regions of  $f_{\text{con}} < f_c$  and  $f_{\text{con}} \geq f_c$  in terms of Jonscher’s two exponents universal dielectric response in Chap. 6. The experimental investigation of electrical properties of the random ICC/PCC ( $R$ – $C$  networks) across  $f_c$  is yet to be investigated universally for  $f_{\text{con}} < f_c$  and  $f_{\text{con}} \geq f_c$ , respectively, although very few experimental systems have been investigated [3, 4]. Also, the electrical properties of the PCC using CIS [6] have received little attention which is a very convenient and non-destructive powerful experimental technique that enables us to study the electrical behavior of the composites over a range of frequency and  $f_{\text{con}}$ . A strong confirmation regarding the universal modeling of electrical equivalent of material for PCC/ICC undergoing continuum ideal percolation is to be proposed based on our experimental results and earlier theoretical as well as experimental results. The role of  $f_{\text{con}}$  in the PCC is to be explored and how it plays the analogous role as that played by temperature in the case of ionic conductors (ceramics) is very interesting. In ionic conductors with the increase of temperature the charge carriers gain energy and try to overcome the attractive potential barrier created by the nearest neighbor sites and undergo an insulator (only ac conduction) to a mixed conduction behavior (both ac and dc conduction) as a function of temperature. Hence, temperature is the parameter/external source to overcome the potential barrier and gives rise to long-range dc conductivity as a function of temperature in the case of ionic conductors. In the case of PCC, electrons are the only free charge carriers in the metallic clusters and are prevented by the insulating polymer layer that acts as the potential barrier. With the increase of  $f_{\text{con}}$  in the composite, the thickness of the insulating layer between the filler clusters decreases, thereby decreasing the height of the potential barrier and the composite undergoes an IMT transition from its pure insulating ac conduction behavior to a behavior in which a mixed conduction behavior (dc and ac conductivity) is expected. Hence, we understand that with the increase of  $f_{\text{con}}$ , a decrease of the height of the potential barrier occurs which is indirectly equivalent to the increase of the activation energy of the free electrons present in the conducting filler clusters. The experimental results on various PCC give exactly similar types of electrical properties across  $f_c$ . The detailed discussion of electrical properties of all the PCC in the following subsections across  $f_c$  and found that the physics associated with the various relaxation processes, and the microstructure of all the PCC remains identical and universal.

To have a complete understanding of the dynamics of electrical response on the variety of PCC across  $f_c$  understudy, an analysis of the frequency-dependent CIS result is presented. Various formalisms, such as complex impedance spectrum, complex modulus spectrum, and conductivity spectrum approach, have been adopted

**Table 7.1** Preparation method and notation for the particular series under study

Name of the series of composites	Preparation method	Notation for the particular series
PVDF/ $\mu$ -Ni	Room temperature consolidation	A
PVDF/ $n$ -Ni	Room temperature consolidation	B
PVDF/ $n$ -QC	Room temperature consolidation	C
PVDF/ $\mu$ -Ni	Compression hot molding	D
PVDF/ $n$ -Ni	Compression hot molding	E
PVDF/ $n$ -Ni-NiO	Compression hot molding	F
LDPE/ $n$ -Ni	Compression hot molding	G

to probe the electrical response across  $f_c$ . This has enabled us to understand and generalize the electrical relaxation behavior in the broad class of PCC across  $f_c$ .

## 7.2 Samples Reported

In this chapter, to universalize the electrical properties (behavior of different electrical parameters) of a PCC across  $f_c$ , the different varieties of PCC have been studied (same series of samples as having been studied in Chap. 6 with different possible types of conductors and insulating polymers). The different series of samples along with their preparation method and notations used for the particular series is given in the form of Table 7.1. Before discussing the results, it would be very much useful to keep in mind the respective  $f_c$  values obtained for different PCC are given by 0.57, 0.28, 0.23, 0.26, 0.07, 0.30, 0.06 for series A, B, C, D, E, F, and G, respectively.

## 7.3 Results and Discussion

### 7.3.1 Microstructure

The effect of process conditions on tailoring of the microstructure of the PCC is described in Chap. 5. Here our emphasis is to correlate the changes in PCC microstructure with filler loading across  $f_c$  [7–9]. Polarized optical microscopy is used to see the distribution of metallic filler clusters in the polymer matrix of the PCC.

Some of the typical optical micrographs of the PCC corresponding to  $f_{\text{con}} \ll f_c$ ,  $f_{\text{con}} \rightarrow f_c$ , and  $f_{\text{con}} \geq f_c$  are given in Fig. 7.1. The typical morphological features for all the composites are composed of two-phase components in which one component shows the brighter region and the other region is the background. Due to the presence of metallic clusters in the polymer matrix, the reflection of the polarized light from the metallic clusters occurs and that corresponds to the brighter regions in the composites. For  $f_{\text{con}} \ll f_c$ , the filler clusters (brighter regions) are well-isolated from each other, and for  $f_{\text{con}} \rightarrow f_c$  the filler clusters approach and become very close to each other. The extent of heterogeneity of the distribution of the filler particles increases with the increase of  $f_{\text{con}}$  and the filler clusters are found to be overlapped with each other for  $f_{\text{con}} \geq f_c$  (refer to optical micrographs of Chap. 5 also). Such tailoring in the morphological features, controlled by dispersion of conducting fillers of variable geometrical shape, size, and loading in the PCC, may be expected to modulate their physical properties and electrical response on the application of an ac electric field across it. To confirm this hypothesis CIS has been carried out on each of the seven series of samples over a wide range of frequency. It is described in the next section.

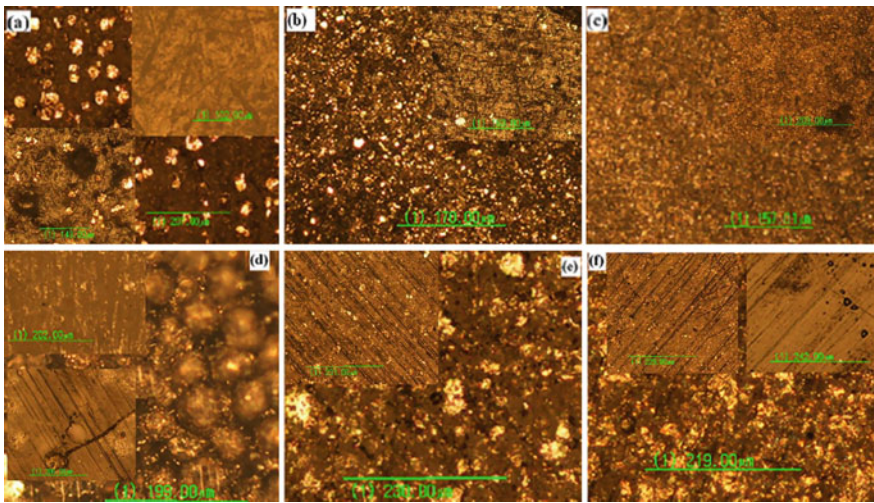


**Fig. 7.1** Typical optical micrographs of the some of the samples corresponding to various series of PCC, **a** series A,  $f_{\text{con}} = 0.57$ , upper inset: pure PVDF, lower inset:  $f_{\text{con}} = 0.20$ , **b** series B,  $f_{\text{con}} = 0.28$ , inset:  $f_{\text{con}} = 0.10$ , **c** series C,  $f_{\text{con}} = 0.24$ , inset:  $f_{\text{con}} = 0.17$ , **d** series D,  $f_{\text{con}} = 0.26$ , upper inset: pure PVDF, lower inset:  $f_{\text{con}} = 0.10$ , **e** series E,  $f_{\text{con}} = 0.07$ , inset:  $f_{\text{con}} = 0.03$ , **f** series F,  $f_{\text{con}} = 0.06$ , left inset:  $f_{\text{con}} = 0.03$ , right inset: pure LDPE

### 7.3.2 Impedance Spectroscopy

The complex-plane impedance spectrum (Nyquist plots) for all the PCC are shown in Fig. 7.2. We observe that for  $f_{\text{con}} < f_c$ , the Nyquist plot typically displays a straight line for all the series of PCC. The straight-line response is attributed to the pure insulating nature of the polymer arising due to only the capacitive behavior. Further, it is observed that the profile of the Nyquist plot changes from straight-line behavior to an arc; i.e., the evolution of impedance spectra shows a slight decrease of resistance with an increase of  $f_{\text{con}}$  in the region of  $f_{\text{con}} \leq f_c$ . In all PCC, it is observed a single depressed semicircle with the center below the real axis for  $f_{\text{con}} \geq f_c$ , with the frequency decreasing from left to right. The presence of a single semicircle indicates a single relaxation process originating from the Maxwell, Wagner, Sillars, (MWS) interfacial polarization at the host polymer-conducting filler interface. An inspection of the CIS spectrum suggests that the purely capacitive response (indicated by the vertical spike) undergoes a drastic modification into a semicircular arc pattern at a specific loading of the conductor component in the PCC. The appearance of semicircle in the electrical impedance response at  $f_{\text{con}} \geq f_c$ , irrespective of the PCC series confirms the electrical behavior of the PCC. It suggests an effective role of the resistive component in the impedance response in conjunction with the capacitive behavior. The combined resistive ( $R$ )–capacitive ( $C$ ) effect begins at  $f_c$ . The  $f_c$  value observed from the Nyquist plots agrees well with earlier values of  $f_c$  for all the series of PCC found from earlier investigations and also from the dielectric analysis (Chap. 6). In general, percolation in PCC typically causes a transition from an insulating electrical response to a more conducting behavior, consistent with CIS results described here. The larger the radius of the semicircle larger is the resistance and vice-versa. Hence, a relative decrease in the radii of arcs with increasing filler loading causes electrical phase transition from an insulating to a conducting behavior across  $f_c$ . In general, whether a full, partial, or no semicircle is observed depends on the strength of the relaxation and the experimentally available frequencies. It is observed that in the region of  $f_{\text{con}} \geq f_c$ , the dc resistance of the sample (where the semicircle cuts the real axis) decreases with the increase of  $f_{\text{con}}$  with a few exceptions which can be accepted within the experimental error. The absence of the first semicircle suggests that the effective contribution of the bulk material to impedance is not there because of the conducting nature of the metallic clusters/particles. An analysis of the CIS spectrum shows that the semicircle exhibits some depression degree instead of a semicircle centered on the abscissa. The most acceptable approach to interpreting the depression of semicircles is the statistical distributions of relaxation times [10, 11]. According to Debye's model, a material having a single relaxation time gives rise to an ideal semicircle in the Nyquist plot centered on the real axis. The shape of Nyquist plots for the PCC suggests that the electrical response is composed of one relaxation phenomenon with different relaxation frequencies. The value of peak relaxation frequency ( $f_{\text{max}}$ ) increases with an increase of  $f_{\text{con}}$  which can be understood based on an increment of long-range dc conductivity like  $f_{\text{max}}$  increases with the increase of temperature [12]. The semicircle arc is attributed to the interfacial

polarization or MWS polarization formed at the interface of the two components. The non-Debye-type electrical relaxation is an outcome of the two-parameter functions, expressed by Havriliak–Negami formalism which is a combination of the Cole–Davidson and Cole–Cole formalism. The depressed semicircle represents typically a phenomenon with a distribution (spread) of relaxation time. It is also observed that in the region of  $f_{\text{con}} \geq f_c$ , the area of the semicircle gradually decreases with an increase of  $f_{\text{con}}$  in PCC with a few exceptions due to the experimental error.

An equivalent circuit is commonly used in impedance spectroscopy analysis to provide a complete picture of the system and establish the microstructure–property relationship of the material systems under investigation. The impedance data of all the PCC have been fitted using the commercially available software ZSIMP WIN Version 2 and are shown in Fig. 7.2g, h. The solid line is the fitted curve used to estimate the impedance of the composite. The theoretical and experimental patterns appear to be in good agreement.

To give the electrical equivalent circuit model of the composites in the region of  $f_{\text{con}} < f_c$ , an equivalent circuit of series resistance ( $R_s$ ), in connection with a CPE (Q) in series was used to fit the experimental data (see equivalent circuit model of Fig. 7.2g). The CPE is used in place of a capacitor to account for deviations from a perfect capacitor behavior causing depression. The CPE is attributed to the electrically insulating behavior of the polymer. The series resistance used to fit the experimental data is attributed to the wire resistance and the contact resistance of the samples. Similarly in the region of  $f_{\text{con}} \geq f_c$ , an equivalent circuit comprising of  $R_s$  in series with another R and Q being in parallel gives the best fit to the experimental data (see equivalent circuit model of Fig. 7.2h). At  $f_c$ , due to the overlapping of the effective tunneling range of the filler particles, the conducting fillers particles/clusters act as a resistor and the thin dielectric insulating layer acts as a CPE (i.e., a capacitor). The series resistance is also attributed to the wire resistance and the contact resistance of the samples. The impedance associated with the CPE (Q) is defined by Eq. (2.18) which is given as  $Z_{\text{CPE}} = \frac{1}{Q_0(i\omega)^u}$ . The estimated values of the electrical parameters from the “equivalent electrical circuit” are given in Table 7.2. A comparison of the values of  $R_s$ ,  $R$ ,  $Q$ , and  $u$  suggests that  $f_{\text{con}}$  affects the electrical properties of the composites markedly. The value of  $R$  decreases with an increase of  $f_{\text{con}}$  due to the increase of density of filler particles leading to the overlapping of effective tunneling range of the filler particles. It is also observed that the magnitude of CPE increases with an increase of  $f_{\text{con}}$ , thereby increasing the value of the capacitance. The magnitude of the dielectric constant (not shown in the table) calculated from the fitted value of CPE matches well with the earlier reported values of the dielectric constant. The magnitude of ‘ $u$ ’ associated with the CPE lies in between  $0.6 < u < 1$  for all the PCC samples confirming the agreement between theoretical and experimental impedance response, i.e., the behavior of a CPE. We observe from Table 7.2 that the value of ‘ $u$ ’ undergoes a drastic change in its value, i.e., from  $0.9 < u < 1$  (for  $f_{\text{con}} < f_c$ ) to  $0.6 < u < 0.9$  (for  $f_{\text{con}} \geq f_c$ ). This can be understood on the basis that the purely capacitive/insulating behavior is markedly affected by  $f_{\text{con}}$  in the composite. As we know from Eq. (2.17), given by  $Z(\omega) = R_\infty + \frac{R}{1+j(\omega/\omega_0)^{1-\alpha}}$  and Eq. (2.18) given above (See theoretical description of impedance spectroscopy in Chap. 2), that

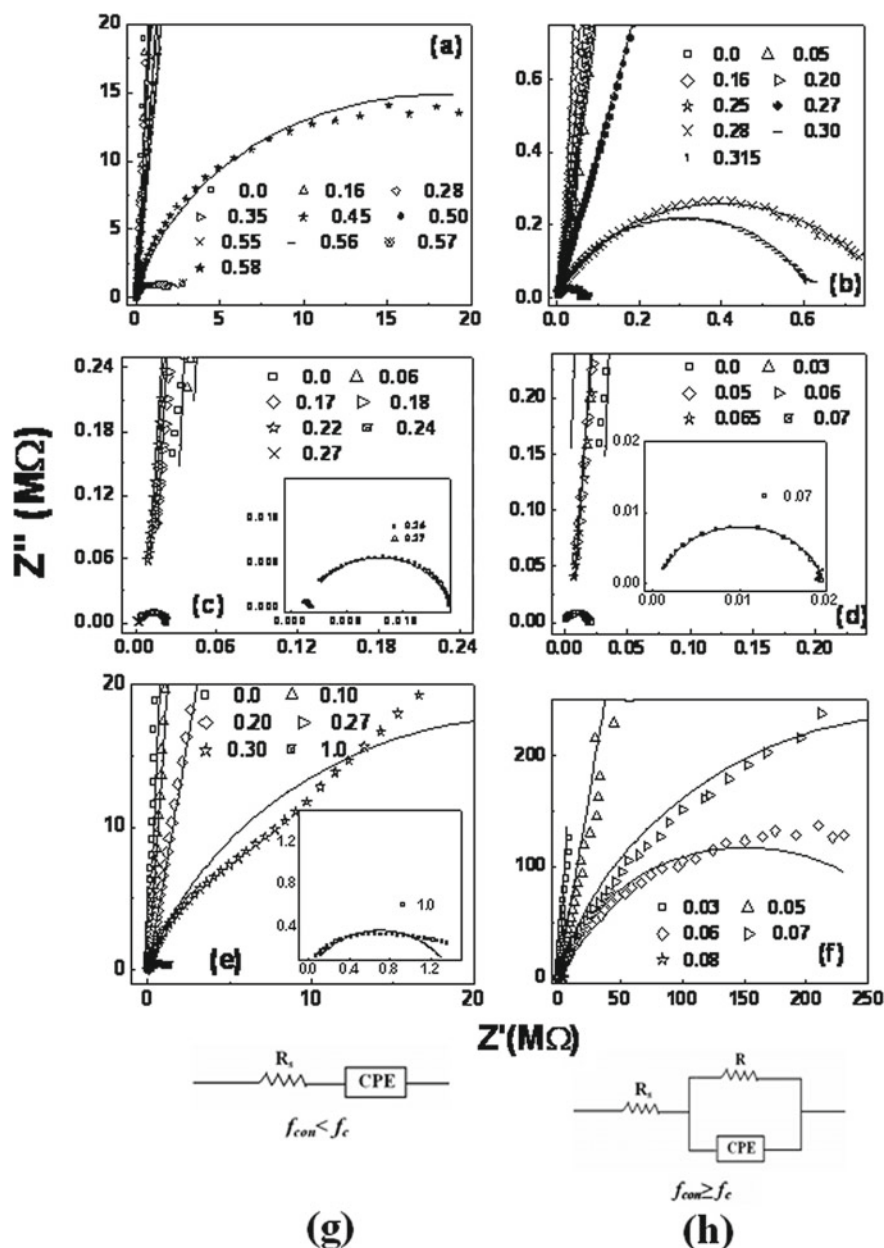


**Fig. 7.2** Complex impedance plots,  $Z''$  versus  $Z'$ , at several  $f_{con}$  for the various PCC series. **a** series A, **b** series B, **c** series C, **d** series E, **e** series F, **f** series G composites, respectively. The high coincidence between the overall fitting (solid curve) and the experimental contributions (dot points curve) is an indicator of the occurrence of the relaxation processes across the interface; Electrical equivalent circuit model of PCC for **g**  $f_{con} < f_c$ , **h**  $f_{con} \geq f_c$

the values of 'u' and 'α' are related to each other by  $u = 1 - \alpha$  and for  $f_{\text{con}} \geq f_c$ , 'α' determines the extent of depression of the semicircle below the real axis. The 'α' value lies in between  $0 < \alpha < 0.4$  as given in Table 7.2 for  $f_{\text{con}} \geq f_c$ , for all the PCC. From Table 7.2, we observe that the values of R and Q also indicate that the CPE attributed to the interfacial/grain boundary semicircle is found to be a function of  $f_{\text{con}}$ . The intercept of the high-frequency semicircular arc with the real axis gives an estimate of the bulk (dc) resistance (R) and its value becomes different for different  $f_{\text{con}}$ , i.e., R decreases with the increase of  $f_{\text{con}}$  in the composite (Fig. 7.2).

Figure 7.3 shows the typical variation of real and imaginary parts of impedance (Z) with frequency for various  $f_{\text{con}}$  for all the PCC series of samples. In all the PCC,  $Z'$  decreases linearly with frequency for  $f_{\text{con}} < f_c$ . But for  $f_{\text{con}} \geq f_c$ , a constant plateau in  $Z'$  versus frequency is observed up to a certain frequency due to the appearance of long-range dc conduction, and then  $Z'$  decreases with frequency. Similarly in observation with the variation of  $Z'' \sim$  frequency (Fig. 7.3), clearly indicates that  $Z''$  decreases linearly with frequency for  $f_{\text{con}} < f_c$  for all PCC. For  $f_{\text{con}} \geq f_c$ , it can be seen that  $Z'' \sim$  frequency pattern display broad and low-intensity peaks with additional features, such as (i) appearance of a peak at a particular frequency (known as relaxation frequency,  $f_{\text{max}}$ ) (ii) decrease in the magnitude of  $Z''$  with a clear shift in the peak frequency toward higher frequency as a function of  $f_{\text{con}}$  (iii) peak broadening with a rise in  $f_{\text{con}}$  and (iv) relaxation over several decades of frequency. The peak location gives the maximum relaxation frequency ( $f_{\text{max}}$ ) which has been calculated in accordance with Eq. (2.20), i.e.,  $f_{\text{max}} = \frac{1}{2\pi RC}$  and  $\tau_0 = \frac{1}{2\pi f_{\text{max}}}$  for all the PCC in the region of  $f_{\text{con}} \geq f_c$ . It is given in Table 7.2. The  $f_{\text{max}}$  shifts to its higher value on increasing  $f_{\text{con}}$  in good analogy with an increase in  $f_{\text{max}}$  as a function of temperature. This behavior has been reported for several materials with evidence of assisted by a hopping type mechanism as electrons start to hop between two filler clusters due to the gradual decrease in distance between the filler clusters/particles due to an increase of  $f_{\text{con}}$ . These behaviors may be related to the  $f_{\text{con}}$  dependence of electrical relaxation phenomena in the PCC. The observed relaxation peak for the PCC for  $f_{\text{con}} \geq f_c$  in the lower frequency region is due to the development of long-range dc conductivity. So, the relaxation is attributed to the conductivity relaxation/MWS relaxation arising due to interfacial polarization. It occurs in the low-frequency regions as compared to the dipolar relaxation of the virgin polymer matrix occurring in the high-frequency region. After the relaxation,  $Z''$  decreases with frequency in the higher frequency region. To investigate and analyze the dynamics of the MWS relaxation mechanism, the impedance master curves are plotted in Fig. 7.4. The normalized impedance versus frequency shows that a peak in the  $Z''$  is observed for all the PCC for  $f_{\text{con}} \geq f_c$ . The peak frequency shifts toward higher frequency with an increase of  $f_{\text{con}}$  due to the appearance of enhanced long-range dc conductivity in the PCC. All the relaxations are endowed with a distribution of relaxation times, and the extent of distribution of relaxation times (i.e., the broadening) is different for different  $f_{\text{con}}$ . This causes a significant effect on the dynamics of charge carriers. This is reflected in the normalized impedance master curve shown in the inset of the corresponding PCC series of the sample of Fig. 7.4. It is observed that the curves don't coincide with each other and the dynamics of charge carriers are merely a function of  $f_{\text{con}}$ .

**Table 7.2** Estimated values of the electrical parameters corresponding to  $f_{con} < f_c$  and  $f_{con} \geq f_c$  for all the series of PCC

Series	$f_{con}$	$R_s$ (k $\Omega$ )	$Q$ (pF)	$R$ (M $\Omega$ )	$u$	$\alpha$	$f_{max}$ (Hz)	$\omega_H$ (Hz)	Series	$f_{con}$	$R_s$ (k $\Omega$ )	$Q$ (pF)	$R$ (M $\Omega$ )	$u$	$\alpha$	$f_{max}$ (Hz)	$\omega_H$ (Hz)
A	0.0	26	1.64		0.98				D	0.0	27	1.6		0.99			
	0.16	17	2.44		0.98					0.10	15	1.8		0.99			
	0.28	12	3.5		0.97					0.16	8.2	3.11		0.98			
	0.35	6.4	7.5		0.96					0.20	5.6	5.9		0.97			
	0.45	3.3	15.4		0.95					0.23	2.4	15.7		0.95			
	0.50	2.9	15.5		0.96					0.25	0.6	27.3		0.93			
	0.55	2.7	18.4		0.95												
	0.56	2.4	25.8		0.95												
	0.57	0.77	193	2.46	0.89	0.11	894	2621									
	0.58	1.3	93	36	0.87	0.13	108	1033	E								
B	0.0	26	1.64							0.03	1	1.7		0.98			
	0.05	29	2.5							0.05	5	5.5		0.95			
	0.16	13	2.95							0.06	6.5	6.22		0.96			
										0.065	5.5	9.5		0.96			
	0.20	13	9.4							0.07	0.5	493	0.002	0.89	0.11	73759	166401
	0.25	4.5	14.6														
	0.27	1.5	98														
	0.28	0.0	1420	0.8	0.73	0.27	1665	5096	F								
	0.30	0.0	440	0.62	0.78	0.22	5770	19425		0.0	27	1.6		0.98			
	0.315	0.0	640	0.066	0.80	0.20	47740	132123		0.10	18	2.32		0.96			
C	0.0	26	1.64		0.98					0.20	11	12.56		0.9			

(continued)



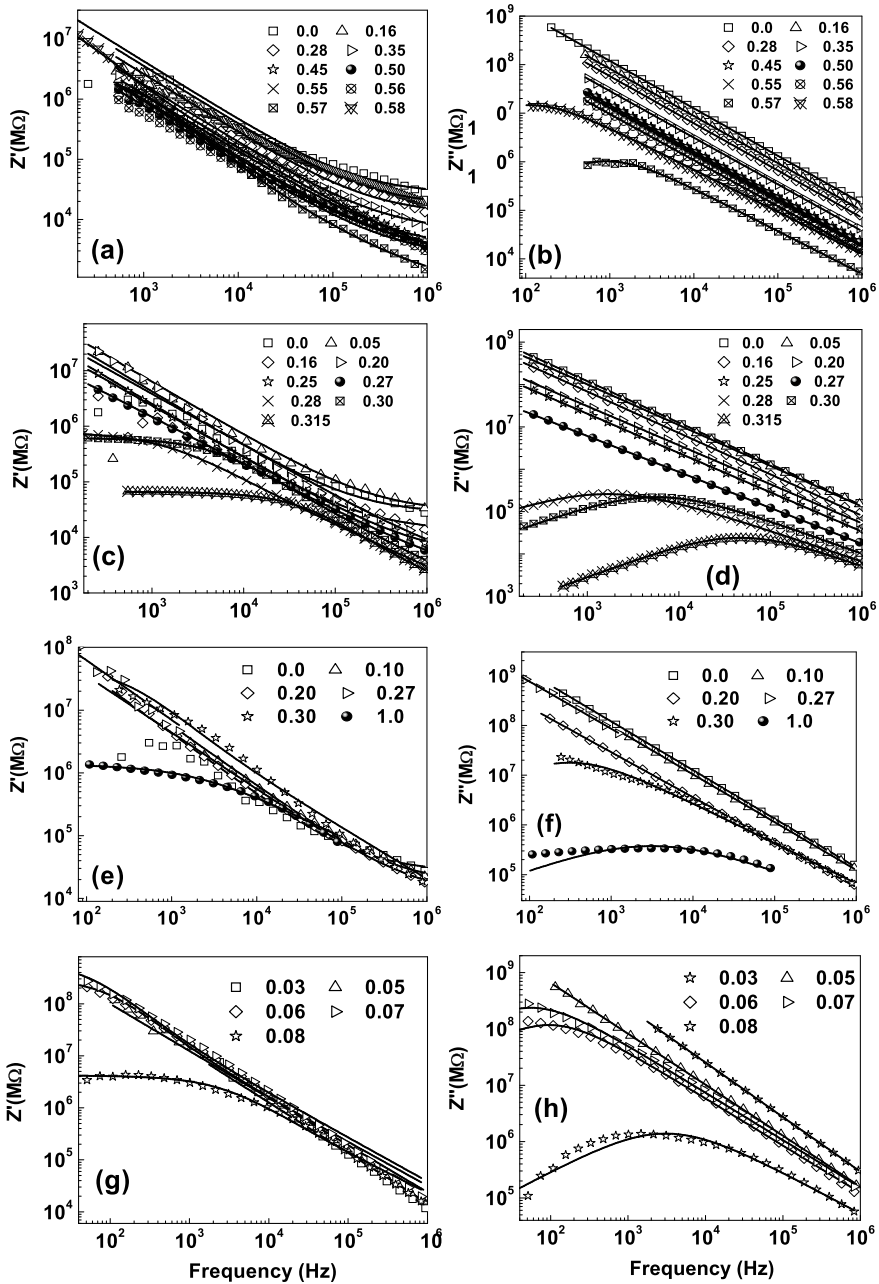


**Fig. 7.3** Typical variation of the real and imaginary part of impedance as a function of frequency for various series of PCC, respectively, **a** series A, **b** series A, **c** series B, **d** series B, **e** series F, **f** series F, **g** series G, **h** series G. The solid lines are the fits to the experimental data

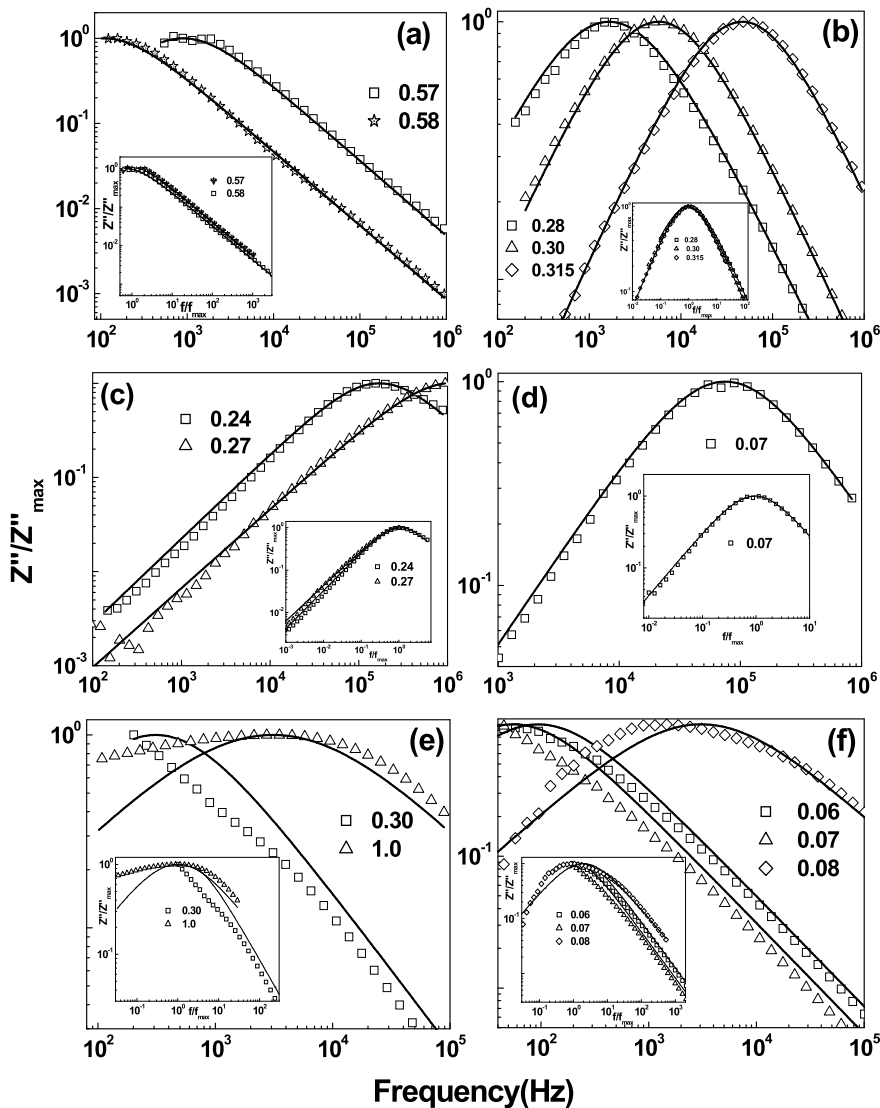


**Fig. 7.4** Normalized imaginary parts of the impedance  $Z''/Z''_{\max}$  as a function of frequency for  $f_{\text{con}} \geq f_c$  for various series of PCC and the corresponding insets represent the normalized impedance master curves of the corresponding PCC for  $f_{\text{con}} \geq f_c$ , **a** series A, **b** series B, **c** series C, **d** series E, **e** series F, **f** series G, respectively

### 7.3.3 Modulus Spectroscopy

In the foregoing sections, it is discussed that the interfacial relaxation occurs for the composites with  $f_{\text{con}} \geq f_c$ . But from earlier Chap. 6, we have found that dipolar relaxation for polar PCC is the universal mechanism for all the composites with  $f_{\text{con}} < f_c$ . Hence, the evidence of both conductivity and dipolar relaxation from modulus spectroscopy analysis is also expected. The real and imaginary part of modulus has been calculated based on Eq. (2.22) for all the PCC. It is shown systematically in Fig. 7.5. This shows the variation of real and imaginary parts of electric modulus as a function of frequency over a range of  $f_{\text{con}}$  for all the PCC. The advantage of representing electrical relaxation in modulus formalism is that the electrode polarization effects are suppressed in this representation [10, 11]. The variation  $M''$  as a function of frequency over a range of  $f_{\text{con}}$  (Fig. 7.5) is characterized by (i) two resolved peaks in the pattern appearing at a different frequency for different  $f_{\text{con}}$  (ii) significant asymmetry in the peak with their positions lying in the dispersion region of  $M'(\omega)$  versus frequency pattern and (iii) the tendency of the peak positions to shift toward the higher frequency side with the rise in  $f_{\text{con}}$ . The low-frequency side of the  $M''$  peak represents the range of frequencies in which charge carriers can move over a long distance; i.e., charge carriers can perform successful hopping from one site to a neighboring site for  $f_{\text{con}} \geq f_c$ . The high-frequency side of the  $M''$  peak represents the range of frequencies in which the dipoles of the polymer flip and give rise to finite charge displacement and thus could make a localized motion for  $f_{\text{con}} < f_c$ . The higher peak frequency ( $f_{\text{max}}$ ) corresponding to the maximum value of  $M''$  is called the dipolar relaxation frequency which shows a higher value as compared to the dielectric relaxation data shown in Chap. 6 for PCC based on PVDF in the region of  $f_{\text{con}} < f_c$ , as it is well known that for the same physical process the time constants are related as  $\tau_e > \tau_M$  [13]. Similarly, the peak frequency in the low-frequency region is called the MWS relaxation frequency. We observe from Fig. 7.5(f) that no signature of dipolar relaxation for  $f_{\text{con}} < f_c$  as the PCC is based on polymer LDPE that does not contain any dipoles in it.

To see if the dynamics of dipolar relaxation behavior are dependent on  $f_{\text{con}}$  or not for  $f_{\text{con}} < f_c$ , the modulus master curve corresponding to all the samples is shown in Fig. 7.6. All the curves merge during the dipolar relaxation frequency and the slight deviation from the coincidence in the low-frequency region is attributed to the formation of MWS dipoles giving rise to interfacial polarization. Similarly, to see the dynamics of MWS dipoles in the region of  $f_{\text{con}} \geq f_c$ , the variation of normalized complex electric modulus with normalized frequency is shown in Fig. 7.7. This is known as the modulus master curve, which enables us to have an insight into the dielectric process occurring in the material as a function of  $f_{\text{con}}$ . A non-exponential or non-symmetrical conductivity relaxation behavior will be governed by Eq. (2.24)

$$\phi(t) = \exp\left(-\left(\frac{t}{\tau}\right)^\beta\right) \text{ with } 0 \leq \beta \leq 1$$

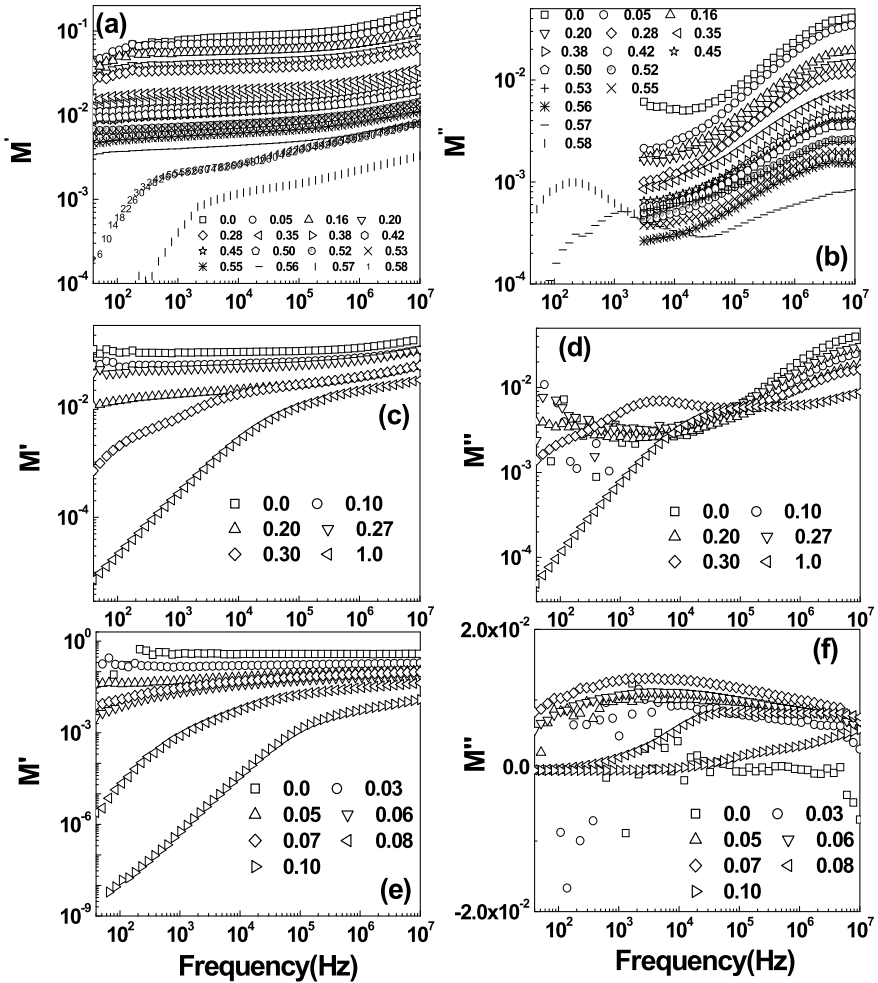


**Fig. 7.5** Typical representative plots of variation of real and imaginary parts of modulus with frequency for all PCC corresponding to  $f_{con} < f_c$  and  $f_{con} \geq f_c$ . **a** series A, **b** series A, **c** series F, **d** series F, **e** series G, **f** series G, respectively

suggests the possibility of electron migration that takes place via hopping. The modulus master curve (Fig. 7.7) shows (a) a small shift in the modulus peak pattern, (b) identical shape and pattern with slight variation in full width at half maximum (FWHM) with a rise in  $f_{con}$  and (c) the asymmetric nature of the curves which indicates the non-exponential behavior of conductivity that can be described by Kohlrausch-Williams-Watts (KWW) [13] function. The FWHM of the peaks is wider than that of the Debye peak (1.14 decades) [14], even reaches 2 decades (Fig. 7.7) which also suggests the presence of non-Debye-type relaxation phenomena.

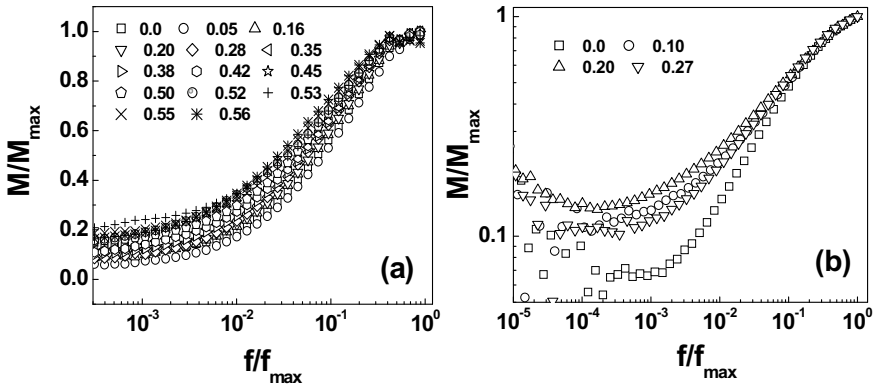


Fig. 7.6 Typical representative pattern of modulus master curve for  $f_{con} < f_c$  for two series of PCC, a series A, b series F, respectively

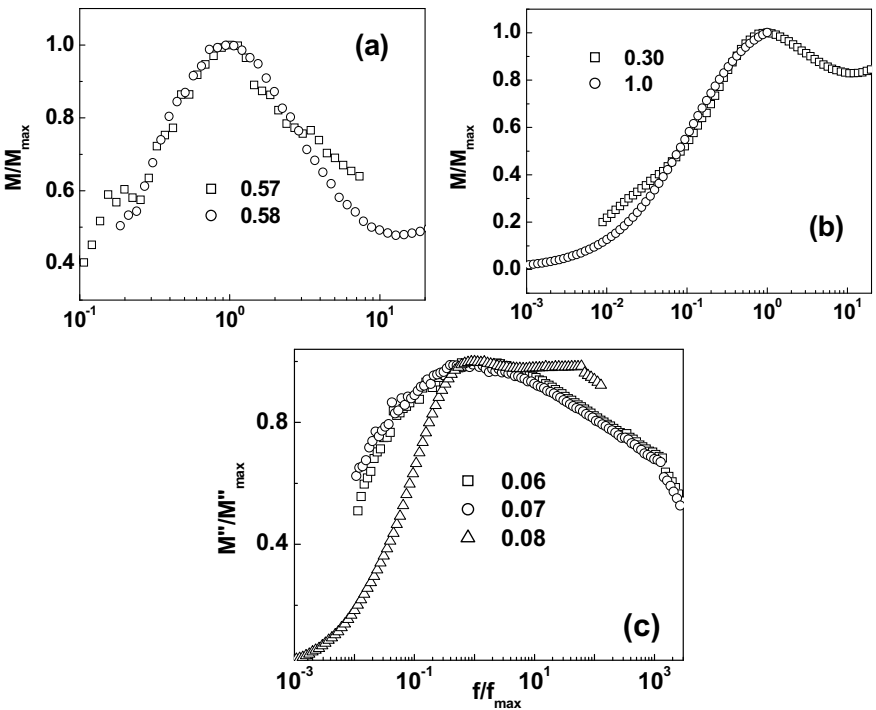
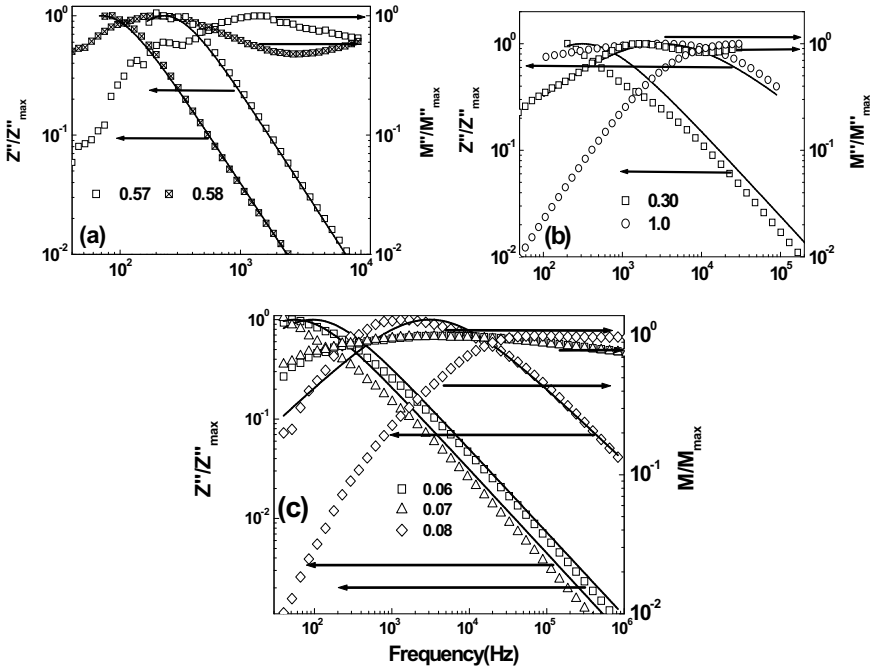


Fig. 7.7 Typical variation of normalized modulus with normalized frequency, i.e., the modulus master curve for  $f_{con} \geq f_c$  for various PCC, a series A, b series F and c series G

The impedance and modulus spectroscopy plots ( $Z''$  and  $M''$  vs. frequency) are complementary to each other. As suggested by Sinclair et al. [15, 16], a combined plot of imaginary modulus ( $M''$ ) and impedance ( $Z''$ ) as a function of frequency is useful to detect the effect of the smallest capacitance and the largest resistance as the peak heights are proportional to  $R$  for the  $Z''$  versus frequency plot and to  $C^{-1}$  for the  $M''$  peak. It is advantageous to plot  $Z''$  and  $M''$  versus frequency simultaneously which helps in distinguishing whether a relaxation process is due to short-range or long-range movement of charge carriers. If the process is long-range, then the peak in  $M''$  versus frequency and  $Z''$  versus frequency will occur at the same frequency. On the other hand, if the process is localized with charge migration occurring via hopping, these peaks will occur at different frequencies. Figure 7.8 shows the representative plots of  $Z''$  and  $M''$  versus frequency of some of the samples corresponding to  $f_{\text{con}} \geq f_c$  for various PCC. This figure exhibits an appreciable mismatch between the  $Z''$  and  $M''$  peaks for different  $f_{\text{con}}$  concentrations of the various PCC. It is observed that the peaks in  $Z''$  and  $M''$  versus frequency spectra occur at different frequencies and the peak frequency of  $M''$  is greater than the peak frequency of  $Z''$ . It is well known that for the same physical processes the different physical quantities will have different relaxation times (i.e., the time constants) and they are related as  $\tau_Z \geq \tau_M$ . Again on increasing  $f_{\text{con}}$  peaks in  $Z''$  and  $M''$  versus frequency spectra shifts toward higher frequency region (with the exception in case of Fig. 7.8a that may be attributed to the experimental error) which is due to the development of long-range dc conductivity in the samples and is in accordance with the same variation with the increase of temperature in the earlier kinds of literature [12]. The appreciable separation between these peaks suggests the presence of localized movement of charge carriers and a clear departure from ideal Debye-like behavior for all samples with  $f_{\text{con}} \geq f_c$  for various PCC. The broad and asymmetric peaks of the samples irrespective of  $f_{\text{con}}$  suggest the existence of a distribution of relaxation times. In addition to the above, it has been found that the  $Z''$  peaks are broadened in the low-frequency region of the peak (maxima), whereas the  $M''$  peaks are broadened in the high-frequency regions. Hence, the two peak maxima in  $Z'' \sim$  frequency and  $M'' \sim$  frequency plots (which are not frequency coincident) suggest a departure from ideal Debye behavior. It seems logical and justified due to the presence of a CPE and agreement with Jonscher's power-law of Eq. (2.25); given by  $\sigma_{\text{ac}}(\omega) = \sigma_{\text{dc}} + A\omega^k$  where  $\sigma_1(\omega) = A\omega^k$ , which plays an important role in the interpretation of electrical behavior of the PCC. We also observe from Fig. 7.8 that the relaxation time decreases with an increase of  $f_{\text{con}}$  in the composites systematically which is attributed to the decrease in the thickness of the polymer layer. It plays the same role as if the height of the potential barrier gradually decreases with an increase in  $f_{\text{con}}$ .

### 7.3.4 Conductivity Spectroscopy

The variation of ac conductivity (which has been calculated as  $\sigma_{\text{ac}} = \omega \epsilon_0 \epsilon \text{Tan} \delta$ ) as a function of frequency (conductivity spectrum) at different  $f_{\text{con}}$  is shown in Fig. 7.9. It



**Fig. 7.8** Typical variation of normalized impedance and modulus with frequency for  $f_{con} \geq f_c$  for various PCC, **a** series A, **b** series F, **c** series G

can be observed that the plot shows dispersion of ac conductivity with frequency for all the PCC series corresponding to  $f_{con} < f_c$  and that variation agree with Eq. (2.25), i.e.,  $\sigma_{ac}(\omega) = \sigma_{dc} + A\omega^k$  with the  $\sigma_{dc}$  part becoming zero. The experimental data for the samples with  $f_{con} < f_c$  well-satisfied Eq. (2.27) and the corresponding value of 'k' found from the fits are plotted against  $f_{con}$  in Fig. 7.10. But for the samples with  $f_{con} \geq f_c$ , a mixed conductivity is found, i.e., a dc plateau up to a certain frequency separated by ac conductivity beyond that frequency. The plateau in the conductivity spectrum occurs due to the appearance of long-range dc conductivity. The frequency at which dispersion in the ac conductivity starts shifts to the higher frequency side with a rise in  $f_{con}$ . At higher frequency, the conductivity becomes more or less  $f_{con}$  dependent. This frequency at which the change in slope takes place is known as the "hopping or critical frequency  $\omega_H$ " which obeys Eq. (2.26), is given by  $\sigma_{ac} = \sigma_{dc}[1 + (\frac{\omega}{\omega_H})^k]$  with the value of  $\omega_H = (\frac{\sigma_{dc}}{A})^{\frac{1}{k}}$  and the corresponding calculated value of ' $\omega_H$ ' for  $f_{con} \geq f_c$ , is given in Table 7.2. We observe that the magnitude of ' $\omega_H$ ' is always greater than  $f_{max}$ , and they are always different for all the samples in the region of  $f_{con} \geq f_c$ , as they have been extracted from the two different physical parameters corresponding to the same physical process which deals with the same type of charge carrier. This can be also well-understood as hopping and relaxation are different mechanisms that occur over different regions of frequencies

as they have different time constants. The value of ' $k$ ' found from the fit of Eq. (2.25) to the experimental data is shown in Fig. 7.10. We observe that the slope of the straight line of the log–log plot (Fig. 7.9) at the lower frequency side for  $f_{\text{con}} \geq f_c$ , approximately equals to 0 which is the natural result of the frequency-independent conduction while the value of the slope at higher frequencies lies in between 0 and 1. The curves tend to flatten with increasing  $f_{\text{con}}$ , especially in the low-frequency regions, suggesting dc conduction behavior. The frequency-independent plateau in the 10–100 kHz range indicates conductivity relaxation across the interface found from the above impedance spectroscopy analysis and thereby a corresponding  $f_{\text{max}}$  is given in Table 7.2. From Fig. 7.10, it is observed that the value of ' $k$ ' remains constant up to a certain  $f_{\text{con}}$  and it starts decreasing with an increase of  $f_{\text{con}}$  in the vicinity of  $f_{\text{con}} \geq f_c$ . This can be understood as due to the appearance of long-range dc conductivity the value of ' $k$ ' approaches 0. However, in all cases, the value of ' $k$ ' lies well within the universal regime [0, 1] suggesting the validity of Jonscher's power-law in all the PCC in the present studies.

## 7.4 Summary

Microstructural and ac electrical characterization of various insulating PCC as a function of frequency and  $f_{\text{con}}$  have been correlated. Correlation between the microstructural and electrical equivalent of the material is established through CIS across the  $f_c$  for all PCC. CIS analysis shows that PCC with  $f_{\text{con}} \geq f_c$  undergo a conductivity/interfacial relaxation due to the formation of MWS polarization at  $f_c$  and the relaxation frequency increases with the increase of  $f_{\text{con}}$ . The dielectric and modulus spectroscopy analysis show the presence of two types of relaxations in different frequency ranges for different samples, such as (i) dipolar relaxation associated with the flipping of dipoles present in the pure polymer for  $f_{\text{con}} < f_c$  and (ii) the conductivity/interfacial relaxation is due to the formation of artificial MWS dipoles at the interface of the two components and the appearance of long-range dc conductivity for  $f_{\text{con}} \geq f_c$ . The two respective relaxation mechanisms are discerned to occur (i) inside the grains of the polymer phase and (ii) the grain boundary/interface of the two-component phases, respectively. The value of relaxation frequency found from the modulus ( $M$ ) data is higher as compared to the impedance ( $Z$ ) data corresponding to the same physical process (electrical relaxation) which is in accordance with the literature; i.e., the relaxation times are related as  $\tau_Z \geq \tau_M$ . A long-range dc conductivity appears at  $f_{\text{con}} \geq f_c$  and Jonscher's universal fractional power-law is well-satisfied for both the regions of  $f_{\text{con}} < f_c$  and  $f_{\text{con}} \geq f_c$  in all PCC. The exponent of the power-law decreases as a function of  $f_{\text{con}}$  due to a decrease of the rate of dispersion arising due to the increase of dc conductivity. This study gives the idea that PCC shows a microstructure and electrical properties which are universal across  $f_c$  and the parameter  $f_c$  in PCC plays the analogous role as that played by temperature in the case of ionic conductors. In all the PCC, the value of the exponent corresponding to the CPE for  $f_{\text{con}} < f_c$  is always less than 0.85, while its value

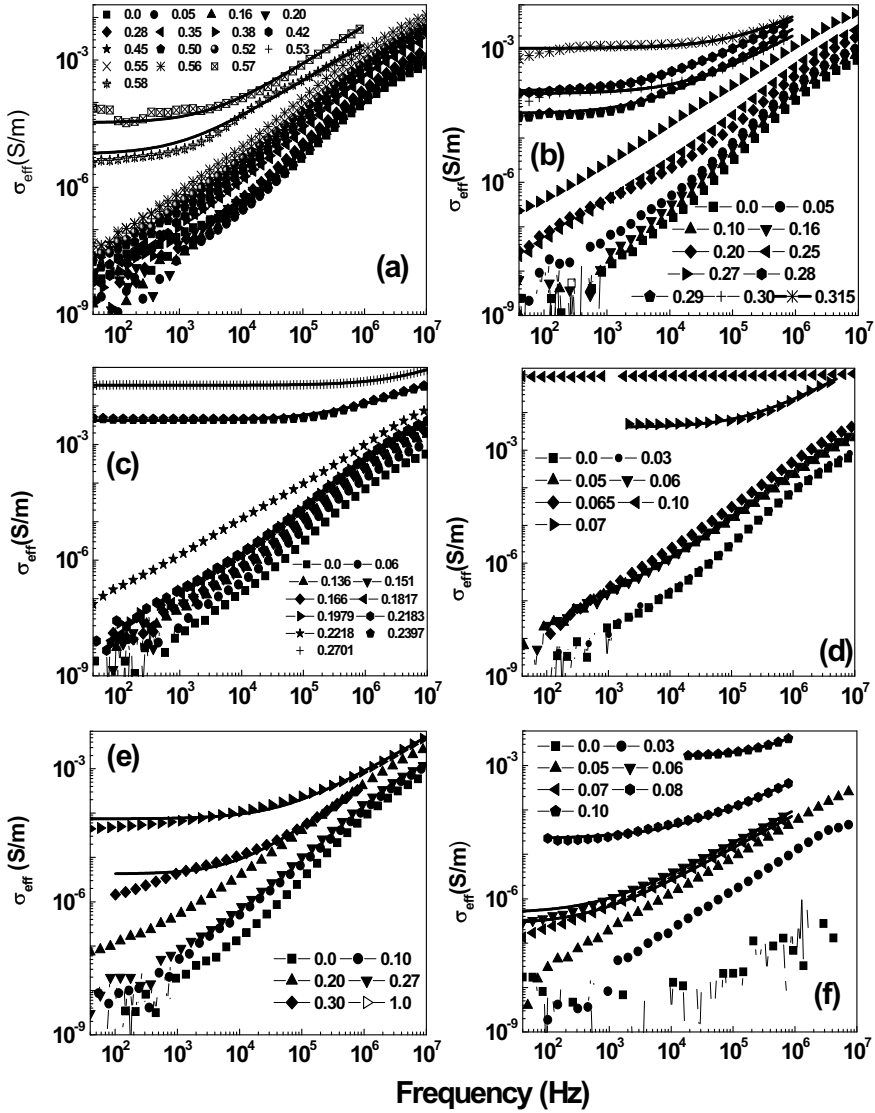
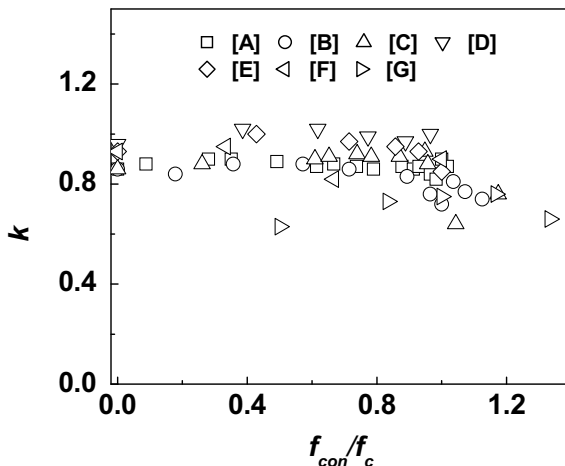


**Fig. 7.9** Variation of ac conductivity with frequency for the non-percolative as well as percolative composites for all the series of samples under study. The solid lines are the fit to Jonscher's universal fractional power-law for all the PCC with  $f_{\text{con}} \geq f_c$ , **a** series A, **b** series B, **c** series C, **d** series E, **e** series F, **f** series G

**Fig. 7.10** Variation of Jonscher's universal exponent ' $k$ ' with  $f_{\text{con}}/f_c$  for all the composites for a series of PCC



undergoes a sharp transition at  $f_c$  and lies in between 0.7 and 1, i.e., the dominant behavior of a capacitor. All the PCC undergo a percolation transition as a function of  $f_{\text{con}}$ , and for a particular  $f_{\text{con}}$ , in the PCC a long-range dc conductivity appears for the sample. Jonscher's universal fractional power-law holds good for all the samples with the exponent ' $k$ ' being found in the universal regime. In the region of  $f_{\text{con}} \geq f_c$ , it is found that the dynamics of charge carriers are  $f_{\text{con}}$  dependent.

## References

1. Almond DP, Vainas B (1999) The dielectric properties of random R-C networks as an explanation of the universal power-law dielectric response of solid. *J Phys: Cond Matt* 11:9081–9093
2. Bouamrane R, Almond DP (2003) The emergent scaling phenomenon and the dielectric properties of random resistor-capacitor networks. *J Phys: Cond Matt* 15:4089–4100
3. Almond DP, Bowen CR, Rees DAS (2006) Composite dielectrics and conductors: simulation, characterization and design. *J Phys D: Appl Phys* 39:1295
4. Almond DP, Bowen CR (2004) Anomalous power law dispersions in ac conductivity and permittivity shown to be characteristics of micro-structural electrical networks. *Phys Rev Lett* 92:157601
5. Calame JP (2003) Evolution of Davidson-Cole relaxation behavior in random conductor–insulator composites. *J Appl Phys* 94:5945
6. Macdonald JR (1987) *Impedance spectroscopy: emphasizing solid materials and systems*. Wiley, New York
7. Panda M, Srinivas V, Thakur AK (2014) Universal microstructure and conductivity relaxation of polymer-conductor composites across the percolation threshold. *Curr Appl Phys* 14:1596–1601
8. Panda M, Srinivas V, Thakur AK (2014) Dielectric spectroscopy of polymer-metal composites across the percolation threshold. *J Adv Dielectr* 04:14500271–14500276
9. Panda M, Srinivas V, Thakur AK (2014) Percolation behaviour of polymer-metal composites on modification of filler. *Modern Phys Lett B* 28(1–6):1450055

10. Nobre MAL, Lanfredi S (2003) Ferroelectric state analysis in grain boundary of  $\text{Na}_{0.85}\text{Li}_{0.15}\text{NbO}_3$  ceramic. *J Appl Phys* 93:5557
11. Nobre MAL, Lanfredi S (2003) Grain boundary electric characterization of  $\text{Zn}_7\text{Sb}_2\text{O}_{12}$  semiconducting ceramic: a negative temperature coefficient thermistor. *J Appl Phys* 93:5576
12. Gerhardt R (1994) Impedance and dielectric spectroscopy revisited: distinguishing localized relaxation from long-range conductivity. *J Phys Chem Solids* 55:1491–1506
13. Cao W, Gerhardt R (1990) Calculation of various relaxation times and conductivity for a single dielectric relaxation process. *Solid State Ion* 42:213
14. Nye JF (1990) *Physical properties of crystals*. Clarendon Press, Oxford
15. Sinclair DC, West AR (1989) Impedance and modulus spectroscopy of semiconducting  $\text{BaTiO}_3$  showing positive temperature coefficient of resistance. *J Appl Phys* 66:3850
16. Sinclair DC, West AR (1994) Effect of atmosphere on the PTCR properties of  $\text{BaTiO}_3$  ceramics. *J Mater Sci* 29:6061–6068

# Chapter 8

## Magnetic and Rheological Behavior of Polymer Composites



In this chapter, among all the polymer/conductor composites (PCC), only the composites of ferroelectric polymer (PVDF) and ferromagnetic metal, nanocrystalline Ni ( $n$ -Ni) composites are studied for their dielectric, ferroelectric and ferromagnetic properties. For the rheological study, the samples of the polymers PVA, PEG, PVDF, and PVDF/NiO composites are studied. Electrical and magnetic properties of PVDF/ $n$ -Ni composites have been investigated as a function of volume fractions of  $n$ -Ni ( $f_{\text{con}}$ ) and frequency of the applied electric signal for investigating the concept of magnetic percolation. Rheological investigations showed that PVDF (polar dielectric) shows comparatively better viscoelastic properties as compared to the non-polar dielectrics (PVA/PEG) due to the existence of permanent dipole moment in its polymer chain structure and its higher crystalline (50–60%) nature. The viscoelastic properties, the mechanical stability, and the nonlinear elastic behavior of the PVDF/NiO composite samples were analyzed using rheological measurements. All the polymers and the composites of PVDF/NiO show non-Newtonian-like fluid behavior. The effect of NiO in these composites was investigated and was found that the mechanical properties are enhanced, being supporting pieces of evidence for their suitability as flexible dielectrics.

### 8.1 Introduction

The synthesis of materials that exhibit simultaneous ferromagnetic (FM) and ferroelectric (FE) characteristics has recently attracted a great deal of attention not only from the fundamental physics point of view but also because of their potential applications in practical electronic devices [1–3]. However, there are only a few single-phase materials that can exhibit both ferromagnetic and ferroelectric properties for multifunctional applications. The study of composite materials has been the subject of considerable interest in recent years because of their possible technological applications. Among the various polymer composites magnetic polymer

composites have received recent attention due to their magneto-electric effects, a coupled magnetic and dielectric/ferroelectric effect by the appearance of electric and magnetic polarizations on applications of an electric or magnetic field. For technological applications, magneto-electric materials must exhibit high magneto-electric coefficients. The soft magnetic nanocomposites (SMC)/insulating polymer magnetic nanocomposites (PMC) with nanosized metallic inclusions are common in established industrial applications because of the following properties/reasons. The SMC also shows a drastic change in their magnetic properties at a critical concentration of the magnetic component called magnetic percolation threshold [4–6]. The composite of magnetic metal and insulator shows a divergence in the variation of inductance and imaginary part of permeability like that of ICC at  $f_c$  [7–11]. In discussion with a ferromagnetic metal nanoparticle, the nanodimensional metal granule is considered as a ferromagnetic particle possessing an intrinsic magnetic moment equal to the sum of magnetic moments of the atoms contained in this granule. If the energy of the magnetostatic interaction between granules is below  $kT$  ( $k$  being Boltzmann constant and  $T$  is absolute temperature), no correlation between the magnetization vectors of such particles takes place, and the composite is expected to show its paramagnetic/superparamagnetic properties. When an infinite network of contacting granules is formed, at a critical concentration of the magnetic filler particle called magnetic percolation threshold ( $m_c$ ) [4], conditions favoring exchange interaction between the atoms of the neighboring granules in the matrix are expected and the material should acquire a drastic change in its magnetic properties (such as dc magnetic susceptibility, coercivity, and dc magnetization). The observation of both ferroelectricity and ferromagnetism individually in PVDF/ $n$ -Ni composites is reported [12]. The magneto-electric effect also could be expected in such a system of PVDF/ $n$ -Ni composites. To achieve multifunctional properties for a particular composite of SMC/PMC, along with the study of  $m_c$ ,  $f_c$ , divergence/anomaly in inductance and magnetic permeability in these composites, a composite composed of an insulating polar polymer PVDF and a magnetostrictive metallic filler in its nanocrystalline form, such as  $n$ -Ni is investigated in its two different forms of the samples, such as thick films and bulk composites of PVDF/ $n$ -Ni.

As polymer dielectrics have considerable potential interest in energy storage and dielectric applications because of their easy processing, flexibility, easily designing, nontoxic, biocompatible, and low cost. The insulating polymer–conductor composites (PCC) are finding a lot of recent interest from the point of energy storage materials, electromagnetic interference applications, transistors, photovoltaic devices, electrical insulations, etc. This PCC undergoes an insulator-to-metal transition (IMT) at a critical concentration of conductor/metal in an insulating matrix, which is called as percolation threshold ( $f_c$ ) [13–15]. In particular, as the filler concentration approaches  $f_c$  from below, the effective ac electrical conductivity ( $\sigma_{\text{eff}}$ ) and the dielectric constant ( $\epsilon_{\text{eff}}$ ) of the composites increase dramatically. It is observed that the enhancement in  $\epsilon_{\text{eff}}$  values with low dielectric loss ( $\text{Tan } \delta$ ) at  $f_c$  is attained at lower filler concentrations for PCC as compared to polymer-ceramic composites. On the other hand, polymer-metal composites (PMC) show relatively new electrical characteristics close to those of metals, whereas the mechanical properties and processing

methods are typical of plastics. The electrical properties of PMC depend on several factors, including the kind of conducting filler, their spatial distribution, the interaction between polymer and filler, and the contact interaction between the particles. In the development of these PMC materials for energy storage applications, specifically, the electrostrictive polymers such as PVDF and PVDF (TrFE) have been highly beneficial and give a very high value of dielectric constant with low loss tangent. The composites of electrostrictive polymer and ferromagnetically magnetostrictive components in their reduced form have gained recent interest because of their room-temperature magnetism, multiferroic, and high magneto-electric coupling coefficients and they are finding a large number of applications such as multi-state memory elements. PVDF is a semicrystalline thermoplastic having a remarkable high piezoelectric coefficient, excellent thermal stability, and chemical resistance compared with other polymers. It has been found that PVDF/Ni and PVDF/NiO composites have proven themselves as very good materials from the point of energy storage, EMI shielding, Photovoltaic, multiferroic, magneto-electric, and various other applications. Although flexibility in the polymer-based composites is required from the solving the designing problem, however the mechanical and the viscoelastic properties are also required at a particular level and range. Although a lot of studies have dealt with the electrical, thermal, magnetic, mechanical, etc., however a systematic study of the viscoelastic properties of these PMC is required and will be interesting in finding their suitability from the application point of view [16–18]. Many rheological and mechanical properties of these polymer dielectrics play an important role in determining their suitability for high K applications. From this point of view, detailed information and investigation about mechanical stability, thermal stability, as well as viscoelastic properties of these polymer dielectric materials, are required. Hence, a comparative study of viscoelastic properties of two non-polar dielectrics (PVA and PEG) versus the polar polymer (PVDF) has also been compared and later on the study was focused on the PVDF/NiO composite dielectrics for finding their suitability as high K dielectric materials.

## 8.2 Samples Reported

The polymer PVDF was purchased from the Alfa Aesar and (PVA, PEG, and NiO) was purchased from Loba Chemie in solid powder form. The size of NiO has been reduced by the ball-milling of NiO by taking 10:1 as the ball-to-powder ratio in a toluene environment. The samples studied in this chapter are in two forms, such as thick films of the composites for their ferroelectric characterization and bulk powder/pellet for the magnetic characterization. The thick films of ferroelectric polymer PVDF and *n*-Ni composites were prepared through a simple tape casting technique in the form of thick films with Ni concentrations varying from 0 to 5 wt% [12]. Appropriate amounts of PVDF powder were dissolved in an organic solvent, such as acetone. Continuous magnetic stirring was done to homogenize the material for 10 h. Subsequently, varying weight percentage (1–5 wt% of PVDF) of *n*-Ni

powder ( $\sim 20$  nm) was added to the solution. With the help of a Sonicator, a homogeneous composition of  $n$ -Ni, PVDF, and acetone was obtained. Thick films ( $\sim 50$   $\mu\text{m}$ ) of the composite (PVDF and  $n$ -Ni) were obtained with the help of a glass tape caster. Similarly, the synthesis of bulk PVDF/ $n$ -Ni composites is reported in Chap. 3 [14]. The structural, electrical, and magnetic properties of the as-prepared samples were carried out at room temperature. The viscous fluid form of all the polymers has been prepared by swelling the polymers in an acetone environment with the help of a magnetic stirrer [16]. The composite samples of PVDF/NiO in viscous form have been prepared by magnetic stirring and ultrasonication for 45 min to prepare the composite fluid. The samples prepared were in the ratio of weight percentage of NiO in the composite, and they were of weight fraction of NiO as 0, 5, 10, and 15%. The rheological data on these composite fluids were taken with the help of the rotational Rheometer given in Chap. 3.

## 8.3 Results and Discussion

### 8.3.1 Magnetic Properties

#### (i) Thick Films

From the XRD Pattern (Fig. 8.1a), it is observed that with the increase of weight fraction of  $n$ -Ni ( $W_{\text{con}}$ ) concentration in the composites, the intensity of Ni peaks is increasing and the result is consistent with the data reported in the literature. It is confirmed that there is no molecular-level interaction between the  $n$ -Ni clusters and PVDF matrix (Fig. 8.1b). From the optical micrographs (Fig. 8.2a), it can be observed that with the increase of  $n$ -Ni concentration in the polymer matrix the bright portions are increasing and are getting distributed homogeneously indicating those portions as  $n$ -Ni. It is also observed the density of distribution of  $n$ -Ni clusters increases with the increase of  $W_{\text{con}}$  from Fig. 8.2b.

The effective dielectric constant ( $\epsilon_{\text{eff}}$ ) of the thick film PMC increases with the increase of  $W_{\text{con}}$  and  $\epsilon_{\text{eff}}$  decreases as a function of frequency (Fig. 8.3a). The loss tangent ( $\tan \delta$ ) shows the presence of dipolar relaxation in the matrix PVDF (Inset: Fig. 8.3a). It is observed that there is no significant change in the FE hysteresis loop area (Fig. 8.3b) and the shape of the hysteresis loops isn't undergoing any change even with the addition of a conducting component, i.e.,  $n$ -Ni.

This is due to the high resistivity ( $\sim 10^{12}$   $\Omega$  cm) of the polymer matrix. The marked feature is that  $P_r$  and  $P_{\text{max}}$  for all composites are in the neighborhood of  $0.1$   $\mu\text{C}/\text{cm}^2$  and  $0.2$ – $0.3$   $\mu\text{C}/\text{cm}^2$ , respectively. However, the coercivity ( $E_c$ ) of all composites almost remains constant while retentivity ( $P_r$ ) of the composites shows a trend in small decrement with concentration up to 5% (Inset, Fig. 8.3b). It can be seen from Fig. 8.3c that the composite materials exhibit typical magnetic hysteresis loops as well as remnant magnetization which indicates the magnetic phase is ordered. The saturation magnetizations ( $M_s$ ) of 1 and 5% PMC composites are given by 0.46 and

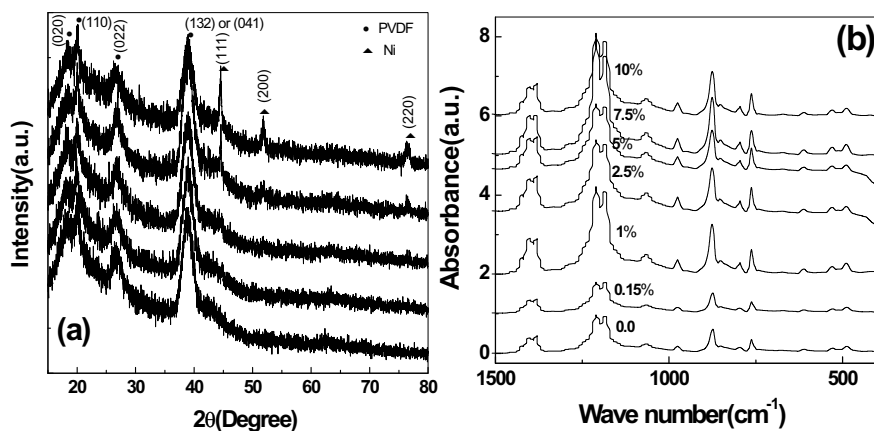


**Fig. 8.1** **a** X-ray diffractometry data of the samples 0–5% from bottom to top. **b** FTIR spectrum of the samples from 0 to 10%

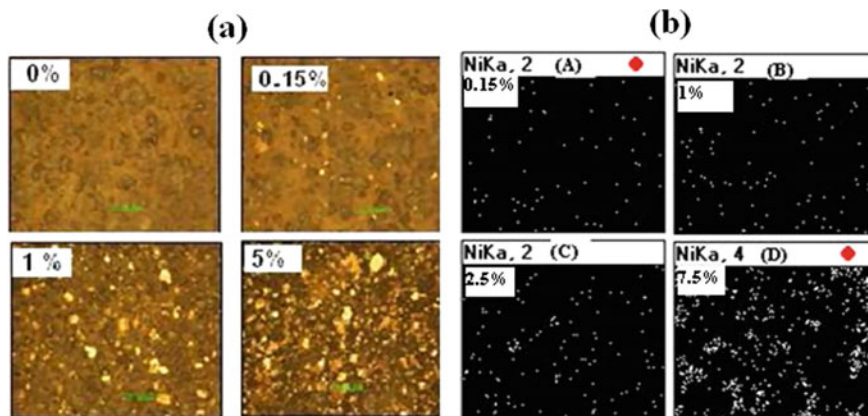


**Fig. 8.2** **a** Optical micrographs of the samples from 0 to 5%. **b** X-ray dot mapping micrographs of the samples from 0.15 to 7.5%

2.56  $\mu\text{g/g}$ , whereas pure *n*-Ni is having  $M_s$  of 30  $\mu\text{g/g}$  as shown in Fig. 8.4a, b. The retentivity ( $M_r$ ) of 1% and 5% PMC is about 0.035  $\mu\text{g/g}$  & 0.4  $\mu\text{g/g}$ , respectively. The coercivity ( $H_c$ ) of 1 and 5% PMC is given by 100 Gauss and 110 Gauss which show no change in coercivity with the increase of concentration of *n*-Ni. At lower concentrations, the interaction between magnetic particles is minimized because of the diamagnetic polymer (PVDF) matrix [12]. Thus, the addition of *n*-Ni in the composites increases the FM behavior while at the same time, retaining the ferroelectric behavior of the PVDF matrix.

### (ii) Bulk Composites

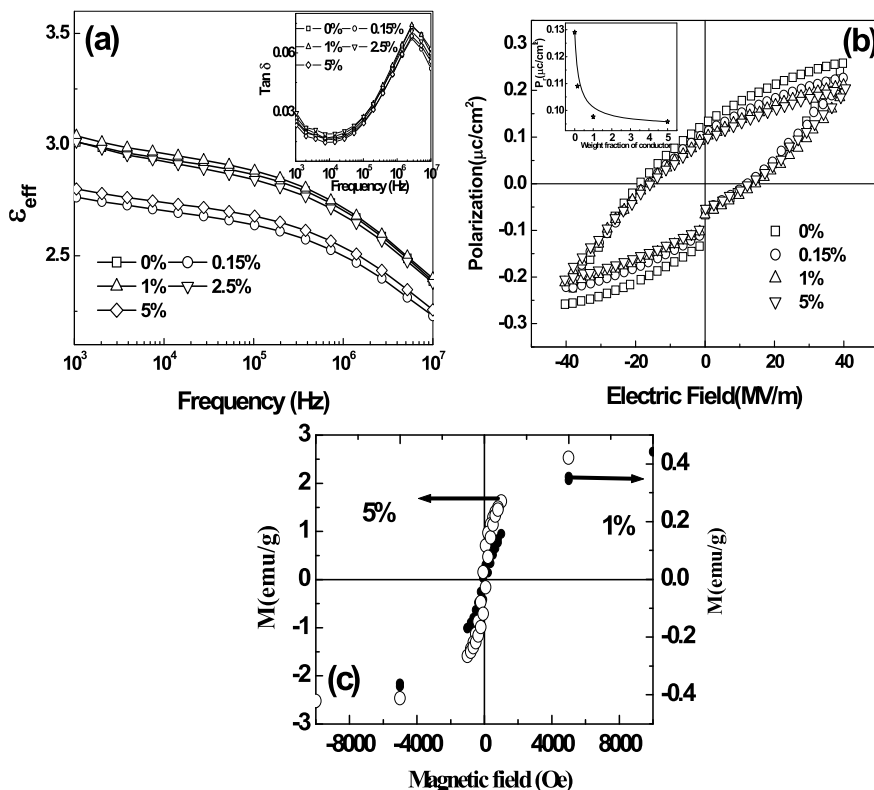


**Fig. 8.3** **a** Dielectric constant  $\sim$  frequency for the samples 0–5%. **b** Ferroelectric hysteresis of the unpoled samples from 0 to 5% (Inset:  $P_r \sim W_{con}$ ). **c** Ferromagnetic hysteresis of 1 and 5% composite samples

The structure and morphological details of the bulk composites already have been discussed in Chap. 4. Hence, here will only concentrate on their simultaneous dielectric and magnetic properties. The  $\epsilon_{eff}$  and the saturation magnetization ( $M_s$ ) of the composites as a function of  $f_{con}$  are shown in Fig. 8.4a.

All the composites show typical ferromagnetic hysteresis (Fig. 8.4b and its Inset) along with their magnetic saturation (Inset, Fig. 8.4a). The value of  $M_s$  increases from  $7 \text{ e}\mu/\text{g}$  for  $f_{con} = 0.05$ – $24 \text{ e}\mu/\text{g}$  for  $f_{con} = 0.28$  with increase of  $f_{con}$  (Fig. 8.4a). To extract the magnetic parameters, the room temperature  $M$ – $H$  curves of all the composite samples are fitted to the usual function [14, 19] customarily used to fit ferromagnetic hysteresis which is given by

$$M(H) = \frac{2M_s}{\pi} \tan^{-1} \left[ \frac{H \pm H_C}{H_C} \tan \left( \frac{\pi S}{2} \right) \right] \quad (8.1)$$

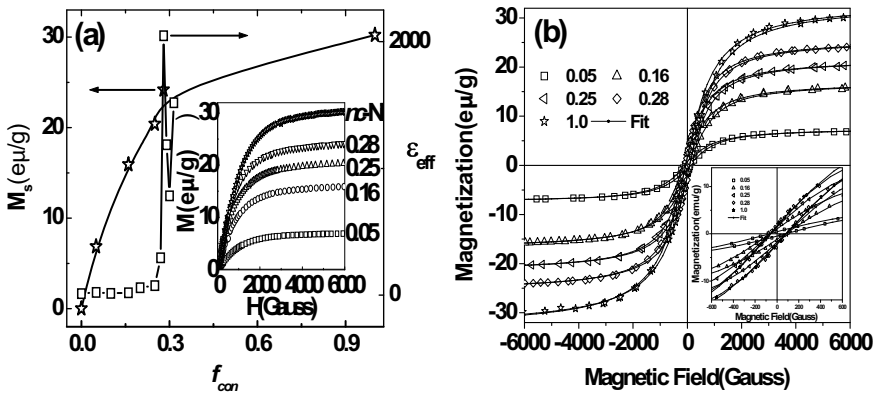


**Fig. 8.4** **a**  $M_s \sim f_{con}$  and  $\epsilon_{eff} \sim f_{con}$  for the composite samples with different  $f_{con}$  at 300 K. Inset: Initial Magnetization ~ Magnetic field plot for the composite samples ( $f_{con} = 0.05-0.28$ ) and  $n$ -Ni at 300 K. **b**  $M \sim H$  plots at 300 K for all the composite samples ( $f_{con} = 0.05$  to  $0.28$ ) and for pure  $n$ Ni ( $f_{con} = 1.0$ ). Inset: Expanded view of the plots showing hysteresis

The quantities  $M_s$  and  $H_c$  give, respectively, the saturation magnetization and coercivity of the samples where ‘S’ is known as “squareness” of the ferromagnetic loop and is defined by the ratio of remnant magnetization to saturation magnetization of the ferromagnetic loop, i.e.,  $S = M_r/M_s$ . Reasonably good fits of Eq. (8.1), to the magnetization curves, have been obtained for all the composite samples (Fig. 8.4b and its Inset). As expected we observe from Table 8.1 that the values of  $M_s$  and  $M_r$  increase with the increase of  $f_{con}$  while  $H_c$  remains constant for all the composites. For single-domain particles, the  $H_c$  value is expected to vary linearly with the packing fraction. However, the present discussion doesn’t show any change in  $H_c$  with packing fraction, suggesting the particles/clusters to be multi-domain. These results suggest that the non-interaction of nickel with the polymer may be due to the complete phase separation of nickel from the polymer. The rate of increment of  $M_s$  with  $f_{con}$  decreases with the increase of  $f_{con}$  as can be observed from Fig. 8.4a that the slope ( $dM_s/df_{con}$ ) of  $M_s \sim f_{con}$  curve decreases with the increase of  $f_{con}$ . This may be attributed to at lower  $f_{con}$  the particles/clusters are well-separated from one another and the magnetic dipolar interaction between them is weak, which is also minimized because of the insulating diamagnetic polymer matrix forbidding the interaction between the particles. So  $M_s$  decreases linearly with the decrease of  $f_{con}$  in the region of  $f_{con} \ll f_c$  that can be understood based on dilution effect. As  $f_{con} \rightarrow f_c$ , the particles are very close to each other and the coupling between the magnetic moments of two or more clusters becomes prominent because of the increased dipolar interaction and that leads to lowering of the rate of increment of  $M_s$  with  $f_{con}$  for  $f_{con} \geq f_c$ . The  $M_s$  for all the composites is achieved for the magnetic field, well above 3000 Oe (Inset, Fig. 8.4a).

Figure 8.5 shows the real part of permeability/initial zero fields effective permeability ( $\mu'$ ) as a function of  $f_{con}$  for various frequencies. The magnitude of  $\mu'$  remains

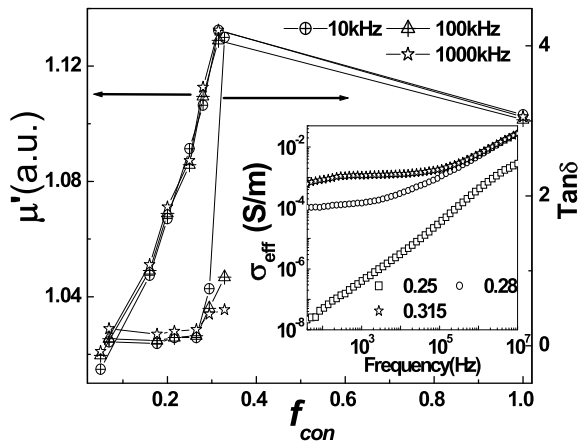
**Table 8.1** Magnitude of the fitting parameters  $M_s$ ,  $M_r$ ,  $H_c$ ,  $S$  for all the composite samples ( $f_{con} = 0.0$  to 1.0)

$f_{con}$	$M_s$ (e $\mu$ /g)	$M_r$ (e $\mu$ /g)	$H_c$ (Gauss)	Squareness ratio ( $S = M_r/M_s$ )
0.0	0	0	0	0
0.05	7.6	0.46	74	0.06
0.16	17.0	1.14	72	0.07
0.25	21.8	1.66	74	0.08
0.28	25.8	1.95	73	0.08
1.0	33.2	1.9	74	0.06

constant with the variation of frequency up to 10 MHz (shown up to 1 MHz in Fig. 8.5). The magnitude of permeability is considered due to both the ferromagnetic properties of  $n$ -Ni and the generation of eddy currents by an alternating magnetic field [7–11]. The  $\mu'$  of the composites for various  $f_{con}$  increases with the increase of Ni content linearly even beyond  $f_c$ , i.e., up to  $f_{con} = 0.315$  and falls for pure  $n$ -Ni. Although the observed  $f_c$  value, in this case, is for  $f_{con} = 0.28$ , the observation of magnetic anomaly beyond  $f_{con} = 0.315$  unlike that of earlier literature [7–11] may be attributed to the following reasons.

From earlier results, it is observed that the magnitude of  $\text{Tan } \delta$  increases with the increase of  $f_{con}$  (Fig. 8.5) and the conductivity for the composite ( $f_{con} = 0.25$ ) is of pure ac conduction while the conductivity for ( $f_{con} = 0.28$  and 0.315) are of mixed type, i.e., the dc conduction in the lower-frequency region followed by ac conduction in the higher-frequency region (Inset, Fig. 8.5). This type of mixed conductivity is the complete signature of a microstructure (Fig. 8.2a), in which the conducting particles are isolated from each other by a thin insulating polymer layer that prevents the generation of eddy current in the samples. Hence due to the non-setting of eddy current in the samples,  $\mu'$  increases linearly up to  $f_{con} = 0.315$  since the magnetic

**Fig. 8.5** Variation of Zero field initial effective permeability and dielectric loss tangent of the composites as a function of  $f_{con}$  for different frequencies. Inset: AC conductivity versus frequency for the non-percolative and percolative composites



flux is more concentrated. But in the case of pure  $n$ -Ni,  $\mu'$  decreases as compared to  $f_{\text{con}} = 0.315$  (Fig. 8.5) which may be due to the combined effect of ferromagnetic properties of  $n$ -Ni and the generation of eddy currents by an alternating magnetic field.

### 8.3.2 Rheological Properties

All the possible rheological parameters and their dependence on other parameters are shown in this section [16]. Figure 8.6a–c shows the variation of torque as a function of speed, shear rate, and strain%, respectively, for the variety of polymers under investigation. The value of torque is quite high ( $\sim 10^3$   $\mu\text{Nm}$  or even more) for the PVDF polar polymer as compared to the PVA ( $\sim 10^2$   $\mu\text{Nm}$ ) & PEG ( $\sim 1$   $\mu\text{Nm}$ ). For PEG, all the graphs show a change in torque with respect to different parameters under investigation but within a very small variation. However, the torque remains very high and also remains constant for PVA & PVDF with respect to all the parameters such as speed, shear rate, and strain%, respectively. This observation shows that PVA shows little similarity with PVDF but PVDF always has a higher value of torque in comparison with PVA and PEG. The higher value of torque, as well as the constancy of torque, is attributed to the higher crystallinity and presence of permanent dipole moments in the PVDF polymer matrix as compared to PVA and PEG. Similarly, the higher value of torque for PVA as compared to PEG is due to the presence of dipole contributions in the PVA polymer matrix as compared to PEG.

Figure 8.7a–c shows the variation of viscosity of PVA, PEG, and PVDF with respect to speed, shear rate, and strain%, respectively. All the three polymers are showing a nonlinearity in the variation of viscosity with respect to all the parameters under investigation and the viscosity also decreases as a function of these parameters. From observations, it is obvious that PEG has the least value of viscosity ( $\sim 10^{-3}$  Pa.S) and remains constant with respect to speed, shear rate, and strain%, respectively, while the value of viscosity is of the order of ( $\sim 10^2$  Pa.S) for PVDF and is of the order of ( $\sim 10$  Pa.S) for PVA. The viscosity of these two polymers (PVDF & PVA) decreases nonlinearly with respect to speed, shear rate, and strain%, respectively, as it is a conventional behavior of all polymers. In all manners, PVDF is always showing a mechanically rich behavior which is good for making a composite with any kind of filler (CNT/metal/graphite/CB/etc.) for finding their suitability for high K dielectric materials.

Figure 8.8 shows the similar behavior of the polymers in terms of shear stress as mechanical properties as that of Fig. 8.6. The value of shear stress is quite high in the case of PVDF as compared to PVA and PEG has been attributed to the higher crystallinity (50–60%), presence of permanent dipole moment and high static dielectric constant ( $\sim 10$ ) of the PVDF polymer matrix.

So, from the above investigations (Figs. 8.6, 8.7, and 8.8) of viscoelastic properties, it is found that always polar polymer/ferroelectric polymer (e.g., PVDF) shows the higher value of mechanical and rheological parameters. From earlier investigations,

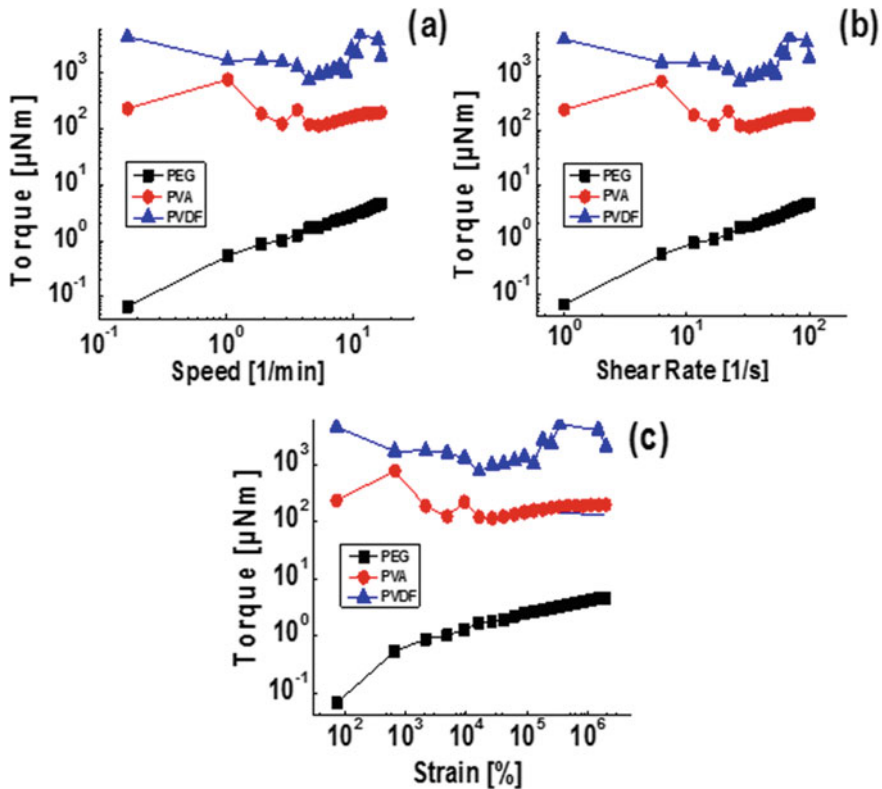


**Fig. 8.6** Variation of torque as a function of **a** speed, **b** shear rate and **c** strain% for all the three pure polymers (PEG, PVA, and PVDF)

it is also found that definitely in the development of flexible high K materials only the ferroelectric polymers should be taken preferentially in comparison to non-polar polymers since the presence of permanent dipole moment and high dielectric constant of the polar polymers play a major role in the enhancement of dielectric constant in case of PMC [20]. As a specific investigation of the dielectric materials, also it has been observed recently that PVDF/*n*-Ni@NiO (core-shell composite with polymer PVDF) is a very good dielectric material [21] and hence under this investigation the rheological investigation on PVDF/NiO composites was investigated.

In Fig. 8.9, the results of the PVDF/NiO composite of the various compositions of NiO in the composite as 0, 5, 10, and 15% are shown. The results show that the value of shear stress for the pure polymer PVDF or its composites, either remains constant or slightly increases with the increase of the NiO content into the polymer matrix in the composite. It is also observed that shear stress has an increasing behavior but after a certain value the graph shows a sudden fall in shear stress but in the case of the PVDF/NiO (15%) composite, it is not as sudden as other compositions, i.e., hardness of the composite is probably increasing.

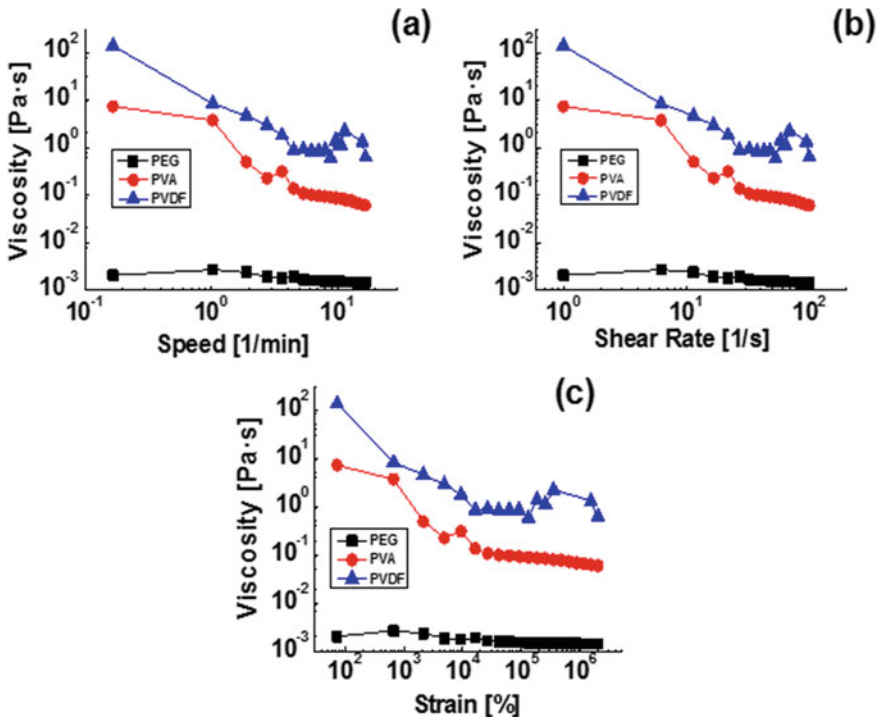


**Fig. 8.7** Variation of viscosity as a function of **a** speed, **b** shear rate and **c** strain% for all the three pure polymers (PEG, PVA, and PVDF)

In Fig. 8.10, the viscosity provides a piece of important information, where lowering in viscosity in these composites has a constant behavior over a long range of the parameters, such as speed, shear rate, strain%, and time, which can be seen in these logarithmic graphs Fig. 8.9a–d. One of the most important behaviors of PVDF/NiO composite is that which have a well-known change of range of viscosity with respect to the compositions and also with respect to the different parameters, such as speed, shear rate, strain%, and time.

In Fig. 8.11, the variation of torque as a function of speed, shear rate, strain%, and time is shown. The torque for all the composites remains constant up to a certain value of all the parameters shown in the fig, and after that, it undergoes a decrement in its value and that change in value isn't becoming a substantial change in the values.

So from the above results and the observations, it is found that the comparative study of PEG, PVA, and PVDF shows that the viscosity of PEG, PVA, and PVDF changes with respect to shear rate which defines that these polymers behave like non-Newtonian fluids. From all observations, it is obvious that PVDF shows high mechanical stability and a high value of viscosity (Figs. 8.6, 8.7 and 8.8). In the case of PVA, PEG, and PVDF, the viscosity decreases with respect to shear rate and strain%, which makes them a pseudoplastic material or called as showing the

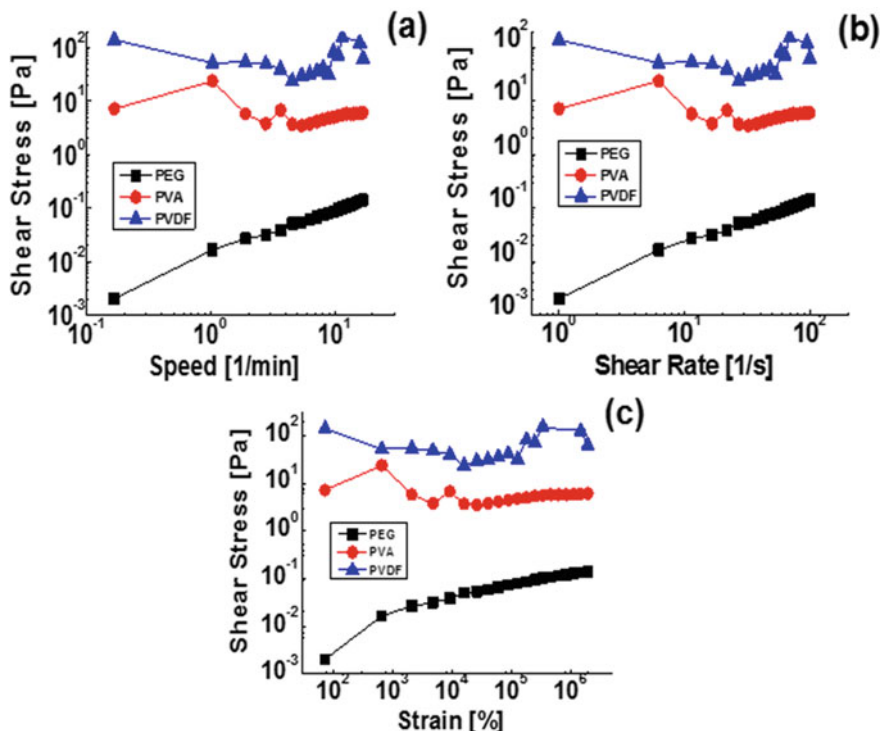


**Fig. 8.8** Variation of shear stress as a function of **a** speed, **b** shear rate and **c** strain% for all the three pure polymers (PEG, PVA, and PVDF)

shear thinning behavior. PVDF and its composites always have a high mechanical and elastic behavior as compared to the other polymers and also always maintain a time-dependent behavior. It is also found that the PVDF/NiO composites of different compositions are showing the non-Newtonian flow behavior and decrease in viscosity with respect to increment in shear rate [22]. In Fig. 8.5, the various compositions of PVDF/NiO composite give the decrement under shear rate and strain% and the curve of PVDF/NiO (15%) has a tendency to minimum thinning under shear rate and strain%. All the polymers and the PVDF/NiO composites are behaving like a thixotropic fluid which is taking a finite time to attain equilibrium viscosity when introduced to a step change in shear rate [22].

## 8.4 Summary

The ferroelectric (FE) and ferromagnetic (FM) behaviors of the composites (thick films) have undergone modifications with the increase of concentration of  $n$ -Ni in the composites. FE and FM contributions in the composites come individually from

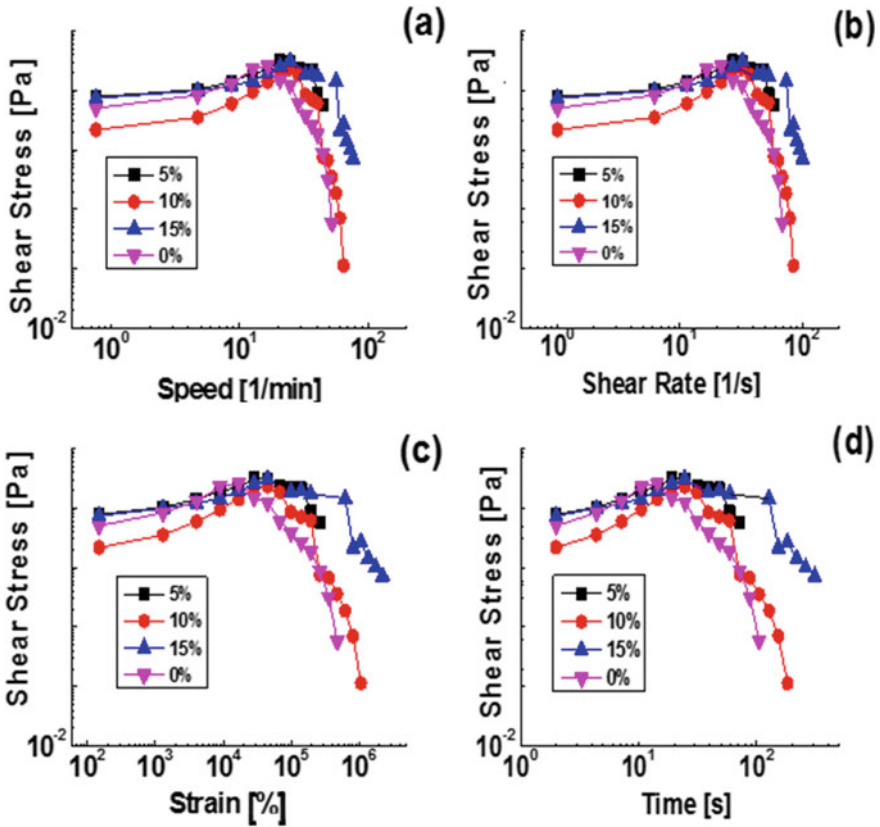


**Fig. 8.9** Variation of shear stress as a function of **a** speed, **b** shear rate, **c** strain% and **d** time for PVDF/NiO composites of NiO weight fractions ranging from 0 to 15%

PVDF and Ni, respectively. However, the concentration change of *n*-Ni hasn't significantly modulated the FE properties of PVDF while FM behavior increases with the increase of concentration of Ni. This suggests that possibly PVDF-Ni nanocomposites may be a good candidate for ME applications which can be confirmed only after further investigation. Similarly, in the case of bulk composites, electrical and magnetic properties have been investigated as a function of volume fractions of *n*-Ni ( $f_{con}$ ). A significant enhancement in saturation magnetization of 24  $\mu\text{g}$ , measure of the permeability of 1.11, and dielectric constant of 2050 at 100 Hz is observed at the electrical percolation threshold ( $f_c$ ) of the composite. The decrease of magnetization of the composite with the decrease in  $f_{con}$  is attributed to the dilution effect and magnetic dipolar interaction. The measure of permeability ( $\mu'$ ) increases linearly with the increase of  $f_{con}$  as the magnetic flux concentrates over individual *n*-Ni clusters/particles even beyond  $f_c$ . On the other hand,  $\mu'$  decreases for pure *n*-Ni probably due to the increased connectivity among the *n*-Ni clusters/particles and hence being a conductor result in eddy current generation in the alternating magnetic field. The

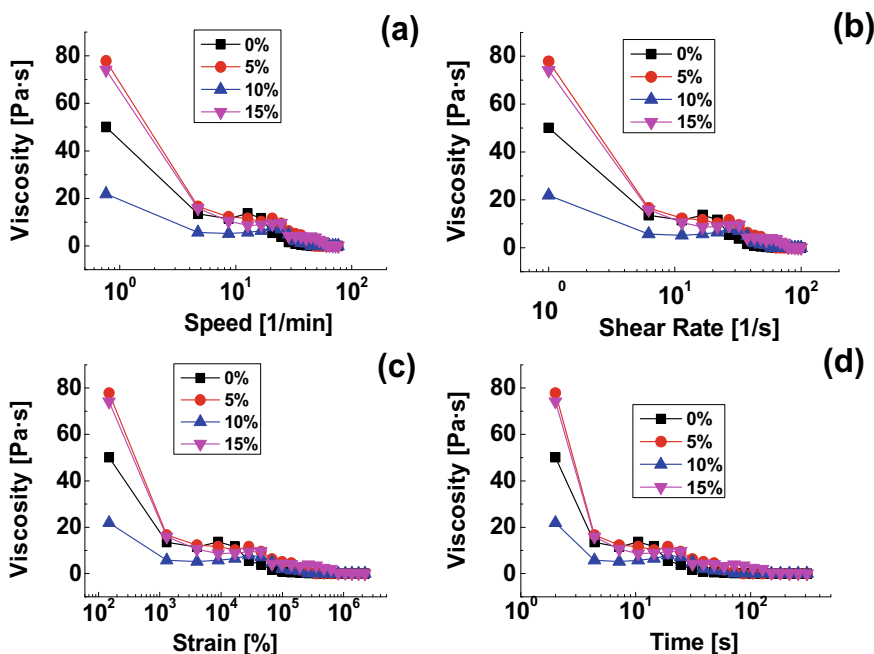


**Fig. 8.10** Variation of viscosity as a function of **a** speed, **b** shear rate, **c** strain%, **d** time for PVDF/NiO composites of NiO with weight fractions ranging from 0 to 15%

concept of  $m_c$  could not be realized which may be attributed to the presence of larger  $n$ -Ni clusters in the polymer matrix giving rise to their nature of ferromagnetism arising due to their multi-domain nature. At  $f_c$  of the composite, i.e., at  $f_{con} = 0.28$  the value of  $\varepsilon_{eff} = 2050$ ,  $M_s = 24 \text{ e}\mu/\text{g}$  which is very close to  $M_s$  of pure  $n$ -Ni ( $30 \text{ e}\mu/\text{g}$ ) along with a higher value of  $\mu' = 1.11$  may make the material suitable for multifunctional applications, such as high charge storage capacitors, magnetic memories, and high-frequency applications. PVDF shows very strong viscoelastic and mechanical properties and also with the addition of NiO to the PVDF matrix, the mechanical and viscoelastic properties are either enhanced or at least remain constant. This study confirms that PVDF or other ferroelectric/polar polymers should be given preference for the development of the PMC for their energy storage and dielectric applications as these polymers also show higher viscoelastic properties.

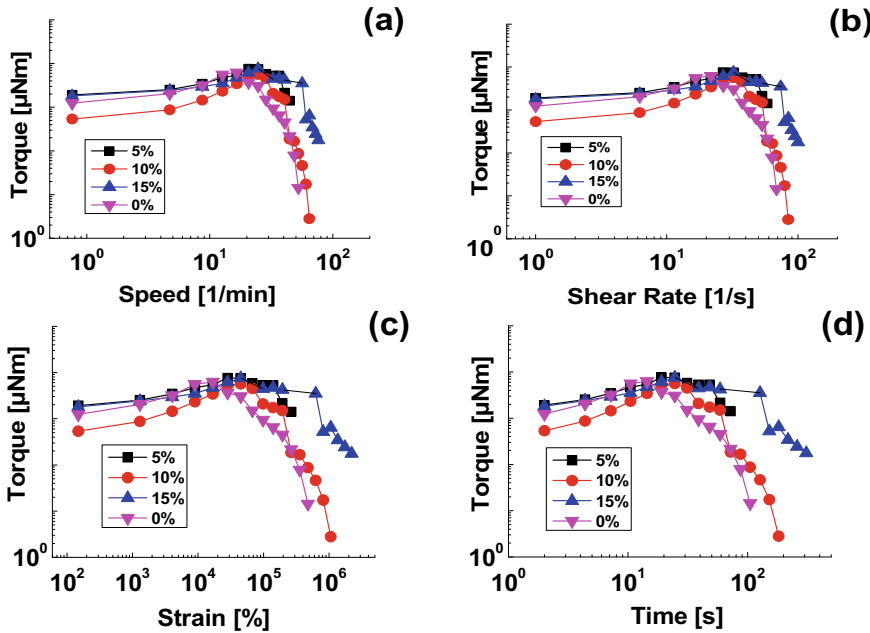


**Fig. 8.11** Variation of torque as a function of **a** speed, **b** shear rate, **c** strain%, **d** time for PVDF/NiO composites of NiO with weight fractions ranging from 0 to 15%

## References

1. Nan CW, Bichurin MI, Dong S, Viehland D, Srinivasan G (2008) Multiferroic magnetoelectric composites: historical perspective, status, and future directions. *J Appl Phys* 103:031101–031135
2. Fiebig M (2005) Revival of the Magneto-electric effect. *J Phys D: Appl Phys* 38:R123
3. Makarova LA, Rodionova VV, Alekhina YA, Rusakova TS, Omelyanchik AS, Perov NS (2017) New multiferroic composite materials consisting of ferromagnetic, ferroelectric, and polymer components. *IEEE Trans Magn* 53:1–7
4. Kalinin YE, Sitnikov AV, Skryabina NE, Spivak LV, Artem AA, Shadrin A (2004) Barkhausen effect and percolation threshold in metal-dielectric nanocomposites. *J Mag Magn Mat* E893:272–276
5. Guo Z, Park S, Hahn HT, Wei S, Moldovan M, Karki AB, Young DP (2007) Magnetic and electromagnetic evaluation of the magnetic nanoparticle filled polyurethane nanocomposites. *J Appl Phys* 101(09M):511
6. Shekhar S, Sajitha EP, Prasad V, Subramanyam SV (2008) High coercivity below percolation threshold in polymer nanocomposite. *J Appl Phys* 104:0839101–0839104
7. Gennes PGD (1981) Colloidal suspensions in a critical binary mixture. *C R Acad Sci* 292:701
8. Panina LV, Antonov AS, Satychev AK, Paramonov VP, Tmasheva EV, Lagarikov AN (1994) Magnetic anomaly in insulator-conductor composite materials near the percolation threshold. *J Appl Phys* 76:636
9. Drnovsek B, Bregar VB, Pavlin M (2009) Numerical study of effective permeability of soft-magnetic composites with conductive inclusions. *J Appl Phys* 105:07D546-11
10. Nicklasson GA, Grangvist CG (1984) Optical properties and solar selectivity of coevaporated  $\text{CoAl}_2\text{O}_3$  composite films. *J Appl Phys* 55:3382

11. Vinogradov AP, Lagarkov AN, Sarychev AK (1984) *Pis'ma Zh. Eksp. Teor. Fiz* 40:296
12. Panda M, Adyam V, Srinivas V, Thakur AK (2008) Synthesis and characterization of Ni-PVDF nano-composites. *AIP conf proc* 1003:43–45
13. Clerc JP, Giraud G, Laugier JM, Lucks JM (1990) The electrical conductivity of binary disordered systems, percolation clusters, fractals, and related models. *Adv Phys* 1:191
14. Panda M, Srinivas V, Thakur AK (2016) Multiferroic properties of PVDF/Ni nano composites. *Indian J Pure Appl Phys* 54:144
15. Dey R, Bhunia R, Hussain S, Dutta P, Chatterjee S, Bhar R, Pal AK (2016) Room temperature magnetism in free-standing nano-Ni/PVDF composites. *Polym Plast Technol Eng* 56:1213
16. Panda M, Soni S (2018) A comparative study of viscoelastic properties of non-polar and polar polymer dielectrics. *Mater Today: Proc* 05:2123–2130
17. Barnes HA, Hutton JF, Walters K (1991) *An introduction to rheology*. Elsevier, Amsterdam
18. Macosko CW (1994) *Rheology: principles, measurements, and applications*. New-Jercy, Weinheim Cambridge VCH, New York
19. Stearns MB, Cheng Y (1994) Determination of para and ferromagnetic components of magnetization and magnetoresistance of granular Co/Ag film (invited). *J Appl Phys* 75:6894
20. Panda M (2017) Major role of process conditions in tuning the percolation behavior of polyvinylidene fluoride based polymer/metal composites. *Appl Phys Lett* 111(1–5):082901
21. Panda M, Srinivas V, Thakur AK (2014) Percolation behavior of polymer-metal composites on modification of filler. *Modern Phys Lett B* 28(1–6):1450055
22. Nalwa HS (1995) *Ferroelectric polymers*. Marcel Dekkar, New York

# Chapter 9

## Non-percolative Polymer Composites



In this chapter, the microstructure, dielectric behavior, and electrical properties of polymer/ceramic composites (PCC) based on ferroelectric polymer [polyvinylidene fluoride (PVDF)] and nanobarium titanate ( $n$ -BaTiO<sub>3</sub>) prepared under the novel cold pressing method are reported. Large enhancement of effective dielectric constant ( $\epsilon_{\text{eff}} \sim 450$ ) with lower loss tangent ( $\text{Tan } \delta \sim 0.9$ ) at 50 Hz was observed for the PCC with 0.60 as the volume fraction of  $n$ -BaTiO<sub>3</sub> into the PVDF matrix. The enhancement of  $\epsilon_{\text{eff}}$  is attributed to the large interfacial polarization arising due to the charge storage at the spherulites of PVDF and the polymer/filler interfaces of PCC. The achieved lower  $\text{Tan } \delta$  for the PCC as compared to the polymer/metal composites (PMC) is attributed to the highly insulating nature of PVDF and semiconducting  $n$ -BaTiO<sub>3</sub>. The thermal stability of the composites is also maintained due to the higher melting temperature (170 °C) of PVDF. The cold-pressed PCC based on PVDF will act as a better polymer dielectric for electrical energy storage applications as compared to the reported cold-pressed PMC.

### 9.1 Introduction

Polymer dielectrics (PD) with higher energy density and lower loss tangent ( $\text{Tan } \delta$ ) with higher breakdown field strength are the emerging materials of future for electrostatic energy storage applications due to their flexibility, non-toxicity, biocompatibility, low cost, higher viscoelastic properties, etc. [1–5]. For this application, the maximum stored energy density is an important parameter, and for a linear dielectric, the maximum stored energy per unit volume is  $U = \frac{1}{2} K \epsilon_0 E_{\text{max}}^2$ , where  $K$  is the relative dielectric constant and  $E_{\text{max}}$  is the maximum electric field, which can be applied to the material (proportional to the breakdown field of the material). In the development of this PD, over the last two decades of research, the ferroelectric polymers, e.g., polyvinylidene fluoride (PVDF) matrix, have been preferred due to their high

static dielectric constant ( $\sim 15$ ) and higher viscoelastic properties and higher insulating nature as compared to other non-polar polymers. The varieties of fillers, such as micron and nanoparticles of metal, ceramic, carbon nanotube, carbon black, graphite, graphene, conducting polymer, are under continuous use in the development of this PD. However, the development of the polymer-ceramic composites (PCC) has been dormant over the last decade of research, as the effective dielectric constant ( $\epsilon_{\text{eff}}$ ) for these composites was found to be very low, i.e.,  $\epsilon_{\text{eff}} \sim 100$  at low frequencies due to the low dielectric constant of the polymers as well as due to the conventional hot molding process conditions. In the preparation of this PCC, a very high dielectric constant ferroelectric ceramic, such as PMN-PT,  $\text{BaTiO}_3$ ,  $\text{PbTiO}_3$  with particles of size order of microns is used to have an improvement in the value of  $\epsilon_{\text{eff}}$  with lower  $\text{Tan } \delta$ . However, due to the low dielectric constant of the polymers, even with the PVDF matrix (whose static dielectric constant  $\sim 17$ ), a much higher value of  $\epsilon_{\text{eff}}$  with lower  $\text{Tan } \delta$  could not be achieved. Hence, to have large interfacial polarization, the nanoparticles of the same ferroelectric ceramics also have been used in the PVDF matrix through hot molding, and partially, the approach becomes effective to get better PD [6–10].

In the development of these PCC based on PVDF, the traditional mixed technique (solution casting followed by hot molding) is used, during which the spherulites of PVDF get lost [8–10], which results in getting the lower value of  $\epsilon_{\text{eff}}$ . Recently, our group has developed the cold pressing technique in preparing the PD based on PVDF, due to which the spherulites of PVDF are retained, and they help additionally in the storage of electrical charge due to their additional interfaces, which results in higher interfacial polarization, and hence, the higher value of  $\epsilon_{\text{eff}}$  is achieved [10].

In developing this PD, among the variety of fillers, except the insulating ceramic fillers, mostly, the polymer/metal or conductor composites (PMC) have undergone research in the last two decades by various research groups, since a very high value of  $\epsilon_{\text{eff}}$  is achieved in these composites due to the percolative second-order insulator-to-metal transition (IMT) at the percolation threshold ( $f_c$ ) of these PMC. At  $f_c$ , the  $\epsilon_{\text{eff}}$ ,  $\text{Tan } \delta$ , and effective AC conductivity ( $\sigma_{\text{eff}}$ ) undergo sharp increment due to the IMT, and  $f_c$  becomes the point of discontinuity for  $\epsilon_{\text{eff}}$  in case of PMC. However, the main drawback of these PMC, which inhibits them from their technological applications, is the unwanted higher value of  $\text{Tan } \delta$  and  $\sigma_{\text{eff}}$ .

Hence, to overcome the major difficulty of this PD (higher value of  $\text{Tan } \delta$ ) based on PMC, the interest in the PCC-based PD should be focused on a novel method of preparation to have a lower value of  $\text{Tan } \delta$  along with the higher value of  $\epsilon_{\text{eff}}$ . One of the very simple methods in finding the true percolation behavior of PMC is the preparation of cold-pressed composites by Panda et al. [8–10], in which the spherulites of PVDF are retained, and higher  $\epsilon_{\text{eff}}$  is observed due to the additional storage of electrical charge at the interfaces of the spherulites.

Hence, it is believed that by changing the traditional process condition (hot molding of the thick films prepared from solution casting) to cold pressing developed by Panda et al. [8–10] in which the spherulites of PVDF will be retained for the case of PCC (like that of the PMC), definitely higher value of  $\epsilon_{\text{eff}}$  will be achieved, with lower  $\text{Tan } \delta$  due to the high dielectric constant insulating ferroelectric ceramics.

Hence, a PCC with high  $\epsilon_{\text{eff}}$  and lower  $\tan \delta$ , ferroelectric polymer (PVDF), and high dielectric constant nanoceramic ( $n$ -BaTiO<sub>3</sub>) with particle size  $\sim 100$  nm (having large surface area) have prepared and have undergone the microstructural, dielectric, and electrical conductivity measurements for finding their suitability to energy storage applications.

## 9.2 Samples Reported

A series of PCC based on PVDF with varying volume fraction of  $n$ -BaTiO<sub>3</sub> ( $f_{\text{BaTiO}_3}$ ) from 0.0 to 0.60 were prepared. The composite powders of PVDF (Alfa Aesar) and the  $n$ -BaTiO<sub>3</sub> (Aldrich) with particle size  $< 100$  nm were prepared with different  $f_{\text{BaTiO}_3}$ , and the final samples were taken in the form of pellets under room temperature consolidation at a pressure of 30 MPa. The microstructure investigation on the samples was carried out with the help of FESEM from *FEI Company of USA (SE Asia) PTE LTD.* (Model No. SEM 450). The electrical measurements were made on all the PCC in the frequency range of 50 Hz–5 MHz and in the temperature range of room temperature to 100 °C with the help of the LCR HITESTER (Model No. HIOKI 3520).

## 9.3 Results and Discussion

### 9.3.1 Microstructure

The FESEM micrographs of the cold-pressed pure PVDF (Fig. 9.1a, b) and PVDF/ $n$ -BaTiO<sub>3</sub> composites with different  $f_{\text{BaTiO}_3}$  up to 0.60 are shown in Fig. 9.1c–f. Figure 9.1a, b shows the presence of spherulites (the spherical semicrystalline regions of the polymer) in the cold-pressed PVDF, while both the spherulites and large created voids/rod-like structures (due to the cold pressing) are observable from the micrographs (Fig. 9.1c–f), which are going to be helpful in storing the additional electric charge. The diameter of the spherulites present in the polymer is of the order of  $\sim 0.1$   $\mu\text{m}$  (Fig. 9.1a, b). Interestingly, the  $n$ -BaTiO<sub>3</sub> taken is of size 100 nm, i.e., 0.1  $\mu\text{m}$ , i.e., of the order of the diameter of the spherulites. During cold pressing, the  $n$ -BaTiO<sub>3</sub> clusters have taken the shape of vertical rods (Fig. 9.1c–f) inside the polymer matrix and created large voids in the matrix, which will be of large benefit in the storage of electrical charge.

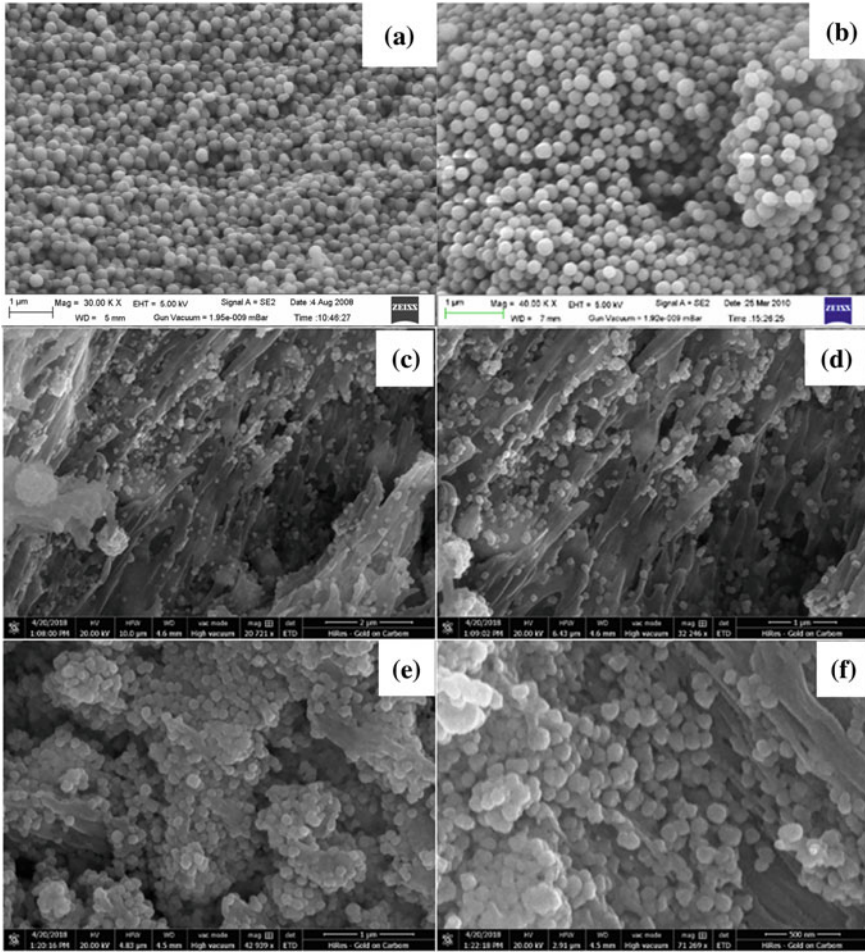


**Fig. 9.1** FESEM micrographs of cold-pressed PCC: **a** pure PVDF (lower resolution), **b** pure PVDF (higher resolution), **c**  $f_{\text{BaTiO}_3} = 0.2$  (lower resolution), **d**  $f_{\text{BaTiO}_3} = 0.2$  (higher resolution), **e**  $f_{\text{BaTiO}_3} = 0.6$  (lower resolution), **f**  $f_{\text{BaTiO}_3} = 0.6$  (higher resolution)

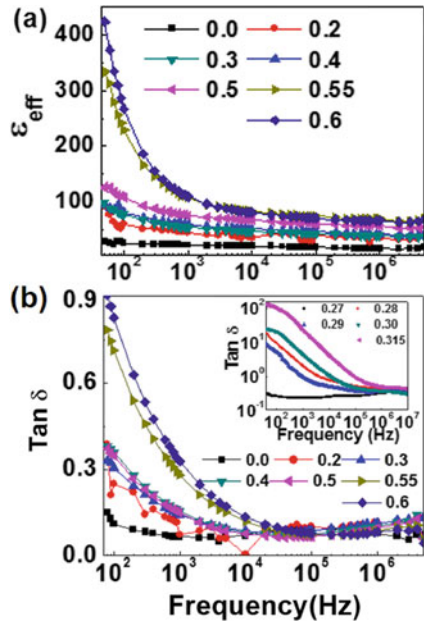
### 9.3.2 Dielectric Properties

The variation of  $\epsilon_{\text{eff}}$  and  $\tan \delta$  of the prepared series of PCC as a function of frequency at 300 K is shown in Fig. 9.2a, b, respectively. The value of  $\epsilon_{\text{eff}}$  at 50 Hz for the 0.0 sample is 16, while this value increases up to 120 linearly up to the PCC with  $f_{\text{BaTiO}_3} = 0.5$ , and after that, it increases up to the value of 330 & 420 for the samples with  $f_{\text{BaTiO}_3} = 0.55$  and  $f_{\text{BaTiO}_3} = 0.60$ , respectively. The higher value of  $\epsilon_{\text{eff}}$  for the  $f_{\text{BaTiO}_3} = 0.55$  and  $f_{\text{BaTiO}_3} = 0.60$  is due to the large interfacial polarization arising both due

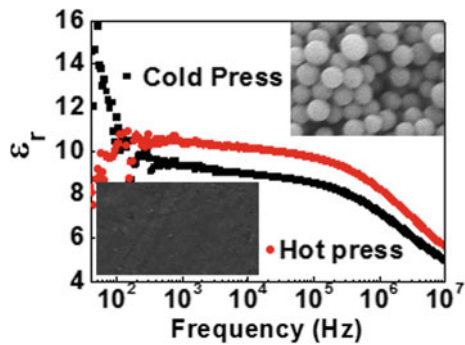
to the presence of spherulites and created larger voids/rod-like structures during cold pressing, while the spherulites are lost for the hot-molded samples (Fig. 9.3).

Figure 9.3 shows the static dielectric constant ( $\epsilon_r$ ) of the cold-pressed pure PVDF is  $\sim 16$ , i.e., higher than the  $\epsilon_r$  of hot-molded pure PVDF ( $\sim 10$ ) due to the loss of spherulites (Inset, Fig. 9.3) of the polymer. The value of  $\epsilon_{\text{eff}}$  decreases with an increase of frequency for all the PCC due to the absence of contribution from interfacial polarization at higher frequencies where only the contribution from dipolar and atomic polarization exists. A very low  $\text{Tan } \delta$  for the PCC with  $f_{\text{BaTiO}_3} = 0.6$  (having highest  $\epsilon_{\text{eff}} = 420$  observed at 50 Hz) was found to be only 0.9 at 50 Hz and that value also decreases with the increase of frequency and the trend of decrement is also observed for all the PCC. However, in the recently reported PMC, the  $\text{Tan } \delta$  value

**Fig. 9.2** (Color online) Variation of **a**  $\epsilon_{\text{eff}}$  and **b**  $\text{Tan } \delta$  as a function of frequency at 300 K for the PD, Inset:  $\text{Tan } \delta \sim \text{frequency}$  for some typical percolative PMC samples



**Fig. 9.3** FESEM micrograph of the hot-molded PVDF showing the loss of spherulites at a temperature higher than the room temperature



was reported to be 10 at 50 Hz (Inset, Fig. 9.2b) for the percolative sample, with  $\epsilon_{\text{eff}} \sim 2000$ . Hence, the PMC at  $f_c$  shows 10 times higher value of  $\text{Tan } \delta$  in comparison to the result of PCC.

The  $\epsilon_{\text{eff}}$ ,  $\sigma_{\text{eff}}$  and  $\text{Tan } \delta$  of the composites as a function of  $f_{\text{BaTiO}_3}$  at different frequencies are shown in Fig. 9.4. The  $\epsilon_{\text{eff}}$  rises linearly from 16 to 120 when  $f_{\text{BaTiO}_3}$  increases from 0.0 to 0.50 at 100 Hz, while due to the large interfacial polarization occurring due to the presence of spherulites and interfaces at the PCC, the  $\epsilon_{\text{eff}}$  increases largely from 120 to 350 & 420 for  $f_{\text{BaTiO}_3} = 0.55$  & 0.60, respectively. It was found that the expression developed by Yamada et al. [11] (which is a model for explaining the sum properties of the composite) can fit the dielectric data well (Fig. 9.4b) at frequency 1000 Hz or above.

$$\epsilon_{\text{eff}} = K_{\text{PVDF}} \left[ 1 + \frac{n f_{\text{BaTiO}_3} (K_{\text{BaTiO}_3} - K_{\text{PVDF}})}{n K_{\text{PVDF}} + (K_{\text{BaTiO}_3} - K_{\text{PVDF}})(1 + f_{\text{BaTiO}_3})} \right] \quad (9.1)$$

where  $\epsilon_{\text{eff}}$  is the effective dielectric constant of the composite,  $K_{\text{PVDF}}$  and  $K_{\text{BaTiO}_3}$  are the dielectric constants of the polymer matrix and the ceramic, respectively,  $f_{\text{BaTiO}_3}$  is the volume fraction of the ceramic, and 'n' is a parameter related to the geometry of ceramic particles [12]. The values of  $K_{\text{PVDF}}$ ,  $K_{\text{BaTiO}_3}$ , and  $n$  obtained from the fitting of Eq. (9.1) to the experimentally measured dielectric data of the composites are 17, 1600, and 10, which is in good agreement with the earlier found geometrical exponent ( $n = 10.6$  for PVDF/PZT composites [11]). The important point is that we would like to communicate here that the Yamada model could not hold good with the experimental dielectric data at 100 Hz, as the additional contributions of electrical charge (in addition to the presence of sum properties of both the components) at the

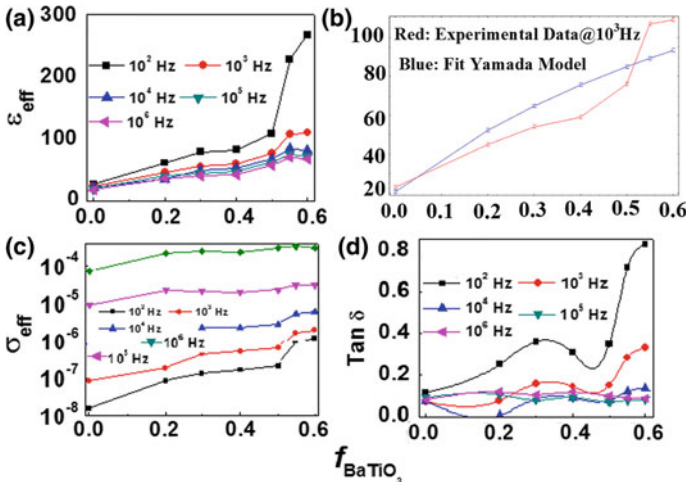


**Fig. 9.4** (Color online) Variation of **a**  $\epsilon_{\text{eff}}$  experimentally, **b** fitting of  $\epsilon_{\text{eff}}$  experimental data at 1 kHz with Yamada model, **c**  $\sigma_{\text{eff}}$  and **d**  $\text{Tan } \delta$  as a function of  $f_{\text{BaTiO}_3}$  for various frequencies at 300 K for the PCC

interface of the spherulites (due to cold pressing) give rise to rapid enhancement of  $\epsilon_{\text{eff}}$ , which suggest that a modified Yamada model is to be developed, remained as a challenge in taking care of the spherulites in his type of cold-pressed PCC.

The  $\sigma_{\text{eff}}$  and  $\text{Tan } \delta$  for all the composites increases with the increase of  $f_{\text{BaTiO}_3}$  in the PCC slowly suggests the semiconducting nature of the  $\text{BaTiO}_3$  nanoceramic, thereby becoming very helpful in the reduction of  $\text{Tan } \delta$  with achieved higher  $\epsilon_{\text{eff}}$  ( $\sim 400$ ). With  $f_{\text{BaTiO}_3} = 0.6$ , the  $\sigma_{\text{eff}}$  value varies within  $10^{-8}$ – $10^{-4} \Omega^{-1} \text{ cm}^{-1}$  for frequency varying between 50 Hz and 5 MHz, while the value of  $\text{Tan } \delta$  is maintained in between 0.1 and 0.8. The value of  $\sigma_{\text{eff}}$  &  $\text{Tan } \delta$  also is found to be increasing with an increase of frequency, suggesting primarily a hopping type of AC conduction in the PCC. Similarly,  $\sigma_{\text{eff}}$  value for all the PCC was found to be very low, i.e., less than  $10^{-4} \Omega^{-1}$  for all the PCC, and that value also almost remains constant over the entire frequency range. The  $\text{Tan } \delta$  increases slowly as a function of  $f_{\text{BaTiO}_3}$  and was found to be less than 0.8 even with the PCC having  $f_{\text{BaTiO}_3} = 0.6$ .

The thermal stability of the PCC was checked by measuring the electrical parameters as a function of temperature and is given in Fig. 9.5. It was found that for  $f_{\text{BaTiO}_3} = 0.4$  (Fig. 9.5a) and  $f_{\text{BaTiO}_3} = 0.50$  (Fig. 9.5b), the low-frequency (50 Hz) value of  $\epsilon_{\text{eff}}$  is maintained at a thermal stabilized value of 90 and 130 (with their corresponding decrement as a function of frequency) as a function of temperature from 40 to 100 °C. The stabilization of  $\epsilon_{\text{eff}}$  is attributed due to the major effective contribution coming from the sum properties of the dielectric constant of both the components. However, for the samples with  $f_{\text{BaTiO}_3} = 0.55$  & 0.6, the reached  $\epsilon_{\text{eff}} \sim 350$  & 420 value arises due to the sum properties of the dielectric constant of both the components as well as due to the major contribution of the spherulites. Hence, with the increase of temperature, the  $\epsilon_{\text{eff}}$  decreases due to the melting of the spherulites of the PCC (Fig. 9.5c, d). Hence, the spherulites are useful at room temperature in the case of PCC for achieving the high value of  $\epsilon_{\text{eff}}$  with low  $\text{Tan } \delta$ .

### 9.3.3 Conductivity Properties

The variation of AC conductivity (which has been calculated as  $\sigma_{\text{ac}} = \omega \epsilon_0 \epsilon' \text{Tan } \delta$ ) as a function of frequency (conductivity spectrum) at different  $f_{\text{BaTiO}_3}$  is shown in Fig. 9.6. The  $\sigma_{\text{eff}}$  as a function of frequency was found to be the hopping types of conductivity satisfying Jonscher's law of AC conduction [13–15]. It can be observed that the plot shows the dispersion of AC conductivity with frequency for all the PCC corresponding to  $f_{\text{BaTiO}_3} \leq 0.20$ , agrees very well with Eq. (9.2), i.e.,

$$\sigma_{\text{ac}}(\omega) = \sigma_{\text{dc}} + A\omega^k \quad (9.2)$$

with the  $\sigma_{\text{dc}}$  part becoming zero and the value of  $k \sim 1$ . The absence of DC conductivity for the samples with  $f_{\text{BaTiO}_3} \leq 0.20$  can be interpreted as the non-presence of percolating paths (being formed from the semiconducting  $\text{BaTiO}_3$  nanoceramics in the PVDF matrix) due to the insufficient  $f_{\text{BaTiO}_3}$ . It can also be observed that the

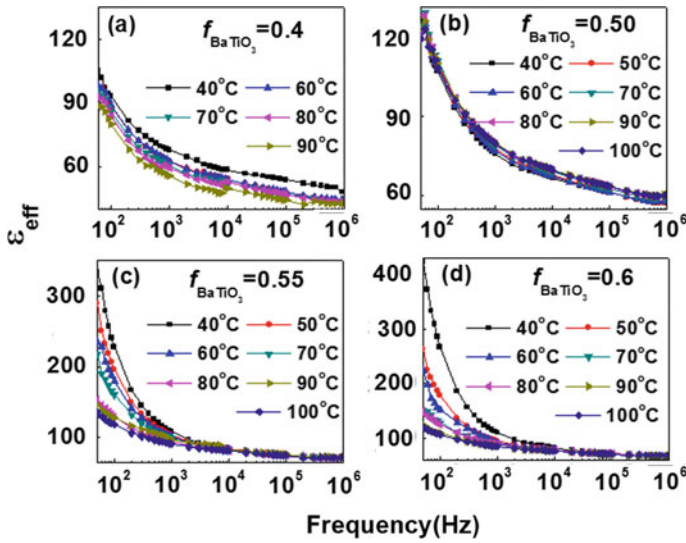
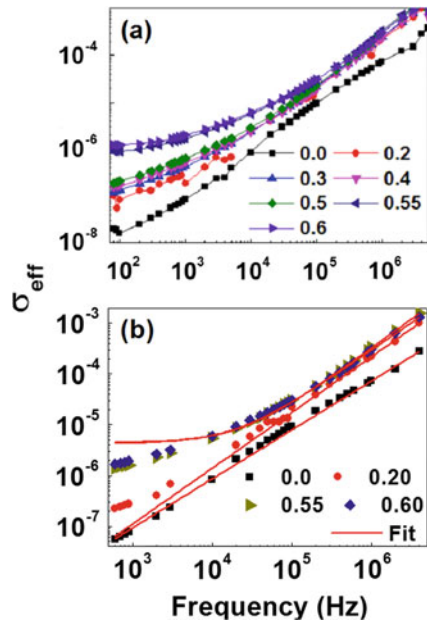


**Fig. 9.5** (Color online) Variation of  $\epsilon_{eff}$  as a function of frequencies for the temperature varying from 40 to 100 °C for varying  $f_{BaTiO_3}$ , **a** 0.40, **b** 0.50, **c** 0.55, **d** 0.60

**Fig. 9.6** (Color online) Variation of **a**  $\sigma_{eff}$  experimentally and **b** fitted with Jonscher’s power law, as a function of frequencies



long-range DC conduction starts to appear for  $f_{\text{BaTiO}_3} = 0.3\text{--}0.5$ , but a good fit of Eq. (9.2) could not be obtained for them as the percolating paths weren't sufficient. But interestingly, for the samples with  $f_{\text{BaTiO}_3} \geq 0.55$ , a mixed conductivity is found, i.e., a DC plateau up to a certain frequency separated by AC conductivity beyond that frequency. The plateau in the conductivity spectrum occurs due to the appearance of long-range DC conductivity. At higher frequency, the conductivity becomes more or less  $f_{\text{BaTiO}_3}$  dependent. This frequency at which the change in slope takes place is known as the "hopping or critical frequency  $\omega_H$ ," and it can be observed that  $\omega_H$  increases with the increase of  $f_{\text{BaTiO}_3}$ .

However, in all cases, the value of 'k' lies well within Jonscher's universal regime [0, 1] suggesting the validity of Jonscher's power law in all the PCC.

## 9.4 Summary

The microstructural and AC electrical characterization of a specific PCC as a function of frequency and  $f_{\text{con}}$  have been studied. It is found that the enhancement of  $\epsilon_{\text{eff}}$  of PCC based on PVDF matrix is largely enhanced by the cold pressing process conditions, due to the retention of the spherulites during sample preparation. It is also found that this cold pressing method is more suitable to the PCC based on PVDF matrix (since a very low value of  $\text{Tan } \delta \sim 0.9$  is observed) in comparison to PMC based on PVDF matrix in which a large value of  $\text{Tan } \delta \sim 10\text{--}100$  is observed. The spherulites present in the PVDF matrix are always helpful in maintaining the  $\epsilon_r$  and in increasing the  $\epsilon_{\text{eff}}$  of PCC/PMC. A long-range DC conductivity appears at  $f_{\text{con}} \geq f_c$  and Jonscher's universal fractional power law is well satisfied for both the regions of  $f_{\text{con}} < f_c$  and  $f_{\text{con}} \geq f_c$  in all PCC. The exponent of the power law decreases as a function of  $f_{\text{con}}$  due to a decrease of the rate of dispersion arising due to the increase of DC conductivity. In the region of  $f_{\text{con}} \geq f_c$ , it is found that the dynamics of charge carriers are  $f_{\text{con}}$  dependent. Again to have the applications of PD, the focus of research should be concentrated on achieving the lower  $\text{Tan } \delta$ , which increases the dielectric field strength as well as the high-energy density, suitable for electrical energy storage applications.

## References

1. Jawaid M, Khan MM (2018) Polymer-based nanocomposites for energy and environmental applications. Netherland, Wood head Publishing, Elsevier, Amsterdam
2. Lin Z, Yang Y, Zhang A (2017) Polymer-engineered nanostructures for advanced energy applications. Springer, Switzerland
3. Thakur VK, Kessler MR (2014) Polymer nanocomposites: new advanced dielectric materials for energy storage applications, in advanced energy materials. Wiley, Hoboken, New-Jersey
4. Panda M (2022) Tuned dielectric and percolation behavior of cold-pressed polyvinylidene fluoride nanocomposites caused by filler. Indian J Phys 96:1699-1703

5. Panda M, Mishra A, Shukla P (2019) Effective enhancement of dielectric properties in cold-pressed polyvinylidene fluoride/Barium Titanate nanocomposites. *SN Appl Sci* 01:230
6. Huang XY, Jiang PK, Kim CU (2007) Electrical properties of polyethylene/aluminium nanocomposites. *J Appl Phys* 102:124103
7. Gonon P, Boudefel A (2006) Electrical properties of epoxy/silver nanocomposites. *J Appl Phys* 99:024308
8. Panda M, Srinivas V, Thakur AK (2008a) On the question of percolation threshold in polyvinylidene fluoride/nanocrystalline nickel composites. *Appl Phys Lett* 92:132905–132907
9. Panda M, Srinivas V, Thakur AK (2008b) Surface and interfacial effect of filler particle on electrical properties of polyvinylidene fluoride/nickel composites. *Appl Phys Lett* 93:242908–242910
10. Panda M (2017) Major role of process conditions in tuning the percolation behavior of polyvinylidene fluoride-based polymer/metal composites. *Appl Phys Lett* 111:0829011–0829015
11. Yamada T, Ueda T, Kitayama T (1982) Piezoelectricity of a high-content lead zirconate titanate/polymer composite. *J Appl Phys* 53:4328
12. Zhang L, Bass P, Cheng ZY (2014) Revisiting the percolation phenomena in dielectric composites with conducting fillers. *Appl Phys Lett* 105:042905
13. Dyre JC, Schroder TB (2000) Universality of ac conduction in disordered solids. *Rev Modern Phys* 72:873
14. Gerhardt R (1994) Impedance and dielectric spectroscopy revisited: distinguishing localized relaxation from long-range conductivity. *J Phys Chem Solids* 55:1491–1506
15. Sinclair DC, West AR (1989) Impedance and modulus spectroscopy of semiconducting BaTiO<sub>3</sub> showing positive temperature coefficient of resistance. *J Appl Phys* 66:3850

# Chapter 10

## Ferroelectric Polymer Dielectrics



In this chapter, the dielectric behavior of a variety of ferroelectric polymer dielectrics (FPD), which may be the materials for future electrostatic energy storage applications has been discussed. The variety of polymer dielectrics, comprising of the ferroelectric polymer [polyvinylidene fluoride (PVDF)]/non-polar polymer [low-density polyethylene (LDPE)] and different sizes of metal particles (Ni, quasicrystal of Al–Cu–Fe) as filler, prepared through different process conditions (cold press/hot press) are explained. Very high values of effective dielectric constants ( $\epsilon_{\text{eff}}$ ) with low loss tangent ( $\tan \delta$ ) were observed for all the prepared FPD at their respective percolation thresholds ( $f_c$ ). The enhancement of  $\epsilon_{\text{eff}}$  and  $\tan \delta$  at the insulator to metal transition (IMT) is explained through the boundary layer capacitor effect and the percolation theory, respectively. The non-universal  $f_c$ /critical exponents across the IMT have been explained through percolation theory and are attributed to the filler particle size and shape, the interaction between the components, method of preparation, adhesiveness, connectivity, and homogeneity of the samples. Recent results on developed FPD with high  $\epsilon_{\text{eff}}$  and low  $\tan \delta$  prepared through cold press have proven themselves to be better candidates for low frequency and static dielectric applications.

### 10.1 Introduction

In the present-day scenario, the commercial materials used for energy storage, capacitor, and low-frequency dielectric applications are the high dielectric constant ceramic materials, such as  $\text{BaTiO}_3$ ,  $\text{PbTiO}_3$ , and PMN-PT. However, these ceramic materials are associated with several disadvantages, such as toxicity, high cost, lack of moldability, requiring longer time and higher energy consumption for their processing. To overcome these disadvantages, a recent area of research is regarding the development of polymer dielectrics (PD)/polymer composites as energy storage materials, composed of polymer/filler [1–20]. In this process of development, the physics of insulator-to-metal transition (IMT), associated with the enhancement of effective

dielectric constant ( $\epsilon_{\text{eff}}$ ) and effective ac conductivity ( $\sigma_{\text{eff}}$ )/loss tangent ( $\text{Tan } \delta$ ) at the percolation threshold ( $f_c$ ) is underuse. In the study of this PD, a variety of polymers with different kinds of fillers have undergone a lot of investigations for the last two decades of research. Out of these investigations, ferroelectric polymer dielectrics (FPD) have proven themselves as very good electrical energy storage materials [1–13]. A detailed investigation of the observed superior dielectric behavior of a large number of FPD [comprising of polyvinylidene fluoride (PVDF) and a variety of metal fillers] in comparison to the non-polar polymer dielectrics [comprising of low-density polyethylene (LDPE)] and nanocrystalline Ni (*n*-Ni)] are to be explained here.

## 10.2 Samples Reported

The various series of polymer/metal composites (PMC) comprising of PVDF/LDPE and different sizes of Ni/quasicrystal of Al–Cu–Fe are prepared through different process conditions (cold press/hot press) are given in Table 10.1. The details of the sample preparation and experimental measurements can be found from the earlier chapters as well as from the references [7–13].

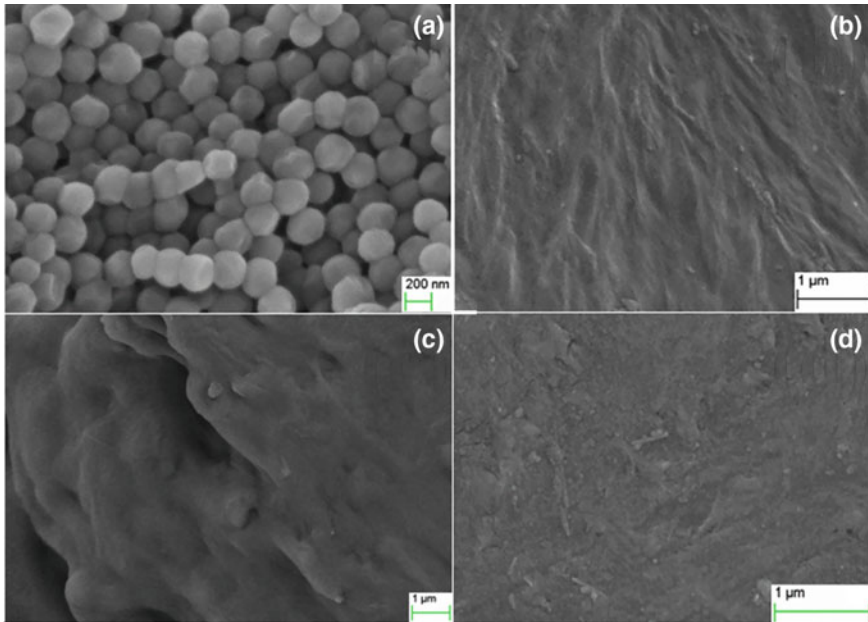
## 10.3 Results and Discussion

The micrographs of the non-polar and polar/ferroelectric polymers of the prepared PMC show interesting features regarding the role of polymer spherulites and permanent dipole moment of the polymer in storing the electrical charge [13]. If in a material, the challenge is to store electrical charge by creating defects in the system (i.e., by preparing polymer composites), and additionally the presence of spherulites is also there in the virgin polymer, then definitely those materials are going to be better dielectrics. The FESEM micrographs of the PVDF/LDPE prepared through the cold-pressed and hot-pressed methods are shown in Fig. 10.1a–d.

The interesting features of the presence of spherulites in the cold-pressed PVDF (Fig. 10.1a) and cold-pressed PMC and the presence of their dipolar polarization (Fig. 10.2) are highly beneficial in storing the electrical charge and hence in the development of high  $\epsilon_{\text{eff}}$  materials. However, the loss of spherulites in the hot-molded PVDF (Fig. 10.1b), lowers the static value of dielectric constant ( $\epsilon_r$ ) (Fig. 10.2), may inhibit the hot-molded FPD although the dipolar polarization contribution in the frequency ranges 40–10<sup>7</sup> Hz is present (Fig. 10.2). The non-presence of spherulites (Fig. 10.1c, d) and dipolar polarization (Fig. 10.2) in both the cold/hot-pressed LDPE inhibits them in the development of PD. The static  $\epsilon_r$  value for cold-pressed PVDF ~16 and hot-pressed PVDF ~10 (due to loss of spherulites) and gradual dispersion of  $\epsilon_r$  with an increase of frequency can be observed (Fig. 10.2). In contrast, the static  $\epsilon_r$  value for both cold/hot-pressed LDPE is ~2 and this value remains constant

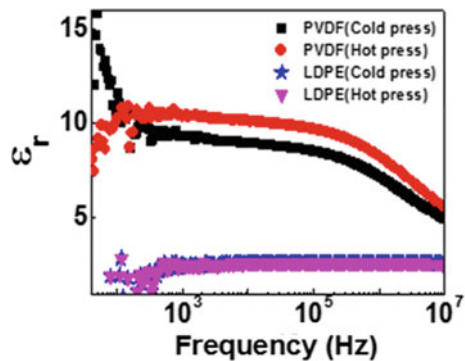
within the frequency range ( $40\text{--}10^7$  Hz) attributed to the non-presence of interfacial (spherulites) and dipolar polarization (Fig. 10.2) in the polymer.

The detailed observation of homogeneity and distribution of metal fillers in the polymer matrices of all the PMC and their dielectric/percolation behavior can be found from the published pieces of literature [7–12]. In a broad sense, from the detailed investigation of a large number of PMC, it can be summarized here that a large variation of  $f_c$  [0.07–0.57] independent of frequency, variation of  $\epsilon_{\text{eff}}$  and Tan



**Fig. 10.1** FESEM micrographs of **a** Cold-pressed PVDF. **b** Hot-pressed PVDF. **c** Cold-pressed LDPE. **d** Hot-pressed LDPE

**Fig. 10.2** Comparison of dielectric behavior of cold/hot-pressed PVDF/LDPE



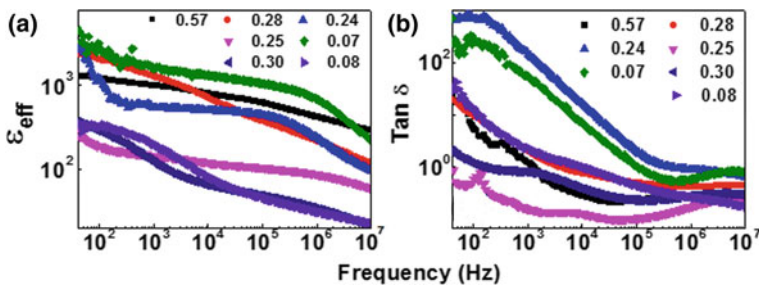


**Fig. 10.3** Achieved **a**  $\epsilon_{\text{eff}}$  and **b**  $\text{Tan } \delta$  of the variety of PMC at their respective  $f_c$  & their variation with frequency

$\delta$  with frequency (Fig. 10.3) and a range of static values of  $\epsilon_{\text{eff}}$  &  $\text{Tan } \delta$  [ $\epsilon_{\text{eff}} \sim 344$  to 2405 &  $\text{Tan } \delta \sim 2.01$  to 711] were observed (Table 10.1).

All the PMC undergo an IMT at their respective  $f_c$  and the enhancement of  $\epsilon_{\text{eff}}$  and  $\sigma_{\text{eff}}$  is explained through the boundary layer capacitor effect and the percolation theory [14]. Across the IMT, i.e., around the critical region, the  $\epsilon_{\text{eff}}$  and  $\sigma_{\text{eff}}$  as a function of volume fraction of conductor ( $f_{\text{con}}$ ) satisfies the power-law Eqs. 1.3 and 1.4 as

$$\epsilon_{\text{eff}} \propto (f_c - f_{\text{con}})^{-s} \text{ for } f_{\text{con}} < f_c$$

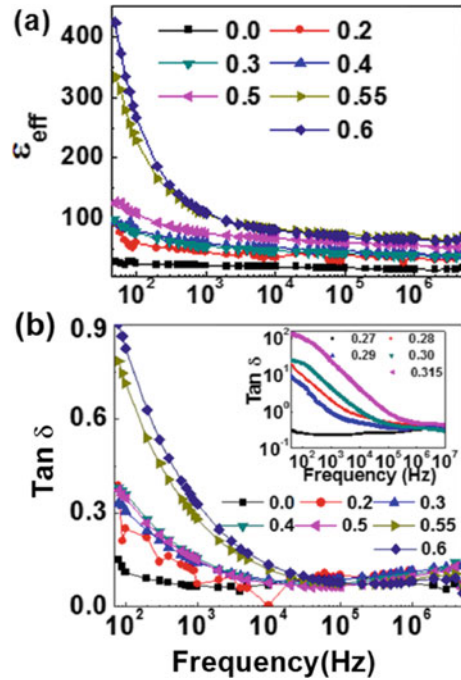
$$\sigma_{\text{eff}} \propto (f_c - f_{\text{con}})^{-s'} \text{ for } f_{\text{con}} < f_c$$

and the obtained non-universal critical exponents ( $s$  &  $s'$ ) are explained through the swiss cheese/inverted Swiss cheese model. As a representative pattern, Fig. 10.3a, b shows the variation of  $\epsilon_{\text{eff}}$  and  $\text{Tan } \delta$  as a function of frequency only for the percolative samples of all the series of PMC. It is observed that the LDPE/ $n$ -Ni composites prepared through hold molding show the weakest dielectric behavior and don't fit to be a good dielectric. However, all the FPD based on PVDF shows good dielectric behavior and may be suitable for applications. Among all the FPD, the best dielectric results are observed for cold-pressed PVDF/ $n$ -Ni composites with  $\epsilon_{\text{eff}} \sim 2405$  and  $\text{Tan } \delta \sim 19$  at  $f_c \sim 0.28$ . Also the achieved high value of  $\epsilon_{\text{eff}}$  and low  $\text{Tan } \delta$  for cold pressed PVDF/BaTiO<sub>3</sub> polymer/ceramic composites will be of high importance for the static and low-frequency dielectric applications over the traditional hot-molded dielectrics (Fig. 10.4) [9].

## 10.4 Summary

FPD is showing superior dielectric properties over other PD and is of definite help in storing the electrical charge and are going to be the future materials for electrostatic energy storage applications. It is found that the enhancement of  $\epsilon_{\text{eff}}$  of PCC based

**Fig. 10.4** Variation of **a**  $\epsilon_{\text{eff}}$  and **b**  $\text{Tan } \delta$  as a function of frequency for polymer-ceramic composites



on PVDF matrix is largely enhanced by the cold pressing process conditions, due to the retention of the spherulites during sample preparation. It is also found that this cold pressing method is more suitable to the PCC based on PVDF matrix (since a very low value of  $\text{Tan } \delta \sim 0.9$  is observed) in comparison with PMC based on PVDF matrix in which a large value of  $\text{Tan } \delta \sim 10\text{--}100$  is observed. The spherulites present in the PVDF matrix are always helpful in maintaining the  $\epsilon_r$  and in increasing the  $\epsilon_{\text{eff}}$  of PCC/PMC. In the current scenario, the most important investigation that should carry out is to develop new methods in lowering the static  $\text{Tan } \delta$  value of FPD to make them more suitable as the emerging materials (since recently it has also been reported that polymer nanocomposites are successful as high-temperature dielectrics [5]).

## 10.5 Scope for Future Possibilities

Although the present book reports a detailed investigation regarding the percolation and its non-universality, scaling and the non-universality of the critical exponents, the universality of the relaxation behavior across  $f_c$ , the multiferroic and rheological properties, and also some of the non-percolative systems, by studying their dielectric, electrical, magnetic, and rheological transport properties, still the following

works can be undertaken to improve the importance of these materials for various multifunctional applications. They are listed as:

- (1) Metals are very good conductors and they have the limitation of being used as EMI shielding materials due to their disadvantages, such as heavyweight, expensive, and their corrosion properties. However, as PMC/PCC composites are showing a high value of  $\text{Tan } \delta$  at their respective  $f_c$ /above it and are also flexible and don't undergo corrosion; nowadays, they are attracted to be used as EMI shielding materials. Hence, the EMI shielding coefficient measurement in these PMC can provide information about the applicability of these materials for high-frequency applications.
- (2) Since the composite of piezoelectric and piezomagnetic components is finding interest as magneto-electric materials for multifunctional applications, the polymer magneto-electrics with high magneto-electric coefficient can be developed.
- (3) Due to the occurrence of both ME and EMI shielding properties, these PMC/PCC will find a lot of multifunctional applications, such as high charge storage capacitors, high-frequency applications, and multistate memory elements.
- (4) Again to have the applications of FPD, the focus of research should be concentrated on achieving the lower  $\text{Tan } \delta$ , which increases the dielectric field strength as well as the high-energy density, suitable for electrical energy storage applications.
- (5) The most interesting part will be in the development of high-temperature polymer dielectric materials for dielectric capacitors to work in a high-temperature environment such as avionic and automotive industries, wind turbine generators, and advanced propulsion system [in which high power, high current, and elevated temperature conditions are the default environmental conditions] should be developed.
- (6) Polymer nanocomposites are going to be the upcoming multifunctional materials for any type of applications in the future.

**Tab. 10.1** Various series of PMC along with the achieved  $\epsilon_{\text{eff}}$  and  $\text{Tan } \delta$  at 40 Hz at their respective  $f_c$

Series of PMC	Method of preparation	$f_c$	$\epsilon_{\text{eff}}$ at 40 Hz	$\text{Tan } \delta$ at 40 Hz
PVDF/ $\mu$ -Ni	Cold Press	0.57	1284	25
PVDF/ $n$ -Ni	Cold Press	0.28	2405	19
PVDF/ $n$ -QC	Cold Press	0.24	3016	711
PVDF/ $\mu$ -Ni	Hot Press	0.25	310	2.11
PVDF/ $n$ -Ni	Hot Press	0.07	9440	693
PVDF/ $n$ -Ni@NiO	Hot Press	0.30	363	2.01
LDPE/ $n$ -Ni	Hot Press	0.08	344	34.46

## References

1. Dang ZM (2018) Dielectric polymer materials for high-density energy storage. Netherland, William Andrew, Elsevier, Amsterdam
2. Lin Z, Yang Y, Zhang A (2017) Polymer-engineered nanostructures for advanced energy applications. Springer International Publishing, Switzerland
3. Prateek, Thakur VK, Gupta RK (2016) Recent progress on ferroelectric polymer-based nanocomposites for high energy density capacitors: synthesis, dielectric properties, and future aspects. *Chem Rev* 116(7):4260–4317
4. Chen Q, Shen Y, Zhang S, Zhang QM (2015) Polymer-based dielectrics with high energy storage density. *Ann Rev Mater Res* 45:433–458
5. Li Q, Chen L, Gadinski MR, Zhang S, Zhang G, Li HU, Iagodkine E, Haque AC, Long-Qing J, Thomas N, Wang Q (2015) Flexible high-temperature dielectric materials from polymer nanocomposites. *Nature* 523:576–579
6. Li Q, Yao FZ, Liu Y, Zhang G, Wang H, Wang Q (2018) High-temperature dielectric materials for electrical energy storage. *Ann Rev Mater Res* 48:219–243
7. Panda M (2010) Scaling and relaxation behavior of polymer-metal composites across the percolation threshold. Ph.D. thesis. Indian Institute of Technology Kharagpur
8. Panda M (2018) Ferroelectric polymer dielectrics: emerging materials for future electrostatic energy storage applications. *AIP Conf Proc* 1953(1–4):020001
9. Panda M, Mishra A, Shukla P (2019) Effective enhancement of dielectric properties in cold-pressed polyvinylidene fluoride/barium titanate nanocomposites. *SN Appl Sci* 01:230–236
10. Panda M, Trivedi A (2021) Ferroelectric and piezoelectric properties of cold pressed polyvinylidene fluoride/barium titanate nano-composites. *Ferroelectrics* 572:246–257
11. Panda M (2022) Tuned dielectric and percolation behavior of cold-pressed polyvinylidene fluoride nanocomposites caused by filler. *Ind J Phys* 96:1699–1703
12. Panda M (2021) Ferroelectric, piezoelectric and dielectric properties of novel polymer nanocomposites. In: Multifunctional ferroelectric materials. Intech Open Publishing, Intechopen, London. <https://doi.org/10.5772/intechopen.96593>. ISBN: 978-1-83968-992-5
13. Panda M (2017) Major role of process conditions in tuning the percolation behavior of polyvinylidene fluoride-based polymer/metal composites. *Appl Phys Lett* 111(1–5):082901
14. Stauffer D, Aharony A (1992) Introduction to percolation theory. Taylor and Francis, London
15. Lin Z, Yang Y, Zhang A (2017) Polymer-engineered nanostructures for advanced energy applications
16. Thakur VK, Kessler MR (2014) Polymer nanocomposites: new advanced dielectric materials for energy storage applications. *Adv Energy Mater* 207–257
17. Sun W, Mao J, Wang S et al (2021) Review of recent advances of polymer based dielectrics for high-energy storage in electronic power devices from the perspective of target applications. *Front Chem Sci Eng* 15:18–34
18. Behera R, Elanseralathan K (2022) A review on polyvinylidene fluoride polymer based nanocomposites for energy storage applications. *J Enegrgy Storage* 48:103788
19. Huan TD, Boggs S, Teyssedre G, Laurent C, Cakmak M, Kumar S, Ramprasad R (2016) Advanced polymeric dielectrics for high energy density applications. *Progr Mater Sci* 83:236–269
20. Hu X, Yi K, Liu J, Chu B (2018) High energy density dielectrics based on PVDF-based polymers. *Energy Technol* 6(5):849–864

# Appendix

## Calculation of Volume Fraction of Any Component in a Composite

Let the two components in a composite are of weight  $xg$  and  $yg$ , respectively, where  $xg$  is the weight of filler and  $yg$  is the weight of the matrix.

Let the total weight of composite be  $zg$ .

Hence, the relationship between  $x$ ,  $y$ , and  $z$  can be written as  $x + y = z$ .

The weight fraction for the first component, i.e., filler is given by  $W_f = x/x + y = x/z$ .

The weight fraction for the second component, i.e., matrix is given by  $W_f = y/x + y = y/z = 1 - x/z$ .

Let the density of two components, such as filler and matrix, be  $\rho_f$  and  $\rho_m$ , respectively.

The volume fraction of any component in the composites, e.g., for filler can be calculated as:

$$V_f = \frac{W_f}{W_f + (1 - W_f) \frac{\rho_f}{\rho_m}}$$

where  $W_f$  is the weight fraction and  $V_f$  is the volume fraction of the filler, used respectively.

# Bibliography

1. Du B (2017) Properties and applications of polymer dielectrics. Intech Open, UK
2. Nicolais L, Carotenuto G (2005) Metal-polymer nanocomposites. Wiley, USA
3. Mai Y-W, Tjong SC (2010) Physical Properties and applications of polymer nanocomposites. Wood Head publishing, Elsevier, Amsterdam, Netherlands
4. Hoque ME, Kumar R, Sharif A (2022) Advanced polymer nanocomposites: science, technology and applications. Woodhead Publishing in Materials, Amsterdam, Netherlands
5. Tavares MIB, Silva EO, da Silva PRC, da Menezes LR, de (2017) Polymer nanocomposites. In: Nanostructured materials—Fabrication to applications. Intech open, London
6. Willard HH, Merritt LLJ, Dean JA, Settle FAJ (1974) Instrumental methods of analysis. Van Nostrand, New York-Wokingham